REGULATION OF MITOCHONDRIAL GENOME DIVISION AND BASAL BODY DUPLICATION IN THE AFRICAN TRYPANOSOME

by

CATHERINE SULLENBERGER

(Under the Direction of Kojo Mensa-Wilmot)

ABSTRACT

Trypanosoma brucei is a protozoan parasite responsible for health and economic burden in some regions of sub-Saharan Africa. In *T. brucei* the mitochondrial genome is housed within a nucleoid termed the kinetoplast. The kinetoplast is physically connected to a cytoplasmic basal body (microtubule-organizing center for the flagellum). Duplication of both the kinetoplast and basal body are coordinated with trypanosome S-phase. Regulatory pathways which promote S-phase entry and control duplication of the kinetoplast and basal body are poorly understood in *T. brucei*. Here we describe a small molecule kinase inhibitor, AEE788, which inhibits duplication of the kinetoplast and basal body, and prevents DNA synthesis; effectively blocking trypanosome entry into S-phase. We developed an AEE788 “block-and-release” protocol for enriching bloodstream *T. brucei* in G1. Thus, for the first time we experimentally documented the kinetics of DNA synthesis (in the kinetoplast and nucleus), basal body duplication, kinetoplast division, and mitosis during trypanosome division, establishing AEE788 as a useful

chemical tool for the study of trypanosome biology. A second study in this work demonstrates that reduced levels of a trypanosome casein kinase 1, TbCK1.2, caused amplification of basal bodies, while increased TbCK1.2 levels inhibited duplication of the organelle. Further, we detected TbCK1.2 at basal bodies, and demonstrated that phosphorylation of basal body proteins was altered after knockdown of the kinase. Interestingly, knockdown of TbCK1.2 inhibited kinetoplast division without preventing kinetoplast DNA (kDNA) replication, basal body duplication/separation, or flagellum biogenesis. These data are at odds with current dogma which describes basal body separation as the cause of kinetoplast division. Accordingly, we hypothesize that a regulatory pathway, dependent on TbCK1.2, is required to promote decatenation of the interlocked kDNA network. Taking into account our work, and other published data, we propose that proteins required for kinetoplast division ("kinetoplast division factors") direct decatenation of the kDNA network to prevent asymmetric division. Collectively this work: i) identifies AEE788 as a chemical tool to reversibly enrich pre-S-phase bloodstream *T. brucei*, ii) demonstrates the role of TbCK1.2 in controlling basal body copy number, and iii) offers a new perspective on the regulatory pathways which are required for kinetoplast division.

INDEX WORDS: *Trypanosoma brucei* (*T. brucei*), basal body, kinetoplast, casein kinase 1, AEE788, chemical biology, cell division cycle

REGULATION OF MITOCHONDRIAL GENOME DIVISION AND BASAL BODY DUPLICATION IN THE AFRICAN TRYPANOSOME

by

CATHERINE SULLENBERGER

B.S., University of Central Florida, 2011

A Dissertation Submitted to the Graduate Faculty of The University of Georgia in Partial Fulfillment of the Requirements for the Degree

DOCTOR OF PHILOSOPHY

ATHENS, GEORGIA

2017

REGULATION OF MITOCHONDRIAL GENOME DIVISION AND BASAL BODY DUPLICATION IN THE AFRICAN TRYPANOSOME

by

CATHERINE SULLENBERGER

Major Professor:	Kojo Mensa-Wilmot
Committee:	Karl Lechtreck
	Roberto Docampo
	Drew Etheridge

Electronic Version Approved:

Suzanne Barbour
Dean of the Graduate School
The University of Georgia
August 2017

DEDICATION

I would like to dedicate this dissertation to my family: my father (John Sullenberger), mother (Suzanne Sullenberger), and brother (Thomas Sullenberger). I am forever thankful to have grown up with such a supportive group of people in my life.

ACKNOWLEDGEMENTS

I have many people to thank for reaching this academic achievement in my life. I would first like to acknowledge Dr. Kojo-Mensa-Wilmot for his guidance, patience, and sense of humor, after all if you can't learn to laugh in the face of failure, it is difficult to overcome. Additionally, I would like to thank the faculty members who served on my committee, Dr. Karl Lechtreck, Dr. Roberto Docampo, Dr. Drew Etheridge, and Dr. Eileen Kennedy, for insightful discussion and fresh perspectives. I also acknowledge Julie Nelson and Dr. Muthugapatti for their guidance in flow cytometry and microscopy, respectively.

I have been lucky to form friendships with some amazing people who were just as willing to trouble-shoot my experiments with me as to have a drink after a long day. I would therefore like to thank Dr. Snehal Chaudari, Zach Detwiler, Dr. Justin Fellows, Dr. Sarah Thomas, Robert Ng, Zhibo Ma, Kyona Jarrett, Penny Louka, Riju Balachandran, Mayukh Guha, Bratati Karmakar, Madhumati Mukherjee, and Bryanna Thomas.

Additionally, I want to thank members of the Mensa-Wilmot lab, past and present (Paul Guyett, Sarah Thomas, Daniel Piqué, Justin Wiedeman, Bry Thomas, Halely Vale, Amrita Sharma, and Ben Hoffman) for providing a super positive, fun, and collaborative (but still productive) working environment. I would especially like to thank Paul, Sarah, and Justin for technical help and advice.

Lastly, I would like to thank my family (Sullenberger, Bensebat, Faulk, McArthur, and Canter clans) and friends (Jill Carey, Sam Bellflower, Stori Johnson, Ann Wolfgang, and Ben Whitener) for their unconditional love and support.

TABLE OF CONTENTS

Page

LIST OF TABLES

Page

LIST OF FIGURES

Page

CHAPTER 1

INTRODUCTION AND LITERATURE REVIEW

1.1 Introduction to research interests and approach

Protein kinases act as molecular switches by transferring a phosphate group onto protein substrates which can lead to changes in protein localization, activity, or protein-protein interactions (reviewed in [1, 2]). There are 176 protein kinases encoded in the genome of *Trypanosoma brucei* [3]. The function of many trypanosome kinases remains unclear but a number of pathways including endocytosis [4, 5], cell cycle progression or organelle duplication [6-14], and trypanosome morphology [13, 15, 16] have been linked to phospho-signaling events. The African trypanosome is an early-branching [17] eukaryotic pathogen and at least 50% of trypanosome genes lack homologs, at the protein sequence level, in other eukaryotes [3, 18]. Thus, the trypanosome field cannot rely strictly on sequence alignments to assign protein function or to predict components of regulatory networks. Consequently, trypanosome substrates and downstream effectors are unknown for the vast majority of protein kinases.

Our lab is particularly interested in understanding how phospho-regulatory networks regulate S-phase entry and promote organelle duplication during this stage of the trypanosome division cycle. In Chapter 2 the effect of an anti-trypanosomal kinase inhibitor, AEE788, on S-phase entry, transferrin endocytosis, and trypanosome morphology is reported. Additionally, we identified putative

phospho-proteins affected by the inhibitor and describe the utility of using small molecules to identify novel phospho-regulatory proteins in the African trypanosome (Figure 1.1).

Several important events occur during the trypanosome S-phase including replication of the mitochondrial genome and duplication of the basal body (microtubule-organizing center for the flagellar axoneme) [19]. In *T. brucei* the mitochondrial genome is sequestered within a catenated mitochondrial nucleoid termed the kinetoplast which is tethered to a basal body [20]. A trypanosome casein kinase 1, TbCK1.2, influences division of the replicated kinetoplast [7], a process associated with separation of duplicated basal bodies [21]. In Chapter 3 we characterize defects in kinetoplast division associated with loss of TbCK1.2 activity and demonstrate the enzyme's role in control of basal body duplication.

The following literature review will describe the health risks posed by *Trypanosoma brucei* (Chapter 1.2) and unique aspects of the parasite's cellular organization (Chapters 1.3-1.4). Subsequently, the physiological pathways relevant to the research presented in Chapters 2 and 3 will be reviewed including: the cell division cycle (Chapter 1.5), organelle duplication (Chapter 1.5), transferrin endocytosis (1.6), and the function of casein kinase 1 in trypanosomes and other eukaryotes (Chapter 1.7). Finally, conclusions from our studies are discussed in Chapter 4.

1.2 Pathogenesis and life cycle of *Trypanosoma brucei*

Trypanosoma brucei is a kinetoplastid protozoan parasite endemic to parts of sub-Saharan Africa. Two sub-species, *T. brucei rhodesiense* and *T. brucei gambiense*,

cause human African trypanosomiasis (HAT), which is fatal if left untreated. There are 60-70 million people at risk of HAT infection [22]. The third sub-species, *T. brucei brucei* does not infect humans, but causes a wasting disease, nagana, in cattle. Consequently, *T. brucei* is the cause of health and economic burden in 36 countries in sub-Saharan Africa, particularly in rural communities where infrastructure and access to healthcare are lacking. Our lab uses *T. brucei brucei* as a model to study trypanosome biology.

T. brucei is an extracellular pathogen that resides in the blood and lymph during early stages of infection (stage I). Stage I symptoms include fever, joint pain, swollen lymph nodes, and headache [23]. Onset of these symptoms can be observed weeks or months after initial exposure to the parasite depending on the type of infection; *T. brucei rhodesiense* (~2% of cases [24]) causes acute infection while *T. brucei gambiense* (>97% of cases [24]) causes chronic infection [23]. The infection reaches stage II (i.e. late stage) when parasites cross the blood-brain barrier and enter the central nervous system (CNS). Stage II symptoms include confusion, poor coordination, and disruption of the circadian rhythm, ultimately leading to death [23].

Vaccine development against HAT has been unsuccessful due in large part to the parasite's ability to evade the host immune system through antigenic variation; a process during which trypanosome subpopulations express distinct variant surface glycoproteins (VSGs) which prevents immune clearance of the entire population (reviewed in [25-27]). There are currently five anti-HAT chemotherapies (pentamidine, suramin, melarsoprol, eflornithine, or nifurtimox-

eflornithine combination treatment), each with their own advantages and disadvantages (reviewed in [28, 29]). Some treatments have toxic side effects and all require delivery by injection, which is far from optimal for treatment of patients with limited access to clinics. The difficulty associated with identifying anti-trypanosomal compounds that cross the blood-brain barrier have made it difficult to develop treatments for stage II HAT. Only two compounds, fexinidazole SCYX-7158, are in clinical trials to treat African trypanosomiasis [29]. Thus, new drugs to combat HAT are still in need.

The geographic distribution of trypanosomiasis is confined by the parasite vector, the Tsetse fly (*Glossina spp*). In order to adapt to the environment of the mammalian host or insect vector, *T. brucei* transitions between two developmental stages (Figure 1.2). Differentiation of the insect procyclic form parasite (PCF) into the human-infective bloodstream from (BSF) stage (reviewed in [30]) is accompanied with many physiological changes [31-39]. Accordingly, it is not surprising that in many cases, genetic knockdown of the same protein in PCF or BSF parasites results in different phenotypes [6, 13, 40-45]. Studies presented in this work were performed with BSF trypanosomes.

1.3 Trypanosome cytoskeleton and morphology

The vermiform morphology of *T. brucei* is maintained by an intracellular microtubule-based cytoskeleton [19, 46, 47]. Cytoskeletal microtubules, or subpellicular microtubules, form a single layer beneath the plasma membrane [19, 46, 47]. Crosslinks between parallel subpellicular microtubules, and to the plasma membrane, form a cage-like structure around the entire cell periphery which is

maintained throughout the cell cycle [31]. Surprisingly, analysis of the cytoskeleton by electron microscopy (EM) failed to detect the presence of actin filaments [47], nor does actin appear to be required to maintain the subpellicular corset [41]. Conversely, genetic knockdown of α-tubulin in *T. brucei* causes swelling of the posterior tip and cell rounding [48].

1.4 The trypanosome basal body and associated organelles

Basal bodies of Trypanosoma brucei

The trypanosome basal body is a microtubule-organizing center that contains two centriole-like structures: a mature basal body (mBB) and an adjacent immature probasal body (pBB) (Figure 1.3) [19]. Centrioles and basal bodies are microtubule-based cylindrical structures with 9-fold symmetry (Figure 1.4). In many eukaryotes, symmetry of the microtubule barrel is, in part, established by the protein SAS6 which self-assembles into a cartwheel-like structure with 9-fold symmetry (Figure 1.4) [49-53]. Trypanosome basal bodies, similar to human centrioles, are composed of nine triplet microtubules (Figure 1.4) [54].

A set of 14 “ancestral centriolar proteins” (δ-tubulin, ε-tubulin, centrin2, WDR16, SAS4, SAS6, POC1, CEP164, DIP13, VFL1/CLERC, CEP76, CEP135/Bld10, POC5, and CEP110/centriolin) can be identified across 45 organisms, from different phyla, which contain either basal bodies or centrosomes (centriole-derived microtubule-organizing centers) [55]. Trypanosomes possess protein homologs to all “ancestral centriolar proteins” with the exception of CEP110/centriolin [55-59], consistent with conserved basal body structure in the parasite. However, in some cases conserved proteins have divergent functions

and fail to localize to the basal body [60], and in several cases the localization/function of conserved proteins have not been experimentally tested in *T. brucei*.

To date approximately 50-60 proteins have been detected at the trypanosome basal body, and approximately half of them are unique to kinetoplastids [10, 42, 56-58, 61-74]. Thus, there are likely novel regulatory pathways that govern basal body biogenesis in the trypanosome. Functional studies have identified several trypanosome basal body proteins that are important for duplication, segregation, or copy number control of the organelle (Table 1.1). Importantly, there are still many unknowns concerning the regulatory mechanisms that initiate basal body biogenesis and the pathways which coordinate this process with the trypanosome division cycle.

Basal bodies are microtubule-organizing centers (MTOCs) that nucleate a flagellar axoneme (reviewed in [75-79]). In addition to facilitating assembly of the flagellum [19], trypanosome basal bodies are important for cytokinesis, inheritance of the mitochondrial genome [21], and formation of the flagellar pocket [80]. To execute its various functions, the trypanosome basal body is closely associated with the mitochondrion, mitochondrial genome, flagellum, and other cytoskeletal structures which are discussed in the following sections.

Organization of the mitochondrion and mitochondrial genome

Trypanosomes have a single mitochondrion that runs from the posterior to the anterior of the cell (Figure 1.3) [81, 82]. Mitochondrial structure in the BSF parasites is simpler than in PCF parasites with less branches extending from the

main mitochondrial tubule [81], likely a reflection of metabolic differences between the developmental stages [39]. BSF parasites rely on glycolysis for ATP production but maintenance of mitochondrial membrane potential is essential for parasite viability [39, 82-85]. Unlike other eukaryotes, fission and fusion events of the mitochondrion in *T. brucei* do not occur throughout cell division [81]. The mitochondrial genome is organized into a single network of interlocked covalently closed, circular DNAs (reviewed in [86-88]); undoubtedly one of the most intriguing aspects of trypanosome biology.

The mitochondrial nucleoid, or kinetoplast, is anchored in the posterior of the cell to the mitochondrial membrane (Figures 1.3 and 1.4) [20]. The kinetoplast DNA (kDNA) network is composed of two classes of circular DNAs: several thousand minicircles (1 kb in size) and a few dozen maxicircles (23 kb in size) [89]. Maxicircles encode mitochondrial proteins [90] and minicircles encode guide RNAs required for post-transcriptional processing (RNA editing) of maxicircle transcripts [91-94]. Each minicircle is topologically interlocked with two or three neighboring minicircles [95]. Maxicircles in *T. brucei* are threaded through the catenated minicircle network and additionally linked with each other, forming a network within a network [96]. In vivo, the kDNA network is condensed into a circular disk (Figures 1.3 and 1.4) [88]. Sequestration of the single-copy mitochondrial genome within the kinetoplast requires faithful duplication and segregation of the kDNA network to ensure trypanosome viability (reviewed in [97]). Curiously, the trypanosome basal body is associated with segregation of the mitochondrial genome through a

“tripartite attachment complex” (TAC) which physically connects the basal body and kinetoplast [20, 21].

Components of the TAC are anchored to the proximal end of the cytoplasmic basal body and traverse the mitochondrial membrane to attach to the kDNA network [20]. “Exclusion zone filaments” bridge the basal body to the outer mitochondrial membrane, while “unilateral filaments” connect the inner mitochondrial membrane to the kinetoplast (Figure 1.4) [20]. Several proteins have been localized to the TAC [98-102], however, composition of TAC itself remains elusive. Though often described as a filamentous network (Figure 1.4) [20, 86, 87], individual filaments are not clearly discerned when the structure is viewed by electron microscopy (EM) [20]. Nonetheless, detergent extraction of trypanosome flagella revealed that the kinetoplast remains attached to the flagellar basal body, implying that the kDNA network is physically linked with the basal body [20, 21]. After replication of both the kinetoplast and basal body (described in Chapter 1.5), the TAC likely facilitates kinetoplast segregation [19].

The flagellum and accessory structures

Two of the triplet microtubules from the mature basal body elongate to form the flagellar axoneme (the A- and B-tubules), maintaining the same 9-fold symmetry observed in the basal body (Figure 1.4) [19]. Elongation of the basal body gives rise to a specialized region between the basal body and flagellum termed the transition zone (Figure 1.4) [103, 104]. The transition zone is capped by the basal plate from which the central pair microtubules of the flagellar axoneme are nucleated (Figure 1.4) [105, 106]. Central pair microtubules are associated with

motile flagella (reviewed in [107, 108]). Thus, transition from the basal body to the flagellum can be identified by the microtubule organization of each region: the basal body (mature and immature) has nine triplet microtubules with no central pair (9+3+0), the transition zone has nine doublet microtubules and lacks a central pair (9+2+0), and the flagellar axoneme is defined by nine doublet microtubules with a central pair (9+2+2) (Figure 1.4).

After assembly, the flagellum exits the cell body from the posterior end of the trypanosome (Figures 1.3 and 1.4). Upon exiting the cell, the flagellum associates with the paraflagellar rod (PFR), an electron-dense structure unique to kinetoplastids, euglenoids, and dinoflagellates (Figure 1.4) [109, 110]. The PFR resides within the flagellar membrane and is important for trypanosome motility [111]. The flagellum and PFR remain in contact with the outer cell membrane for the entire length of the cell [112]. Attachment of the flagellum to the cell body is achieved through the flagellar attachment zone (FAZ) (Figures 1.3 and 1.4) which consists of a group of four microtubules (microtubule quartet) and a filamentous structure (reviewed in [113]). Genetic knockdown of proteins that localize to the FAZ can cause detachment of the flagellum from the cell body [45, 69, 114, 115]. Flagellar biogenesis, trypanosome motility, and attachment of the flagellum to the cell membrane are essential for proper completion of the cell division cycle and trypanosome viability [69, 114, 116-119].

The flagellar pocket (reviewed in [120]) is an invagination of the plasma membrane, towards the interior of the cell (Figures 1.3 and 1.4), from which the flagellum exits the cell body [121]. When viewed by EM, an electron dense

structure encircling the neck of the flagellar pocket is observed [121] and referred to as the flagellar pocket collar (FPC). The only identified protein component of the FPC is TbBILBO-1 [43]. Knockdown of TbBIBLO-1 in procyclic trypanosomes blocked duplication of the FP and caused flagellar detachment [43]. Fascinatingly, knockdown of the same protein in bloodstream trypanosomes had a markedly different phenotype characterized by cell rounding with no defects in flagellar attachment [43].

The trypanosome bilobe

The bilobe is found in proximity to the basal body, FPC, FAZ, and Golgi [99, 122]. The hook-like structure of the bilobe curves around the flagellar pocket while the anterior region of the structure runs parallel to the FAZ (Figure 1.3) [122, 123]. Co-immunoprecipitation of bilobe proteins identified components of the basal body, TAC, and FAZ leading to the hypothesis that these cytoskeletal structures form a continuous cytoskeletal network [99]. The bilobe is essential for duplication of the Golgi in PCF parasites [62]. Interestingly, several proteins which localize to the basal body, flagellum, or FAZ are also localized to the bilobe [56, 62, 66, 71] which supports the idea of an interconnected cytoskeletal network.

1.5 Cell division cycle of *T. brucei*

Cell cycle overview

The trypanosome cell cycle, similar to other eukaryotes, has four distinct phases: G1, S, G2, and M (reviewed in [124, 125]). After mitosis (M), cytokinesis divides the cell, segregating replicated organelles into two identical daughter

trypanosomes (reviewed in [126]). The first (G1) and second (G2) gap phases allow the cell to prepare for DNA synthesis during S-phase and chromosome segregation during mitosis (M), respectively. Cell cycle checkpoints block transition from one stage of the cycle to the next if events of the preceding phase are not properly executed (reviewed in [127, 128]). Additionally, a complex series of phospho-signaling networks dictate entry and exit from each stage of the cell cycle [129] (reviewed in [130-132]). The absence of well characterized cell cycle regulators in the trypanosome genome suggests novel regulatory networks drive cell cycle progression in the parasite. Further, cell cycle regulators and cell cycle checkpoints differ between BSF or PCF trypanosomes. Chapters 2 and 3 will describe chemical or genetic perturbation of progression across the G1/S border, kinetoplast division, and basal body duplication. Consequently, the following sections will describe these events in the context of the trypanosome cell division cycle.

Order of organelle duplication during the trypanosome division cycle

Cytological assessment of the number of kinetoplasts, basal bodies, and nuclei per trypanosome can be used to estimate the cell cycle stage of individual cells (Figure 1.5) [19, 133]. Trypanosomes in G1 have a single round kinetoplast (K), one nucleus (N), and one flagellated basal body (1K1N 1BB) (Figure 1.5) [19, 134]. Transition into S-phase correlates with a structural change in the kinetoplast; kDNA synthesis, measured by incorporation of a thymidine analog, correlates with kinetoplast elongation (Ke) (Figure 1.5) [133, 135, 136]. Nuclear DNA content is increased in 1Ke1N trypanosomes [137], suggesting that 1Ke1N trypanosomes

are in nuclear S-phase. Duplication of the basal body (2 BB), flagellum, and bilobe is also observed during S-phase (1Ke1N 2BB) (Figure 1.5) [19, 62, 126, 133, 136]. Division of the kinetoplast occurs prior to mitosis yielding 2K1N 2BB trypanosomes (Figure 1.5) [19, 133], each of which is associated with a basal body through the TAC (Chapter 1.4). The kinetoplast-basal body complexes separate during G2 in preparation for segregation during cytokinesis [19] (Figure 1.5). The replicated nucleus divides during mitosis (M) generating 2K2N 2BB trypanosomes (Figure 1.5) [19, 133] that will undergo cytokinesis to produce two 1K1N 1BB daughter cells.

The transition from G1 to S

In many eukaryotes cyclin-dependent kinases (CDKs) and their activating partners, cyclins, are major regulators of cell cycle transitions (reviewed in [138, 139]). Mammalian cells progress through G1 in response to extracellular growth signals which stimulate transcription of G1 cyclins (cyclin D and cyclin E) (reviewed in [140-142]). Cyclin D forms an active complex with either CDK4 or CDK6 and helps to activate the cyclin E-CDK2 complex which drives transition from G1 to S [143-146]. Transcription of G1 cyclins and assembly of active CDK complexes are enhanced by different phospho-signaling pathways which are stimulated by environmental cues (reviewed in [140-142]). In particular, receptor tyrosine kinases (RTKs) stimulate mitogen-activated protein kinase (MAPK) cascades in response to various growth factors (reviewed in [140-142]). Additionally, a phosphatidylinositol-3-kinase (PI3K)/AKT-directed signaling pathway stimulates the mammalian target of rapamycin (mTOR), as part of a nutrient signaling

pathway, which promotes cyclin E-CDK2 activity and cell proliferation [140, 147, 148].

The observation that bloodstream trypanosomes arrest in G1 after serum starvation [149] and in response to a trypanosome-secreted differentiation factor (SIF) [150] suggests that, like other eukaryotes, nutrients in the extracellular environment influence trypanosome division. Trypanosomes lack homologs to RTKs [3], but encode homologs of TOR protein kinase which may be involved in progression from G1 to S [151, 152]. Knockdown of either TbTOR1 or TbTOR4 in BSF trypanosomes enriched cells in G1 while simultaneously decreasing S and G2/M populations (based on nuclear DNA content) [151, 152]. However, further studies measuring DNA synthesis are needed to confirm these findings. Trypanosomes express a single PI3K homolog which does not function in G1 progression [153].

The trypanosome genome encodes eleven cdc2-related kinases (TbCRKs) and ten cyclins (TbCYC) [125]. Studies have shown that TbCRK1, TbCRK2, and TbCYC2 are important for efficient progression through the G1/S boundary [6, 44, 154-156]. Knockdown of TbCYC2, TbCRK1, or TbCRK2 in both BSF and PCF parasites enrich the fraction of G1 cells (based on nuclear DNA content) and increase the percentage of 1K1N (G1) trypanosomes [6, 154-156]. However, DNA synthesis (in the kinetoplast and nucleus) in only inhibited in PCF cells [155, 156]. A triple knockdown of TbCRK1/CRK2/CYC2 in BSF inhibited DNA synthesis in just 15% of the population suggesting that progression into S-phase was delayed, but not blocked [44].

Thus, there is still much to be learned about the phospho-signaling pathways that promote G1 progression and S-phase entry, especially in BSF trypanosomes. Currently there are no approaches for the synchronization of bloodstream trypanosomes in G1. In search of a chemical tool which could aid in characterization of the G1/S boundary, we present data suggesting that an RTK inhibitor, AEE788, can be used as a novel tool for the enrichment of pre-S-phase trypanosomes (Chapter 2). Additionally, we discuss the utility of AEE788 for identification of putative phospho-proteins that may regulate the G1/S transition in BSF trypanosomes.

Kinetoplast DNA synthesis

Kinetoplast DNA and nuclear DNA are synthesized in two distinct, but overlapping, S-phases [133]. Approximately 30-40 proteins have been implicated in kDNA synthesis or post-replication division of the network (reviewed in [86, 87, 157]). The complexity of this process has led researchers to predict that 100-150 proteins are likely involved in the event [87], thus there is still much to learn about the pathways responsible for kinetoplast duplication. The process of KDNA replication and a few key proteins known to be involved in this pathway are described below.

Minicircle and maxicircle DNA replication occur in different regions surrounding the kinetoplast (reviewed in [86, 87]). Minicircles are enzymatically released from the kDNA network [158] and replicated within the mitochondrion proximal to differentiated mitochondrial membranes occupied by components of the TAC (kinetoflagellar zone or KFZ) (Figure 1.6A) [159]. Minicircle DNA synthesis is unidirectional and proceeds through theta intermediates (Figure 1.6A) [158, 160]

(theta type replication is reviewed in [161]). Following replication, the mother and daughter minicircles are directed to protein assemblies at the poles of the kinetoplast (antipodal sites) where nicks and gaps are filled in by replicative proteins before reattachment to the network (Figure 1.6A) [159, 162]. At least one nick or gap is retained in the minicircle when it is reconnected to the network and has been proposed to serve as a marker for replicated minicircles to prevent re-replication of kDNA [87, 158]. Prior to division of the replicated network, which has doubled in size, all nicks and gaps in minicircles or maxicircles are repaired [86, 87]. Maxicircle DNA replication is not well understood, but is proposed to occur within the kDNA network, without detachment, through theta intermediates (Figure 1.6B) [163]. Nuclear DNA synthesis is not dependent on kDNA synthesis; knockdown of a replicative mitochondrial DNA polymerase prevented kDNA synthesis but had no effect on duplication of the nucleus or subsequent cytokinesis [164].

Several proteins involved in kDNA synthesis are localized to the KFZ, antipodal sites, or the kDNA disk (reviewed in [86, 87]). Mitochondrial topoisomerase II localizes to the antipodal sites [165] and is postulated to release minicircles from the network [86, 87, 165]. However, this hypothesis is not consistent with data from genetic knockdown of the single mitochondrial topoisomerase II which implicates the protein in reattachment of minicircles to the kDNA network [87, 165-167]. Universal minicircle binding proteins (UMBSP I and II) and p38 bind the origin of free minicircles and are important for initiation of minicircle replication [168-171]. UMSBP proteins localize to the KFZ [171] (site of

minicircle DNA synthesis) whereas p38 was detected at the antipodal sites [170]. Three mitochondrial DNA helicases are involved in either minicircle replication (TbPIF1) [172], maxicircle replication (TbPIF2) [173], or kDNA network organization (TbPIF8) [174]. Mitochondrial primases are localized to the antipodal sites to prime minicircles and maxicircles for replication [175, 176]. Of the seven mitochondrial DNA polymerases (pol) identified in trypanosomes, experimental evidence suggests that DNA Pol IB, Pol IC, and Pol 1D are replicative polymerases [164, 177, 178]. DNA Pol 1B and Pol 1C localize to two foci in the KFZ [178] whereas Pol ID localizes throughout the mitochondrion but is recruited to the antipodal sites during kDNA S-phase [179]. Two DNA Pol β-like enzymes work in concert with DNA ligases to fill in gaps and seal nicks in minicircle and maxicircle DNAs [134, 180, 181]. DNA Pol β and ligase κβ localize to the antipodal sites to repair minicircles prior to network reattachment [134, 181]. Pol β-PAK and ligase κ-α are localized within the kDNA disk suggesting that they repair nicks within the network before division of the kinetoplast [134, 181]. Protein kinases may influence the timing of kinetoplast S-phase by controlling transcript stability of proteins required for kDNA synthesis [182-184].

Nuclear DNA synthesis

Replicative proteins that facilitate DNA synthesis are recruited to specific sites in the genome (origin of replication) where they form the replisome (reviewed in [185, 186]). Assembly of the replisome is staged [187] and its activity is controlled by protein phosphorylation (reviewed in [188, 189]). Protein components of the origin recognition complex (ORC1-6) assemble at the origin and recruit proteins required

to load the DNA helicase [190-192]. In mammalian cells, the proteins Cdc6 and Cdt1 bind ORC [193-195] and are essential for loading the MCM complex (DNA helicase) onto the origin [195-197]. Together ORC, Cdc6, Cdt1, and the MCM complex (Mcm2-7) form the pre-replicative complex (pre-RC) (reviewed in [185, 186]). Formation of the pre-RC is regulated by the availability of nuclear Cdc6 and Cdt1, which are consequently referred to as licensing factors [198]. After the MCM complex has been loaded onto the origin, Cdc6 and/or Cdt1 are degraded, exported from the nucleus, and/or sequestered to prevent licensing of the origin outside of S-phase [199-202].

Activation of the MCM complex requires protein phosphorylation which promotes interaction of the MCM complex with Cdc45, the GINS complex (Sld5, Psf1, Psf2, and Psf3), and other replicative proteins (reviewed in [203, 204]). The active helicase is consequently referred to as the CMG complex (**C**dc45, **M**CM complex, and **G**INs complex). An S-phase CDK promotes binding between the MCM complex, Cdc45, replicative DNA polymerases, and the GINs complex (reviewed in [188]). A second protein kinase, Dbf4-dependent kinase (DDK/Cdc7) phosphorylates subunits of the MCM complex promoting further interaction with Cdc45 and GINs (reviewed in [188]). Subsequently, DNA polymerases α, δ, and ε work together to replicate both strands of the double-stranded DNA (reviewed in [203, 205]).

Five ORC subunits have been identified in *T. brucei,* most of which are highly divergent: TbOrc1/Cdc6, TbOrc4, TbOrc1b, Tb3120, and Tb7980 [206-208]. TbOrc1 shares homology to both Orc1 and Cdc6 but its constant association with

chromatin over the trypanosome cell division cycle suggests that it does not function as a licensing factor [206]. TbOrc1/Cdc6 is the only trypanosome Orc that has been directly implicated in the control of DNA synthesis [209]. The CMG complex is well conserved in trypanosomes and is required for DNA replication [208]. Additionally, replicative DNA polymerases (α, δ, and ε) are conserved amongst kinetoplastids [210, 211]. A Cdt1 homolog, however, has not been identified in *T. brucei* and it is currently unclear how the trypanosome MCM complex is loaded onto the origins. Further, proteins which function as licensing factors in the parasite are not well understood. The observation that TbCdc45 is exported from the nucleus after S-phase suggests that TbCdc45 may have a licensing function in trypanosomes [208].

Intriguingly, there have not been any trypanosome protein kinases implicated in the control of DNA synthesis. Despite the presence of CDKs in the trypanosome [125], there is no evidence that a functional homolog of the S-phase CDK is present. Additionally, trypanosomes lack homologs to Dbf4 and DDK/Cdc7. How phosphorylation events may regulate assembly or activity of the CMG complex in trypanosomes remains an open question, especially given the fact that phosphorylated forms of TbMcm4 and TbMcm7 are detected in the trypanosome phosphoproteome [212, 213]. Intriguingly, phosphorylation of Mcm4 by DDK/Cdc7 in mammalian cells is required for DNA synthesis [214].

Duplication of trypanosome basal bodies

At the start of the trypanosome cell cycle two centriole-like structures, the mature basal body (mBB) and adjacent immature probasal body (pBB), exist and are

considered to be a single basal body (1mBB/1pBB) (Figures 1.5 and 1.7A) [19]. Before duplication occurs, the preexisting probasal body matures (2mBB) and becomes competent to: i) nucleate the axoneme of a daughter flagellum, and ii) direct assembly of a new probasal body (Figure 1.7A) [19]. Basal body maturation is associated with docking of the basal body to the plasma membrane via transition fibers (Figure 1.7A) [121], similar to other flagellated organisms (reviewed in [215]). Recruitment of TbRP2 (a retinitis pigmentosa homolog) to trypanosome transition fibers can be used as a marker for probasal body maturation; TbRP2 is detected by the antibody YL1/2 [64]. During basal body duplication, new probasal bodies are simultaneously assembled adjacent to both mature basal bodies (Figure 4A) (2mBB/2pBB) [19, 80, 136].

The newly matured basal body is initially detected anterior to the preexisting mature basal body [80]. Subsequently the new mBB/pBB pair migrates to the posterior side of the preexisting basal body; this movement is important in formation of the daughter flagellar pocket [80]. Basal body duplication occurs during the trypanosome S-phase, prior to kinetoplast division (Figures 1.5 and 1.7A) [133, 136]. Technical limitations have prevented synchronization of BSF trypanosomes in G1 [216, 217] and consequently experimental determination of a precise timeline of basal body duplication, with respect to the kinetoplast and nuclear S-phase, has not been obtainable. In Chapter 2 we use the small molecule AEE788 as a chemical tool to experimentally document the time-line of kDNA synthesis, nuclear DNA synthesis, basal body duplication, and kinetoplast division.

Biogenesis of the basal body or centriole can follow a templated or *de novo* assembly pathway (reviewed in [77]). In the templated pathway centrioles/basal bodies are assembled adjacent to a mature centriole/basal body (Figure 1.7B), while in the *de novo* pathway, they are assembled in the absence of a preexisting centriole/basal body. Trypanosomes appear to follow the templated pathway, however the capacity to form basal bodies *de novo* may exist, given the increasing evidence that many cells can execute both pathways [75, 218, 219]. In either case, the proteins required for centriole/basal body biogenesis are similar [220].

A signaling pathway involving polo-like kinase 4 (or its functional homolog Zyg-1 in *C. elegans* and SAK in *D. melanogaster*) is necessary to initiate assembly of nascent centrioles [221-224]. However, PLK4 is only conserved amongst holozoans [59] and the pathways responsible for initiation of centriole or basal body biogenesis in other organisms have not been well described. Centriole/basal body assembly in many eukaryotes begins with the formation of a cartwheel-like structure (Figure 1.7B) composed of SAS6 and BLD10/CEP135 (reviewed in [79, 225]). The cartwheel plays an important role in organization of 9-fold symmetry within the centriole [50] and for stabilizing the basal body against forces generated during ciliogenesis [226]. Nucleation of centriole/basal body microtubules (Figure 1.7B) is influenced by γ-tubulin [227, 228]. Loss of γ-tubulin can lead to aberrant centriole/basal body morphology [229]. Subsequently δ-tubulin, ε-tubulin, and SAS4/CPAP promote incorporation of triplet microtubules and centriole elongation (Figure 1.7B) [230-234]. In non-mammalian cells, it appears that SAS4 plays an earlier role in probasal body assembly [235, 236], suggesting that the protein may

have species-specific functions in centriole or basal body biogenesis. While many proteins have essential functions in centriole/basal body duplication (reviewed in [54, 76, 225]), SAS6, SAS4/CPAP, and BLD10/CEP135 have the highest degree of conservation across many organisms [59].

Centriole/basal body duplication is often coordinated with the cell division cycle and tightly regulated such that biogenesis of the organelle occurs once per cell division [237-239]. The availability of proteins required for centriole/basal body assembly limits the number of procentrioles/probasal bodies produced by single mother [240]. Consequently, overexpression of proteins such as PLK4 and SAS6 permit centriole/basal body amplification [221, 223, 224, 241]. Additionally, reduplication or centrioles is blocked by the proximity of the daughter centriole to the mother [242, 243]. In mammalian cells, PLK1-dependent maturation and distancing of the daughter centriole during G2/M allows the mother to form a new daughter centriole in the subsequent cell cycle [244-247]. Centriole overduplication correlates with genomic instability [248] and tumor formation in mammalian cells [249, 250].

SAS6 and BLD10 are conserved in trypanosomes, consistent with detection of cartwheel-like scaffolds at the base of trypanosome basal bodies (Figure 1.4) [55-57, 59]. The cartwheel is maintained at the basal body throughout trypanosome division [106]. Accordingly, SAS6 and BLD10 localize to both mature and immature basal bodies [56, 57]. Knockdown of either TbSAS6 or TbBLD10 disrupts probasal body assembly without disrupting maturation of the preexisting probasal body leading to the emergence of trypanosomes with two mature basal

bodies, each lacking an adjacent probasal body (2mBB/0pBB) [56, 57]. While these studies suggest a conserved function of cartwheel proteins in biogenesis of the trypanosome basal body, the upstream signaling pathways which initiate cartwheel assembly are unknown. Intriguingly, phosphorylation of TbSAS6 has been detected in-vivo [212]. Phosphorylation of SAS6 in *C. elegans* promotes procentriole assembly [251]. γ-tubulin is also conserved in *T. brucei* and localizes to the basal body where it functions in duplication of the organelle and nucleation of the central pair microtubules found in the flagellum [74]. Both δ-tubulin and ε-tubulin are present in the trypanosome genome. Loss of δ-tubulin, by genetic knockdown, causes defects in the assembly of triplet microtubules at the basal body [58]. Interestingly, while SAS4 is conserved in trypanosomes, studies in PCF *T. brucei* did not detect the protein at the basal body and demonstrated that it was not required for duplication of the organelle [60]. Additional trypanosome proteins which have been localized to the basal body and functionally characterized are described in Table 1.1.

Mechanisms that coordinate basal body duplication with the cell cycle in *T. brucei* differ from those described in other eukaryotes. For example, overexpression of TbSAS6 does not lead to basal body amplification [57] as reported in other eukaryotes [224, 241]. Furthermore, TbPLK1 is not required for probasal body maturation or assembly in trypanosomes [71]. Thus, mechanisms which regulate probasal body maturation and distancing from the mature basal body have not been identified. Importantly, overduplication of trypanosome basal bodies has been observed after genetic knockdown or overexpression of several

trypanosome basal body proteins (Table 1.1). These data imply that basal body copy number is normally regulated in the parasite. In Chapter 3 we propose that a protein kinase, TbCK1.2, plays an important role in this process.

In order to maintain the kinetoplast-basal body connection during cell division, the TAC (Chapter 1.4) must be remodeled such that each mBB/pBB is associated with a replicated kDNA network [20]. During kDNA synthesis and basal body duplication, ultrastructural studies using electron microscopy suggest that the TAC remains intact [20, 80], though unilateral filaments are only observed proximal to the mature basal body [20]. Strikingly, two proteins detected at unilateral filaments are recruited to the TAC only after probasal body maturation [100, 101]. Further characterization of TAC composition is necessary to gain a better understanding of its biological functions and dynamics during trypanosome division.

Relationship between kinetoplast division and basal body separation

After basal body duplication, the two mBB/pBB pairs migrate away from each other towards the kinetoplast poles [252]. Scission of the kDNA network occurs prior to division of the single-copy mitochondrion (Figure 1.5) [81]. Once the kinetoplast has completed division, the kinetoplast-basal body complexes separate [19] in preparation for cytokinesis when they are segregated into daughter cells. The apparent coincidence of kinetoplast division and basal body separation led researchers to hypothesize that the events were linked. This theory of interdependence was further supported by two observations: i) identification of the TAC, which physically tethers the kinetoplast with the basal body [20] and ii)

demonstration that a microtubule-depolymerizing agent, ansamitocin, inhibited both basal body separation and kinetoplast division [21]. Hence, the idea that basal body separation drives kinetoplast division remains the prevailing dogma in the field [86, 87]. The TAC would consequently play a fundamental role in basal body-mediated kinetoplast division. Consistent with this idea, knockdown of TAC-associated proteins results in asymmetric kinetoplast division [98-102]. Additionally, defects in kinetoplast division are frequently associated with impaired basal body duplication/segregation (Table 1.1).

However, it was also demonstrated that small molecule inhibitors of topoisomerase II blocked kinetoplast division, but had no effect on basal body separation [21]. This data can be used to argue that basal body movements alone are not sufficient to drive kinetoplast scission. This hypothesis is consistent with the complexity of the interlocked kDNA network which is unlikely to be broken by a mechanical force. Rather, topoisomerase II decatenation activity is likely to be involved [86, 87, 157, 159], consistent with effects observed by treating *T. brucei* with topoisomerase II inhibitors [21]. In Chapter 3 we present genetic data demonstrating that basal body separation is not sufficient to cause division of the kinetoplast and propose a new hypothesis in which TbCK1.2 regulates activity of proteins that are biochemically competent to resolve the interlocked kDNA network.

Failure of the kinetoplast to divide does not prevent mitosis as evidenced by the production of trypanosomes with a single kinetoplast and two nuclei (1K2N) following genetic perturbations [7, 42, 56]. Cytokinesis often fails in 1K2N cells

which can result in the emergence of multinucleated trypanosomes (1KxN) [14, 42, 56]; thus kinetoplast division and cytokinesis may be linked [253]. Protein kinases and protein phosphatases have both been implicated in the control of kDNA network division [7, 14].

Progression from G2 through mitosis

The second gap phase, G2, allows cells to prepare for mitosis during which replicated nuclear chromosomes will be segregated. Mitotic entry in many eukaryotes, including humans [254] and yeast [255, 256], is regulated by a mitotic cyclin-CDK complex (reviewed in [139, 257]). In trypanosomes, the transition between G2 and mitosis is governed by TbCRK3 and TbCYC6 [6, 258, 259]. Genetic knockdown of either proteins in PCF or BSF trypanosomes inhibits mitosis [6, 258, 259]. In BSF parasites this results in an increase in the number of 2K1N trypanosomes [6, 258]. Surprisingly, inhibition of mitosis did not prevent cytokinesis in PCF parasites resulting in cell division of 2K1N trypanosomes and the production of anucleate daughter cells, or zoids (1K0N), and 1K1N cells with fully replicated nuclear chromosomes [6, 258].

The nuclear genome of *T. brucei*, (reviewed in [260]) is comprised of three types of linear chromosomes: 11 pairs of megabase chromosomes (1-6 Mb), 3-5 intermediate chromosomes (200-500 kb), and approximately 100 minichromosomes (50-150 bp), which serve as VSG reservoir [261]. Segregation of megabase chromosomes and minichromosomes is mediated by a microtubule-based bipolar mitotic spindle [262], while the mechanisms that regulate intermediate chromosomes separation are unclear. Trypanosomes undergo

closed mitosis (nuclear envelope remains intact) and the mitotic spindle is assembled within the nucleus [263]. Thus, basal bodies, which remain at the flagellar pocket throughout the cell cycle, do not promote spindle assembly. Instead, spindle microtubules originate from electron-dense structures localized to opposite poles of the nuclear envelope [263].

Mitochondrial dynamics during the trypanosome division cycle

Mitochondrial network growth is associated with the formation of individual mitochondrial loops and branches (Figure 1.5) [81]. Mitochondrial growth peaks between G2 and cytokinesis (2K1N and 2K2N trypanosomes) [81] with the number of secondary structures increasing after division of the kinetoplast (2K1N). In post-mitotic cells (2K2N) a large mitochondrial complex can be detected (Figure 1.5) [81]; while two discrete mitochondria are not apparent at this time, the main branch of the daughter mitochondrion can be distinguished opposite the main tubule of the pre-existing mitochondrion (Figure 1.5) [81]. (Figure 1.5) The daughter kinetoplast is repositioned into the principal branch of the new mitochondrion just before cytokinesis and mitochondrial segregation [81].

Cytokinesis in T. brucei

Cytokinesis is the process that physically divides the cytoplasm of a duplicated cell to generate two daughters. In animals and yeast this process involves selection of a division plane, assembly of an actomyosin contractile ring, followed by its constriction and disassembly, and remodeling of the plasma membrane (reviewed in [264-266]). Trypanosomatids lack myosin II and actin is not essential in PCF

cells, nor does it appear essential for cytokinesis in BSF trypanosomes [41]. Accordingly, cytokinesis in *T. brucei* does not depend on an actomyosin ring.

Cytokinesis in trypanosomes is initiated at the anterior end of the cell and proceeds to the posterior end along the longitudinal cell axis between the mother and daughter flagella (reviewed in [126, 267]). The point of furrow ingression is determined by the anterior tip of the daughter FAZ [252, 268]. Consequently, defects in elongation of the new flagellum or FAZ can lead to misplacement of the cleavage furrow resulting in the formation of smaller daughter cells [69, 119, 252].

Several trypanosome signaling pathways play important roles in regulating cytokinesis. An Aurora kinase B homolog, TbAUK1, forms the chromosomal passenger complex (TbCPC) which is essential for initiation of cytokinesis [269]. Genetic knockdown of TbPLK disrupts cytokinesis [71, 72, 270], but also inhibits basal body separation [71, 270], kinetoplast division [72], and FAZ assembly [71] making it difficult to discern whether TbPLK1 directly regulates cytokinesis as in other eukaryotes [271, 272]. Knockdown of TbRHP (a Rho-like GTPase) and its associated GAP (GTPase-activating protein), TbORCL, cause defects in spindle assembly and cytokinesis [273].

1.6 Transferrin Endocytosis

Endocytosis facilitates internalization of membrane proteins and lipids, as well as extracellular nutrients (reviewed in [274, 275]). Endocytic ligands can be internalized through receptor-mediated pathways or taken up by fluid phase endocytosis (reviewed in [274, 275]). Internalization of iron is an important physiological process, necessary for the activity of iron-dependent enzymes

(reviewed in [276]). Transferrin is an iron-binding protein that facilitates iron transport into mammalian cells [277]. In most cases transferrin endocytosis is mediated through a transferrin receptor at the plasma membrane [276]. Iron-transferrin interactions are susceptible to low pH which allows release of iron, from transferrin, in acidic endosomal compartments [278, 279]. Following the release of iron, 85% to 95% of transferrin-transferrin receptor complexes are recycled back to the membrane while the remaining complexes are trafficked to the lysosome for degradation [280].

Clathrin-mediated endocytosis (CME) is the major pathway used for internalization of the transferrin receptor [281]. CME involves the recruitment of clathrin to the plasma membrane where it assembles into a curved lattice structure [282]. Studies in humans and yeast suggest that nucleation of clathrin-coated pits is initiated at specific sites on the plasma membrane where proteins have caused the membrane to become slightly curved [283, 284]. Subsequently these nucleation proteins are thought to recruit adapter protein complexes [284] which integrate cargo selection with clathrin recruitment (reviewed in [285]).

CME is most frequently associated with the AP-2 adaptor complex [286]. Endocytosis of the transferrin receptor in mammalian cells is influenced by its interaction with AP-2 [287, 288]. Accessory proteins like epsins, BAR domain-containing proteins, and actin, are important for curvature of the membrane during invagination of clathrin-coated pits (reviewed in [274, 275]). The neck of the budding endocytic vesicle is severed from the membrane by a GTPase, dynamin [289]. Transferrin endocytosis can be regulated by Src tyrosine kinases [290].

Trypanosomes require iron for proliferation [291, 292]. *T. brucei* expresses a divergent transferrin receptor that can bind and internalize transferrin from the host [293, 294]. The transferrin receptor is a heterodimer of ESAG-6 and ESAG-7 gene products which are anchored to the plasma membrane by a glycosylphosphatidylinositol (GPI) anchor [294]. After binding of transferrin, the transferrin receptor is internalized, iron is released in acidic endosomes, the transferrin receptor is recycled to the plasma membrane, and transferrin is delivered to the lysosome [295].

CME in trypanosomes depends on clathrin [40], an epsin-related protein [296], and actin [41], similar to mammalian cells. The role of the trypanosome dynamin homolog (TbDLP) in endocytosis has been controversial; one study found that knockdown TbDLP inhibited mitochondrial fission, cytokinesis, and endocytosis [297], while a second study reported that mitochondrial fission was disrupted but endocytic pathways were not [298]. Trypanosomes lack the AP-2 adaptor complex, one of the major components of the CME pathway in other organisms. Consequently, the control of cargo selection and clathrin recruitment during formation of endocytic vesicles has not been characterized. A recent study identified clathrin-interacting proteins (TbCAPs) and found eight proteins that are restricted to trypanosomatids [299], suggesting that unique regulatory mechanisms govern endocytic pathways in *T. brucei*. Inhibitors of serine/threonine and tyrosine kinases block transferrin endocytosis in trypanosomes [5, 16], implying that the pathway is regulated by phospho-signaling events. Recently

trypanosome glycogen synthase kinase 3 (TbGSK3) has been implicated in the control of transferrin endocytosis [300].

1.7 Functions of casein kinase 1 in *T. brucei* and other eukaryotes

Members of the casein kinase 1 (CK1) family belong to the serine/threonine protein kinase superfamily, but have also been shown to phosphorylate tyrosine residues [301, 302]. Seven mammalian CK1 isoforms have been identified: CK1 α, CK1β (found only in cows), CK1δ, CK1ε, CK1γ 1-3. The N-terminal catalytic domain is highly conserved across all isoforms which differ in regards to their C-terminal and N-terminal extensions (reviewed in [303-305]). CK1 family members are ubiquitously expressed and their activity does not depend on phosphorylation of an activation loop [306].

Trypanosomes possess four casein kinase 1 isoforms [3], of which TbCK1.1 and TbCK1.2 are the best characterized [307]. TbCK1.1 and TbCK1.2 are most similar, at the protein sequence level, to CK1 δ/ε (70% sequence similarity). Of the two, only TbCK1.2 is essential for trypanosome proliferation [307]. Genetic knockdown of TbCK1.2 disrupts cell cycle progression [7, 307]. We have been particularly interested in the role of TbCK1.2 in kinetoplast division; knockdown of the protein inhibited scission of the kinetoplast producing trypanosomes with a single kinetoplast and two nuclei (1K2N) [7]. There are several instances in the literature in which defects in kinetoplast division correlate with genetic perturbation of basal body proteins (Table 1.1). Intriguingly, CK1 δ/ε have been localized to microtubule-organizing centers (MTOCs) in yeast and mammalian cell lines [308-314]. Taken together these data could suggest that TbCK1.2 influences kinetoplast

division by controlling trypanosome basal bodies; a hypothesis which is addressed in Chapter 3.

Microtubule dynamics influence segregation of the mitochondrial genome (kinetoplast) [21, 136]. Thus, in other eukaryotes, the function of CK1 δ/ε in chromosome segregation [315-319] and microtubule dynamics [313, 314, 320] could have parallels with the function of TbCK1.2 in kinetoplast division. Genetic or chemical inhibition of CK1 δ/ε in mammalian cells is associated with defects in spindle assembly and centrosome amplification [248, 309, 310]. In yeast the CK1δ homolog, Hrr25, associates with the γ-tubulin small complex at the spindle pole body (yeast MTOC) to regulate nucleation of cytoplasmic microtubules and positioning of the mitotic spindle [321]. CK1δ regulates microtubule dynamics through phosphorylation of tubulin and microtubule associated proteins (MAPs) in response to DNA damage [308]. Additionally CK1δ promotes centrosome repositioning in T cells through phosphorylation of EB1 [314], a plus-end binding MAP. In Chapter 3 we characterize the role of TbCK1.2 in controlling kinetoplast division and basal body copy number.

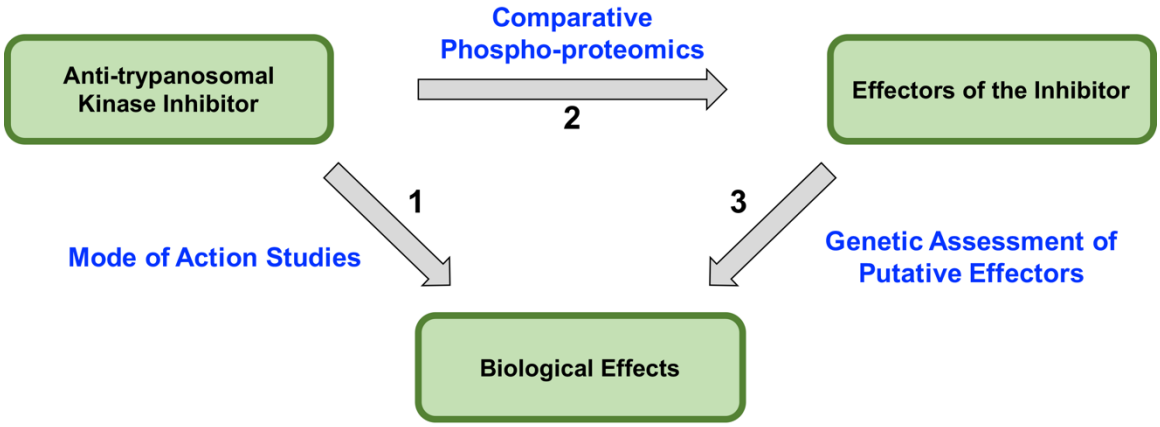

Figure 1.1 *Discovery chemical biology approach for the identification of phospho-protein effectors of antitrypanosomal inhibitors***.** Schematic of an unbiased "discovery chemical biology" approach which links uncharacterized phospho-proteins to specific biological pathways disrupted by anti-trypanosomal drugs. In this strategy, phenotypic assays are used to determine biological pathways disrupted by an inhibitor (arrow 1). Comparative phospho-proteomics can then be employed to identify proteins with altered phosphorylation following exposure to the inhibitor (arrow 2). We hypothesize that these proteins (effectors) function in biological pathways disrupted by the drug. This hypothesis can be tested by determining if genetic knockdown or overexpression of putative effectors has similar biological effects as treatment of *T. brucei* with the inhibitor (arrow 3).

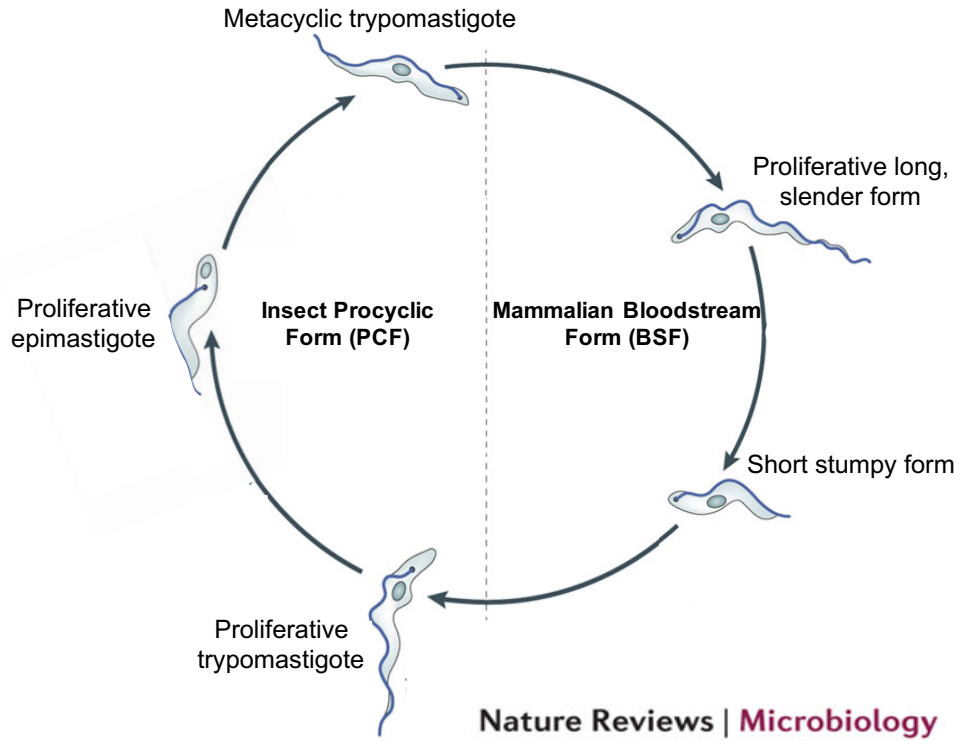

Figure 1.2 *The life cycle of Trypanosome brucei*. Developmental stages of the African trypanosome cycle between the insect vector and mammalian host (modified from [322]). Two distinct forms of the bloodstream parasite (BSF) can be identified from infected mammals: the long, slender form which proliferates in the blood or fluid of the central nervous system and the cell cycle-arrested short, stumpy form which can be taken up by the Tsetse fly (insect vector). Inside the midgut of the Tsetse fly, trypanosomes transition into proliferative procyclic form (PCF) trypomastigotes. PCF trypomastigotes subsequently transition into proliferative epimastigotes which migrate from the insect midgut to the salivary glands. In the salivary glands, epimastigotes become cell cycle-arrested and differentiate into metacyclic trypomastigotes which are injected into the mammalian host during the bite of a Tsetse fly.

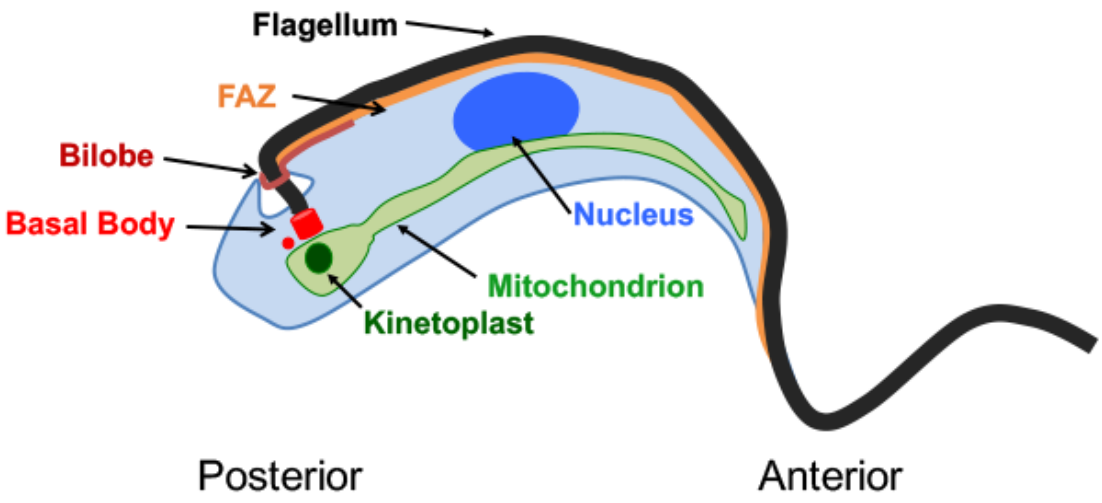

Figure 1.3 *Organization of the trypanosome basal body and associated structures*. The trypanosome basal body is found at the posterior end of the cell and consists of a mature basal body (mBB) and an adjacent immature probasal body (pBB). The mature basal body nucleates the axoneme of the flagellum which exits the cell body at the flagellar pocket (FP) [121]. Outside of the cell, the flagellum remains attached to the plasma membrane for the length of the parasite. The flagellar attachment zone (FAZ) mediates contact between the flagellum and plasma membrane [113]. The trypanosome bilobe is a cytoskeletal structure proximal to the flagellum and neck of the flagellar pocket [122, 123]. It has a hook-like structure with the posterior end curving around the neck of the flagellar pocket, while the anterior portion is found parallel to the FAZ [122, 123]. The kinetoplast, a nucleoid which contains the mitochondrial genome (kDNA), is found within the single-copy mitochondrion below the cytoplasmic basal body [86]. The nucleus is found in the mid-region of the trypanosome.

Figure 1.4 *Schematic of the "tripartite attachment complex" (TAC), basal body, and associated structures* (modeled after [322]). "Unilateral filaments" connect the inner mitochondrial membrane to the kinetoplast [20]. "Exclusion zone filaments" link the proximal end of the basal body to the outer mitochondrial membrane [20]. The distal end of the mature basal body is anchored to the flagellar pocket (FP) by transition fibers [106]. Cross sections of the proximal region of the basal body (BB), transition zone (TZ), and flagellar axoneme (Ax) depict microtubule organization of each structure. Both the mature basal body and adjacent probasal body are composed of nine triplet microtubules (9+3) organized around a cartwheel-like structure [106]. A- and B-microtubules extend from the mature basal body to a basal plate (BP) from which central pair microtubules of the flagellum are nucleated [106]. The TZ is characterized by nine doublet microtubules which lack central pair microtubules (9+2+0) that are present in the flagellar axoneme (9+2+2) [106]. After exiting the cell, the flagellum is associated with the paraflagellar rod (PFR), both of which remain attached to the cell body [112] via the flagellar attachment zone (FAZ) [113].

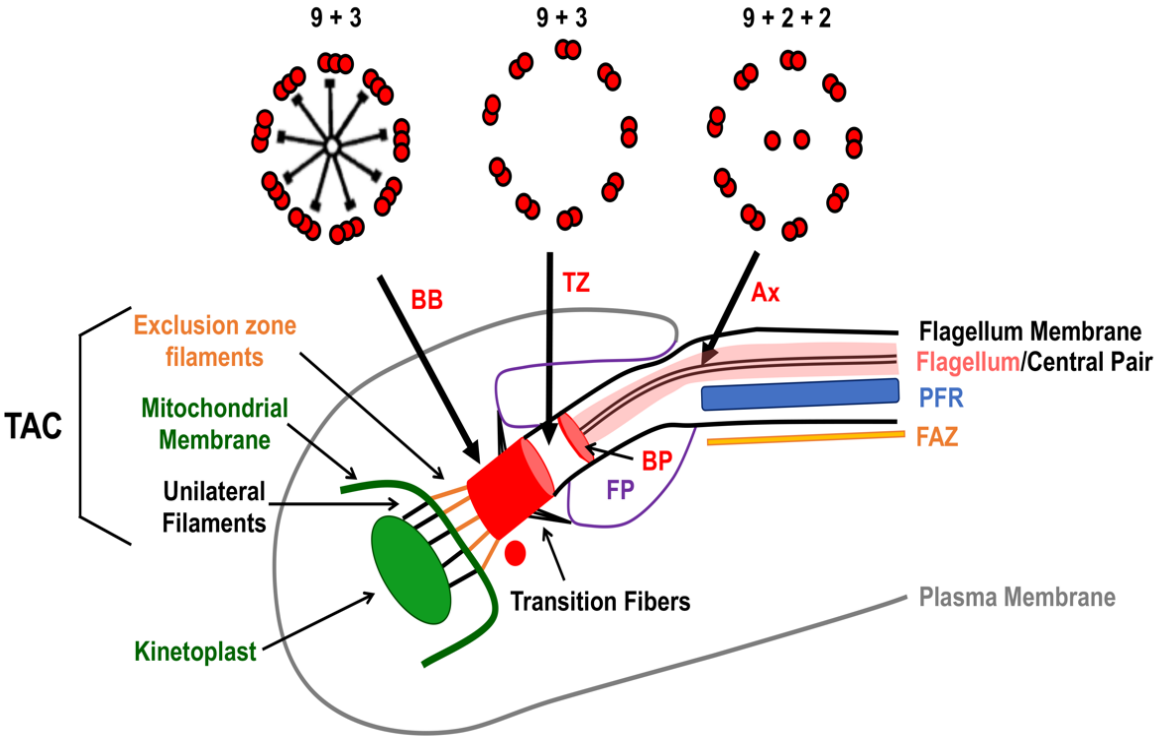
9 + 3
9 + 3
9 + 2 + 2
BB
TZ
Ax
Exclusion zone filaments
Mitochondrial Membrane
Unilateral Filaments
TAC
Flagellum Membrane
Flagellum/Central Pair
PFR
FAZ
BP
FP
Transition Fibers
Plasma Membrane
Kinetoplast

Figure 1.5 *Cell Division Cycle of BSF trypanosomes*. *T. brucei* in G1 have a single kinetoplast (K), nucleus (N), and basal body (mature (mBB) and probasal body (pBB)) (1K1N 1BB). In S-phase, kDNA synthesis results in elongation of the kDNA network (Ke) [136]. The probasal body matures and two new probasal bodies are formed (2mBB/2pBB) (1Ke1N 2BB) [19]. The newly matured basal body nucleates a daughter flagellum which associates with a new flagellar attachment zone (FAZ). Mitochondrial branches extend from the main tubule of 1Ke1N trypanosomes [81] and duplication of the bilobe and flagellar pocket (FP) occurs. Nuclear DNA replication is detectable in 1Ke1N cells [137]. Prior to mitosis, the kinetoplast divides, coincident with basal body separation (2K1N 2BB). Division of the nuclear genome occurs during mitosis (2K2N 2BB). Post-mitotic trypanosomes have an extended mitochondrial network which segregates during cytokinesis. Cytokinesis starts at the anterior end of the cell forming a cleavage furrow (CF) between the two flagella, and proceeds towards the posterior forming two 1K1N 1BB daughter cells.

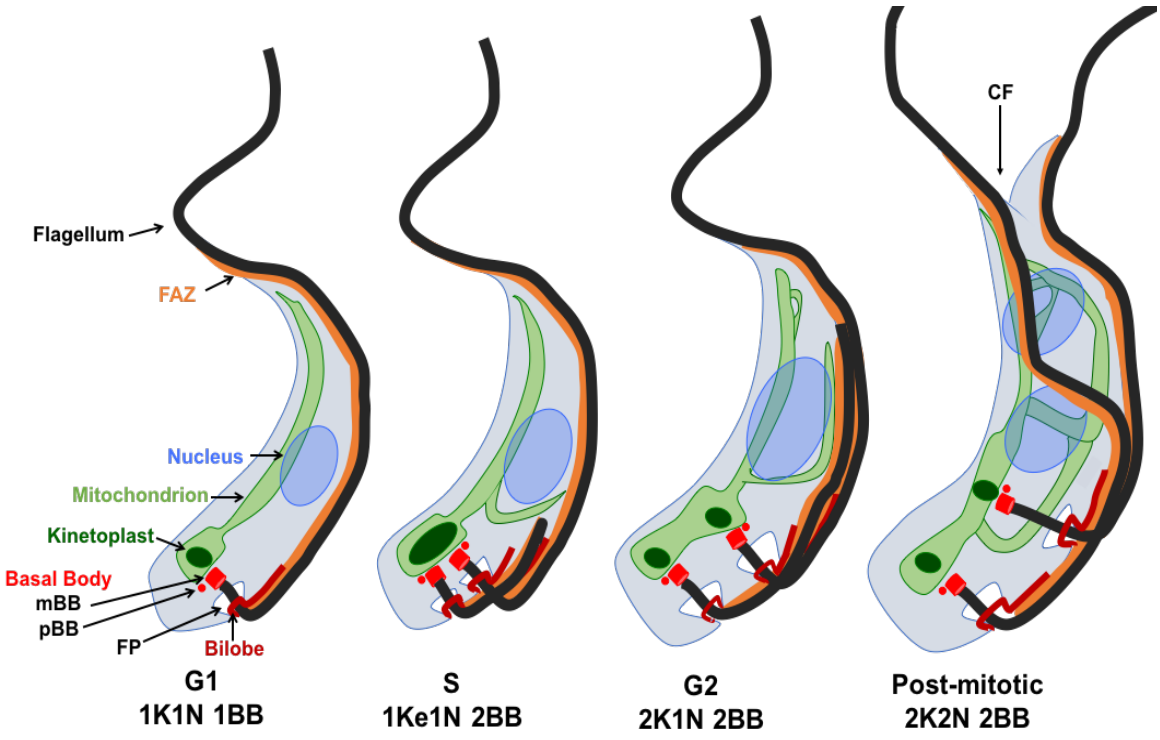
Flagellum
FAZ
Nucleus
Mitochondrion
Kinetoplast
Basal Body
mBB
pBB
FP
Bilobe
CF
G1
1K1N 1BB
S
1Ke1N 2BB
G2
2K1N 2BB
Post-mitotic
2K2N 2BB

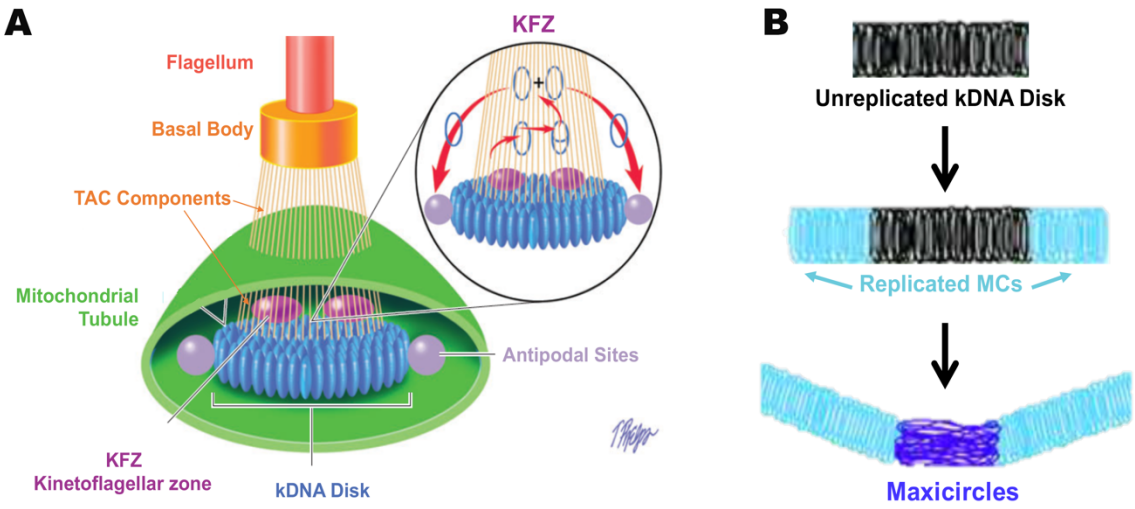

Figure 1.6 *Current model of kinetoplast DNA (kDNA) replication*. ***(A)*** Diagram of minicircle DNA synthesis (adapted from [87]). Minicircles are enzymatically released from the catenated kDNA network. Free minicircles are replicated through theta intermediates in the kinetoflagellar zone (KFZ). Replicated minicircles are reattached at the poles of the kDNA network near antipodal sites (assembly of replicative proteins). At the antipodal sites nicks and gaps in the minicircle are repaired prior to network reattachment. **(B)** Organization of minicircles and maxicircles during kDNA replication (modified from [157]). Release of unreplicated minicircles and reattachment, following replication, at the kinetoplast poles is thought to separate the replicated minicircle network. Because maxicircles are synthesized within the kDNA network, it is believed that they would link the minicircle networks. Thus, at a later stage of kinetoplast division, decatenation activity of a topoisomerase is thought to be required to biochemically resolve the kDNA network.

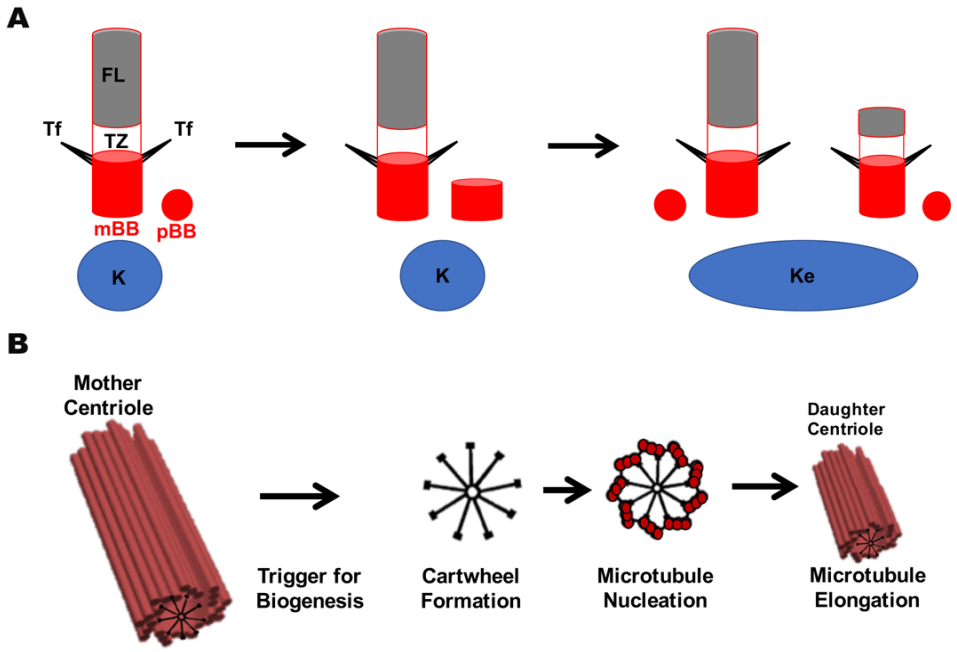

Figure 1.7 *Basal body duplication*. ***(A)*** Duplication of trypanosome basal bodies in the context of kinetoplast DNA (kDNA) network elongation. At the beginning of the cell cycle a basal body is associated with a single kinetoplast (K) through the tripartite attachment complex (not shown). The mature basal body (mBB) is anchored to the plasma membrane by transition fibers (Tf) and is tethered to a transition zone (TZ) which gives rise to the flagellum (FL). During the G1/S transition the probasal body (pBB) begins to elongate [19]. In S-phase the probasal body matures and can direct assembly of a new TZ and FL, as well as assembly of a new probasal body. Assembly of new probasal bodies occurs simultaneously and correlates with kinetoplast elongation (Ke) [19, 136]. ***(B)*** Major events of centriole/basal body biogenesis in organisms that form a cartwheel (modified from [323]). A signaling event triggers assembly of the daughter centriole/basal body resulting in the formation of a cartwheel-like structure with 9-fold symmetry. Centriole/basal body microtubules are nucleated at the cartwheel and elongate to form the daughter centriole/basal body.

Table 1.1 Trypanosome basal body proteins which are important for biogenesis of the organelle. Proteins which have been experimentally localized to the trypanosome basal body, and implicated in regulation of the organelle through genetic studies, are shown. The developmental stage used for genetic studies is indicated (PCF = procyclic form; BSF = bloodstream form). Defects associated with basal body biogenesis, as well as kinetoplast division (kDiv), are indicated (N/A = effect on kinetoplast division not reported).

Protein	Genetic Perturbation	Basal Body Phenotype	Defective kDiv	Ref
TbCen1	PCF knockdown	Inhibits probasal body maturation and assembly	Yes	63
TbCen2	PCF knockdown	Inhibits probasal body maturation and assembly	Yes	63
TbBLD10	PCF knockdown	Inhibits probasal body assembly	Yes	57
TbSAS6	PCF knockdown	Inhibits probasal body assembly	Yes	58
TbBBP65	PCF knockdown	Inhibits probasal body assembly	Yes	57
TbPOC11	PCF knockdown	Inhibits probasal body assembly	Yes	57
TbCen4	PCF knockdown	Results in overduplication	No	74
TbBBP46	PCF knockdown	Results in overduplication	Yes	57
TbCEP57	PCF knockdown	Results in overduplication	Yes	57
TbLRTP1	PCF knockdown	Results in overduplication	Yes	64
TbPLK1	PCF knockdown	Inhibits basal body separation	Yes	72; 271
TbSPBB1	PCF knockdown	Inhibits basal body segregation	Yes	66
TbCC2D	PCF knockdown	Inhibits basal body segregation	Yes	70
TbKMP-11	PCF knockdown	Inhibits basal body segregation	Yes	42
TbKMP-11	BSF knockdown	Inhibits basal body segregation	Yes	42
Tb*γ*-tubulin	PCF knockdown	Loss of triplet microtubules	N/A	75
Tbδ-tubulin	PCF knockdown	Loss of triplet microtubules	N/A	59
TbTBCCD1	PCF knockdown	Detection of basal bodies distant from a kinetoplast	Yes	67
TbSAS6	PCF overexpression	Inhibits probasal body assembly	Yes	58
TbNRKC	PCF overexpression	Results in overduplication	Yes	10
TbLRTP1	PCF overexpression	Inhibits probasal body maturation and assembly	Yes	64

1.8 References

1. Taylor, S.S. and A.P. Kornev, *Protein kinases: evolution of dynamic regulatory proteins.* Trends Biochem Sci, 2011. **36**(2): p. 65-77.

2. Shchemelinin, I., L. Sefc, and E. Necas, *Protein kinases, their function and implication in cancer and other diseases.* Folia Biol (Praha), 2006. **52**(3): p. 81-100.

3. Parsons, M., et al., *Comparative analysis of the kinomes of three pathogenic trypanosomatids: Leishmania major, Trypanosoma brucei and Trypanosoma cruzi.* BMC Genomics, 2005. **6**: p. 127.

4. Guyett, P.J., et al., *Glycogen Synthase Kinase 3β Promotes the Endocytosis of Transferrin in the African Trypanosome.* ACS Infectious Diseases, 2016. **2**(7): p. 518-528.

5. Subramanya, S. and K. Mensa-Wilmot, *Diacylglycerol-stimulated endocytosis of transferrin in trypanosomatids is dependent on tyrosine kinase activity.* PLoS One, 2010. **5**(1): p. e8538.

6. Tu, X. and C.C. Wang, *The involvement of two cdc2-related kinases (CRKs) in Trypanosoma brucei cell cycle regulation and the distinctive stage-specific phenotypes caused by CRK3 depletion.* J Biol Chem, 2004. **279**(19): p. 20519-28.

7. Jones, N.G., et al., *Regulators of Trypanosoma brucei Cell Cycle Progression and Differentiation Identified Using a Kinome-Wide RNAi Screen.* PLoS Pathog, 2014. **10**(1): p. e1003886.

8. Ma, J., et al., *Nuclear DBF-2-related kinases are essential regulators of cytokinesis in bloodstream stage Trypanosoma brucei.* J Biol Chem, 2010. **285**(20): p. 15356-68.

9. de Graffenried, C.L., H.H. Ho, and G. Warren, *Polo-like kinase is required for Golgi and bilobe biogenesis in Trypanosoma brucei.* J Cell Biol, 2008. **181**(3): p. 431-8.

10. Pradel, L.C., et al., *NIMA-related kinase TbNRKC is involved in basal body separation in Trypanosoma brucei.* J Cell Sci, 2006. **119**(Pt 9): p. 1852-63.

11. Tu, X. and C.C. Wang, *Pairwise knockdowns of cdc2-related kinases (CRKs) in Trypanosoma brucei identified the CRKs for G1/S and G2/M transitions and demonstrated distinctive cytokinetic regulations between*

two developmental stages of the organism. Eukaryot Cell, 2005. **4**(4): p. 755-64.

12. Li, Z., S. Gourguechon, and C.C. Wang, *Tousled-like kinase in a microbial eukaryote regulates spindle assembly and S-phase progression by interacting with Aurora kinase and chromatin assembly factors.* J Cell Sci, 2007. **120**(Pt 21): p. 3883-94.

13. Gourguechon, S. and C.C. Wang, *CRK9 contributes to regulation of mitosis and cytokinesis in the procyclic form of Trypanosoma brucei.* BMC Cell Biol, 2009. **10**: p. 68.

14. Rothberg, K.G., et al., *Identification of a protein phosphatase 2A family member that regulates cell cycle progression in Trypanosoma brucei.* Mol Biochem Parasitol, 2014. **194**(1-2): p. 48-52.

15. Li, Z., T. Umeyama, and C.C. Wang, *The chromosomal passenger complex and a mitotic kinesin interact with the Tousled-like kinase in trypanosomes to regulate mitosis and cytokinesis.* PLoS One, 2008. **3**(11): p. e3814.

16. Guyett, P.J., et al., *Novel Effects of Lapatinib Revealed in the African Trypanosome by Using Hypothesis-Generating Proteomics and Chemical Biology Strategies.* Antimicrob Agents Chemother, 2017. **61**(2).

17. Cavalier-Smith, T., *Kingdoms Protozoa and Chromista and the eozoan root of the eukaryotic tree.* Biol Lett, 2010. **6**(3): p. 342-5.

18. Berriman, M., et al., *The genome of the African trypanosome Trypanosoma brucei.* Science, 2005. **309**(5733): p. 416-22.

19. Sherwin, T. and K. Gull, *The cell division cycle of Trypanosoma brucei brucei: timing of event markers and cytoskeletal modulations.* Philos Trans R Soc Lond B Biol Sci, 1989. **323**(1218): p. 573-88.

20. Ogbadoyi, E.O., D.R. Robinson, and K. Gull, *A high-order trans-membrane structural linkage is responsible for mitochondrial genome positioning and segregation by flagellar basal bodies in trypanosomes.* Mol Biol Cell, 2003. **14**(5): p. 1769-79.

21. Robinson, D.R. and K. Gull, *Basal body movements as a mechanism for mitochondrial genome segregation in the trypanosome cell cycle.* Nature, 1991. **352**(6337): p. 731-3.

22. World Health, O. *Human African trypanosomiasis*. Epidemiological situation 2016 11-08-2016 [cited 2017 2-24]; Available from: http://www.who.int/trypanosomiasis_african/country/en/.

23. CDC. *Parasites-African Trypanosomiassis (also known as Sleeping Sickness)*. Disease 8-29-2012 [cited 2017 2-24]; Available from: https://www.cdc.gov/parasites/sleepingsickness/disease.html.

24. World Health, O. *Global Health Observatory (GHO) data*. Human African trypanosomiasis: Situation and Trends 9-23-2016 [cited 2017 2-24]; Available from: http://www.who.int/gho/neglected_diseases/human_african_trypanosomiasis/en/.

25. Cross, G.A., *Cellular and genetic aspects of antigenic variation in trypanosomes.* Annu Rev Immunol, 1990. **8**: p. 83-110.

26. La Greca, F. and S. Magez, *Vaccination against trypanosomiasis: can it be done or is the trypanosome truly the ultimate immune destroyer and escape artist?* Hum Vaccin, 2011. **7**(11): p. 1225-33.

27. McCulloch, R., *Antigenic variation in African trypanosomes: monitoring progress.* Trends Parasitol, 2004. **20**(3): p. 117-21.

28. Brun, R., et al., *Human African trypanosomiasis.* Lancet, 2010. **375**(9709): p. 148-59.

29. Babokhov, P., et al., *A current analysis of chemotherapy strategies for the treatment of human African trypanosomiasis.* Pathog Glob Health, 2013. **107**(5): p. 242-52.

30. Matthews, K.R., J.R. Ellis, and A. Paterou, *Molecular regulation of the life cycle of African trypanosomes.* Trends Parasitol, 2004. **20**(1): p. 40-7.

31. Vickerman, K., *Developmental Cycles and Biology of Pathogenic Trypanosomes.* British Medical Bulletin, 1985. **41**(2): p. 10.

32. Brun, R., et al., *A quantitative ultrastructural study on the transformation of Trypanosoma brucei metacyclic to bloodstream forms in vitro.* Acta Trop, 1984. **41**(2): p. 117-29.

33. Matthews, K.R., T. Sherwin, and K. Gull, *Mitochondrial genome repositioning during the differentiation of the African trypanosome between life cycle forms is microtubule mediated.* J Cell Sci, 1995. **108 (Pt 6)**: p. 2231-9.

34. Seed, J.R., *Antigenic Similarity among Culture Forms of the 'Brucei' Group of Trypanosomes.* Parasitology, 1964. **54**: p. 593-6.

35. Overath, P., et al., *Repression of glycoprotein synthesis and release of surface coat during transformation of Trypanosoma brucei.* EMBO J, 1983. **2**(10): p. 1721-8.

36. Cross, G.A., *Identification, purification and properties of clone-specific glycoprotein antigens constituting the surface coat of Trypanosoma brucei.* Parasitology, 1975. **71**(3): p. 393-417.

37. Shapiro, S.Z., et al., *Analysis by flow cytometry of DNA synthesis during the life cycle of African trypanosomes.* Acta Trop, 1984. **41**(4): p. 313-23.

38. Matthews, K.R. and K. Gull, *Evidence for an interplay between cell cycle progression and the initiation of differentiation between life cycle forms of African trypanosomes.* J Cell Biol, 1994. **125**(5): p. 1147-56.

39. Brown, R.C., D.A. Evans, and K. Vickerman, *Changes in oxidative metabolism and ultrastructure accompanying differentiation of the mitochondrion in Trypanosoma brucei.* Int J Parasitol, 1973. **3**(5): p. 691-704.

40. Allen, C.L., D. Goulding, and M.C. Field, *Clathrin-mediated endocytosis is essential in Trypanosoma brucei.* EMBO J, 2003. **22**(19): p. 4991-5002.

41. Garcia-Salcedo, J.A., et al., *A differential role for actin during the life cycle of Trypanosoma brucei.* EMBO J, 2004. **23**(4): p. 780-9.

42. Li, Z. and C.C. Wang, *KMP-11, a basal body and flagellar protein, is required for cell division in Trypanosoma brucei.* Eukaryot Cell, 2008. **7**(11): p. 1941-50.

43. Bonhivers, M., et al., *Biogenesis of the trypanosome endo-exocytotic organelle is cytoskeleton mediated.* PLoS Biol, 2008. **6**(5): p. e105.

44. Tu, X., et al., *Distinct cytoskeletal modulation and regulation of G1-S transition in the two life stages of Trypanosoma brucei.* J Cell Sci, 2005. **118**(Pt 19): p. 4353-64.

45. Sunter, J.D., et al., *Modulation of flagellum attachment zone protein FLAM3 and regulation of the cell shape in Trypanosoma brucei life cycle transitions.* J Cell Sci, 2015. **128**(16): p. 3117-30.

46. Sherwin, T., et al., *Distinct localization and cell cycle dependence of COOH terminally tyrosinolated alpha-tubulin in the microtubules of Trypanosoma brucei brucei.* J Cell Biol, 1987. **104**(3): p. 439-46.

47. Kohl, L. and K. Gull, *Molecular architecture of the trypanosome cytoskeleton.* Mol Biochem Parasitol, 1998. **93**(1): p. 1-9.

48. Ngo, H., et al., *Double-stranded RNA induces mRNA degradation in Trypanosoma brucei.* Proc Natl Acad Sci U S A, 1998. **95**(25): p. 14687-92.

49. Gibbons, I.R. and A.V. Grimstone, *On flagellar structure in certain flagellates.* J Biophys Biochem Cytol, 1960. **7**: p. 697-716.

50. Nakazawa, Y., et al., *SAS-6 is a cartwheel protein that establishes the 9-fold symmetry of the centriole.* Curr Biol, 2007. **17**(24): p. 2169-74.

51. Kitagawa, D., et al., *Structural basis of the 9-fold symmetry of centrioles.* Cell, 2011. **144**(3): p. 364-75.

52. van Breugel, M., et al., *Structures of SAS-6 suggest its organization in centrioles.* Science, 2011. **331**(6021): p. 1196-9.

53. Leidel, S., et al., *SAS-6 defines a protein family required for centrosome duplication in C. elegans and in human cells.* Nat Cell Biol, 2005. **7**(2): p. 115-25.

54. Azimzadeh, J. and W.F. Marshall, *Building the centriole.* Curr Biol, 2010. **20**(18): p. R816-25.

55. Hodges, M.E., et al., *Reconstructing the evolutionary history of the centriole from protein components.* J Cell Sci, 2010. **123**(Pt 9): p. 1407-13.

56. Dang, H.Q., et al., *Proximity Interactions among Basal Body Components in Trypanosoma brucei Identify Novel Regulators of Basal Body Biogenesis and Inheritance.* MBio, 2017. **8**(1).

57. Hu, H., et al., *The Centriole Cartwheel Protein SAS-6 in Trypanosoma brucei Is Required for Probasal Body Biogenesis and Flagellum Assembly.* Eukaryot Cell, 2015. **14**(9): p. 898-907.

58. Gadelha, C., et al., *Basal body and flagellum mutants reveal a rotational constraint of the central pair microtubules in the axonemes of trypanosomes.* J Cell Sci, 2006. **119**(Pt 12): p. 2405-13.

59. Carvalho-Santos, Z., et al., *Stepwise evolution of the centriole-assembly pathway.* J Cell Sci, 2010. **123**(Pt 9): p. 1414-26.

60. Hu, H., Q. Zhou, and Z. Li, *SAS-4 Protein in Trypanosoma brucei Controls Life Cycle Transitions by Modulating the Length of the Flagellum Attachment Zone Filament.* J Biol Chem, 2015. **290**(51): p. 30453-63.

61. Scott, V., T. Sherwin, and K. Gull, *gamma-tubulin in trypanosomes: molecular characterisation and localisation to multiple and diverse microtubule organising centres.* J Cell Sci, 1997. **110 (Pt 2)**: p. 157-68.

62. He, C.Y., M. Pypaert, and G. Warren, *Golgi duplication in Trypanosoma brucei requires Centrin2.* Science, 2005. **310**(5751): p. 1196-8.

63. Morgan, G.W., et al., *An evolutionarily conserved coiled-coil protein implicated in polycystic kidney disease is involved in basal body duplication and flagellar biogenesis in Trypanosoma brucei.* Mol Cell Biol, 2005. **25**(9): p. 3774-83.

64. Andre, J., et al., *An Alternative Model for the Role of RP2 Protein in Flagellum Assembly in the African Trypanosome.* J Biol Chem, 2014. **289**(1): p. 464-75.

65. Hu, H., Q. Zhou, and Z. Li, *A Novel Basal Body Protein That Is a Polo-like Kinase Substrate Is Required for Basal Body Segregation and Flagellum Adhesion in Trypanosoma brucei.* J Biol Chem, 2015. **290**(41): p. 25012-22.

66. Andre, J., et al., *The tubulin cofactor C family member TBCCD1 orchestrates cytoskeletal filament formation.* J Cell Sci, 2013. **126**(Pt 23): p. 5350-6.

67. Dilbeck, V., et al., *Characterization of a coiled coil protein present in the basal body of Trypanosoma brucei.* J Cell Sci, 1999. **112 (Pt 24)**: p. 4687-94.

68. Akiyoshi, B. and K. Gull, *Evolutionary cell biology of chromosome segregation: insights from trypanosomes.* Open Biol, 2013. **3**(5): p. 130023.

69. Zhou, Q., et al., *A coiled-coil- and C2-domain-containing protein is required for FAZ assembly and cell morphology in Trypanosoma brucei.* J Cell Sci, 2011. **124**(Pt 22): p. 3848-58.

70. Shi, J., et al., *Centrin4 coordinates cell and nuclear division in T. brucei.* J Cell Sci, 2008. **121**(Pt 18): p. 3062-70.

71. Ikeda, K.N. and C.L. de Graffenried, *Polo-like kinase is necessary for flagellum inheritance in Trypanosoma brucei.* J Cell Sci, 2012. **125**(Pt 13): p. 3173-84.

72. Hammarton, T.C., et al., *Trypanosoma brucei Polo-like kinase is essential for basal body duplication, kDNA segregation and cytokinesis.* Mol Microbiol, 2007. **65**(5): p. 1229-48.

73. Selvapandiyan, A., et al., *Centrin1 is required for organelle segregation and cytokinesis in Trypanosoma brucei.* Mol Biol Cell, 2007. **18**(9): p. 3290-301.

74. McKean, P.G., et al., *Gamma-tubulin functions in the nucleation of a discrete subset of microtubules in the eukaryotic flagellum.* Curr Biol, 2003. **13**(7): p. 598-602.

75. Marshall, W.F., *Centriole evolution.* Curr Opin Cell Biol, 2009. **21**(1): p. 14-9.

76. Avidor-Reiss, T. and J. Gopalakrishnan, *Building a centriole.* Curr Opin Cell Biol, 2013. **25**(1): p. 72-7.

77. Beisson, J. and M. Wright, *Basal body/centriole assembly and continuity.* Curr Opin Cell Biol, 2003. **15**(1): p. 96-104.

78. Dawe, H.R., H. Farr, and K. Gull, *Centriole/basal body morphogenesis and migration during ciliogenesis in animal cells.* J Cell Sci, 2007. **120**(Pt 1): p. 7-15.

79. Winey, M. and E. O'Toole, *Centriole structure.* Philos Trans R Soc Lond B Biol Sci, 2014. **369**(1650).

80. Lacomble, S., et al., *Basal body movements orchestrate membrane organelle division and cell morphogenesis in Trypanosoma brucei.* J Cell Sci, 2010. **123**(Pt 17): p. 2884-91.

81. Jakob, M., et al., *Mitochondrial growth during the cell cycle of Trypanosoma brucei bloodstream forms.* Sci Rep, 2016. **6**: p. 36565.

82. Tyler, K.M., K.R. Matthews, and K. Gull, *The bloodstream differentiation-division of Trypanosoma brucei studied using mitochondrial markers.* Proc Biol Sci, 1997. **264**(1387): p. 1481-90.

83. Bienen, E.J., et al., *Mitochondrial development in Trypanosoma brucei brucei transitional bloodstream forms.* Mol Biochem Parasitol, 1991. **45**(2): p. 185-92.

84. Brown, S.V., et al., *ATP synthase is responsible for maintaining mitochondrial membrane potential in bloodstream form Trypanosoma brucei.* Eukaryot Cell, 2006. **5**(1): p. 45-53.

85. Nolan, D.P. and H.P. Voorheis, *The mitochondrion in bloodstream forms of Trypanosoma brucei is energized by the electrogenic pumping of protons catalysed by the F1F0-ATPase.* Eur J Biochem, 1992. **209**(1): p. 207-16.

86. Liu, B., et al., *Fellowship of the rings: the replication of kinetoplast DNA.* Trends Parasitol, 2005. **21**(8): p. 363-9.

87. Jensen, R.E. and P.T. Englund, *Network news: the replication of kinetoplast DNA.* Annu Rev Microbiol, 2012. **66**: p. 473-91.

88. Shapiro, T.A. and P.T. Englund, *The structure and replication of kinetoplast DNA.* Annu Rev Microbiol, 1995. **49**: p. 117-43.

89. Kleisen, C.M., et al., *The structure of kinetoplast DNA. 2. Characterization of a novel component of high complexity present in the kinetoplast DNA network of Crithidia luciliae.* Eur J Biochem, 1976. **64**(1): p. 153-60.

90. Simpson, L., et al., *Comparison of the maxicircle (mitochondrial) genomes of Leishmania tarentolae and Trypanosoma brucei at the level of nucleotide sequence.* J Biol Chem, 1987. **262**(13): p. 6182-96.

91. Corell, R.A., et al., *Trypanosoma brucei minicircles encode multiple guide RNAs which can direct editing of extensively overlapping sequences.* Nucleic Acids Res, 1993. **21**(18): p. 4313-20.

92. Benne, R., et al., *Major transcript of the frameshifted coxII gene from trypanosome mitochondria contains four nucleotides that are not encoded in the DNA.* Cell, 1986. **46**(6): p. 819-26.

93. Aphasizhev, R. and I. Aphasizheva, *Mitochondrial RNA processing in trypanosomes.* Res Microbiol, 2011. **162**(7): p. 655-63.

94. Simpson, L., et al., *Mitochondrial proteins and complexes in Leishmania and Trypanosoma involved in U-insertion/deletion RNA editing.* RNA, 2004. **10**(2): p. 159-70.

95. Chen, J., et al., *The topology of the kinetoplast DNA network.* Cell, 1995. **80**(1): p. 61-9.

96. Shapiro, T.A., *Kinetoplast DNA maxicircles: networks within networks.* Proc Natl Acad Sci U S A, 1993. **90**(16): p. 7809-13.

97. Schnaufer, A., G.J. Domingo, and K. Stuart, *Natural and induced dyskinetoplastic trypanosomatids: how to live without mitochondrial DNA.* Int J Parasitol, 2002. **32**(9): p. 1071-84.

98. Zhao, Z., et al., *p166, a link between the trypanosome mitochondrial DNA and flagellum, mediates genome segregation.* EMBO J, 2008. **27**(1): p. 143-54.

99. Gheiratmand, L., et al., *Biochemical characterization of the bi-lobe reveals a continuous structural network linking the bi-lobe to other single-copied organelles in Trypanosoma brucei.* J Biol Chem, 2013. **288**(5): p. 3489-99.

100. Ochsenreiter, T., et al., *Alternative RNA editing produces a novel protein involved in mitochondrial DNA maintenance in trypanosomes.* Mol Cell Biol, 2008. **28**(18): p. 5595-604.

101. Trikin, R., et al., *Correction: TAC102 Is a Novel Component of the Mitochondrial Genome Segregation Machinery in Trypanosomes.* PLoS Pathog, 2016. **12**(7): p. e1005750.

102. Schnarwiler, F., et al., *Trypanosomal TAC40 constitutes a novel subclass of mitochondrial beta-barrel proteins specialized in mitochondrial genome inheritance.* Proc Natl Acad Sci U S A, 2014. **111**(21): p. 7624-9.

103. Dean, S., et al., *Cilium transition zone proteome reveals compartmentalization and differential dynamics of ciliopathy complexes.* Proc Natl Acad Sci U S A, 2016. **113**(35): p. E5135-43.

104. Szymanska, K. and C.A. Johnson, *The transition zone: an essential functional compartment of cilia.* Cilia, 2012. **1**(1): p. 10.

105. Vaughan, S., M. Shaw, and K. Gull, *A post-assembly structural modification to the lumen of flagellar microtubule doublets.* Curr Biol, 2006. **16**(12): p. R449-50.

106. Vaughan, S. and K. Gull, *Basal body structure and cell cycle-dependent biogenesis in Trypanosoma brucei.* Cilia, 2015. **5**: p. 5.

107. Satir, P. and S.T. Christensen, *Overview of structure and function of mammalian cilia.* Annu Rev Physiol, 2007. **69**: p. 377-400.

108. Mitchell, D.R., *Speculations on the evolution of 9+2 organelles and the role of central pair microtubules.* Biol Cell, 2004. **96**(9): p. 691-6.

109. Cachon, M. and M.P. Cosson, *Ciliary and flagellar apparatuses and their associated structures.* Biol Cell, 1988. **63**(2): p. 115.

110. Schlaeppi, K., J. Deflorin, and T. Seebeck, *The major component of the paraflagellar rod of Trypanosoma brucei is a helical protein that is encoded by two identical, tandemly linked genes.* J Cell Biol, 1989. **109**(4 Pt 1): p. 1695-709.

111. Bastin, P., T. Sherwin, and K. Gull, *Paraflagellar rod is vital for trypanosome motility.* Nature, 1998. **391**(6667): p. 548.

112. Kohl, L., T. Sherwin, and K. Gull, *Assembly of the paraflagellar rod and the flagellum attachment zone complex during the Trypanosoma brucei cell cycle.* J Eukaryot Microbiol, 1999. **46**(2): p. 105-9.

113. Sunter, J.D. and K. Gull, *The Flagellum Attachment Zone: 'The Cellular Ruler' of Trypanosome Morphology.* Trends Parasitol, 2016. **32**(4): p. 309-24.

114. Vaughan, S., et al., *A repetitive protein essential for the flagellum attachment zone filament structure and function in Trypanosoma brucei.* Protist, 2008. **159**(1): p. 127-36.

115. Zhou, Q., et al., *Assembly and maintenance of the flagellum attachment zone filament in Trypanosoma brucei.* J Cell Sci, 2015. **128**(13): p. 2361-72.

116. Broadhead, R., et al., *Flagellar motility is required for the viability of the bloodstream trypanosome.* Nature, 2006. **440**(7081): p. 224-7.

117. Ralston, K.S., et al., *Flagellar motility contributes to cytokinesis in Trypanosoma brucei and is modulated by an evolutionarily conserved dynein regulatory system.* Eukaryot Cell, 2006. **5**(4): p. 696-711.

118. Absalon, S., et al., *Intraflagellar transport and functional analysis of genes required for flagellum formation in trypanosomes.* Mol Biol Cell, 2008. **19**(3): p. 929-44.

119. Kohl, L., D. Robinson, and P. Bastin, *Novel roles for the flagellum in cell morphogenesis and cytokinesis of trypanosomes.* EMBO J, 2003. **22**(20): p. 5336-46.

120. Field, M.C. and M. Carrington, *The trypanosome flagellar pocket.* Nat Rev Microbiol, 2009. **7**(11): p. 775-86.

121. Lacomble, S., et al., *Three-dimensional cellular architecture of the flagellar pocket and associated cytoskeleton in trypanosomes revealed by electron microscope tomography.* J Cell Sci, 2009. **122**(Pt 8): p. 1081-90.

122. Esson, H.J., et al., *Morphology of the trypanosome bilobe, a novel cytoskeletal structure.* Eukaryot Cell, 2012. **11**(6): p. 761-72.

123. Morriswood, B., et al., *Novel bilobe components in Trypanosoma brucei identified using proximity-dependent biotinylation.* Eukaryot Cell, 2013. **12**(2): p. 356-67.

124. Li, Z., *Regulation of the cell division cycle in Trypanosoma brucei.* Eukaryot Cell, 2012. **11**(10): p. 1180-90.

125. Hammarton, T.C., *Cell cycle regulation in Trypanosoma brucei.* Mol Biochem Parasitol, 2007. **153**(1): p. 1-8.

126. Zhou, Q., H. Hu, and Z. Li, *New insights into the molecular mechanisms of mitosis and cytokinesis in trypanosomes.* Int Rev Cell Mol Biol, 2014. **308**: p. 127-66.

127. Lukas, J., C. Lukas, and J. Bartek, *Mammalian cell cycle checkpoints: signalling pathways and their organization in space and time.* DNA Repair (Amst), 2004. **3**(8-9): p. 997-1007.

128. Kastan, M.B. and J. Bartek, *Cell-cycle checkpoints and cancer.* Nature, 2004. **432**(7015): p. 316-23.

129. Bettencourt-Dias, M., et al., *Genome-wide survey of protein kinases required for cell cycle progression.* Nature, 2004. **432**(7020): p. 980-7.

130. Nigg, E.A., *Mitotic kinases as regulators of cell division and its checkpoints.* Nat Rev Mol Cell Biol, 2001. **2**(1): p. 21-32.

131. Lindqvist, A., V. Rodriguez-Bravo, and R.H. Medema, *The decision to enter mitosis: feedback and redundancy in the mitotic entry network.* J Cell Biol, 2009. **185**(2): p. 193-202.

132. Vermeulen, K., D.R. Van Bockstaele, and Z.N. Berneman, *The cell cycle: a review of regulation, deregulation and therapeutic targets in cancer.* Cell Prolif, 2003. **36**(3): p. 131-49.

133. Woodward, R. and K. Gull, *Timing of nuclear and kinetoplast DNA replication and early morphological events in the cell cycle of Trypanosoma brucei.* J Cell Sci, 1990. **95 (Pt 1)**: p. 49-57.

134. Saxowsky, T.T., et al., *Trypanosoma brucei has two distinct mitochondrial DNA polymerase beta enzymes.* J Biol Chem, 2003. **278**(49): p. 49095-101.

135. Robinson, D.R. and K. Gull, *The configuration of DNA replication sites within the Trypanosoma brucei kinetoplast.* J Cell Biol, 1994. **126**(3): p. 641-8.

136. Gluenz, E., et al., *The kinetoplast duplication cycle in Trypanosoma brucei is orchestrated by cytoskeleton-mediated cell morphogenesis.* Mol Cell Biol, 2011. **31**(5): p. 1012-21.

137. Siegel, T.N., D.R. Hekstra, and G.A. Cross, *Analysis of the Trypanosoma brucei cell cycle by quantitative DAPI imaging.* Mol Biochem Parasitol, 2008. **160**(2): p. 171-4.

138. Pavletich, N.P., *Mechanisms of cyclin-dependent kinase regulation: structures of Cdks, their cyclin activators, and Cip and INK4 inhibitors.* J Mol Biol, 1999. **287**(5): p. 821-8.

139. Suryadinata, R., M. Sadowski, and B. Sarcevic, *Control of cell cycle progression by phosphorylation of cyclin-dependent kinase (CDK) substrates.* Biosci Rep, 2010. **30**(4): p. 243-55.

140. Fisher, R.P., *Getting to S: CDK functions and targets on the path to cell-cycle commitment.* F1000Res, 2016. **5**: p. 2374.

141. Foster, D.A., et al., *Regulation of G1 Cell Cycle Progression: Distinguishing the Restriction Point from a Nutrient-Sensing Cell Growth Checkpoint(s).* Genes Cancer, 2010. **1**(11): p. 1124-31.

142. Sherr, C.J. and J. Bartek, *Cell Cycle–Targeted Cancer Therapies.* Annual Review of Cancer Biology, 2017. **1**(1): p. 41-57.

143. Meyerson, M. and E. Harlow, *Identification of G1 kinase activity for cdk6, a novel cyclin D partner.* Mol Cell Biol, 1994. **14**(3): p. 2077-86.

144. Musgrove, E.A., B. Sarcevic, and R.L. Sutherland, *Inducible expression of cyclin D1 in T-47D human breast cancer cells is sufficient for Cdk2 activation and pRB hyperphosphorylation.* J Cell Biochem, 1996. **60**(3): p. 363-78.

145. Prall, O.W., et al., *c-Myc or cyclin D1 mimics estrogen effects on cyclin E-Cdk2 activation and cell cycle reentry.* Mol Cell Biol, 1998. **18**(8): p. 4499-508.

146. Ohtsubo, M., et al., *Human cyclin E, a nuclear protein essential for the G1-to-S-phase transition.* Mol Cell Biol, 1995. **15**(5): p. 2612-24.

147. Moreno-Torres, M., M. Jaquenoud, and C. De Virgilio, *TORC1 controls G1-S cell cycle transition in yeast via Mpk1 and the greatwall kinase pathway.* Nat Commun, 2015. **6**: p. 8256.

148. Wang, X. and C.G. Proud, *Nutrient control of TORC1, a cell-cycle regulator.* Trends Cell Biol, 2009. **19**(6): p. 260-7.

149. Morgan, G.A., E.A. Hamilton, and S.J. Black, *The requirements for G1 checkpoint progression of Trypanosoma brucei S 427 clone 1.* Mol Biochem Parasitol, 1996. **78**(1-2): p. 195-207.

150. Vassella, E., et al., *Differentiation of African trypanosomes is controlled by a density sensing mechanism which signals cell cycle arrest via the cAMP pathway.* J Cell Sci, 1997. **110 (Pt 21)**: p. 2661-71.

151. Barquilla, A., J.L. Crespo, and M. Navarro, *Rapamycin inhibits trypanosome cell growth by preventing TOR complex 2 formation.* Proc Natl Acad Sci U S A, 2008. **105**(38): p. 14579-84.

152. Barquilla, A., et al., *Third target of rapamycin complex negatively regulates development of quiescence in Trypanosoma brucei.* Proc Natl Acad Sci U S A, 2012. **109**(36): p. 14399-404.

153. Hall, B.S., et al., *TbVps34, the trypanosome orthologue of Vps34, is required for Golgi complex segregation.* J Biol Chem, 2006. **281**(37): p. 27600-12.

154. Hammarton, T.C., M. Engstler, and J.C. Mottram, *The Trypanosoma brucei cyclin, CYC2, is required for cell cycle progression through G1 phase and for maintenance of procyclic form cell morphology.* J Biol Chem, 2004. **279**(23): p. 24757-64.

155. Tu, X. and C.C. Wang, *Coupling of posterior cytoskeletal morphogenesis to the G1/S transition in the Trypanosoma brucei cell cycle.* Mol Biol Cell, 2005. **16**(1): p. 97-105.

156. Liu, Y., H. Hu, and Z. Li, *The cooperative roles of PHO80-like cyclins in regulating the G1/S transition and posterior cytoskeletal morphogenesis in Trypanosoma brucei.* Mol Microbiol, 2013. **90**(1): p. 130-46.

157. Povelones, M.L., *Beyond replication: division and segregation of mitochondrial DNA in kinetoplastids.* Mol Biochem Parasitol, 2014. **196**(1): p. 53-60.

158. Englund, P.T., *Free minicircles of kinetoplast DNA in Crithidia fasciculata.* J Biol Chem, 1979. **254**(11): p. 4895-900.

159. Drew, M.E. and P.T. Englund, *Intramitochondrial location and dynamics of Crithidia fasciculata kinetoplast minicircle replication intermediates.* J Cell Biol, 2001. **153**(4): p. 735-44.

160. Ryan, K.A. and P.T. Englund, *Synthesis and processing of kinetoplast DNA minicircles in Trypanosoma equiperdum.* Mol Cell Biol, 1989. **9**(8): p. 3212-7.

161. del Solar, G., et al., *Replication and control of circular bacterial plasmids.* Microbiol Mol Biol Rev, 1998. **62**(2): p. 434-64.

162. Engel, M.L. and D.S. Ray, *The kinetoplast structure-specific endonuclease I is related to the 5' exo/endonuclease domain of bacterial DNA polymerase I and colocalizes with the kinetoplast topoisomerase II and DNA polymerase beta during replication.* Proc Natl Acad Sci U S A, 1999. **96**(15): p. 8455-60.

163. Carpenter, L.R. and P.T. Englund, *Kinetoplast maxicircle DNA replication in Crithidia fasciculata and Trypanosoma brucei.* Mol Cell Biol, 1995. **15**(12): p. 6794-803.

164. Bruhn, D.F., et al., *Mitochondrial DNA polymerase POLIB is essential for minicircle DNA replication in African trypanosomes.* Mol Microbiol, 2010. **75**(6): p. 1414-25.

165. Melendy, T., C. Sheline, and D.S. Ray, *Localization of a type II DNA topoisomerase to two sites at the periphery of the kinetoplast DNA of Crithidia fasciculata.* Cell, 1988. **55**(6): p. 1083-8.

166. Wang, Z., et al., *Inhibition of Trypanosoma brucei gene expression by RNA interference using an integratable vector with opposing T7 promoters.* J Biol Chem, 2000. **275**(51): p. 40174-9.

167. Wang, Z. and P.T. Englund, *RNA interference of a trypanosome topoisomerase II causes progressive loss of mitochondrial DNA.* EMBO J, 2001. **20**(17): p. 4674-83.

168. Tzfati, Y., et al., *A single-stranded DNA-binding protein from Crithidia fasciculata recognizes the nucleotide sequence at the origin of replication of kinetoplast DNA minicircles.* Proc Natl Acad Sci U S A, 1992. **89**(15): p. 6891-5.

169. Abu-Elneel, K., et al., *Intramitochondrial localization of universal minicircle sequence-binding protein, a trypanosomatid protein that binds kinetoplast minicircle replication origins.* J Cell Biol, 2001. **153**(4): p. 725-34.

170. Liu, B., et al., *Role of p38 in replication of Trypanosoma brucei kinetoplast DNA.* Mol Cell Biol, 2006. **26**(14): p. 5382-93.

171. Milman, N., et al., *Mitochondrial origin-binding protein UMSBP mediates DNA replication and segregation in trypanosomes.* Proc Natl Acad Sci U S A, 2007. **104**(49): p. 19250-5.

172. Liu, B., et al., *TbPIF1, a Trypanosoma brucei mitochondrial DNA helicase, is essential for kinetoplast minicircle replication.* J Biol Chem, 2010. **285**(10): p. 7056-66.

173. Liu, B., et al., *Trypanosomes have six mitochondrial DNA helicases with one controlling kinetoplast maxicircle replication.* Mol Cell, 2009. **35**(4): p. 490-501.

174. Wang, J., P.T. Englund, and R.E. Jensen, *TbPIF8, a Trypanosoma brucei protein related to the yeast Pif1 helicase, is essential for cell viability and mitochondrial genome maintenance.* Mol Microbiol, 2012. **83**(3): p. 471-85.

175. Hines, J.C. and D.S. Ray, *A mitochondrial DNA primase is essential for cell growth and kinetoplast DNA replication in Trypanosoma brucei.* Mol Cell Biol, 2010. **30**(6): p. 1319-28.

176. Hines, J.C. and D.S. Ray, *A second mitochondrial DNA primase is essential for cell growth and kinetoplast minicircle DNA replication in Trypanosoma brucei.* Eukaryot Cell, 2011. **10**(3): p. 445-54.

177. Bruhn, D.F., M.P. Sammartino, and M.M. Klingbeil, *Three mitochondrial DNA polymerases are essential for kinetoplast DNA replication and survival of bloodstream form Trypanosoma brucei.* Eukaryot Cell, 2011. **10**(6): p. 734-43.

178. Klingbeil, M.M., S.A. Motyka, and P.T. Englund, *Multiple mitochondrial DNA polymerases in Trypanosoma brucei.* Mol Cell, 2002. **10**(1): p. 175-86.

179. Concepcion-Acevedo, J., J. Luo, and M.M. Klingbeil, *Dynamic localization of Trypanosoma brucei mitochondrial DNA polymerase ID.* Eukaryot Cell, 2012. **11**(7): p. 844-55.

180. Torri, A.F., T.A. Kunkel, and P.T. Englund, *A beta-like DNA polymerase from the mitochondrion of the trypanosomatid Crithidia fasciculata.* J Biol Chem, 1994. **269**(11): p. 8165-71.

181. Downey, N., et al., *Mitochondrial DNA ligases of Trypanosoma brucei.* Eukaryot Cell, 2005. **4**(4): p. 765-74.

182. Pasion, S.G., et al., *Periodic expression of nuclear and mitochondrial DNA replication genes during the trypanosomatid cell cycle.* J Cell Sci, 1994. **107 (Pt 12)**: p. 3515-20.

183. Pasion, S.G., et al., *Sequences within the 5' untranslated region regulate the levels of a kinetoplast DNA topoisomerase mRNA during the cell cycle.* Mol Cell Biol, 1996. **16**(12): p. 6724-35.

184. Mittra, B. and D.S. Ray, *Presence of a poly(A) binding protein and two proteins with cell cycle-dependent phosphorylation in Crithidia fasciculata mRNA cycling sequence binding protein II.* Eukaryot Cell, 2004. **3**(5): p. 1185-97.

185. Masai, H., et al., *Eukaryotic chromosome DNA replication: where, when, and how?* Annu Rev Biochem, 2010. **79**: p. 89-130.

186. O'Donnell, M., L. Langston, and B. Stillman, *Principles and concepts of DNA replication in bacteria, archaea, and eukarya.* Cold Spring Harb Perspect Biol, 2013. **5**(7).

187. Tsakraklides, V. and S.P. Bell, *Dynamics of pre-replicative complex assembly.* J Biol Chem, 2010. **285**(13): p. 9437-43.

188. Labib, K., *How do Cdc7 and cyclin-dependent kinases trigger the initiation of chromosome replication in eukaryotic cells?* Genes Dev, 2010. **24**(12): p. 1208-19.

189. Diffley, J.F., *Quality control in the initiation of eukaryotic DNA replication.* Philos Trans R Soc Lond B Biol Sci, 2011. **366**(1584): p. 3545-53.

190. Bell, S.P. and B. Stillman, *ATP-dependent recognition of eukaryotic origins of DNA replication by a multiprotein complex.* Nature, 1992. **357**(6374): p. 128-34.

191. Gossen, M., et al., *A Drosophila homolog of the yeast origin recognition complex.* Science, 1995. **270**(5242): p. 1674-7.

192. Romanowski, P., et al., *The Xenopus origin recognition complex is essential for DNA replication and MCM binding to chromatin.* Curr Biol, 1996. **6**(11): p. 1416-25.

193. Speck, C. and B. Stillman, *Cdc6 ATPase activity regulates ORC x Cdc6 stability and the selection of specific DNA sequences as origins of DNA replication.* J Biol Chem, 2007. **282**(16): p. 11705-14.

194. Randell, J.C., et al., *Sequential ATP hydrolysis by Cdc6 and ORC directs loading of the Mcm2-7 helicase.* Mol Cell, 2006. **21**(1): p. 29-39.

195. Chen, S., M.A. de Vries, and S.P. Bell, *Orc6 is required for dynamic recruitment of Cdt1 during repeated Mcm2-7 loading.* Genes Dev, 2007. **21**(22): p. 2897-907.

196. Hofmann, J.F. and D. Beach, *cdt1 is an essential target of the Cdc10/Sct1 transcription factor: requirement for DNA replication and inhibition of mitosis.* EMBO J, 1994. **13**(2): p. 425-34.

197. Cook, J.G., D.A. Chasse, and J.R. Nevins, *The regulated association of Cdt1 with minichromosome maintenance proteins and Cdc6 in mammalian cells.* J Biol Chem, 2004. **279**(10): p. 9625-33.

198. Nishitani, H. and Z. Lygerou, *DNA replication licensing.* Front Biosci, 2004. **9**: p. 2115-32.

199. Liu, E., et al., *Cyclin-dependent kinases phosphorylate human Cdt1 and induce its degradation.* J Biol Chem, 2004. **279**(17): p. 17283-8.

200. Li, A. and J.J. Blow, *Cdt1 downregulation by proteolysis and geminin inhibition prevents DNA re-replication in Xenopus.* EMBO J, 2005. **24**(2): p. 395-404.

201. Kim, J., H. Feng, and E.T. Kipreos, *C. elegans CUL-4 prevents rereplication by promoting the nuclear export of CDC-6 via a CKI-1-dependent pathway.* Curr Biol, 2007. **17**(11): p. 966-72.

202. Wohlschlegel, J.A., et al., *Inhibition of eukaryotic DNA replication by geminin binding to Cdt1.* Science, 2000. **290**(5500): p. 2309-12.

203. Bochman, M.L. and A. Schwacha, *The Mcm complex: unwinding the mechanism of a replicative helicase.* Microbiol Mol Biol Rev, 2009. **73**(4): p. 652-83.

204. Nougarede, R., et al., *Hierarchy of S-phase-promoting factors: yeast Dbf4-Cdc7 kinase requires prior S-phase cyclin-dependent kinase activation.* Mol Cell Biol, 2000. **20**(11): p. 3795-806.

205. Baker, T.A. and S.P. Bell, *Polymerases and the replisome: machines within machines.* Cell, 1998. **92**(3): p. 295-305.

206. Godoy, P.D., et al., *Trypanosome prereplication machinery contains a single functional orc1/cdc6 protein, which is typical of archaea.* Eukaryot Cell, 2009. **8**(10): p. 1592-603.

207. Tiengwe, C., et al., *Identification of ORC1/CDC6-interacting factors in Trypanosoma brucei reveals critical features of origin recognition complex architecture.* PLoS One, 2012. **7**(3): p. e32674.

208. Dang, H.Q. and Z. Li, *The Cdc45.Mcm2-7.GINS protein complex in trypanosomes regulates DNA replication and interacts with two Orc1-like proteins in the origin recognition complex.* J Biol Chem, 2011. **286**(37): p. 32424-35.

209. Benmerzouga, I., et al., *Trypanosoma brucei Orc1 is essential for nuclear DNA replication and affects both VSG silencing and VSG switching.* Mol Microbiol, 2013. **87**(1): p. 196-210.

210. Chang, L.M., et al., *DNA polymerases in parasitic protozoans differ from host enzymes.* Science, 1980. **208**(4443): p. 510-1.

211. Uzcanga, G., et al., *Nuclear DNA replication and repair in parasites of the genus Leishmania: Exploiting differences to develop innovative therapeutic approaches.* Crit Rev Microbiol, 2017. **43**(2): p. 156-177.

212. Urbaniak, M.D., D.M. Martin, and M.A. Ferguson, *Global quantitative SILAC phosphoproteomics reveals differential phosphorylation is widespread between the procyclic and bloodstream form lifecycle stages of Trypanosoma brucei.* J Proteome Res, 2013. **12**(5): p. 2233-44.

213. Nett, I.R., et al., *The phosphoproteome of bloodstream form Trypanosoma brucei, causative agent of African sleeping sickness.* Mol Cell Proteomics, 2009. **8**(7): p. 1527-38.

214. Masai, H., et al., *Phosphorylation of MCM4 by Cdc7 kinase facilitates its interaction with Cdc45 on the chromatin.* J Biol Chem, 2006. **281**(51): p. 39249-61.

215. Reiter, J.F., O.E. Blacque, and M.R. Leroux, *The base of the cilium: roles for transition fibres and the transition zone in ciliary formation, maintenance and compartmentalization.* EMBO Rep, 2012. **13**(7): p. 608-18.

216. Archer, S.K., et al., *The cell cycle regulated transcriptome of Trypanosoma brucei.* PLoS One, 2011. **6**(3): p. e18425.

217. Mutomba, M.C. and C.C. Wang, *Effects of aphidicolin and hydroxyurea on the cell cycle and differentiation of Trypanosoma brucei bloodstream forms.* Mol Biochem Parasitol, 1996. **80**(1): p. 89-102.

218. Marshall, W.F., Y. Vucica, and J.L. Rosenbaum, *Kinetics and regulation of de novo centriole assembly. Implications for the mechanism of centriole duplication.* Curr Biol, 2001. **11**(5): p. 308-17.

219. Khodjakov, A., et al., *De novo formation of centrosomes in vertebrate cells arrested during S-phase.* J Cell Biol, 2002. **158**(7): p. 1171-81.

220. Rodrigues-Martins, A., et al., *Revisiting the role of the mother centriole in centriole biogenesis.* Science, 2007. **316**(5827): p. 1046-50.

221. Kleylein-Sohn, J., et al., *Plk4-induced centriole biogenesis in human cells.* Dev Cell, 2007. **13**(2): p. 190-202.

222. O'Connell, K.F., et al., *The C. elegans zyg-1 gene encodes a regulator of centrosome duplication with distinct maternal and paternal roles in the embryo.* Cell, 2001. **105**(4): p. 547-58.

223. Bettencourt-Dias, M., et al., *SAK/PLK4 is required for centriole duplication and flagella development.* Curr Biol, 2005. **15**(24): p. 2199-207.

224. Peel, N., et al., *Overexpressing centriole-replication proteins in vivo induces centriole overduplication and de novo formation.* Curr Biol, 2007. **17**(10): p. 834-43.

225. Hirono, M., *Cartwheel assembly.* Philos Trans R Soc Lond B Biol Sci, 2014. **369**(1650).

226. Brian A. Bayless, T.H.G., Jr., Mark Winey and Chad G. Pearson, *Bld10/Cep135 stabilizes basal bodies to resist cilia-generated forces.* Mol. Biol. Cell, 2012. **23**(24): p. 4820-4832.

227. Fuller, S.D., et al., *The core of the mammalian centriole contains gamma-tubulin.* Curr Biol, 1995. **5**(12): p. 1384-93.

228. Ruiz, F., et al., *Basal body duplication in Paramecium requires gamma-tubulin.* Curr Biol, 1999. **9**(1): p. 43-6.

229. O'Toole, E., et al., *The role of gamma-tubulin in centrosomal microtubule organization.* PLoS One, 2012. **7**(1): p. e29795.

230. Kohlmaier, G., et al., *Overly long centrioles and defective cell division upon excess of the SAS-4-related protein CPAP.* Curr Biol, 2009. **19**(12): p. 1012-8.

231. Schmidt, T.I., et al., *Control of centriole length by CPAP and CP110.* Curr Biol, 2009. **19**(12): p. 1005-11.

232. Dutcher, S.K., et al., *Epsilon-tubulin is an essential component of the centriole.* Mol Biol Cell, 2002. **13**(11): p. 3859-69.

233. Dutcher, S.K. and E.C. Trabuco, *The UNI3 gene is required for assembly of basal bodies of Chlamydomonas and encodes delta-tubulin, a new member of the tubulin superfamily.* Mol Biol Cell, 1998. **9**(6): p. 1293-308.

234. Garreau de Loubresse, N., et al., *Role of delta-tubulin and the C-tubule in assembly of Paramecium basal bodies.* BMC Cell Biol, 2001. **2**: p. 4.

235. Gogendeau, D., et al., *Sas-4 proteins are required during basal body duplication in Paramecium.* Mol Biol Cell, 2011. **22**(7): p. 1035-44.

236. Leidel, S. and P. Gönczy, *SAS-4 Is Essential for Centrosome Duplication in C. elegans and Is Recruited to Daughter Centrioles Once per Cell Cycle.* Developmental Cell, 2003. **4**(3): p. 431-439.

237. Brownlee, C.W. and G.C. Rogers, *Show me your license, please: deregulation of centriole duplication mechanisms that promote amplification.* Cell Mol Life Sci, 2013. **70**(6): p. 1021-34.

238. Ruthnick, D. and E. Schiebel, *Duplication of the Yeast Spindle Pole Body Once per Cell Cycle.* Mol Cell Biol, 2016. **36**(9): p. 1324-31.

239. Nigg, E.A., *Centrosome duplication: of rules and licenses.* Trends Cell Biol, 2007. **17**(5): p. 215-21.

240. Rogers, G.C., et al., *The SCF Slimb ubiquitin ligase regulates Plk4/Sak levels to block centriole reduplication.* J Cell Biol, 2009. **184**(2): p. 225-39.

241. Strnad, P., et al., *Regulated HsSAS-6 levels ensure formation of a single procentriole per centriole during the centrosome duplication cycle.* Dev Cell, 2007. **13**(2): p. 203-13.

242. Loncarek, J., et al., *Control of daughter centriole formation by the pericentriolar material.* Nat Cell Biol, 2008. **10**(3): p. 322-8.

243. Wong, C. and T. Stearns, *Centrosome number is controlled by a centrosome-intrinsic block to reduplication.* Nat Cell Biol, 2003. **5**(6): p. 539-44.

244. Loncarek, J., P. Hergert, and A. Khodjakov, *Centriole reduplication during prolonged interphase requires procentriole maturation governed by Plk1.* Curr Biol, 2010. **20**(14): p. 1277-82.

245. Shukla, A., et al., *Plk1 relieves centriole block to reduplication by promoting daughter centriole maturation.* Nat Commun, 2015. **6**: p. 8077.

246. Haren, L., et al., *NEDD1-dependent recruitment of the gamma-tubulin ring complex to the centrosome is necessary for centriole duplication and spindle assembly.* J Cell Biol, 2006. **172**(4): p. 505-15.

247. Wang, W.J., et al., *The conversion of centrioles to centrosomes: essential coupling of duplication with segregation.* J Cell Biol, 2011. **193**(4): p. 727-39.

248. Greer, Y.E., et al., *Lack of Casein Kinase 1 Delta Promotes Genomic Instability - The Accumulation of DNA Damage and Down-Regulation of Checkpoint Kinase 1.* PLoS One, 2017. **12**(1): p. e0170903.

249. Levine, M.S., et al., *Centrosome Amplification Is Sufficient to Promote Spontaneous Tumorigenesis in Mammals.* Dev Cell, 2017. **40**(3): p. 313-322 e5.

250. Chan, J.Y., *A clinical overview of centrosome amplification in human cancers.* Int J Biol Sci, 2011. **7**(8): p. 1122-44.

251. Kitagawa, D., et al., *Phosphorylation of SAS-6 by ZYG-1 is critical for centriole formation in C. elegans embryos.* Dev Cell, 2009. **17**(6): p. 900-7.

252. Robinson, D.R., et al., *Microtubule polarity and dynamics in the control of organelle positioning, segregation, and cytokinesis in the trypanosome cell cycle.* J Cell Biol, 1995. **128**(6): p. 1163-72.

253. Ploubidou, A., et al., *Evidence for novel cell cycle checkpoints in trypanosomes: kinetoplast segregation and cytokinesis in the absence of mitosis.* J Cell Sci, 1999. **112 (Pt 24)**: p. 4641-50.

254. Riabowol, K., et al., *The cdc2 kinase is a nuclear protein that is essential for mitosis in mammalian cells.* Cell, 1989. **57**(3): p. 393-401.

255. Beach, D., B. Durkacz, and P. Nurse, *Functionally homologous cell cycle control genes in budding and fission yeast.* Nature, 1982. **300**(5894): p. 706-9.

256. Fantes, P. and P. Nurse, *Control of cell size at division in fission yeast by a growth-modulated size control over nuclear division.* Exp Cell Res, 1977. **107**(2): p. 377-86.

257. Harashima, H., N. Dissmeyer, and A. Schnittger, *Cell cycle control across the eukaryotic kingdom.* Trends Cell Biol, 2013. **23**(7): p. 345-56.

258. Hammarton, T.C., et al., *Stage-specific differences in cell cycle control in Trypanosoma brucei revealed by RNA interference of a mitotic cyclin.* J Biol Chem, 2003. **278**(25): p. 22877-86.

259. Li, Z. and C.C. Wang, *A PHO80-like cyclin and a B-type cyclin control the cell cycle of the procyclic form of Trypanosoma brucei.* J Biol Chem, 2003. **278**(23): p. 20652-8.

260. Ersfeld, K., S.E. Melville, and K. Gull, *Nuclear and genome organization of Trypanosoma brucei.* Parasitol Today, 1999. **15**(2): p. 58-63.

261. Sloof, P., et al., *Size fractionation of Trypanosoma brucei DNA: localization of the 177-bp repeat satellite DNA and a variant surface glycoprotein gene in a mini-chromosomal DNA fraction.* Nucleic Acids Res, 1983. **11**(12): p. 3889-901.

262. Ersfeld, K. and K. Gull, *Partitioning of large and minichromosomes in Trypanosoma brucei.* Science, 1997. **276**(5312): p. 611-4.

263. Ogbadoyi, E., et al., *Architecture of the Trypanosoma brucei nucleus during interphase and mitosis.* Chromosoma, 2000. **108**(8): p. 501-13.

264. Bathe, M. and F. Chang, *Cytokinesis and the contractile ring in fission yeast: towards a systems-level understanding.* Trends Microbiol, 2010. **18**(1): p. 38-45.

265. Glotzer, M., *The molecular requirements for cytokinesis.* Science, 2005. **307**(5716): p. 1735-9.

266. Barr, F.A. and U. Gruneberg, *Cytokinesis: placing and making the final cut.* Cell, 2007. **131**(5): p. 847-60.

267. Farr, H. and K. Gull, *Cytokinesis in trypanosomes.* Cytoskeleton (Hoboken), 2012. **69**(11): p. 931-41.

268. Linda Kohl, D.R.a.P.B., *New roles for the flagellum in cell morphorgenesis and cytokinesis of trypanosomes.* EMBO J, 2003. **22**(20): p. 5336-5346.

269. Li, Z., et al., *Identification of a novel chromosomal passenger complex and its unique localization during cytokinesis in Trypanosoma brucei.* PLoS One, 2008. **3**(6): p. e2354.

270. Lozano-Nunez, A., et al., *An analogue-sensitive approach identifies basal body rotation and flagellum attachment zone elongation as key functions of PLK in Trypanosoma brucei.* Mol Biol Cell, 2013. **24**(9): p. 1321-33.

271. Seong, Y.S., et al., *A spindle checkpoint arrest and a cytokinesis failure by the dominant-negative polo-box domain of Plk1 in U-2 OS cells.* J Biol Chem, 2002. **277**(35): p. 32282-93.

272. Petronczki, M., et al., *Polo-like kinase 1 triggers the initiation of cytokinesis in human cells by promoting recruitment of the RhoGEF Ect2 to the central spindle.* Dev Cell, 2007. **12**(5): p. 713-25.

273. Abbasi, K., et al., *A novel Rho-like protein TbRHP is involved in spindle formation and mitosis in trypanosomes.* PLoS One, 2011. **6**(11): p. e26890.

274. Doherty, G.J. and H.T. McMahon, *Mechanisms of endocytosis.* Annu Rev Biochem, 2009. **78**: p. 857-902.

275. McMahon, H.T. and E. Boucrot, *Molecular mechanism and physiological functions of clathrin-mediated endocytosis.* Nat Rev Mol Cell Biol, 2011. **12**(8): p. 517-33.

276. Octave, J.N., Schneider, Y. J., Trouet, A., Crichton, R. R., *Iron uptake and uitliazation by mammalian cells. I: Cellular uptake of transferrin and iron.* Trends Biochem Sci, 1983. **8**(6): p. 4.

277. Huebers, H.A. and C.A. Finch, *The physiology of transferrin and transferrin receptors.* Physiol Rev, 1987. **67**(2): p. 520-82.

278. El Hage Chahine, J.M., M. Hemadi, and N.T. Ha-Duong, *Uptake and release of metal ions by transferrin and interaction with receptor 1.* Biochim Biophys Acta, 2012. **1820**(3): p. 334-47.

279. Surgenor, D.M., B.A. Koechlin, and L.E. Strong, *Chemical, clinical, and immunological studies on the products of human plasma fractionation; the metal-combining globulin of human plasma.* J Clin Invest, 1949. **28**(1): p. 73-8.

280. Stein, B.S. and H.H. Sussman, *Demonstration of two distinct transferrin receptor recycling pathways and transferrin-independent receptor internalization in K562 cells.* J Biol Chem, 1986. **261**(22): p. 10319-31.

281. Harding, C., J. Heuser, and P. Stahl, *Receptor-mediated endocytosis of transferrin and recycling of the transferrin receptor in rat reticulocytes.* J Cell Biol, 1983. **97**(2): p. 329-39.

282. Pearse, B.M., *Clathrin: a unique protein associated with intracellular transfer of membrane by coated vesicles.* Proc Natl Acad Sci U S A, 1976. **73**(4): p. 1255-9.

283. Stimpson, H.E., et al., *Early-arriving Syp1p and Ede1p function in endocytic site placement and formation in budding yeast.* Mol Biol Cell, 2009. **20**(22): p. 4640-51.

284. Henne, W.M., et al., *FCHo proteins are nucleators of clathrin-mediated endocytosis.* Science, 2010. **328**(5983): p. 1281-4.

285. Park, S.Y. and X. Guo, *Adaptor protein complexes and intracellular transport.* Biosci Rep, 2014. **34**(4).

286. Blondeau, F., et al., *Tandem MS analysis of brain clathrin-coated vesicles reveals their critical involvement in synaptic vesicle recycling.* Proc Natl Acad Sci U S A, 2004. **101**(11): p. 3833-8.

287. Banbury, D.N., et al., *Tyrphostin A23 inhibits internalization of the transferrin receptor by perturbing the interaction between tyrosine motifs and the medium chain subunit of the AP-2 adaptor complex.* J Biol Chem, 2003. **278**(14): p. 12022-8.

288. Nesterov, A., et al., *Inhibition of the receptor-binding function of clathrin adaptor protein AP-2 by dominant-negative mutant mu2 subunit and its effects on endocytosis.* EMBO J, 1999. **18**(9): p. 2489-99.

289. Kosaka, T. and K. Ikeda, *Reversible blockage of membrane retrieval and endocytosis in the garland cell of the temperature-sensitive mutant of Drosophila melanogaster, shibirets1.* J Cell Biol, 1983. **97**(2): p. 499-507.

290. Cao, H., et al., *SRC-mediated phosphorylation of dynamin and cortactin regulates the "constitutive" endocytosis of transferrin.* Mol Cell Biol, 2010. **30**(3): p. 781-92.

291. Steverding, D., *Bloodstream forms of Trypanosoma brucei require only small amounts of iron for growth.* Parasitol Res, 1998. **84**(1): p. 59-62.

292. Schell, D., N.K. Borowy, and P. Overath, *Transferrin is a growth factor for the bloodstream form of Trypanosoma brucei.* Parasitol Res, 1991. **77**(7): p. 558-60.

293. Steverding, D., et al., *ESAG 6 and 7 products of Trypanosoma brucei form a transferrin binding protein complex.* Eur J Cell Biol, 1994. **64**(1): p. 78-87.

294. Steverding, D., et al., *Transferrin-binding protein complex is the receptor for transferrin uptake in Trypanosoma brucei.* J Cell Biol, 1995. **131**(5): p. 1173-82.

295. Grab, D.J., et al., *Endocytosed transferrin in African trypanosomes is delivered to lysosomes and may not be recycled.* Eur J Cell Biol, 1992. **59**(2): p. 398-404.

296. Gabernet-Castello, C., J.B. Dacks, and M.C. Field, *The single ENTH-domain protein of trypanosomes; endocytic functions and evolutionary relationship with epsin.* Traffic, 2009. **10**(7): p. 894-911.

297. Chanez, A.L., et al., *Ablation of the single dynamin of T. brucei blocks mitochondrial fission and endocytosis and leads to a precise cytokinesis arrest.* J Cell Sci, 2006. **119**(Pt 14): p. 2968-74.

298. Morgan, G.W., D. Goulding, and M.C. Field, *The single dynamin-like protein of Trypanosoma brucei regulates mitochondrial division and is not required for endocytosis.* J Biol Chem, 2004. **279**(11): p. 10692-701.

299. Adung'a, V.O., C. Gadelha, and M.C. Field, *Proteomic analysis of clathrin interactions in trypanosomes reveals dynamic evolution of endocytosis.* Traffic, 2013. **14**(4): p. 440-57.

300. Guyett, P.J., et al., *Glycogen Synthase Kinase 3beta Promotes the Endocytosis of Transferrin in the African Trypanosome.* ACS Infect Dis, 2016. **2**(7): p. 518-28.

301. Pulgar, V., et al., *The recombinant alpha isoform of protein kinase CK1 from Xenopus laevis can phosphorylate tyrosine in synthetic substrates.* Eur J Biochem, 1996. **242**(3): p. 519-28.

302. Hoekstra, M.F., et al., *Budding and fission yeast casein kinase I isoforms have dual-specificity protein kinase activity.* Mol Biol Cell, 1994. **5**(8): p. 877-86.

303. Knippschild, U., et al., *The casein kinase 1 family: participation in multiple cellular processes in eukaryotes.* Cell Signal, 2005. **17**(6): p. 675-89.

304. Cheong, J.K. and D.M. Virshup, *Casein kinase 1: Complexity in the family.* Int J Biochem Cell Biol, 2011. **43**(4): p. 465-9.

305. Knippschild, U., et al., *The CK1 Family: Contribution to Cellular Stress Response and Its Role in Carcinogenesis.* Front Oncol, 2014. **4**: p. 96.

306. Nolen, B., S. Taylor, and G. Ghosh, *Regulation of protein kinases; controlling activity through activation segment conformation.* Mol Cell, 2004. **15**(5): p. 661-75.

307. Urbaniak, M.D., *Casein kinase 1 isoform 2 is essential for bloodstream form Trypanosoma brucei.* Mol Biochem Parasitol, 2009. **166**(2): p. 183-5.

308. Behrend, L., et al., *Interaction of casein kinase 1 delta (CK1delta) with post-Golgi structures, microtubules and the spindle apparatus.* Eur J Cell Biol, 2000. **79**(4): p. 240-51.

309. Stoter, M., et al., *Inhibition of casein kinase I delta alters mitotic spindle formation and induces apoptosis in trophoblast cells.* Oncogene, 2005. **24**(54): p. 7964-75.

310. Behrend, L., et al., *IC261, a specific inhibitor of the protein kinases casein kinase 1-delta and -epsilon, triggers the mitotic checkpoint and induces p53-dependent postmitotic effects.* Oncogene, 2000. **19**(47): p. 5303-13.

311. Milne, D.M., P. Looby, and D.W. Meek, *Catalytic activity of protein kinase CK1 delta (casein kinase 1delta) is essential for its normal subcellular localization.* Exp Cell Res, 2001. **263**(1): p. 43-54.

312. Giamas, G., et al., *Phosphorylation of CK1delta: identification of Ser370 as the major phosphorylation site targeted by PKA in vitro and in vivo.* Biochem J, 2007. **406**(3): p. 389-98.

313. Greer, Y.E. and J.S. Rubin, *The role of centrosomal casein kinase 1 delta in neurite outgrowth and beyond.* Cell Cycle, 2011. **10**(16): p. 2605-6.

314. Zyss, D., H. Ebrahimi, and F. Gergely, *Casein kinase I delta controls centrosome positioning during T cell activation.* J Cell Biol, 2011. **195**(5): p. 781-97.

315. Brockman, J.L., et al., *Cell cycle-dependent localization of casein kinase I to mitotic spindles.* Proc Natl Acad Sci U S A, 1992. **89**(20): p. 9454-8.

316. Wang, L., et al., *Casein kinase 1 alpha regulates chromosome congression and separation during mouse oocyte meiotic maturation and early embryo development.* PLoS One, 2013. **8**(5): p. e63173.

317. Katis, V.L., et al., *Rec8 phosphorylation by casein kinase 1 and Cdc7-Dbf4 kinase regulates cohesin cleavage by separase during meiosis.* Dev Cell, 2010. **18**(3): p. 397-409.

318. Hoekstra, M.F., et al., *HRR25, a putative protein kinase from budding yeast: association with repair of damaged DNA.* Science, 1991. **253**(5023): p. 1031-4.

319. Petronczki, M., et al., *Monopolar attachment of sister kinetochores at meiosis I requires casein kinase 1.* Cell, 2006. **126**(6): p. 1049-64.

320. Ben-Nissan, G., et al., *Arabidopsis casein kinase 1-like 6 contains a microtubule-binding domain and affects the organization of cortical microtubules.* Plant Physiol, 2008. **148**(4): p. 1897-907.

321. Li, C., et al., *A spindle pole antigen gene MoSPA2 is important for polar cell growth of vegetative hyphae and conidia, but is dispensable for pathogenicity in Magnaporthe oryzae.* Curr Genet, 2014. **60**(4): p. 255-63.

322. Langousis, G. and K.L. Hill, *Motility and more: the flagellum of Trypanosoma brucei.* Nat Rev Microbiol, 2014. **12**(7): p. 505-18.

323. Bettencourt-Dias, M. and D.M. Glover, *SnapShot: centriole biogenesis.* Cell, 2009. **136**(1): p. 188-188 e1.

CHAPTER 2

AEE788 INHIBITS BASAL BODY ASSEMBLY AND BLOCKS DNA REPLICATION IN THE AFRICAN TRYPANOSOME[1]

[1] Catherine Sullenberger, Daniel Piqué, Yuko Ogata, and Kojo Mensa-Wilmot. Accepted by *Molecular Pharmacology*. 2017.
Reprinted here with permission of the publisher

2.1 Abstract

Trypanosoma brucei causes human African trypanosomiasis (HAT). The pyrrolopyrimidine AEE788 (a hit for anti-HAT drug discovery) associates with three trypanosome protein kinases. Herein we delineate the effects of AEE788 on *T. brucei* using chemical biology strategies. AEE788 treatment inhibits DNA replication in the kinetoplast (mitochondrial nucleoid) and nucleus. In addition, AEE788 blocks duplication of the basal body and the bilobe without affecting mitosis. Thus, AEE788 prevents entry into S-phase of the cell division cycle. To study kinetics of early events in trypanosome division, we employed an "AEE788 block-and-release" protocol to stage entry into S-phase. A time-course of DNA synthesis (nuclear and kinetoplast DNA (kDNA)), duplication of organelles (basal body, bilobe, kinetoplast, nucleus), and cytokinesis was obtained. Unexpected findings include the following: (i) basal body and bilobe duplication are concurrent, (ii) maturation of probasal bodies, marked by TbRP2 recruitment, is coupled with nascent basal body assembly, monitored by localization of TbSAS6 at newly forming basal bodies, and (iii) kinetoplast division is observed in G2, after completion of nuclear DNA synthesis. Prolonged exposure of trypanosomes to AEE788 inhibited transferrin endocytosis, altered cell morphology, and decreased cell viability. To discover putative effectors for AEE788's pleiotropic effects, proteome-wide changes in protein phosphorylation induced by the drug were determined. Putative effectors include an SR protein kinase, bilobe proteins, TbSAS4, TbRP2, and BILBO-1. Loss of function of one or more of these effectors

can, from published literature, explain the polypharmacology of AEE788 on trypanosome biology.

2.2 Introduction

Trypanosoma brucei is a protozoan parasite that causes Human African Trypanosomiasis (HAT) (reviewed in [1, 2]). Current HAT chemotherapies are administered by injection and have toxic side effects (reviewed in [3]), making them far from ideal. An attractive drug discovery approach for neglected tropical diseases (NTDs), such as HAT, is chemical scaffold repurposing [4]. In this strategy, drugs with proven efficacy against other diseases are screened for activity against HAT, reducing time and cost associated with early-stage drug discovery [5]. We identified a small molecule kinase inhibitor, AEE788 [6, 7], as a "hit" (GI_{50} = 2.5 μM) [8] for HAT drug discovery. Subsequently, AEE788 was established as an anti-trypanosomal lead drug [8]. AEE788 forms complexes with three trypanosome protein kinases [9] suggesting that it is a multi-targeted antagonist or agonist [10] whose toxicity to trypanosomes is likely based on exerting pleiotropic biological effects.

Stages of the trypanosome cell division cycle can be identified by enumeration of single copy organelles, including the kinetoplast (mitochondrial nucleoid containing kinetoplast DNA (kDNA)), basal body, and nucleus [11, 12]. In G1, trypanosomes have a single round kinetoplast (K) and a single nucleus (1K1N) [11]. As cells transition into S-phase, synthesis of kDNA (reviewed in [13]) is associated with kinetoplast elongation [14], generating early S-phase cells with a single elongated kinetoplast (Ke) and one nucleus (1Ke1N) [15]. Division of the

kinetoplast precedes mitosis forming a 2K1N population [12]. 2K2N trypanosomes are formed after mitosis which generate 1K1N cells following cytokinesis [11], completing the division cycle (reviewed in [16-18]).

The basal body is the microtubule-organizing center for the flagellar axoneme. Additionally, the basal body is attached to the kinetoplast [19] and has a role in inheritance of the mitochondrial genome [20]. Accordingly, basal body biogenesis is tightly coordinated with the cell division cycle [11, 12, 14]. Prior to duplication, trypanosomes have a mature basal body adjacent to an immature probasal body [11]. Maturation of the probasal body produces cells with two mature basal bodies, each of which seed a new probasal body [11, 14, 21]. No quantitative time-course study of the conversion of putative intermediates into mature basal bodies has been reported.

The flagellum exits the trypanosome cell body via the flagellar pocket [22]. Duplication of the flagellar pocket depends on basal body duplication and separation [21]. Outside the cell body, the flagellar membrane is conjoined to the plasma membrane by the flagellar attachment zone (FAZ) [11, 23]. Cytokinesis requires duplication of the flagellum and its associated cytoskeletal structures [24, 25]. The bilobe is a cytoskeletal structure closely associated with the FAZ filament [26] and is implicated in FAZ formation [27, 28]. The flagellar pocket is the major site of endocytosis, a process needed for nutrient uptake (reviewed in [29]). Bloodstream trypanosomes require host transferrin (Tf), as a source of iron, for proliferation [30]. Interestingly, trypanosome glycogen synthase kinase

(TbGSK3ß), an AEE788-associated protein kinase [9], regulates Tf endocytosis [31].

In our effort to understand the basis of AEE788 toxicity in *T. brucei*, we show that AEE788 blocks S-phase entry of bloodstream trypanosomes, inhibits transferrin endocytosis, and alters cell morphology. Unexpectedly, we found that AEE788 could be used to enrich pre-S-phase trypanosomes. Using a novel "AEE788 block-and-release" protocol we document the kinetics of DNA replication and subcellular organelle duplication in bloodstream trypanosomes. Finally, we show that AEE788 perturbs phospho-protein homeostasis, offering insight into the putative effector proteins involved in AEE788-disrupted phospho-signaling pathways in the African trypanosome.

2.3 Results

AEE788 inhibits kinetoplast duplication

Our primary objective in these studies was to characterize pharmacological effects of AEE788 on bloodstream trypanosomes. To achieve this goal it was necessary to work with higher cell densities, and therefore higher drug concentrations, than previously used in proliferation inhibition assays [8], to provide adequate numbers of trypanosomes for follow-up phenotypic evaluation. We first identified the optimal AEE788 concentration and treatment time for "mode of action" studies (conditions that inhibit proliferation without death, thereby providing an opportunity to characterize disrupted pathways in living cells). We found that AEE788 (5 µM) arrested proliferation between 4 h and 9 h of treatment, but beyond 9 h the drug caused cell density to decrease (Supplemental Figure 2.1). These data indicate

that AEE788 halts bloodstream trypanosome division within a single duplication cycle (~6-7 h) [32, 33].

One hypothesis to explain the inability of cells to proliferate in the presence of AEE788 (Supplemental Figure 2.1) is that trypanosomes fail to progress through a specific point in the division cycle. To determine if AEE788 interfered with the cell division cycle we used DAPI to quantitate the number of kinetoplasts and nuclei per cell. Following a 4 h incubation with AEE788 the proportion of trypanosomes with one round kinetoplast (1K) and a single nucleus (1N) increased, compared to control cells treated with DMSO (drug vehicle) (Figure 2.1A). Quantitation of the percentage of cells with each "karyotype" (i.e. number of kinetoplasts and nuclei) demonstrated that AEE788 caused a statistically significant change in the cell type distribution as compared to the control population (p = 7.4 x 10^{-19}). The proportion of cells with a 1K1N configuration (*i.e.* G1 trypanosomes) increased from 52.2% to 78.2% (Figure 2.1B). Concomitantly, the percentage of cells in S-phase (i.e 1Ke1N cells [15, 34]) dropped from 28.6% to 9.8% (Figure 2.1B). A decrease in the percentage of 2K1N cells, from 13% in the control (DMSO-treated) to 2.7%, after AEE788 treatment indicated that kinetoplast duplication was blocked (Figure 2.1B). In contrast, the proportion of post-mitotic trypanosomes (2K2N) was unchanged during the 4 h AEE788 treatment, implying that mitosis was not affected (Figure 2.1B).

AEE788 prevents DNA synthesis in the kinetoplast and nucleus

Failure of the kinetoplast to elongate following AEE788 treatment (Figure 2.1) led us to hypothesize that the drug impairs kinetoplast DNA (kDNA) synthesis. We

tested this hypothesis by labeling kinetoplast and nuclear DNA with a thymidine analog, 5-ethynyl-2'-deoxyuridine (EdU) [35], in the absence or presence of AEE788 (Figure 2.2A). EdU labeling was performed for 30 minutes to detect newly synthesized DNA. Unlike nuclear incorporation of EdU, which can be visualized throughout the nucleus, kDNA incorporation of EdU is limited to the ends of the kinetoplast DNA network (Figure 2.2A) where newly synthesized minicircles are attached (reviewed in [36]).

In control trypanosomes (treated with DMSO) 23.8% incorporated EdU into the kDNA network (proportional to the number of 1Ke1N cells (Figure 2.1B), while only 5.5% of kinetoplasts in AEE788-treated trypanosomes incorporated EdU (Figure 2.2B). The distribution of replicating and non-replicating kinetoplasts was significantly altered, as compared to control trypanosomes, by AEE788 treatment ($p = 4.9 \times 10^{-4}$). Nuclear DNA synthesis was also inhibited by AEE788 treatment. Only 14% of AEE788-treated trypanosomes incorporated EdU in the nucleus compared to 52.2% in the control (Figure 2.2C), leading to a statistically significant difference in the distribution of S-phase nuclei ($p = 3.1 \times 10^{-19}$). Inhibition of DNA synthesis in both trypanosome DNA-containing organelles suggests that AEE788 impairs entry into S-phase of the cell cycle, as the protein factors and DNA origins needed for DNA replication in the nucleus and kinetoplast differ (reviewed in [13, 37, 38]). In DMSO-treated populations the percentage of cells synthesizing kDNA is approximately 50% of the proportion synthesizing nuclear DNA (Figures 2.2B-2.2C). This observation may be explained by the fact that: (i) the time-course of DNA synthesis differs between kDNA and chromosomal DNA (Figures 2.5B-2.5C)

[12]; and (ii) the sensitivity of EdU detection is higher in the nucleus which contains more DNA [39].

Effect of AEE788 on duplication of the basal body and bilobe

Trypanosomes in G1 have a single mature basal body (mBB) paired with an immature probasal body (pBB) each containing TbSAS6. TbRP2 (recognized by the antibody YL1/2 [40]) is localized to transitional fibers, found only on mature basal bodies [40]. Maturation of the pBB is thought to precede assembly of new ones [11, 14, 21, 41]. Thus, trypanosomes with two mBBs lacking adjacent pBBs (2mBB/0pBB) are thought to arise first as intermediates in biogenesis of the organelle. Subsequently a new pBB is assembled adjacent to each mBB to form 2mBB/2pBB trypanosomes. Migration of each mBB/pBB pair away from each other correlates with scission of the kinetoplast [11, 14, 20, 21]. Given that AEE788 blocked division of the kinetoplast (Figure 2.1) we hypothesized that the drug inhibited basal body duplication. We tested this possibility using immunofluorescence to detect the number of mBBs and pBBs per trypanosome (Figure 2.3A).

The distribution of basal bodies (i.*e*., number of mBBs or pBBs per cell), was skewed towards trypanosomes with unduplicated basal bodies (1mBB/1pBB) after AEE788 treatment (p = 1.3 x 10^{-18}). In a control population (exposed to DMSO) 35.5% of cells had one mBB and one pBB (1mBB/1pBB) (Figure 2.3B). This population doubled to 73.5% following a 4 h treatment with AEE788 (Figure 2.3B). Additionally, the fraction of trypanosomes with 2mBB/2pBB dropped from 54.2% in the control to 21.5% in AEE788-treated trypanosomes (Figure 2.3B).

Infrequently trypanosomes with 1mBB/0pBB or 2mBB/1pBB were detected, likely a staining artifact, and these populations remained the same after DMSO or AEE788 treatment (Figure 2.3B). The data indicates that in the presence of AEE788, targeting of TbRP2 to the second basal body fails, possibly due to (i) absence of new transitional fibers, and/or (ii) inability to deliver TbRP2 to newly matured basal bodies. Further, AEE788 prevents assembly of new TbSAS6-positive pBBs in the absence of TbRP2 recruitment (Figure 2.3B). Together, these data indicate that AEE788 inhibits basal body duplication by interfering with recruitment of proteins to the organelle.

Failure of AEE788-treated trypanosomes to synthesize DNA (Figure 2.2) indicated that the drug blocked entry of trypanosomes into S-phase. The bilobe, a centrin-containing cytoskeletal structure at the base of the flagellum [26], is duplicated in S-phase [16]. We postulated that because AEE788 prevented S-phase entry (Figure 2.2) the drug would inhibit bilobe duplication. We tested this hypothesis by evaluating the effect of AEE788 on bilobe biogenesis using the antibody 20H5, which detects centrins at the bilobe and basal body [42] (Figure 2.4A). AEE788 increased the fraction of trypanosomes with one bilobe from 54.7% to 77.5%, and decreased the proportion of trypanosomes with two bilobes from 45.3% to 22.5% (Figure 2.4B); a significant change in the distribution of cells with unduplicated and duplicated bilobes ($p = 3.6 \times 10^{-9}$). We conclude that AEE788 prevents bilobe duplication.

A time-course for DNA synthesis, and duplication of cytoskeletal organelles during trypanosome division

Experimental measurement of the kinetics of organelle duplication during bloodstream division has been hampered by the technical difficulties of enriching a pre-S-phase trypanosome population [43-46]. Discovery that AEE788 causes a build-up of pre-S-phase trypanosomes (Figures 2.2-2.4) suggested that a "block-and-release" protocol using the drug might be valuable for time-course studies of organelle duplication during trypanosome division.

We first tested whether DNA synthesis would resume upon removal of AEE788 from the trypanosome culture, indicating re-entry into S-phase. For this objective, trypanosomes were treated with AEE788 (5 μM) for 4 h, washed and resuspended in drug-free HMI-9 medium. Following AEE788 withdrawal, cell aliquots were obtained every hour and incubated with EdU [35] for 30 minutes (1 h to 4 h post-AEE788 washout). During the first hour after AEE788 removal, the percentage of trypanosomes that incorporated EdU into the kinetoplast (or nucleus) was similar to that observed immediately following AEE788 treatment (Figures 2.5A-2.5C). However, by 2 h the percentage of cells with EdU-positive kinetoplasts increased from 5%, immediately following AEE788 washout, to 25% (Figures 2.5A-2.5B). Likewise, the number of nuclei which incorporated EdU increased from 12% to 35% (Figures 2.5A and 2.5C). Using a sigmoidal nonlinear regression curve, we estimated a time at which significant DNA synthesis (*i.e*. 10% of the observed maximum (4 h) for EdU-positive kinetoplasts or nuclei) had occurred, designated as T_{10}. Similarly, we defined the time by which the EdU-

positive population increased to 50% (T_{50}) or 90% (T_{90}) compared to the observed maximum (4 h). Initiation of nuclear DNA synthesis (T_{10} = 1.1 h) and kDNA synthesis (T_{10} = 0.9 h) occurred at similar times following AEE788 removal. However, the T_{50} for kinetoplast EdU incorporation (1.5 h) was reached approximately 30 minutes earlier than that of nuclear incorporation (T_{50} = 2.1 h) and it terminated an hour before nuclear DNA synthesis (T_{90} = 2.1 h and 3 h, respectively) (Figures 2.5B and 2.5C). This data is consistent with kinetoplast S-phase terminating prior to completion of nuclear DNA synthesis [12]. We next performed time-course experiments for duplication of the kinetoplast (Figure 2.5D), nucleus (Figure 2.5D), basal body (Figures 2.6A-2.6B), and bilobe (Figures 6D-2.6E).

Kinetoplast elongation (i.e. appearance of 1Ke1N trypanosomes) was observed between 1 h and 4 h post-AEE788 release (T_{10} = 1.4 h; T_{50} = 2.3 h; T_{90} = 3.3 h) (Figure 2.5D). From 1 h to 4 h the fraction of 1Ke1N trypanosomes increased from 5% to 35% (Figure 2.5D and Supplemental Figure 2.2). Correspondingly, by 4 h the 1K1N population was reduced from 77%, immediately following AEE788 withdrawal, to 39% (Figure 2.5D). Kinetoplast division (defined as an increase in the percentage of 2K1N trypanosomes) was observed between 3 h and 4 h when the 2K1N population increased from 5% to 18.2% (T_{10} = 3 h; T_{50} = 3.4 h; T_{90} = 3.9 h) (Figure 2.5D and Supplemental Figure 2.2). Mitosis was detectable between 4 h and 5 h with the number of 2K2N cells increasing from 2.7% to 17% (T_{10} = 3.9 h; T_{50} = 4.4; T_{90} = 5 h), indicating that mitosis can be completed within one hour (Figure 2.5D and Supplemental Figure 2.2). Between 5

h and 6 h the number of 1K1N trypanosomes increased (35.9% to 56.9%), with a simultaneous decrease in all other populations (Figure 2.5D), demonstrating the completion of cytokinesis and the cell division cycle. This data is consistent with the 6-7 h division time observed in bloodstream trypanosomes [32, 33].

Basal bodies were co-stained using the antibody YL1/2 (for TbRP2-positive mature basal bodies (mBB) [40]) and anti-TbSAS6 for mBBs and immature probasal bodies (pBBs) [47] (Figure 2.6A). Immediately following AEE788 withdrawal, the majority of trypanosomes (73.4%) had 1mBB/1pBB, with 25.3% containing 2mBB/2pBB (Figure 2.6B). Between 2 h and 3 h following AEE788 washout, the percentage of trypanosomes with 2mBB/2pBB increased from 24.4% to 56.6% (Figures 2.6A-2.6B). A nonlinear regression analysis indicated that trypanosomes with 2mBB/2pBB emerged 2.3 h (T_{10}) after AEE788 removal and reached the observed maximum by 2.7 h (T_{90}) (Figure 2.6B). Assuming pBB maturation occurs prior to new pBB assembly [11, 14, 21, 41], one would expect to detect trypanosomes with two mBBs but no probasal bodies (2mBB/0pBB). Surprisingly, we detected a small fraction of trypanosomes (>7%) with 2mBB/0pBB (Figure 2.6B). In fact, the kinetics of TbRP2 recruitment (a marker for pBB maturation) and assembly of new pBBs (monitored by TbSAS6) were remarkably similar (Supplemental Figure 2.3). Our data suggest that TbRP2 recruitment to mBBs coincides with, and may be coordinated with, pBB assembly (Figure 2.6C).

Bilobe duplication was examined using the anti-centrin antibody 20H5 [42] (Figure 2.6D). During the first two hours after AEE788 washout, less than 30% of trypanosomes had two bilobes (Figure 2.6E). By 3 h hours 45% of trypanosomes

had two bilobes (T_{10} = 2 h; T_{50} = 2.4 h; T_{90} = 2.6 h) (Figure 2.6E). Thus, bilobe duplication occurs between two and three hours after release from an AEE788 block, coincident with basal body duplication (Figure 2.7).

A summary of the time-course for organelle duplication after AEE788 washout (Figures 2.5 and 2.6) is presented in Figure 2.7 based on the calculated T_{10}, T_{50} and T_{90} for each event. Briefly, kDNA synthesis and nuclear DNA synthesis begin at similar times following AEE788 removal (T_{10} = 0.9 h and 1.1 h, respectively). Kinetoplast elongation (T_{10} = 1.4 h) is detected approximately 30 minutes after the start of kDNA synthesis and coincides with nuclear DNA synthesis (T_{50} = 2.3 h and 2.1 h, respectively). Basal body and bilobe duplication also occur during nuclear DNA synthesis (T_{50} = 2.5 h and 2.4 h, respectively). Termination of kDNA synthesis (T_{90} = 2.1 h) is detected approximately an hour prior to cessation of nuclear S-phase (T_{90} = 3 h). The end of nuclear DNA synthesis marks the start of kinetoplast division (T_{10}= 3 h), which continues for one hour (T_{90} = 3.8). Mitosis is completed within one hour (T_{10} = 3.9 h; T_{90} = 5 h). Lastly cytokinesis occurs between 5 h and 6 h after trypanosomes have entered S-phase.

Trypanocidal effects of AEE788 are associated with endocytosis defects and changes in cell morphology

The ability of trypanosomes to resume division after a 4 h treatment with AEE788 (Figures 2.5-2.6) indicated that trypanosomes did not commit to death during that period of treatment. However, between 9 h and 16 h of AEE788 treatment trypanosome density decreases (Supplemental Figure 2.1). Accordingly, we postulated that extended exposure to the drug was necessary to impair

trypanosome viability. We tested this idea by staining trypanosomes with propidium iodide (PI) which will not enter trypanosomes with an intact plasma membrane [48]. By 4 h, a small proportion of PI-positive trypanosomes (< 0.4%) was observed in the control group (exposed to DMSO) as well as those treated with AEE788 (Figure 2.8). After 9 h of drug treatment, however, 16.5% of AEE788-treated trypanosomes (compared to 1.5% in the DMSO-treated control) were positive for PI uptake, and by 16 h half of the population stained with PI (Figure 2.8). We conclude that beyond 9 h of treatment, AEE788 (5 μM) decreases trypanosome viability.

AEE788 associates with three trypanosome protein kinases [9]. As such the drug is likely to exert pleiotropic effects on trypanosome biology as a multi-targeted kinase modulator. One AEE788-associated protein, TbGSK3ß [9], regulates transferrin endocytosis [31]. We therefore tested if AEE788 (5 μM) affected trypanosome endocytic pathways. Ligands internalized through glycosylphosphatidylinositiol (GPI) anchored-receptors, such as the transferrin receptor [49], follow a distinct endocytic pathway [50]. We studied the effect of AEE788 treatment on internalization of three endocytic cargos. Transferrin was used for receptor-mediated endocytosis; bovine serum albumin (BSA) was a marker for bulk-phase endocytosis [31, 51]; and tomato lectin (TL) was used to evaluate internalization of carbohydrate-binding proteins [52, 53]. Fluorescent cargo was used to monitor endocytosis following a 9 h treatment with DMSO (drug solvent) or AEE788 (washed off prior to incubation with cargo). Propidium iodide exclusion was used to gate for viable cells (Figure 2.9A) before fluorescence

intensity of endocytic cargo was measured (Figures 2.9B-2.9D). Based on the median fluorescence intensity, AEE788 decreased transferrin endocytosis by 87% (Figure 2.9B) (p = 2.8 x 10^{-3}), but increased BSA internalization by 40% (Figure 2.9C) (p = 3.1 x 10^{-3}), without affecting TL uptake (Figure 2.9D) (p = 0.9). Each cargo demonstrated a unique distribution of fluorescence intensity (proportional to the amount of cargo internalized) within the population (Figures 2.9B-2.9D). For reasons that are unclear to us, AEE788 broadened the distribution of fluorescence associated with BSA or TL internalization (Figures 2.9C-2.9D). These results demonstrate that trypanosomes are metabolically active after 9 h of exposure to AEE788, and that transferrin endocytosis is selectively inhibited.

AEE788 caused morphological changes in trypanosomes in a time-dependent manner (Figure 2.10A). Most trypanosomes had normal morphology following a 4 h treatment with AEE788 (5 μM). However, by 9 h the distribution of trypanosomes with altered morphology or normal shape shifted towards swollen and rounded cells, compared to that found after 4 h of AEE788 treatment (p = 6.6 x 10^{-17}). By 16 h the majority of AEE788-treated trypanosomes had changed morphology, compared to trypanosomes after a 4 h treatment (p = 1.1 x 10^{-64}) or after the 9 h treatment (p = 5.6 x 10^{-25}). Flagella of rounded trypanosomes were not observed by light microscopy (Figure 2.10A). Despite this fact, no detached flagella were detected in the culture medium. This fact prompted us to use alternative methods to detect flagella on rounded trypanosomes. Employing markers for the flagellum (anti-centrin antibody 20H5 [54]) and paraflagellar rod [55] (anti-PFR2) we detected flagella juxtaposed to the periphery of rounded

trypanosomes (Figure 2.10B). The presence of flagella outside rounded trypanosomes was confirmed by scanning electron microscopy (Figure 2.10C).

Changes in phospho-protein homeostasis in AEE788-treated trypanosomes

The presence of AEE788 in complexes with trypanosome protein kinases [9] prompted us to determine whether AEE788 could alter phospho-protein homeostasis in the parasite. We used IMAC enrichment of phospho-peptides, combined with LC-MS/MS, to identify changes in the abundance of protein phosphorylation following trypanosome exposure to AEE788. Because there are phenotypic differences associated with short-term (4 h) as compared to long-term (9 h) AEE788 treatment, we examined trypanosome phospho-peptides obtained after both treatment times. A total of 244 trypanosome peptides (176 unique proteins) showed a 2-fold, or greater, change in phosphorylation after AEE788 treatment (Supplemental Tables 2.1-2.4), confirming that AEE788 influences protein phosphorylation in T. brucei.

After 4 h of AEE788 treatment, 56 unique trypanosome peptides showed decreased phosphorylation and 21 demonstrated increased phosphorylation (Supplemental Tables 2.1 and 2.3). Proteins with decreased phosphorylation after 4 h of AEE788 treatment include a serine-arginine protein kinase (SRPK) (reviewed in [56]), TbSAS4 [57] and a bilobe protein [58] (Table 2.1). Proteins with increased phosphorylation include a protease (calpain-like cysteine peptidase) (Table 2.1).

After 9 h of AEE788 (5 μM) treatment, 115 trypanosome peptides with decreased phosphorylation and 52 peptides with increased phosphorylation were

identified (Supplemental Tables 2.2 and 2.4). Thus, extended exposure to AEE788 affected more peptides (167) than the 4 h treatment (77). Proteins with decreased phosphorylation following a 9 h exposure to AEE788 include a NIMA-related kinase (NEK) (reviewed in [59]), the basal body protein TbRP2 [40], a bilobe protein [58] and a flagellar pocket protein BILBO-1 [60] (Table 2.2). Proteins with increased phosphorylation include a Tb14-3-3-associated kinase (TbAKB1 [61]), a bilobe protein [58], and a ubiquitin-transferase (Table 2.2).

In some cases, the abundance of the phosphorylated peptide, as well as, the abundance of the parent protein (number in parentheses of Tables 2.1-2.2) changed. In most cases the magnitude of change in phospho-peptide abundance exceeds that observed for total protein abundance (*e.g.*, Tb427.01.2100 (Table 2.1) and Tb427.03.3080 (Table 2.2). This data may indicate that phosphorylation influences stability of some trypanosome proteins, as observed in other eukaryotes [62-66]. Additionally, the altered phosphorylation of proteins involved in protein degradation (Tables 2.1-2.2 and Supplemental Tables 2.1-2.4) may influence protein abundance.

2.4 Discussion

A new tool for identification of S-phase regulators in bloodstream trypanosomes

S-phase is the period of DNA synthesis by the replisome (reviewed in [67]). DNA replication is restricted to S-phase to ensure that the genome is replicated only once per division cycle [68]. Kinetoplastids are early branching eukaryotes with a divergent genome [69, 70] and signaling pathways responsible for entry into S-phase are not fully defined in bloodstream trypanosomes (reviewed in [38]). In

higher eukaryotes the Dbf4-dependent kinase (DDK) [71-73] and S-phase cyclin dependent kinase (S-CDK) [73, 74] promote initiation of DNA synthesis. Trypanosomes lack homologs of the DDK complex, and trypanosome homologs to cyclin-dependent kinases (TbCRKs), do not regulate DNA replication in bloodstream trypanosomes; knockdown of TbCRK1 and TbCRK2 arrests procyclic (insect stage) trypanosomes in G1, but does not prevent DNA synthesis in bloodstream trypanosomes [75-77].

AEE788 prevents trypanosome entry into S-phase by inhibiting DNA synthesis in the kinetoplast and nucleus (Figure 2.2). Accordingly, by combining our phenotypic analysis with the identification of AEE788-affected phospho-proteins (Supplemental Tables 2.1-2.4) we envision the use of AEE788 as a small-molecule tool to identify novel proteins (from effectors of the drug's action observed at 4 h (Supplemental Tables 2.1 and 2.3) that regulate S-phase entry in bloodstream trypanosomes. In this strategy, proteins that are dephosphorylated (or hyperphosphorylated) will be knocked down (or overexpressed) genetically to determine their effect on DNA synthesis.

Kinetics of organelle duplication and protein recruitment to the basal body during trypanosome division

A novel strategy using AEE788 in a "block-and-release" protocol was used to enrich pre-S-phase trypanosomes and to study the time-course of organelle duplication in the bloodstream stage parasites (Figures 2.5-2.7). Previous studies of basal body duplication in insect stage trypanosomes identified two groups of 1Ke1N cells based on probasal body formation: (i) 1Ke1N cells with two mBBs

each lacking a pBB (*i.e.,* 2mBB/0pBB); and (ii) 1Ke1N cells with two mBBs paired with adjacent pBBs (*i.e.*, 2mBB/2pBB) [11, 14, 21, 41]. In our quantitation of SAS6/RP2 double-labeled basal bodies, we found less than 7% of trypanosomes with 2mBB/0pBB (Figure 2.6B). The data indicates that 2mBB/0pBB is not a major intermediate for basal body duplication in bloodstream trypanosomes (Figure 2.6C). This conclusion is reinforced by our observation that during duplication of basal bodies, TbRP2 is recruited to mBBs with the same kinetics as TbSAS6 localization at nascent pBBs (Figure 2.6B and Supplemental Figure 2.3). Hence, recruitment of TbRP2 to mBBs is concurrent with new pBB formation. Our observations establish the utility of AEE788 as a small-molecule tool for monitoring the order of protein recruitment during basal body biogenesis (and perhaps of other cytoskeletal organelles).

Our data additionally provides new insight on the sequence of S-phase events; DNA replication, with respect to organelle duplication in bloodstream trypanosomes. We found that kinetoplast elongation occurs throughout nuclear DNA synthesis, consistent with the annotation of 1Ke1N trypanosomes as S-phase cells [15] (Figure 2.7). Second, duplication of the basal body and bilobe are coincident (consistent with the idea of a continuous cytoskeletal network containing both organelles [78]). Duplication of these cytoskeletal structures occurs after kDNA synthesis, but is concurrent with nuclear S-phase and kinetoplast elongation (both of which initiate approximately 30 minutes prior to duplication of the basal body and bilobe) (Figure 2.7). Third, kinetoplast division does not occur immediately after kDNA synthesis, but is observed one hour after termination of

kDNA replication. During the intervening period the basal body is duplicated. This lag between kDNA replication and kinetoplast division may reflect (i) a requirement of two basal bodies to facilitate kinetoplast fission [20, 21], (ii) a slow assembly of factors needed for kinetoplast division, or both. Nuclear DNA synthesis was completed before kinetoplast division (Figure 2.7), revealing that 2K1N trypanosomes are most likely in G2, in accordance with previous work [12, 15]. Mitosis was observed one hour after replication of the nuclear genome, implying that the trypanosome G2 lasts one hour during which kinetoplast division occurs.

Selective inhibition of endocytosis by AEE788

Extended AEE788 treatment (9 h) of trypanosomes inhibited transferrin endocytosis (Figure 2.9B). Interestingly, not all trypanosome endocytic pathways were affected by AEE788 treatment. Internalization of BSA, a marker for fluid phase endocytosis [51], was increased after AEE788 treatment (Figure 2.9C). A similar effect was observed after knockdown of TbGSK3ß [31]. Future studies will address the basis of AEE788's ability to selectively inhibit transferrin endocytosis (Figure 2.9) by knocking down (or overexpressing) putative effectors of the drugs action (Table 2.2, Supplemental Tables 2.2 and 2.4).

Putative effectors of AEE78 action

AEE788 treatment of trypanosomes caused dephosphorylation of some proteins, but resulted in hyperphosphorylation of others (Tables 2.1-2.2 and Supplemental Tables 2.1-2.4). Small molecule kinase inhibitors can paradoxically lead to hyperphosphorylation of proteins [79, 80] through a variety of mechanisms

including; protection of their target from protein phosphatases [81], increasing [82] or decreasing [80] inhibitory autophosphorylation, and activation of negative feedback loops [83].

Proteins with altered phosphorylation after 4 h of AEE788 treatment (Table 2.1) may be involved in biological pathways disrupted during short-term AEE788 exposure (4 h). They might be effectors for S-phase entry (Figure 2.2) or duplication of the basal body (Figure 2.3) and bilobe (Figure 2.4). Of note, a cytoskeletal protein TbSAS4 and a bilobe protein (Tb427.10.3010 [58]) were dephosphorylated (Table 2.1). In other organisms SAS4 is a centriolar protein [84] with essential roles in centriole duplication [85-89]. The role of TbSAS4 in bloodstream trypanosomes remains to be explored.

Extended exposure (9 h) of trypanosomes to AEE788 inhibited transferrin endocytosis (Figure 2.9) and distorted cell morphology (Figure 2.10). These phenotypes may be explained by postulating that two proteins with altered phosphorylation, namely, Tb14-3-3-associated protein kinase (TbAKB1 [61]) (Table 2.2) and BILBO-1 [60] (Table 2.2), are effectors of AEE788 action. Knockdown of Tb14-3-3 reduces the size of recycling endosomes [90], and knockdown of BILBO-1 causes rounding of bloodstream trypanosomes [60], comparable to the morphology of *T. brucei* observed after prolonged AEE788 treatment (Figure 2.10).

The relative abundance of phospho-peptides in DMSO-treated cells (drug vehicle control) and AEE788-treated trypanosomes was determined by spectral counting of LC-MS/MS data. Spectral counting (reviewed in [91]) has been used

to document changes in protein expression [92-94] and phosphorylation [95-97]. However, there are limitations associated with this method: the dynamic range is poor for proteins of low abundance [92]. Additionally, reproducibility of data may be compromised by non-identical sampling of peptides between instrument runs (*e.g.,* control versus experimental). The latter issue is mitigated by replicate runs and statistical analysis to improve confidence in identifying changes in protein levels between controls and experimental samples. Zhang et al showed that the Student's t-test offers the lowest false positive rate (> 1%) for triplicate replicates (used in our analysis) when the fold-change in spectra is greater than two [98]. We reported proteins which were observed in three independent experiments and showed a statistically significant change in levels of phosphorylation as determined by Student's t-tests.

The functions of many phospho-proteins affected by AEE788 are unknown in bloodstream trypanosomes. Hence correlation of their dephosphorylation with the disruption of essential physiological trypanosome pathways, generates hypotheses as to the function of these uncharacterized phospho-proteins. In the future, we will focus on determining the role of these unstudied proteins in: (i) AEE788-perturbed pathways (Figures 2.2-2.4 and 2.9-2.10); and (ii) how their phosphorylation may modulate their biological functions.

2.5 Materials and Methods

Parasite cultures

Bloodstream *T. brucei*, RUMP528 [99] or Lister 427, were cultured in HMI-9 medium supplemented with 10% Fetal Bovine Serum (Atlanta Biologicals; Flowery

Branch, GA), 10% Serum Plus™ (SAFC Biosciences; Lenexa, KS) and 1% antibiotic-antimycotic solution (Corning; Corning, NY) at 37 °C, 5% CO_2 [100]. For all experiments trypanosomes were harvested in logarithmic phase (i.e. less than 1 x 10^6 cells/ml).

Time-dependent inhibition of trypanosome proliferation at a cytostatic concentration of AEE788

T. brucei were resuspended at 5 x 10^5 cells/ml (5 ml), in a Corning 25 cm^2 culture flask, and treated with AEE788 (Novartis; Basel, Switzerland) to achieve a final concentration of 5 µM or equal volume (0.1%) of the drug solvent DMSO (Thermo Fisher; Waltham, MA). Cells were incubated at 37 °C, 5% CO_2. Trypanosome density was measured with a haemocytometer after 4 h, 9 h and 16 h of incubation. Both sides of the haemocytometer were counted twice and averaged for every time point. Biological replicates were performed twice.

DAPI staining of DNA in the kinetoplast and nucleus following AEE788 treatment

T. brucei (5 x 10^5 cells/ml) was treated with AEE788 (5 µM), or equal volume (0.1%) DMSO (drug solvent) for 4 h at 37 °C, 5% CO_2. Treated cells were pelleted (3000 x g for 5 min), resuspended in 1 ml of 4% paraformaldehyde (Affymetrix; Santa Clara, CA) in phosphate-buffered saline (Thermo Fisher), and incubated for 15 min at room temperature. Cells were pelleted by centrifugation, as described previously, and adhered to poly-L-lysine (Sigma Adlrich; St. Louis, MO) coated coverslips for 15 min. Coverslips were briefly washed with phosphate-buffered saline (PBS) before being mounted onto microscope slides with VectaSheild® Mounting Medium (Vector Labs; Burlingame, CA), containing 1.5 µM 4',6-

diamidino-2-phenylindole (DAPI) to stain nuclear and kinetoplast DNA. Trypanosomes were visualized with a high sensitivity interline camera on an EVOS fluorescence (EVOS® FL) microscope (Life Technologies; Grand Island, NY). The number of kinetoplasts and nuclei per cell, in 150 trypanosomes, were scored in four independent experiments.

Time-course for duplication of the kinetoplast and nucleus

Following a 4 h treatment with AEE788 (5 μM), trypanosomes were washed twice and resuspended in drug-free HMI-9 medium (5 x 10^5 cells/ml). Cells were returned to an incubator (37 °C, 5% CO_2) for 1 h, 2 h, 3 h, 4 h, 5 h or 6 h. Cells were fixed and stained with DAPI as described above. Trypanosomes (150) were scored based on their number of kinetoplasts and nuclei (n = 3 for each time point).

Detection of DNA synthesis with 5-ethynyl-2'-deoxyuridine (EdU)

Bloodstream trypanosomes (5 x10^5 cells/ml) were treated with AEE788 (5 μM) or DMSO (0.1%) for 4 h at 37 °C, 5% CO_2. EdU (5-ethynyl-2'-deoxyuridine) (300 μM) (Life Technologies), and 2'-deoxycytidine (200 μM) (Sigma Adlrich), were added to both DMSO and AEE788-treated samples 3.5 h into the 4 h treatment (i.e. 30 min labeling period). Following the 4 h incubation, cells were washed once in phosphate-buffered saline supplemented with 1% glucose (PBSG), fixed with 4% paraformaldehyde (PFA) in PBS (15 min), adhered to poly-L-lysine coated coverslips, and permeabilized with 0.5% Triton X-100 (Thermo Fisher) in PBS for 25 min at room temperature. Permeabilized trypanosomes were washed with PBS and incubated in the dark for 30 min in a click-iT reaction cocktail: 4 mM copper

sulfate (Sigma Adlrich); 60 μM azide conjugated to Alexa Fluor® 488 (Life Technologies); 1 x Tris-buffered saline (20 mM Tris base (Genesee Scientific; San Diego, CA) and 0.14 M NaCl (Sigma Adlrich)); and 300 mM ascorbic acid (Avantor Performance Materials; Center Valley, PA). Cells were washed thrice in PBS (3 min each) before mounting with VectaSheild® Mounting Medium, containing DAPI (1.5 μM), onto microscope slides. Cells were visualized by fluorescence microscopy on the Applied Precision DeltaVision II Microscope System (GE Healthcare; Issaquah, WA) on an Olympus IX-71 inverted microscope (Olympus; Center Valley, PA). Images were captured with a cooled CCD camera. The kinetoplast and nucleus of each trypanosome (n = 100-150) were characterized as EdU-positive or EdU-negative in three independent experiments.

Time-course of DNA synthesis

Trypanosomes were treated for 4 h with AEE788 (5 μM), washed twice and resuspended in drug-free HMI-9 medium (5 x 10^5 cells/ml). Trypanosome aliquots (2 x 10^6 cells) were harvested every hour over a three-hour time-course (1 h to 4 h post AEE788 washout) and incubated in medium containing EdU (300 μM) and 2'-deoxycytidine (200 μM) for 30 min (37 °C, 5% CO_2). Cells were subsequently processed as described above. Cells were first collected from 0 h – 4 h after AEE788 washout to identify the range of DNA synthesis. Subsequently trypanosomes were harvested from 0 h to 3 h post AEE788 wash off (n = 3) to monitor initiation of DNA synthesis. Additionally, cells were collected between 2 h – 4 h after AEE788 washout (n = 2) in attempts to detect termination of DNA synthesis. The kinetoplast and nucleus of 100-150 trypanosome were scored as

EdU-positive or EdU-negative at each time point for all experiments (0 h and 2 h, n = 6; 1 h, n = 4; 3 h and 4 h, n = 3).

Immunofluorescence detection of basal bodies and bilobes

Trypanosomes (5 x 10^5 cells/ml) were treated with AEE788 (5 μM) or an equal volume (0.1%) of DMSO (drug solvent) for 4 h at 37 °C, 5% CO_2. Cells were washed once with PBSG, and adhered to poly-L-lysine coated coverslips for 5 min, quickly air-dried, and fixed with methanol (Thermo Fisher) for 20 min at -20 °C. Coverslips were briefly rinsed with PBS and rehydrated in blocking buffer (1% bovine serum albumin (BSA) (Sigma Aldrich) in PBS) for 1 h. Permeabilized trypanosomes were either co-stained with the primary antibodies YL1/2 (EMD Millipore; Billerica, MA) [40] and anti-TbSAS6 [47] to detect basal bodies or stained with 20H5 (EMD Millipore) [42] for bilobes. The TbSAS6 antibody was a generous gift from Dr. Ziyin Li (University of Texas Health Science Center). Antibodies were diluted (YL1/2 at 1:1000; anti-TbSAS6 and 20H5 at 1:500) in blocking buffer and incubated with cells for 1 h at room temperature. Cells were rinsed thrice, 5 minutes each, in PBS prior to exposure to the secondary antibody at a dilution of 1:2000 in blocking buffer for 1 h at room temperature: Alexa Fluor® 488 goat anti-rat and Alexa Fluor® 594 goat anti-rabbit or Alexa Fluor® 488 goat anti-mouse, respectively (Molecular Probes; Eugene, OR). Cells were rinsed three times, 5 minutes each, in PBS and mounted onto microscope slides with VectaSheild® Mounting Medium supplemented with DAPI (1.5 μM). Cells were then visualized with a DeltaVision Microscope System II, at the Biomedical Microscopy Core (BMC) at the University of Georgia, and images captured with a cooled CCD camera. The number of basal

bodies and bilobes were quantitated in three independent experiments (100-150 trypanosome quantitated per experiment). Basal bodies were considered mature if they were co-labeled with YL1/2 and anti-TbSAS6 or if they were labeled by YL1/2 alone. Basal bodies labeled solely by anti-TbSAS6 were counted as probasal bodies.

Time-course of basal body and bilobe duplication

Trypanosomes (5 x 10^5 cells/ml) were treated with AEE788 (5 μM), for 4 h (37 °C, 5% CO_2), washed twice in drug-free HMI-9 medium and resuspended in drug-free medium. Cells were returned to the incubator for 0 h, 2 h, 2.5 h, 3 h or 3.5 h, collected and prepared for immunofluorescence assays as described above (YL1/2 and anti-TbSAS6 double labeling or 20H5 staining). The time-course was repeated in three independent experiments with the number of basal bodies (in YL1/2 and anti-TbSAS6 stained cells) and bilobes (in 20H5 stained cells) assessed in 100-150 trypanosomes at each time point for all experiments.

Analysis of time-course studies using nonlinear regression curve fitting

Nonlinear regression curves were applied to time-course data documenting the recovery of DNA synthesis and organelle duplication (kinetoplast, basal body, bilobe and nucleus) following an "AEE788 block-and-release" protocol (see above) using GraphPad Prism. GraphPad was used to calculate the time at which 50% (T_{50}) of the maximum activity (*e.g.* DNA synthesis) was achieved based on a sigmoidal function. Calculations for kinetoplast elongation (measured by the percentage of 1Ke1N cells) and cytokinesis (based on the reappearance of 1K1N

cells) were based on time points between 0 h – 4 h, and 5 h – 6 h, respectively, when the minimum and maximum for these events were observed (a 3rd order polynomial nonlinear regression was used to show data trends for these events). Based on the T_{50} and the Hill slope (provided by GraphPad Prism), we calculated the time at which 10% (T_{10}) and 90% (T_{90}) of the maximum was achieved using the following equation provided by GraphPad Software: $T_x = ((x/100\text{-}x)^{1/H})T_{50}$ where H = Hill slope and x = the desired percentage (of maximum).

Assessment of cell viability following AEE788 treatment

Trypanosomes (5 x 10^5 cells/ml) were treated with AEE788 (5 μM) or equal volume (0.1%) DMSO (drug solvent) for 4 h, 9 h, or 16 h. Thereafter, cells from each treatment group (1 ml each) were aliquoted into 1.5 ml microcentrifuge tubes and treated with propidium iodide (3 μM) (Sigma Aldrich). Cells were immediately incubated on ice for 15 min and analyzed using a Beckman Coulter Cyan flow cytometer to measure propidium iodide fluorescence. FlowJo software (FlowJo, LLC; Ashland, OR) was used to gate live cell populations based on size and shape (forward and side scatter) and to quantitate the fluorescence intensity of propidium iodide in 10,000 trypanosomes (n = 2).

Evaluation of trypanosome endocytosis of transferrin (Tf), bovine serum albumin (BSA) and tomato lectin (TL)

Trypanosomes were treated with AEE788 (5 μM) or equal volume (0.1%) DMSO (drug solvent) for 9 h (37 °C, 5% CO_2). Cells were washed and resuspended in serum-free HMI-9 medium devoid of AEE788 or DMSO (5 x 10^5 cells/ml).

Trypanosomes were incubated with fluorescent endocytic cargo for 15 min at 37 °C, 5% CO_2: 25 µg Tf-Alexa Fluor® 488 Conjugate (Thermo Fisher), 25 BSA labeled with Alexa Fluor® 647 (Thermo Fisher), or 10 µg DyLight® 488-TL (Vector Laboratories). Cells were subsequently transferred to an ice-water bath and washed with cold PBSG at 4 °C (3000 x g for 5 min). Cells were resuspended in 1 ml PBSG, with propidium iodide (3 µM), as a marker for non-viable cells, and analyzed on the Beckman Coulter Cyan flow cytometer. FlowJo software (FlowJo, LLC) was used to gate viable trypanosome populations, based on size, shape (forward and side scatter) and propidium iodide exclusion. Fluorescence intensity of endocytic cargo was measured only in viable cell populations (negative for propidium iodide uptake). FlowJo was then used to determine the median fluorescence intensity of each endocytic cargo in trypanosome populations (15,000 events, n = 3).

Quantitation of changes in trypanosome morphology

Trypanosomes (5 x 10^5 cells/ml) were treated with AEE788 (5 µM) or equal volume (0.1%) DMSO (drug solvent) for 4 h, 9 h, or 16 h. After each incubation period cells were transferred to a haemocytometer and visualized (live) with an EVOS XL Core microscope (Thermo Fisher). Cells (100/incubation period) were scored based on morphology in two independent experiments.

Immunofluorescence detection of the paraflagellar rod (PFR) and flagellum

Trypanosomes (5 x 10^5 cells/ml) were treated with DMSO or AEE788 for 16 h (37 °C, 5% CO_2), washed with PBSG and adhered to poly-L-lysine coated coverslips

(5 min). Once adhered, cells were quickly air-dried and fixed with methanol for 20 min at -20 °C. Cells were rehydrated in blocking buffer (PBS supplemented with 1% BSA) for 1 h. Subsequently, trypanosomes were incubated with anti-PFR2 (1:500) and 20H5 (1:500) in blocking buffer for 1 h at room temperature. The polyclonal rabbit antibody against PFR2 was generated by GenScript® (Piscataway Township, NJ). Trypanosomes were washed three times, 5 min each, in PBS before addition of fluorescent secondary antibodies (1:2000 in blocking buffer) for 1 h at room temperature (Alexa Fluor® 488 goat anti-rabbit or Alexa Fluor® 594 goat anti-mouse, respectively). Cells were washed three times in PBS, 5 min each, prior to mounting onto microscope slides with VectaSheild® Mounting Medium containing DAPI (1.5 µM). Cells were visualized by fluorescence microscopy on an Applied Precision DeltaVision II Microscope System (GE Healthcare; Issaquah, WA) with an Olympus IX-71 inverted microscope (Olympus; Center Valley, PA). Images were captured with a cooled CCD camera.

Scanning Electron Microscopy

T. brucei (5×10^5 cells/ml) were treated with AEE788 (5 µM) for 12 h in HMI-9 medium. Cells were centrifuged (1500 x g for 5 min) and washed with ice-cold PBSG. Cells were fixed with 2% glutaraldehyde in PBS for 1 h at room temperature, washed with PBS and adhered to poly-L-lysine coated coverslips. Cells on coverslips were treated with OsO_4 (1%) for 30 min at RT, washed thrice in water and dehydrated with increasing concentrations of ethanol by incubating them sequentially in 25%, 30%, 50%, 75%, 85%, 95%, and 100% ethanol for 5 min each. The samples were dried at critical point with a Tousimis Critical Point

Dryer (Samdri-780 A), and sputter coated (gold) with an SPI Module Sputter Coater following standard protocols. Samples were viewed using a Zeiss 1450EP variable pressure scanning electron microscope at the Center for Advanced Ultrastructural Research (CAUR) at the University of Georgia.

Phospho-peptide enrichment and identification in AEE788-treated trypanosomes

Trypanosomes (5 x 10^5 cells/ml) were treated with either AEE788 (5 μM) or equivalent volume (0.1%) DMSO (drug solvent) at 37 ºC (4 h or 9 h). Trypanosomes (2 x 10^8 cells) were moved to ice, washed with cold PBSG containing 1X HALT Phosphatase Inhibitor Cocktail (PIC)(Thermo Fisher), lysed by sonication in 50 mM HEPES (Thermo Fisher), pH 7.6, 8 M urea (Thermo Fisher), 4 mM DTT (Sigma Aldrich), 1X HALT PIC and alkylated with 9 mM iodoacetamide (Bio-Rad; Hercules, CA) for 30 min (away from light). The lysate was diluted 5-fold with 50 mM HEPES, pH 7.6, and 1X HALT PIC (1.6 M urea final) followed by protein digestion with immobilized trypsin agarose (Thermo Fisher) for 48 at room temperature. After collecting the beads by centrifugation, the peptide supernatant was diluted 10-fold with 0.1% trifluoroacetic acid (TFA) (Thermo Fisher) and desalted over a Sep-Pak C18 column (Waters; Milford MA). A step gradient of acetonitrile (25% followed by 50%) (Thermo Fisher) was used to elute peptides. Eluates were dried via vacuum centrifugation. Phospho-peptides were then enriched by $FeCl_3$ charged metal affinity chromatography (IMAC) made in-house (Proteomics core at Fred Hutchinson Cancer Research Center). Briefly, peptide samples were resuspended in 80% acetonitrile, 0.1% TFA and loaded onto $FeCl_3$ charged IMAC resin (10 μl bed volume). The resin was washed three times

with 150 µl of 80% acetonitrile in 0.1% TFA, then a final wash of 1% TFA (150 µl). The peptides were eluted twice (3 min each) with 150 µl of 500 mM potassium phosphate (pH 7), and desalted using ZipTip™ C18 (Millipore Corporation; Billerica, MA) before MS analysis.

LC-MS/MS analysis was performed with an Easy-nLC 1000 (Thermo Scientific) coupled to an Orbitrap Elite mass spectrometer (Thermo Scientific). The LC system was configured in a vented format [101] consisting of a fused-silica nanospray needle (PicoTip™ emitter, 50 µm ID, New Objective) packed in-house (Fred Hutchinson Proteomics Facility) with Magic C18 AQ 100Å reverse-phase medium (Michrom Bioresources Inc.) (25 cm), and a trap (IntegraFrit™ Capillary, 100 µm ID, New Objective) containing Magic C18 AQ 200Å (2 cm). The peptide sample was diluted in 10 µl of 2% acetonitrile and 0.1% formic acid in water and 8 µl was loaded onto the column for separation using a two-mobile-phase system consisting of 0.1% formic acid in water (A) and 0.1% acetic acid in acetonitrile (B). A 60 or 90-minute gradient from 7% to 35% acetonitrile in 0.1% formic acid at a flow rate of 400 nl/minute was used for chromatographic separation. The mass spectrometer was operated in a data-dependent MS/MS mode over the m/z range of 400-1800 at the 240,000 mass resolutions. For each cycle, the 20 most abundant ions from the scan were selected for MS/MS analysis using 35% normalized collision energy. Selected ions were dynamically excluded for 30 seconds.

Raw MS/MS data were analyzed with Proteome Discoverer software v 1.4 (Thermo Fisher) using SEQUEST [102] as a search engine against TriTrypDB

database version 4.1 (from TritrypDB.org), which included common contaminants such as human keratin. The database contained 8,614 protein entries including contaminants. The following modifications were considered: carbamidomethylation of cysteine as a fixed modification; phosphorylation of serine, threonine, tyrosine, and oxidation of methionine as variable modifications. The enzyme was set to trypsin allowing up to 2 missed cleavages. The precursor and fragment mass tolerances were set to 10 ppm and 0.6 Da respectively. Search results were run through Percolator [103] for scoring. The results were filtered for peptides identified with a false discovery rate lower than 0.05. Phosphorylation sites were evaluated and probability values were calculated using phosphoRS v. 3.1 [104]. Specific phosphorylation sites in Tables 2.1-2.2 and supplemental tables 2.1-2.4 were assigned if the PhosphoRS probability for the site was 80% or greater.

Statistical Analysis

To quantitate the effect of AEE788 on organelle (basal body, bilobe, nucleus, kinetoplast) duplication and trypanosome morphology, the distribution of cells was grouped according to organelle content per trypanosome, or trypanosome shape after treatment with drug or DMSO. To determine if AEE788 caused statistically significant changes in these distributions we compared the distribution obtained after exposure to AEE788 to that observed after treatment with DMSO (*i.e.,* control) using the Pearson chi-squared test of independence ($\alpha = 0.0005$).

A two sample Student's t-test was used to compare the median fluorescence of endocytosed cargo (measure of internalization) between DMSO and AEE788-treated cells ($\alpha = 0.005$).

Figure 2.1. *AEE788 blocks kinetoplast elongation and division*. Trypanosomes (5 x 10^5 cells/ml) were treated with AEE788 (5 μM) or DMSO (0.1%), in HMI-9 medium, for 4 h. Cells were fixed in paraformaldehyde and the kinetoplast and nuclear DNA stained with DAPI. The number of kinetoplasts and nuclei in 150 trypanosomes were quantitated. (***A***) Representative images of DAPI-stained trypanosomes after treatment with DMSO (top) or AEE788 (bottom). The scale bar is 6 μm. (***B***) The average percentage of trypanosomes within each kinetoplast (K) and nucleus (N) configuration are shown. Ke = elongated kinetoplast. Error bars represent standard deviation between 4 biological replicates. The distribution of kinetoplasts and nuclei (per trypanosome) in DMSO-treated and AEE788-treated cells was compared using a Pearson chi-squared test (p = 7.4 x 10^{-19}).

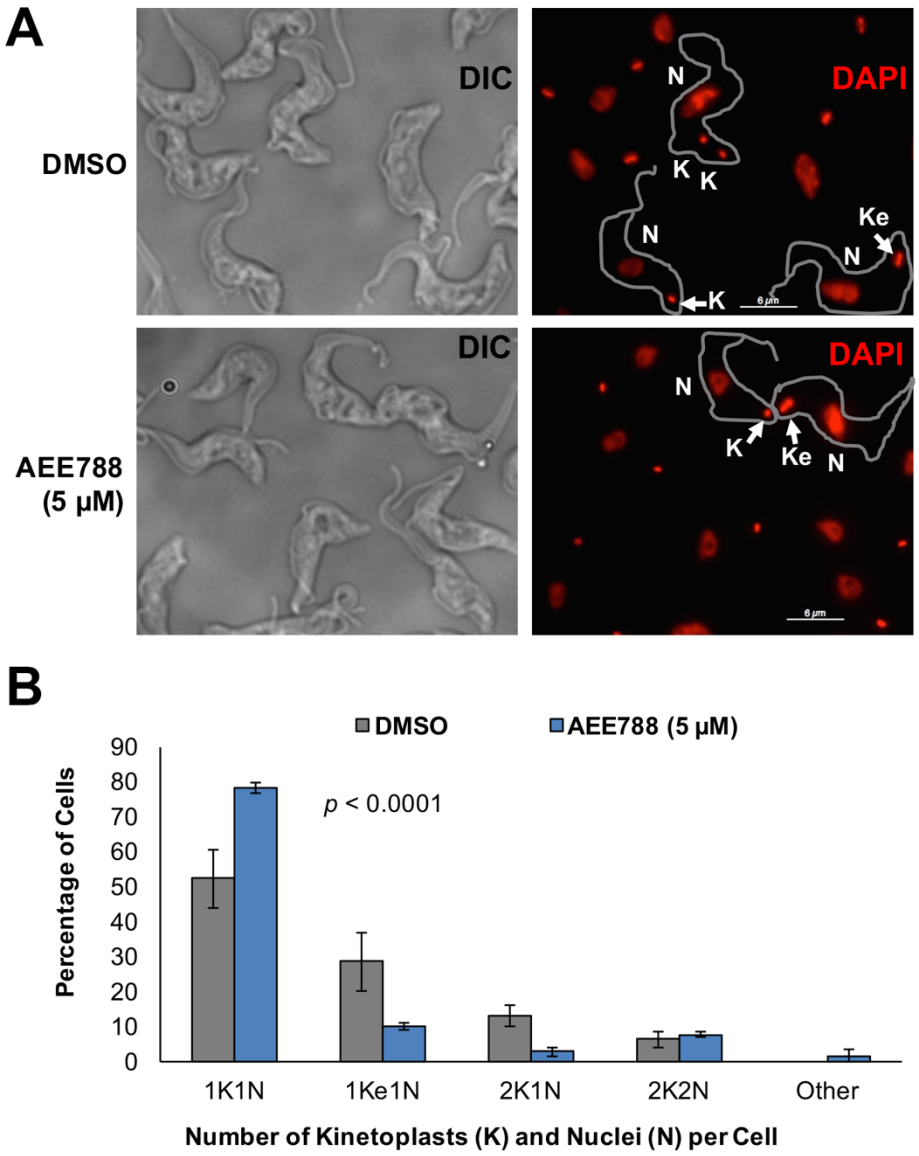
A
DMSO
AEE788
(5 μM)
DIC
DAPI
N
K
Ke
6 μm
B
DMSO
AEE788 (5 μM)
p < 0.0001
Percentage of Cells
90
80
70
60
50
40
30
20
10
0
1K1N
1Ke1N
2K1N
2K2N
Other
Number of Kinetoplasts (K) and Nuclei (N) per Cell

Figure 2.2. *AEE788 decreases DNA synthesis in the kinetoplast and nucleus*. Trypanosomes were treated with AEE788 (5 μM) or DMSO (0.1%) for 4 h. 5-ethynyl-2'-deoxyuridine (EdU) and 2'-deoxycytidine were added to both cultures during the last 30 minutes of treatment. Incorporated EdU was detected in a click-iT reaction with a fluorescent azide. (***A***) Kinetoplasts (K) and nuclei (N) were scored as EdU-positive (K+ or N+) or EdU-negative after treatment with DMSO (top) or AEE788 (bottom). The scale bar is 10 μm. (***B***) Quantitation of the average percentage of trypanosomes (n = 125) with EdU-negative or EdU-positive kinetoplasts following AEE788 or DMSO treatment. (***C***) Quantitation of the average proportion of cells (n = 125) with EdU-negative or EdU-positive nuclei following AEE788 or DMSO treatment. Error bars denote the standard deviation in three independent experiments. Differences in the distribution of trypanosomes between EdU-positive and EdU-negative kinetoplasts or nuclei in cell populations treated with DMSO or AEE788 were assessed with a Pearson chi-squared test ($p = 4.9 \times 10^{-4}$ for the kinetoplast, and $p = 3.1 \times 10^{-19}$ for the nucleus).

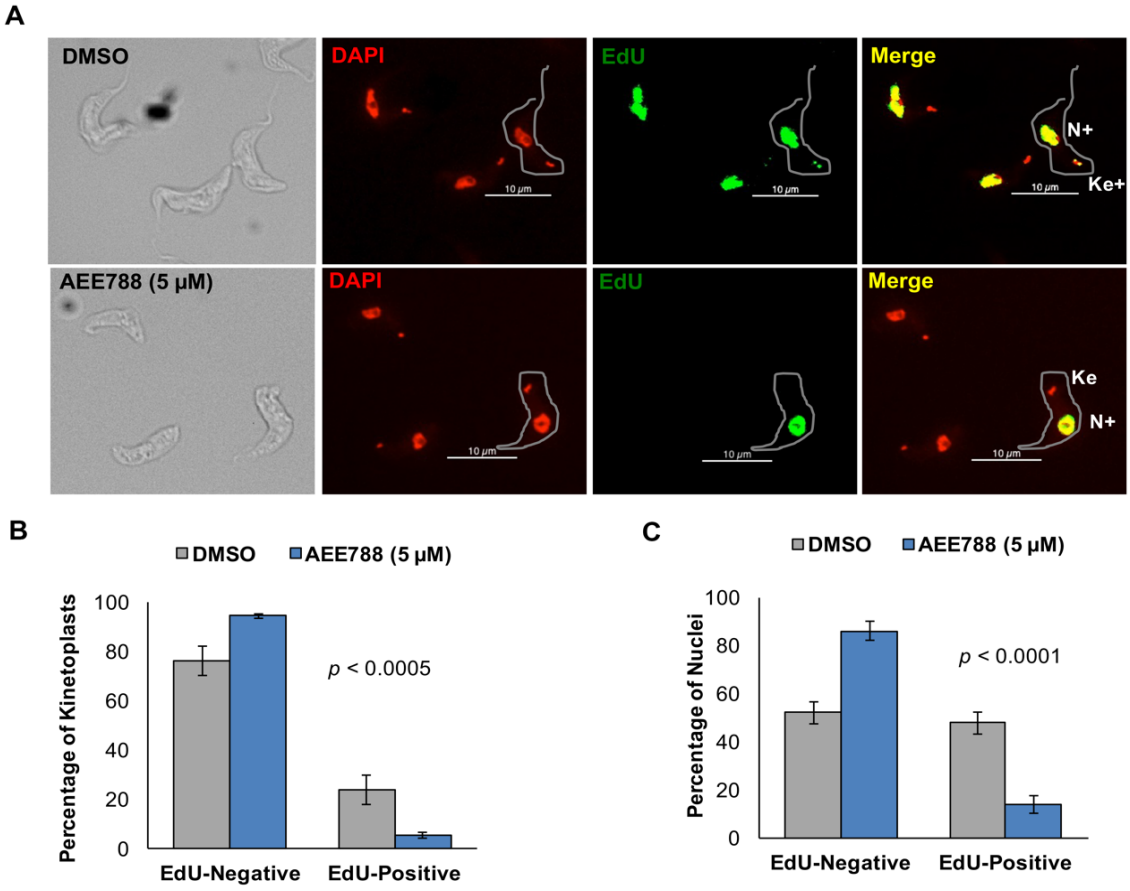
A
DMSO
DAPI
EdU
Merge
N+
Ke+
AEE788 (5 μM)
DAPI
EdU
Merge
Ke
N+
B
DMSO
AEE788 (5 μM)
Percentage of Kinetoplasts
100
80
60
40
20
0
p < 0.0005
EdU-Negative
EdU-Positive
C
DMSO
AEE788 (5 μM)
Percentage of Nuclei
100
80
60
40
20
0
p < 0.0001
EdU-Negative
EdU-Positive

Figure 2.3. *AEE788 prevents basal body duplication*. Anti-TbSAS6 and YL1/2 were used to quantitate the number of mature basal bodies (mBB) and immature probasal bodies (pBB) per trypanosome after treatment with AEE788 (5 μM) or DMSO (0.1%). (***A***) Representative staining pattern of YL1/2 (red) and anti-TbSAS6 (green) after DMSO (top) or AEE788 (bottom) treatment. Cells are counterstained with DAPI (1.5 μM). Red arrows indicate TbRP2+ foci (mBB), green arrows indicate TbSAS6+ foci (pBB), and yellow arrows indicate colocalization of TbRP2 and TbSAS6 (mBB). The scale bar is 6 μm. The basal bodies and associated kinetoplast (K) are enlarged in a single trypanosome for both treatment groups: DMSO (yellow boxes) and AEE788 (orange boxes). (***B***) Average percentage of trypanosomes (n = 125) with the indicated number of mBBs and pBBs following treatment with AEE788 or DMSO. Error bars represent the standard deviation in three independent experiments. Statistical significance of changes in the distribution of the number of basal bodies (per cell) in the trypanosome population was determined with a Pearson chi-squared test ($p = .3 \times 10^{-18}$).

A

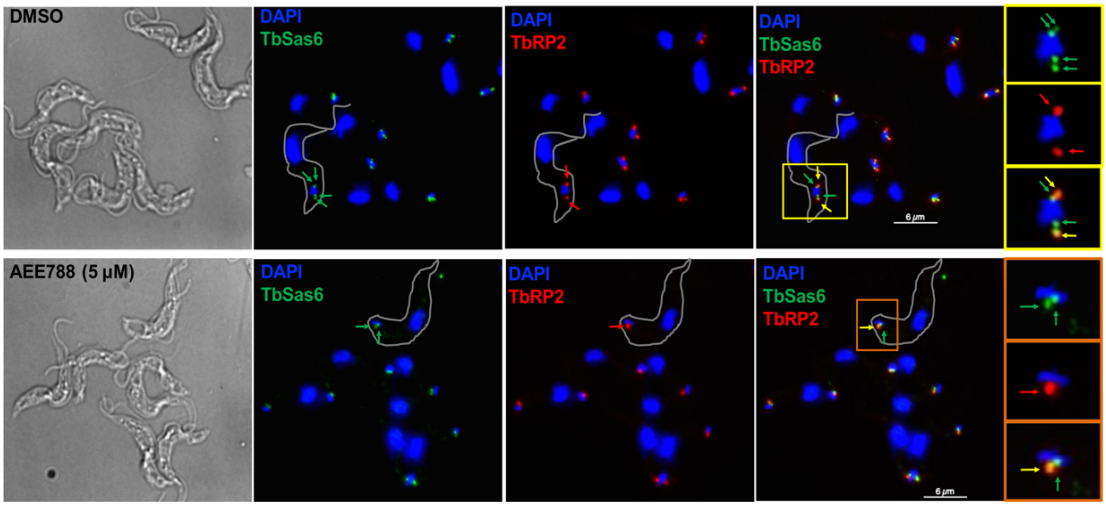
DMSO
DAPI
TbSas6
DAPI
TbRP2
DAPI
TbSas6
TbRP2
6 µm
AEE788 (5 µM)
DAPI
TbSas6
DAPI
TbRP2
DAPI
TbSas6
TbRP2
6 µm

B

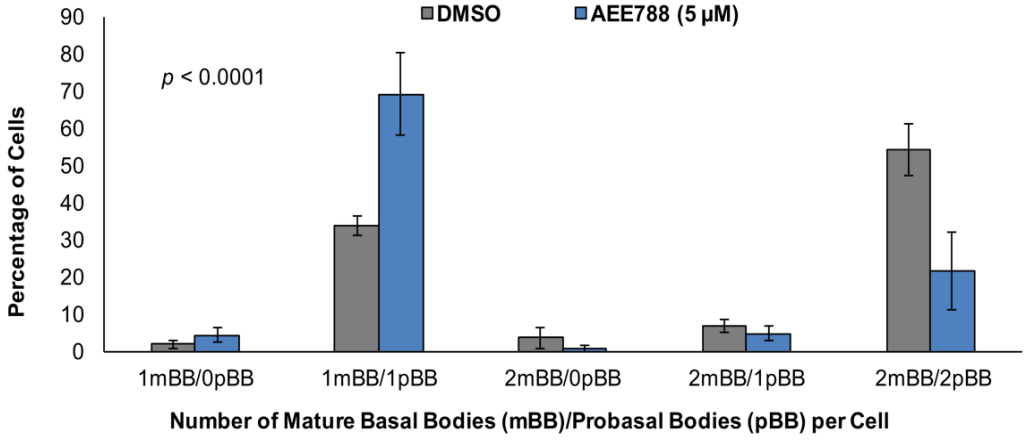
DMSO
AEE788 (5 µM)
p < 0.0001
Percentage of Cells
90
80
70
60
50
40
30
20
10
0
1mBB/0pBB
1mBB/1pBB
2mBB/0pBB
2mBB/1pBB
2mBB/2pBB
Number of Mature Basal Bodies (mBB)/Probasal Bodies (pBB) per Cell

Figure 2.4. *Bilobe duplication is inhibited by AEE788*. Following a 4 h treatment with AEE788 (5 μM) or DMSO (0.1%), trypanosomes were stained with the anti-centrin antibody 20H5 to detect the bilobe. (***A***) Representative images of 20H5-stained trypanosomes after treatment with DMSO (top) or AEE788 (bottom). Centrin is observed at the bilobe (green arrowheads) as well as the basal body (green arrows). DAPI was used to stain kinetoplast and nuclear DNA. K = kinetoplast; N = nucleus. The scale bar is 6 μm. (***B***) Average percentage of cells with one or two bilobes following AEE788 or DMSO treatment. Error bars represent standard deviation between four biological replicates. The distribution of trypanosomes with one or two bilobes in AEE788-treated cells was compared to the distribution observed in control cells (i.e. DMSO-treated) using a Pearson chi-squared test ($p = 3.6 \times 10^{-9}$).

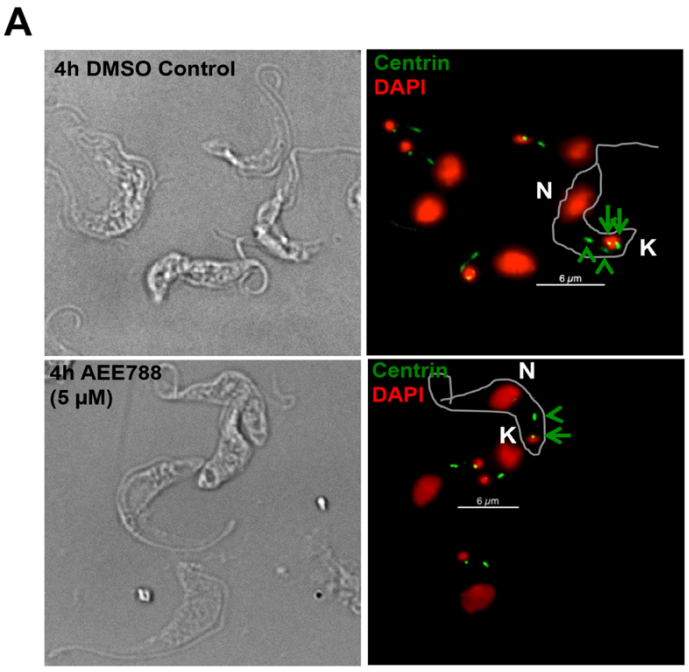
A
4h DMSO Control
Centrin
DAPI
N
K
6 μm
4h AEE788
(5 μM)
Centrin
DAPI
N
K
6 μm
B
DMSO
AEE788
p < 0.0001
Percentage of Cells
90
80
70
60
50
40
30
20
10
0
1 Bilobe
2 Bilobes

Figure 2.5. *Time-course of DNA replication and division in the kinetoplast and nucleus after withdrawal of AEE788*. Trypanosomes were treated with AEE788 (5 μM, 4 h), rinsed, and placed in drug-free HMI-9 medium. The time-course of DNA synthesis was monitored by EdU incorporation and DAPI was used to visualize division of the kinetoplast and nucleus. (***A***) Representative images of trypanosomes directly after AEE788 treatment (0 h, top panel) or 2 h after AEE788 washout (bottom). Kinetoplasts and nuclei, in 100-150 trypanosomes, were scored as EdU-positive (K+ or N+) or EdU-negative. Ke = elongated kinetoplast. Scale bar = 15 μm. The average proportion of cells with EdU-positive kinetoplasts (***B***), or nuclei (***C***), are indicated at every hour following AEE788 withdrawal. Standard deviation between independent experiments are shown (n = 6 for 0 h and 2 h; n = 4 for 1 h; n = 3 for 3 h and 4 h). A sigmoidal nonlinear regression curve was fit to the data points using GraphPad Prism, and the time at which 10% (T_{10}) or 50% (T_{50}) of the population became EdU-positive, compared to the observed maximum (4 h), was calculated for kinetoplast (***B***) and nuclear (***C***) EdU incorporation. (***D***) The average percentage of cells (n = 115) with indicated numbers of kinetoplasts (K) and nuclei (N) is shown for every hour after AEE788 withdrawal. Standard deviation represents standard deviation in three independent experiments. Data trends are represented by nonlinear regression curves using a 3^{rd} order polynomial equation for 1K1N and 1Ke1N data, and a sigmoidal nonlinear regression curve for 2K1N and 2K2N populations. T_{10} and T_{50} (calculated by GraphPad software) for each event is listed. (T_{10} and T_{50} for the appearance of 1Ke1N cells is based on a sigmoidal nonlinear regression curve from 0 h to 4 h (maximum).

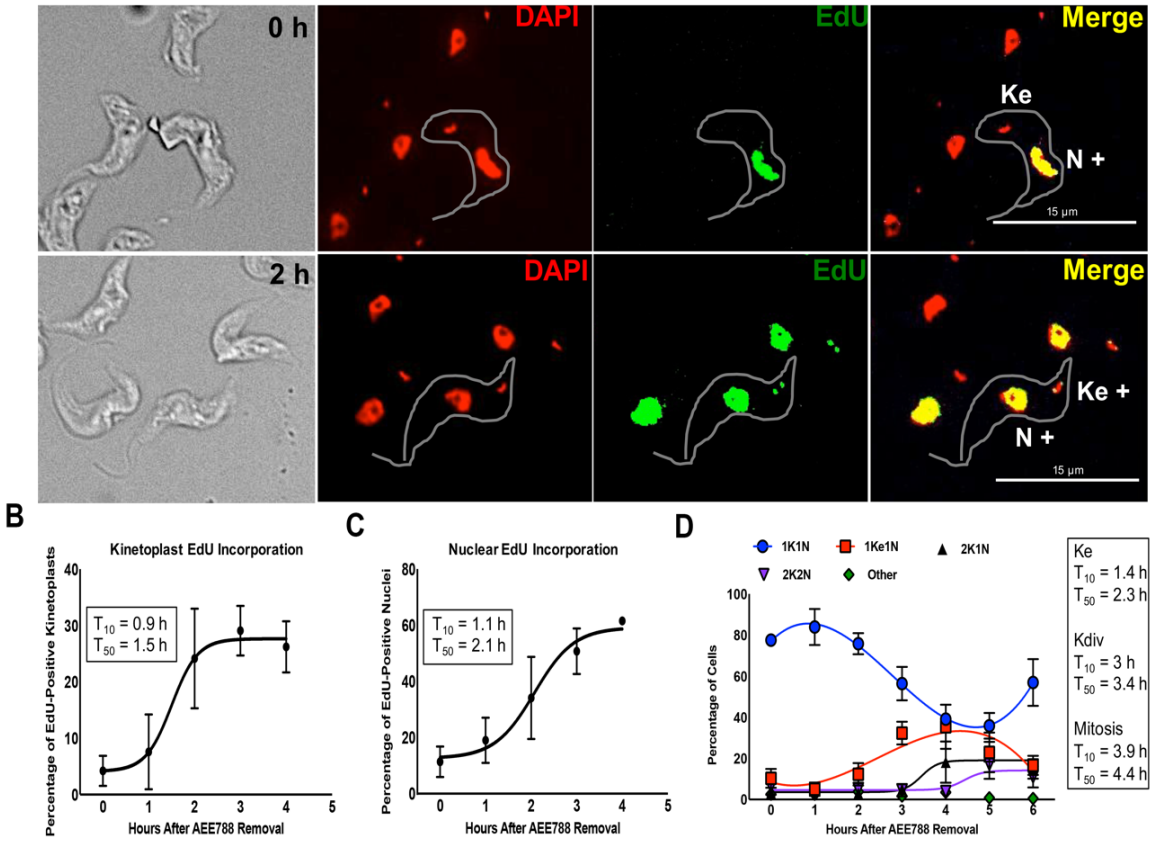
A
0 h
DAPI
EdU
Merge
Ke
N +
15 µm
2 h
DAPI
EdU
Merge
Ke +
N +
15 µm
B
Kinetoplast EdU Incorporation
Percentage of EdU-Positive Kinetoplasts
T10 = 0.9 h
T50 = 1.5 h
Hours After AEE788 Removal
C
Nuclear EdU Incorporation
Percentage of EdU-Positive Nuclei
T10 = 1.1 h
T50 = 2.1 h
Hours After AEE788 Removal
D
1K1N
1Ke1N
2K1N
2K2N
Other
Percentage of Cells
Hours After AEE788 Removal
Ke
T10 = 1.4 h
T50 = 2.3 h
Kdiv
T10 = 3 h
T50 = 3.4 h
Mitosis
T10 = 3.9 h
T50 = 4.4 h

Figure 2.6. *Kinetics of basal body and bilobe duplication*. Trypanosomes were treated with AEE788 (5 μM, 4 h) and then transferred to drug-free HMI-9 medium for up to 3 h. Cells were retrieved every 30 minutes between 2 h and 3 h after AEE788 washout (***A***) Basal body duplication was assessed with YL1/2 and anti-TbSAS6. YL1/2 recognizes mature basal bodies (mBBs) (red arrows) and TbSAS6 localizes to immature probasal bodies (pBB) (green arrows) and mature basal bodies (yellow arrows). The scale bar is 6 μm. An unduplicated basal body (1mBB/1pBB) 1.5 h after AEE788 washout (yellow boxes) and a duplicated basal body (2mBB/2pBB) 3 h after AEE788 washout (orange boxes) are magnified. K = kinetoplast. (***B***) The average percentage of cells with the indicated number of mature basal bodies (mBB) and probasal bodies (pBB) are shown at various times after AEE788 washout. Error bars represent standard deviation between three independent experiments. A sigmoidal nonlinear regression curve was fit to the data points in GraphPad Prism and the time by which 10% (T_{10}) or 50% (T_{50}) of the population, compared to the observed maximum, became 2mBB/2pBB, is listed. (***C***) Schematic of nascent basal body duplication and probasal body maturation (acquisition of TbRP2) occurring in the absence of intermediates with two mature basal bodies and no probasal bodies (2mBB/0pBB). (***D***) The anti-centrin antibody, 20H5, was used to visualize bilobes. Green arrowheads indicate bilobes, green arrows point to basal bodies. K = kinetoplast; N = nucleus. Scale bar is 10 μm. (***E***) Quantitation of the average percentage of bilobes (BL) per cell following AEE788 withdrawal. Error bars represent standard deviation between three independent experiments. A sigmoidal nonlinear regression curve was fit to

the data points in GraphPad Prism, and the T_{10} and T_{50}, describing the formation of cells with duplicated bilobes, are provided.

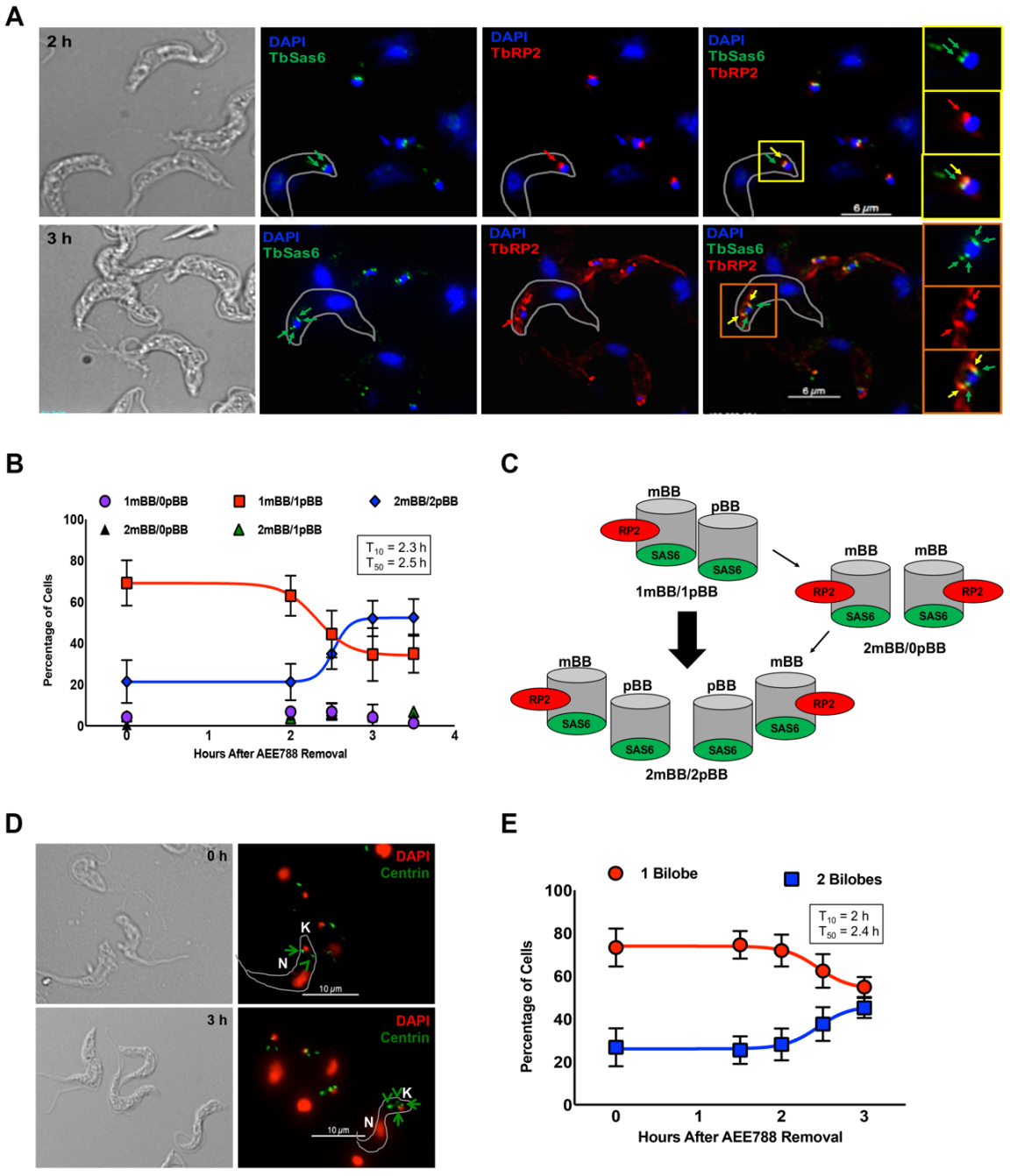

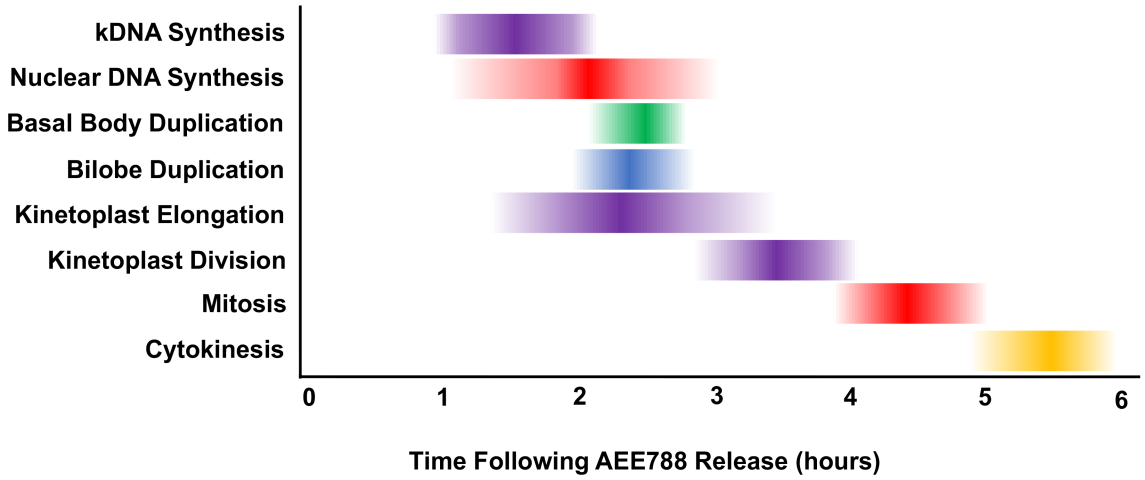

Figure 2.7. *Time-course of major events in the trypanosome division cycle*. AEE788 (5 μM, 4 h) was used to block organelle duplication and DNA synthesis. After removing AEE788 from the medium, the onset and duration of organelle duplication and DNA synthesis were determined. The time at which, 10% (T_{10}) (left border), 50% (T_{50}) and 90% (T_{90}) (right border) of the observed maximum was reached for each event was calculated, based on nonlinear regression curves (Figures 5 and 6). The darkest shading corresponds to the T_{50} (+/- standard error).

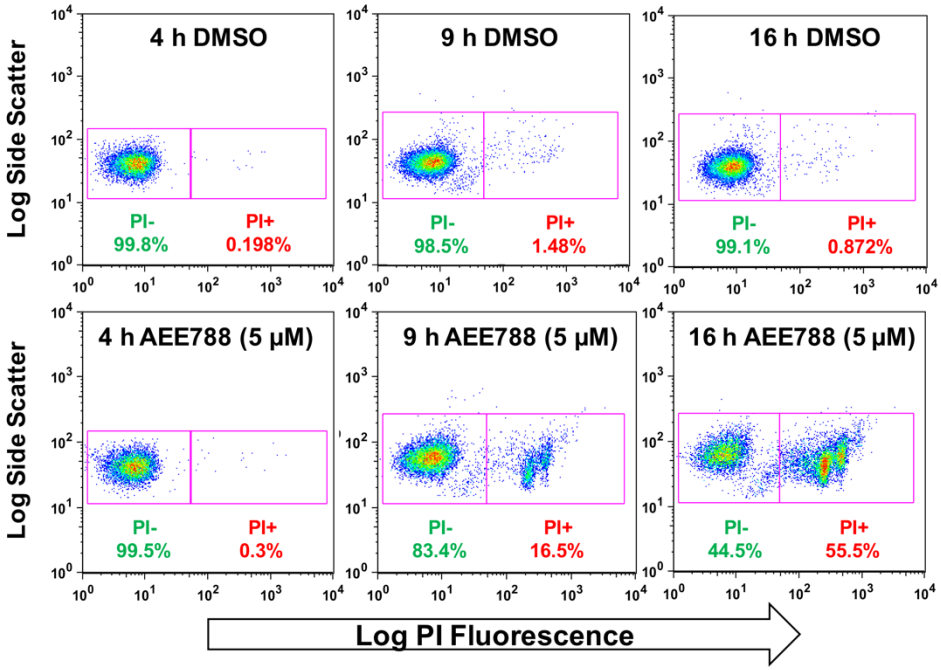

Figure 2.8. *Extended AEE788 exposure decreases trypanosome viability*. Trypanosomes were treated with AEE788 (5 μM) or DMSO (0.1%) for 4 h, 9 h or 16 h, harvested and treated with propidium iodide (3 μM) prior to analysis on a flow cytometer. Trypanosomes were gated based on size and shape (forward and side scatter) and the intensity of propidium iodide (PI) determined.

Figure 2.9. *Effect of AEE788 on endocytic pathways*. Trypanosomes (5 x 10^5 cells/ml) were incubated with AEE788 (5 μM) or DMSO (0.1%) for 9 h. Cells were subsequently washed and resuspended in serum-free medium (without drug or DMSO). Trypanosomes were incubated with fluorescent endocytic cargo (transferrin, BSA, or tomato lectin) for 15 minutes (37 °C). Propidium iodide (3 μM) was used to stain dead cells. A flow cytometer was used to detect fluorescence intensity per cell. (***A***) FlowJo software was used to gate for live trypanosomes based on shape (forward and side scatter) and ability to exclude propidium iodide. Histograms depict fluorescence intensity for transferrin (***B***), BSA (***C***) or tomato lectin (***D***) for every observed cell (n = 15,000 for each cargo). Bar graphs represent the average median fluorescence intensity (calculated with FloJo), with standard deviation between three independent experiments shown, for transferrin (***B***), BSA (***C***) or tomato lectin (***D***) after DMSO or AEE788 treatment. In statistical analysis, the median fluorescence of each cargo was compared between cells treated with DMSO or AEE788 using a Student's t-test (p = 0.002 for Tf, p = 0.003 for BSA and p = 0.9 for TL).

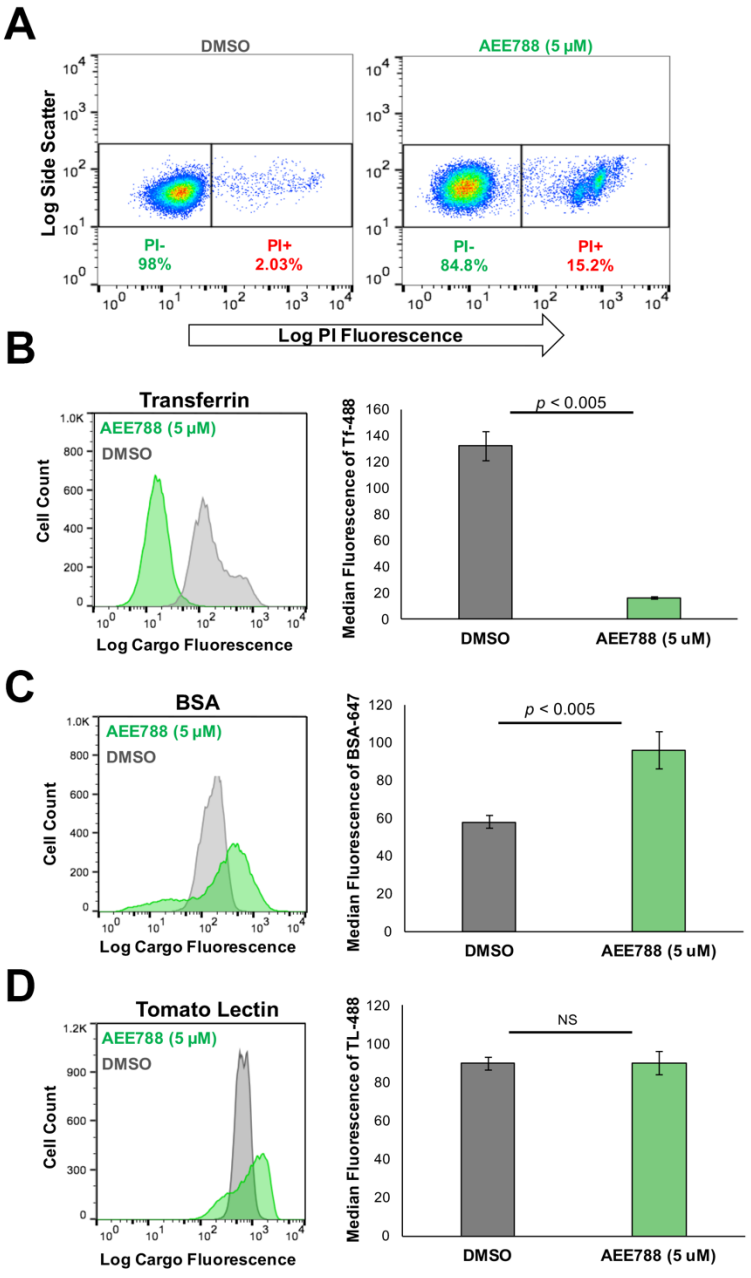
A
DMSO
AEE788 (5 μM)
Log Side Scatter
PI-
98%
PI+
2.03%
PI-
84.8%
PI+
15.2%
Log PI Fluorescence
B
Transferrin
AEE788 (5 μM)
DMSO
Cell Count
Log Cargo Fluorescence
Median Fluorescence of Tf-488
p < 0.005
DMSO
AEE788 (5 uM)
C
BSA
AEE788 (5 μM)
DMSO
Cell Count
Log Cargo Fluorescence
Median Fluorescence of BSA-647
p < 0.005
DMSO
AEE788 (5 uM)
D
Tomato Lectin
AEE788 (5 μM)
DMSO
Cell Count
Log Cargo Fluorescence
Median Fluorescence of TL-488
NS
DMSO
AEE788 (5 uM)

Figure 2.10. *Prolonged AEE788 exposure changes trypanosome morphology.* (***A***) The morphology of live trypanosomes (n = 100) was determined after different durations of AEE788 treatment (examples of trypanosome morphology are demonstrated by paraformaldehyde fixed cells). The standard deviation of two experiments is shown. A Pearson chi-squared test was used to compare the distribution of normal, swollen and rounded cells between different treatment groups; 4 h to 9 h ($p = 6.6 \times 10^{-64}$); 4 h to 16 h ($p = 1.1 \times 10^{-64}$); 9 h to 16 h ($p = 5.6 \times 10^{-25}$). (***B***) Following a 16 h treatment with DMSO (top) or AEE788 (bottom), the paraflagellar rod (PFR) was visualized using an antibody against PFR2 (green) and the flagellum with the antibody 20H5 (red). 20H5 detects centrin at the basal body (arrow), bilobe (arrowhead) and the flagellum. K = kinetoplast; N = nucleus. The scale bar is 6 μm. (***C***) Trypanosomes were treated with AEE788 (5 μM) for 12 h and visualized by SEM. The left panel demonstrates normal trypanosome morphology, the middle panel shows both rounded (left) and swollen (right) cells, and the right panel depicts a round trypanosome with flagellum at the cell periphery (white arrow). The scale bar is 2 μm.

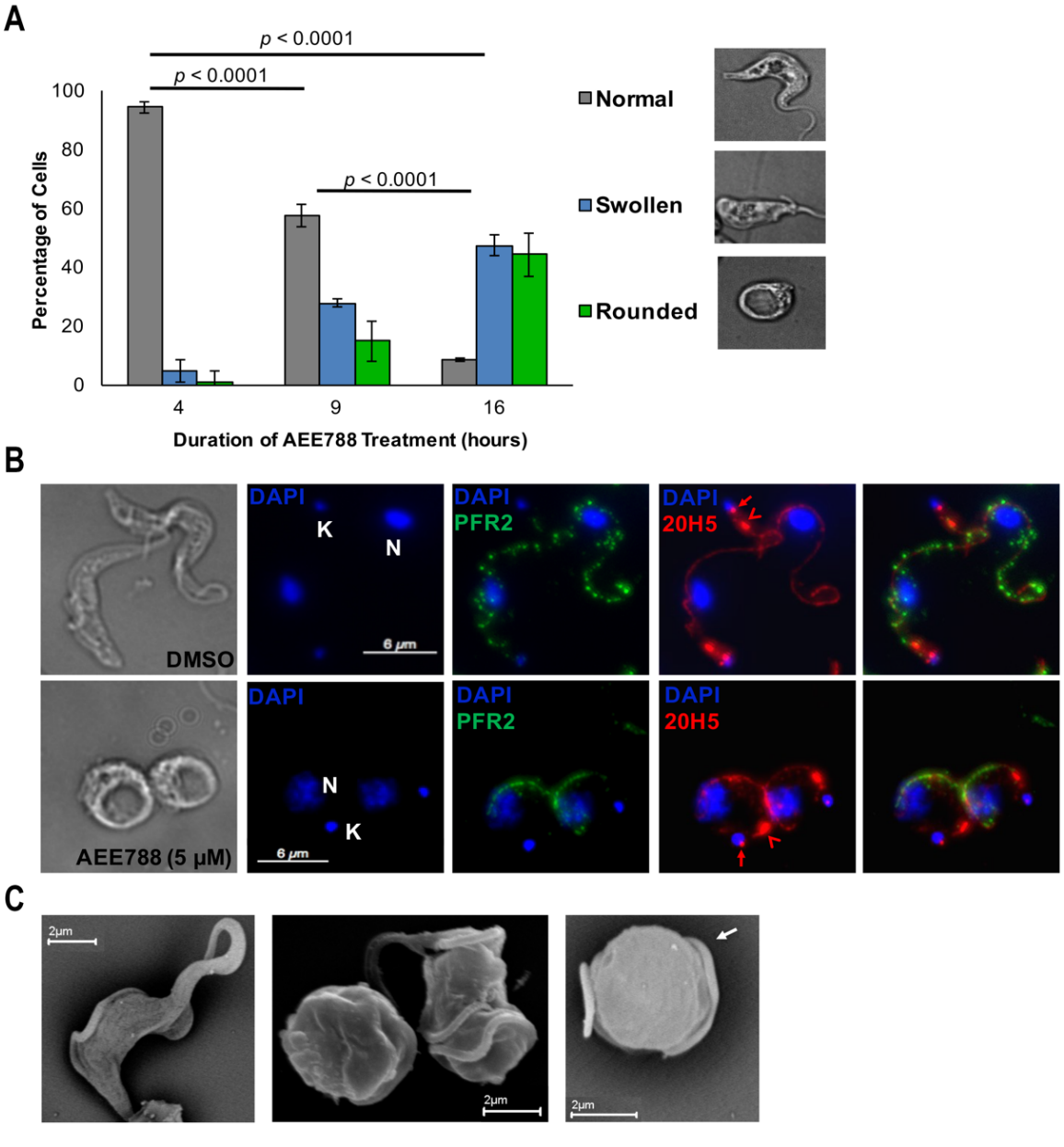
A
p < 0.0001
p < 0.0001
p < 0.0001
100
80
60
40
20
0
Percentage of Cells
4
9
16
Duration of AEE788 Treatment (hours)
Normal
Swollen
Rounded
B
DMSO
AEE788 (5 μM)
DAPI
K
N
6 μm
DAPI
PFR2
DAPI
20H5
C
2μm

Table 2.1. *Select examples of phospho-proteins affected by short-term (4 h) AEE8788 treatment*. After treatment of trypanosomes with DMSO (0.1%) or AEE788 (5 μM) for 4 h, peptides were harvested and phospho-peptides enriched over an IMAC column. LC-MS/MS was used to monitor the abundance of phospho-peptides in three independent experiments. Spectral counts indicate the combined number of times a phospho-peptide was observed over all experiments. The number in parenthesis indicates the total number of peptides observed for the parent protein over all experiments (summation of all peptides observed in the IMAC elution and flow through). The affected peptide is indicated with the phospho-site bolded in lowercase (phosphoRS [104] probability ≥ 80%). A Student's t-test was used to determine if the change in phospho-peptide abundance was statistically significant ($p < 0.05\%$).

Gene ID	Production Description	Identified Phosphopeptide	Spectral Counts		p-value
			DMSO	AEE788	
Decreased					
Tb427.06.4970	SR Protein Kinase (SRPK)	HsASTNGPSQPAHQR	6 (15)	1 (3)	0.038
Tb427.10.3010	Bilobe Protein	sRISTGISFLSK	5 (18)	0 (7)	0.038
Tb427tmp.02.0810	TbSAS4	LAVGDANHSESIGDKSVstK	8 (12)	2 (3)	0.013
Increased					
Tb427.01.2100	Calpain-like Cysteine Peptidase	AEEASPAPSPAGEsDEKAsKSEHESEAK	20 (88)	44 (99)	0.03

Table 2.2. *Select examples of phospho-proteins affected by long-term (9 h) AEE8788 treatment*. After treatment of trypanosomes with DMSO (0.1%) or AEE788 (5 μM) for 4 h, trypanosome phospho-peptides were enriched over an IMAC column. Phospho-peptide abundance was monitored by LC-MS/MS in three independent experiments. Spectral counts indicate the combined number of times a phospho-peptide was observed over all three experiments. The number in parenthesis indicates the total number of peptides observed for the parent protein over all experiments (summation of all peptides observed in the IMAC elution and flow through). The affected peptide is indicated with the phosphosite bolded in lowercase (phosphoRS [104] probability ≥ 80%). A Student's t-test was used to determine if the change in phospho-peptide abundance was statistically significant ($p < 0.05\%$).

Gene ID	Production Description	Identified Phosphopeptide	Spectral Counts		p-value
			DMSO	AEE788	
Decreased					
Tb427.03.3080	NEK Kinase	ADTsDIsLSHEDLsR	12 (16)	0 (7)	0.02
Tb427.10.14010	TbRP2	EATPPEsASRSDSSAPTTPHSR	8 (25)	1 (7)	0.05
Tb427.10.8820	Bilobe Protein	TIGTTSGHSTTNLssHTPEK	6 (17)	0 (5)	0.03
Tb427tmp.01.3960	BILBO-1	LMSEASsFLGNLR	5 (41)	0 (26)	0.04
Increased					
Tb427.10.14770	Associated kinase of Tb14-3-3	LANSsLPVsHTSTR	7 (13)	15 (18)	0.02
Tb427.07.7000	Bilobe Protein	TSSHIsEHGLDR	0 (38)	10 (67)	0.02
Tb427.04.310	Ubiquitin-transferase	TTLSKsAHVsHER	3 (3)	8 (9)	0.04

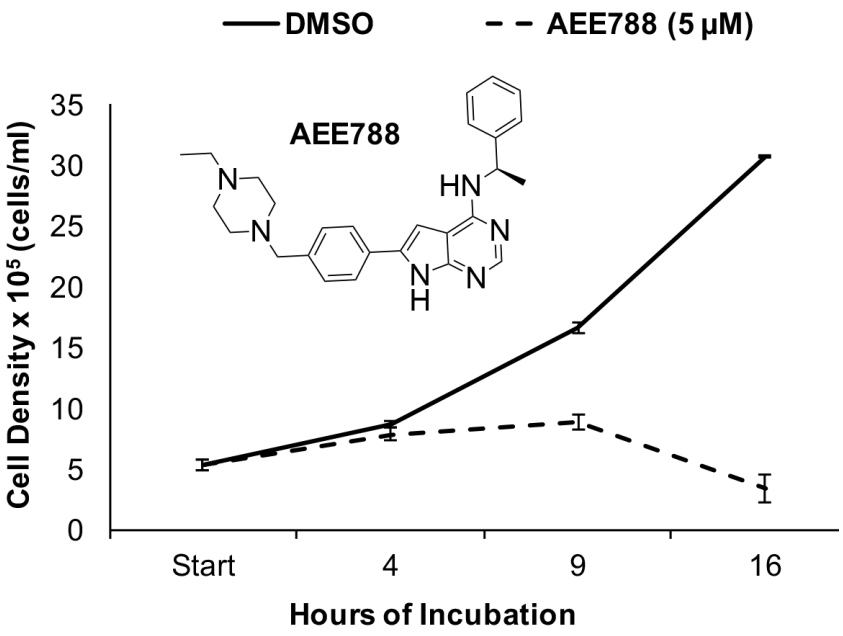

Supplemental Figure 2.1. *Short-term AEE788 treatment arrests proliferation of bloodstream trypanosomes*. Trypanosomes (5 x 10^5 cells/ml) were treated with the indicated concentration of AEE788 (structure shown) or DMSO (0.1%) for 4 h, 9 h or 16 h. Cell density was determined with a haemocytometer at each time point. Averages shown are from two independent experiments with error bars demonstrating standard deviation.

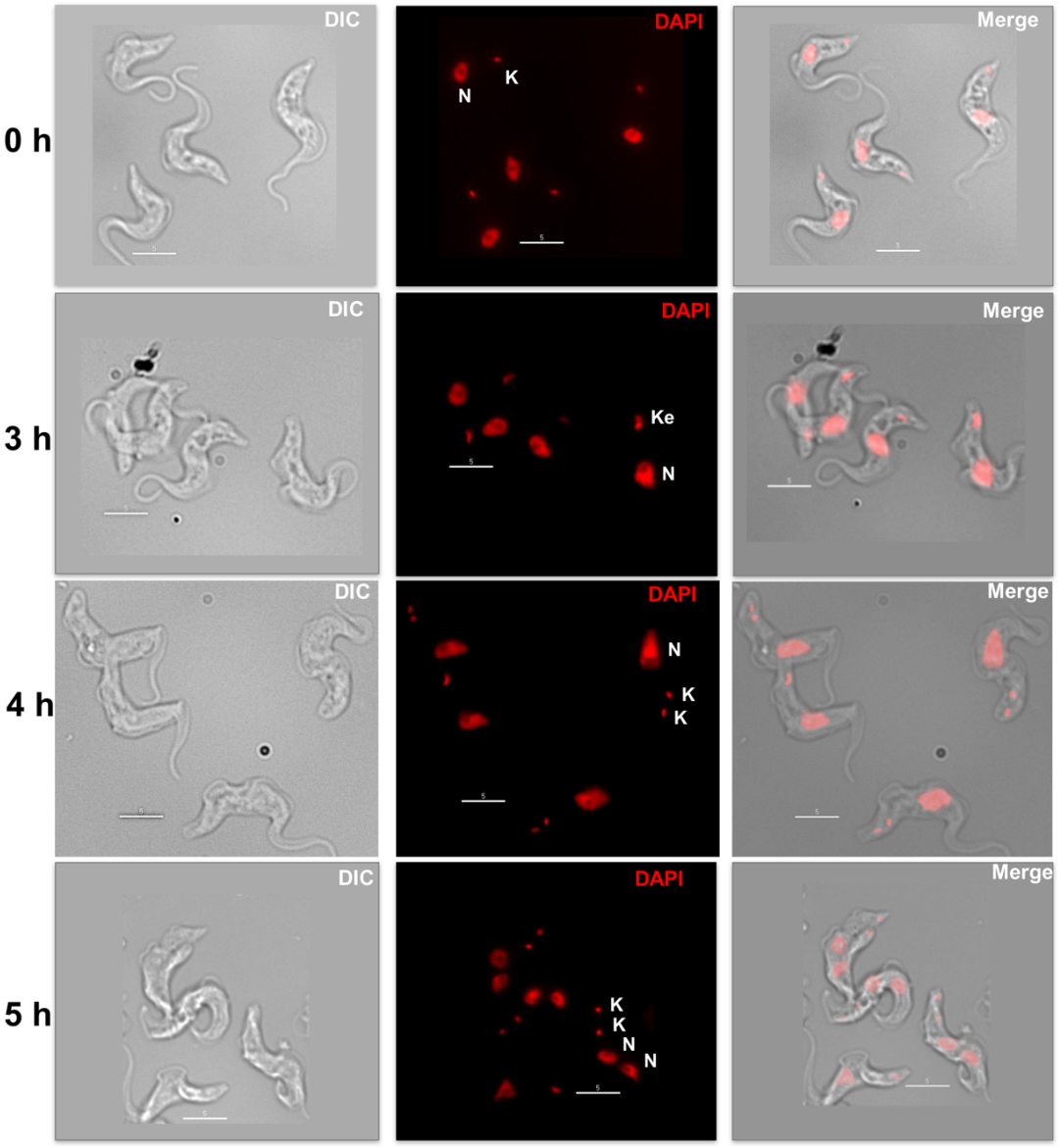

Supplemental Figure 2.2. *Duplication of the kinetoplast and nucleus after AEE788 withdrawal*. Trypanosomes were treated with AEE788 (5 μM) for 4 h, and resuspended in drug-free HMI-9 medium. Trypanosome aliquots were collected every hour for 6 h and stained with DAPI. Images show dominant cell cycle populations observed 0 h, 3 h, 4 h and 5 h after AEE788 withdrawal. K = kinetoplast; Ke = elongated kinetoplast; N = nucleus. Scale bars are 5 μm.

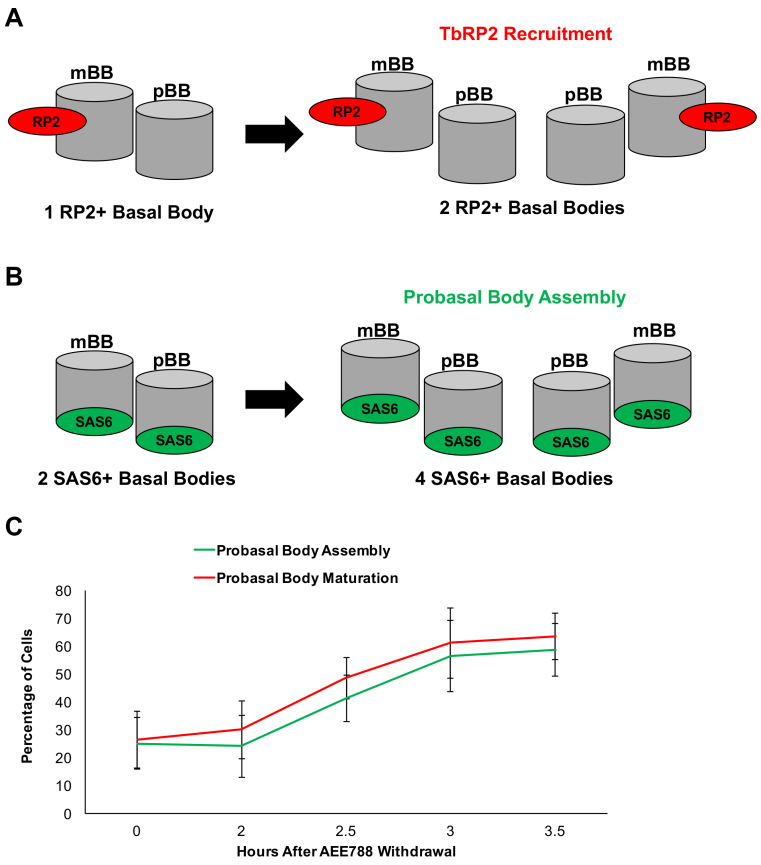

Supplemental Figure 2.3. *TbRP2 recruitment is observed during assembly of TbSAS6 at probasal bodies*. Following a 4 h treatment with AEE788 (5 μM), trypanosomes were washed and incubated in drug-free HMI-9 medium. Trypanosomes were collected every 30 minutes from 2 h to 3.5 h after AEE788 withdrawal. Cells were stained with YL/2 to detect TbRP2 at mature basal bodies, and anti-TbSAS6 to detect mature and immature basal bodies. (***A***) Model for TbRP2 recruitment. (***B***) Model for assembly of TbSAS6-positive probasal bodies. (***C***) Time-course of the formation of trypanosomes with two TbRP2-positive basal bodies (TbRP2 recruitment) and three-four TbSAS6-positive basal bodies (probasal body assembly). Error bars show standard deviation between three independent experiments.

Supplemental Table 2.1. *Phospho-peptides with decreased abundance after treatment with AEE788 (4 h)*. Phospho-peptides from trypanosomes treated with DMSO (0.1%) or AEE788 (5 μM) were enriched over an IMAC column. LC-MS/MS was used to monitor the abundance of observed phospho-peptides over three independent experiments. The phospho-peptides listed here demonstrated a decrease (2-fold, or greater) in abundance in at least two out of three biological replicates. The phosphosite is highlighted in red (phosphoRS [104] score above 80%). Spectral counts indicate the combined number of times a phospho-peptide was observed over the three independent experiments. The number in parenthesis is the summation of all unique peptides detected (IMAC elution and flow through) for each protein reported. A Student's t-test was used to determine if the change in abundance was statistically significant ($p \leq 0.05\%$). For phospho-peptides observed in two out of three experiments, only the two experiments were used for statistical analysis. Phospho-peptides listed in Table 2.1 or Table 2.2 are highlighted in yellow. ** no phosphosite with a phosphoRS probability of at least 80% was identified.

Gene ID	Predicted Protein Product	Peptide Sequence	Spectral Counts		p-Value	# of Repeats
			DMSO	AEE788		
Tb427.01.1880	WD40 repeat-conatining protein	SSEVLNsPLsDLPYTR	7 (5)	2 (3)	0.21	3
Tb427.02.2090	hypothetical protein	DGcGEVSTPTYSVVRPGstPK	**8** (17)	**3** (11)	0.07	3
Tb427.02.3480	Transcription Elongation Factor	DFGGDSSESEFAGGssDDEyGKR	**4** (20)	**0** (19)	0.18	2
Tb427.03.1920	NOT5 protein	GNTslTSTVGGR	**11** (42)	**5** (12)	0.18	3
Tb427.03.3080	serine/threonine-protein kinase Nek1	ADTSDISLSHEDLsR	**10** (10)	**3** (3)	0.06	3
Tb427.03.3940	RNA-binding (DRBD11) protein,	TPLNNESGPGTSSSGSHSSSSNVPVA	**9** (13)	**0** (2)	0.02	3
Tb427.03.5020	Flagellar Member 6 (FLAM6)	LINAAPEPLsDGASDMASLSNVSTTAT	**6** (15)	**0** (7)	0.07	3
Tb427.04.2600	hypothetical protein, conserved	ASTSSVVsQFR	**5** (25)	**2** (21)	0.10	3
Tb427.05.1730	inhibitor of serine peptidase (ISP)	stMGSRVDIDFcKFEEPPSPR	**11** (18)	4 (5)	0.57	2
Tb427.06.3100	IFT complex B protein 46 C terminal,	TTGGSGGDATETsPPtPK	**12** (18)	**6** (12)	0.33	3
Tb427.06.3540	zinc-finger protein, conserved	DSDAAsALTSTSLGSAAVGLHR	**11** (11)	**1** (0)	0.03	3
Tb427.06.4970	ser/arg-rich protein specific kinase	HsASTNGPSQPAHQR	**6** (15)	**1** (3)	0.23	2
Tb427.07.2650	hypothetical protein, conserved	sDRQPssGAPEEEEETEEQIIIR	**21** (161)	**2** (175)	0.21	3
Tb427.07.3080	hypothetical protein, conserved	mQPVDEsDLsESGYSNHR	**22** (28)	**8** (14)	0.06	3
Tb427.07.3550	hypothetical protein, conserved	LDVPPtPsPDRKPPIGK	**17** (205)	**0** (155)	0.21	2
Tb427.07.3550	hypothetical protein, conserved	LSSGHPSGNRDssRR	**15** (205)	**7** (155)	0.21	3
Tb427.07.3740	hypothetical protein, conserved	KVSTTQQSPLsGTDGDFVTK	**9** (52)	**0** (36)	0.16	2
Tb427.07.4410	hypothetical protein, conserved	KssFNAVETHR	**6** (12)	**3** (10)	0.06	3
Tb427.07.4980	ZC3H23 (POMP35)	ALYDQYLADSGSEDssELSK	**7** (6)	**1** (1)	0.14	3
Tb427.07.6290	kinesin (TbKIF9A),	LNASSEsASMLER	**6** (19)	**0** (7)	0.07	3
Tb427.07.6610	hypothetical protein, conserved	SRSSTSGENHSQVTVSSASSR **	**18** (29)	**5** (14)	0.04	3
Tb427.07.6640	hypothetical protein, conserved	GDLFSPLGLPRPDtGsTSSPR	**12** (44)	**0** (22)	0.21	2
Tb427.07.6640	hypothetical protein, conserved	SSLSSsNNLAPGSPR	**5** (44)	**1** (22)	0.23	2
Tb427.07.810	hypothetical protein, conserved	SVTsVEQEPATADTATDIK	**8** (8)	**2** (2)	0.25	2
Tb427.08.5300	hypothetical protein, conserved	HLTPEtLDSAPSTAyGSVGFK	**11** (13)	**1** (2)	0.00	3
Tb427.10.14330	UTP14,	KmEEDADADAFLNAANEDGGGsEAss	**9** (8)	**0** (0)	0.19	3
Tb427.10.15170	hypothetical protein, conserved	SVsPSKSVsPPRPAQVR	**7** (9)	**0** (0)	0.02	3
Tb427.10.15310	hypothetical protein, conserved	KsEsDVcGEGSELLLQQYR	10 (34)	3 (19)	0.04	3
Tb427.10.2080	hypothetical protein, conserved	TAAAtDIPRGADDMIEVKEtK	**10** (11)	**4** (4)	0.10	3
Tb427.10.2920	hypothetical protein, conserved	EADINDLPSSFcPFPPAtLTASSPPVsG	**10** (10)	**2** (2)	0.21	2
Tb427.10.3010	Bilobe protein, conserved	sRISTGISFLSK	**5** (18)	**0** (7)	0.04	3
Tb427.10.5240	cAMP binding protein,	sPSLPSTPR	**9** (10)	**4** (5)	0.04	3
Tb427.10.5880	Proteophosphoglycan,	AsVSEEANNVSSDRPVGK	**5** (40)	**2** (16)	0.35	2
Tb427.10.5890	Galactose oxidase domain containing pr	RGSYIsSHSNEADAAK	**4** (9)	**1** (5)	0.25	2
Tb427.10.5990	hypothetical protein, conserved	HLVNIsGHSAER	**4** (6)	**2** (2)	0.42	2
Tb427.10.8820	Bilobe protein, conserved	mGEPsLEDVEKtIDsFR	**7** (17)	**1** (3)	0.08	3
Tb427.10.8930	paraflagellar rod component (PFC18),	VASSGKEDTEEAPsASSETGVSTPGD	**13** (24)	**1** (10)	0.03	3
Tb427.10.9060	hypothetical protein, conserved	sVPPPsPGSLVSIPR	**8** (8)	**2** (2)	0.01	3
Tb427.10.9910	PSP1 C-terminal conserved region,	SGAAGGcSLPAASTPLsER	**5** (5)	**0** (0)	0.13	2
Tb427tmp.01.0230	hypothetical protein, conserved	ALKFsLsPVtTR	**7** (20)	**1** (15)	0.08	3
Tb427tmp.01.1880	hypothetical protein, conserved	HGsVPYSAADGGNsR	**6** (6)	**0** (0)	0.16	2
Tb427tmp.01.3960	BILBO1	HsAGGSFSQGSR	4 (35)	0 (24)	0.12	2
Tb427tmp.01.4370	hypothetical protein, conserved	GsTSNSGIAAQGR	**10** (22)	**1** (13)	0.17	2
Tb427tmp.01.5010	hypothetical protein, conserved	RTSTVsVSTVEQPIK	**9** (9)	**0** (0)	0.16	2

Supplemental Table 2.2. *Phospho-peptides with decreased abundance after treatment with AEE788 (9 h)*. Phospho-peptides from trypanosomes treated with DMSO (0.1%) or AEE788 (5 μM) were enriched over an IMAC column. LC-MS/MS was used to monitor the abundance of observed phospho-peptides over three independent experiments. The phospho-peptides listed here demonstrated a decrease (2-fold, or greater) in abundance in at least two out of three biological replicates. The phosphosite is highlighted in red (phosphoRS [104] score above 80%). Spectral counts indicate the combined number of times a phospho-peptide was observed over the three independent experiments. The number in parenthesis is the summation of all unique peptides detected (IMAC elution and flow through) for each protein reported. A Student's t-test was used to determine if the change in abundance was statistically significant ($p \leq 0.05\%$). For phospho-peptides observed in two out of three experiments, only the two experiments were used for statistical analysis. Phospho-peptides listed in Table 2.1 or Table 2.2 are highlighted in yellow. ** no phosphosite with a phosphoRS probability of at least 80% was identified.

Gene ID	Predicted Protein Product	Peptide Sequence	Spectral Counts		p-Value	# of Repeats
			DMSO	AEE788		
Tb427.01.4310	hypothetical protein, conserved	GPADGDsESDAASSAVDIR	**27** (240)	**11** (172)	0.10	3
Tb427.01.4310	hypothetical protein, conserved	SAGTPLRsAHNETAR	**4** (240)	**1** (172)	0.27	2
Tb427.01.4310	hypothetical protein, conserved	SVRsssKHSPAGAGR	**6** (240)	**1** (172)	0.08	3
Tb427.02.3020	hypothetical protein, conserved	GFVASPHsTLSEEAPK	**8** (9)	**3** (4)	0.02	3
Tb427.02.3480	Transcription Elongation Factor	EGsAAsADDDVAYVVDmLR	**38** (43)	**10** (10)	0.18	3
Tb427.02.4060	dynein intermediate chain IC 138	STDSKKEVEAAIHVLDNGVDR **	**8** (10)	**2** (2)	0.10	3
Tb427.02.4710	RNA-binding protein (TRRM1)	TTEDVPQADGAGAGsAEDAAGEVSNGANR	**4** (40)	**0** (24)	0.18	2
Tb427.02.5760	Flagellar Member 8 (FLAM8)	ATSTSSlyFSPSSVPPFVR	**31** (54)	**0** (27)	0.16	2
Tb427.03.1900	hypothetical protein, conserved	ETLNSDSSRPAtPQK	**14** (63)	**4** (29)	0.14	3
Tb427.03.1920	NOT5 protein	LGsGSPsPHKGNTSITSTVGGR	**21** (44)	**3** (19)	0.05	3
Tb427.03.3080	serine/threonine-protein kinase Nek1	ADTsDIsLSHEDLsR	**12** (16)	**0** (7)	0.02	3
Tb427.03.3620	hypothetical protein, conserved	SRGGDsAsNEEGKELPPVPPPPR	**13** (13)	**3** (3)	0.21	3
Tb427.03.4270	hypothetical protein, conserved	NAGQGsPSFSPKSPSAPFLFPGPR	**9** (22)	**7** (7)	0.12	3
Tb427.03.5040	hypothetical protein, conserved	SVQSLHSGGDStTGQSQHAANPK	**6** (18)	**1** (12)	0.24	2
Tb427.03.5250	ZC3H8	AEVAHSRVssGIVSINTGAPSVGcTAEGIK	**9** (11)	**2** (4)	0.06	3
Tb427.03.5260	hypothetical protein, conserved	SSSLGsNIAPSPMGGNASR	**8** (10)	**1** (3)	0.19	3
Tb427.03.5370	hypothetical protein, conserved	RVPEPSTPITEALTTPEsVK	**48** (77)	**19** (44)	0.04	3
Tb427.04.2600	hypothetical protein, conserved	AYSPLAmsssDKSELEGGDLAPSSLAR	**26** (34)	**9** (20)	0.04	3
Tb427.04.5020; Tb42	DNA-directed RNA polymerase subunit (RPC160)	DHDAtPFVNNAsLFLR	**7** (28)	**2** (14)	0.37	2
Tb427.05.1900	hypothetical protein, conserved	LETSATPADGGSGELGsDHsDSGGVSGK	**25** (31)	**11** (13)	0.08	3
Tb427.05.2060	cell division control protein (CDC5)	sSSRPSVGSVGDTPVLLDFTSPSGR	**20** (20)	**3** (3)	0.04	3
Tb427.05.2330	hypothetical protein, conserved	RKsSSAAVSGLISGISVK	**10** (17)	**5** (13)	0.33	3
Tb427.05.500	hypothetical protein, conserved	RTsNKDsTYcSNVVGTTGGR	**6** (13)	**1** (4)	0.08	3
Tb427.05.790	casein kinase I isoform 1	IHDTLHPSSDAALEDGDEEsDDtE	**4** (4)	**1** (1)	0.25	2
Tb427.06.3100	IFTB protein 46 C terminal	TTGGSGGDATETsPPtPK	**10** (23)	**3** (14)	0.16	3
Tb427.06.640	kinetoplastid-specific protein phosphatase	HSSNNSSTNsGNDKPIETQAPHR	**17** (27)	**3** (15)	0.26	2
Tb427.07.1650	hypothetical protein, conserved	VLVPILEGGQPmFPmDDTsDSDGER	**15** (17)	**3** (5)	0.23	2
Tb427.07.2650	hypothetical protein, conserved	DDGDGEWSELGsEVTsELR	**32** (193)	**8** (129)	0.25	3
Tb427.07.2650	hypothetical protein, conserved	sDRQPssGAPEEEEETEEQIIIR	**32** (193)	**2** (129)	0.13	3
Tb427.07.3550	hypothetical protein, conserved	DSRLsSGHPSGNR	**5** (198)	**1** (187)	0.05	3
Tb427.07.3980	immunodominant antigen,	RsPAGAAKPASNVLAPTTGTK	**6** (12)	**1** (6)	0.19	2
Tb427.07.4410	hypothetical protein, conserved	KssFNAVETHR	**6** (11)	**3** (9)	0.23	3
Tb427.07.5250	hypothetical protein, conserved	SARTtPSFVVTILPSEATTTPR	**5** (11)	**1** (11)	0.05	3
Tb427.07.650	hypothetical protein, conserved	ARGEQTTAMVAEsERGsSYGmESR	**5** (6)	**0** (0)	0.03	3
Tb427.07.6610	hypothetical protein, conserved	SRSSTsGENHSQVTVSSASSR	**26** (35)	**2** (7)	0.03	3
Tb427.07.7000	Bilobe protein, conserved	sMTHYSPTHDSNR	**5** (38)	**1** (68)	0.23	3
Tb427.07.7400	hypothetical protein, conserved	RGDSVTRPPTSLLsDDYETR	**4** (5)	**0** (2)	0.12	3
Tb427.07.810	hypothetical protein, conserved	SVTsVEQEPATADTATDIK	**4** (4)	**1** (1)	0.25	3
Tb427.08.1050	hypothetical protein, conserved	sVsVPFVSFTDADEQPK	**6** (22)	**2** (20)	0.13	3
Tb427.08.3680	kinetoplastid kinetochore protein 4 (kkt4)	EREGtVSTTPTRPLK	**8** (18)	**3** (10)	0.13	3
Tb427.08.5800	hypothetical protein, conserved	IVAKPTESHSTSSAsAGAAKPR	**4** (4)	**0** (0)	0.12	3
Tb427.08.6790	hypothetical protein, conserved	sHFssEVHDASR	**9** (9)	**3** (3)	0.07	3
Tb427.08.6870	hypothetical protein, conserved	AKSGASSAtGDDKSDLFEPPPINDEVR	**12** (12)	**3** (3)	0.10	3
Tb427.08.6980	hypothetical protein, conserved	IGssEATSPAVTAMASVIDSPISVADR	**35** (48)	**7** (11)	0.00	3
Tb427.08.8000	hypothetical protein, conserved	GVDTRDSLFADGGELDsFYAK	**8** (11)	**4** (5)	0.52	3
Tb427.10.11800	33 kDa inner dynein arm light chain, axonemal	FVLEGGPPssDLGVEL	**7** (8)	**2** (3)	0.11	3
Tb427.10.12640	chaperone protein DNAj	RVSsVGDGSNFNVK	**6** (6)	**3** (3)	0.23	3
Tb427.10.13250	hypothetical protein, conserved	YGDTPGSPLSEITTHSSDSEVPEYFYAGSQT	**10** (12)	**2** (5)	0.21	2
Tb427.10.14010	tubulin cofactor C domain-containing protein (RP2)	EATPPEsASRSDSSAPTTPHSR	**8** (25)	**1** (7)	0.05	3
Tb427.10.14010	tubulin cofactor C domain-containing protein (RP2)	TGAEEWTGNKESssPERGK	**8** (25)	**0** (7)	0.21	2
Tb427.10.15040	hypothetical protein, conserved	NVEFPVVGsDEGNKsR	**6** (8)	**0** (0)	0.03	3
Tb427.10.15080	hypothetical protein, conserved	sIASSTHTVAYLADEFGR	**15** (23)	**2** (2)	0.01	3
Tb427.10.15080	hypothetical protein, conserved	sRsPsITVFTVLNPK	**12** (23)	**0** (2)	0.01	3
Tb427.10.15310	hypothetical protein, conserved	KsEsDVcGEGSELLLQQYR	**6** (25)	**2** (10)	0.18	3
Tb427.10.1890	cysteine peptidase, Clan CA, family C2	sATPAPGESQEEDPDLVEFLR	**9** (9)	**0** (1)	0.12	2
Tb427.10.1970	hypothetical protein, conserved	TRSSLLsRDSIGLLPASGTQQNALSR	**11** (12)	**5** (5)	0.18	3
Tb427.10.2080	hypothetical protein, conserved	TAAAtDIPRGADDMIEVKEtK	**8** (8)	**1** (2)	0.07	3
Tb427.10.2920	hypothetical protein, conserved	EADINDLPSSFcPFPPATLTASSPPVsGR	**7** (8)	**3** (3)	0.37	3

(Supplemental Table 2.2 continued)

Tb427.10.3010	Bilobe protein, conserved	KPPTTSSTPsPAHPVLR	**7** (13)	**1** (6)	0.10	3
Tb427.10.3780	hypothetical protein, conserved	SYVTVLEGsQAsLFK	**6** (16)	**1** (3)	0.07	3
Tb427.10.5200	hypothetical protein, conserved	FGIPLSTETPsERSGGDDVDDIDGSGLAK	**9** (10)	**1** (1)	0.09	3
Tb427.10.5240	cAMP binding protein	sPSLPSTPR	**8** (9)	**2** (2)	0.06	3
Tb427.10.5470	hypothetical protein, conserved	CRLTTNSSTVPSAEVLR **	**6** (7)	**0** (0)	0.12	2
Tb427.10.5880	Proteophosphoglycan,	SLLHPsHSGSsDSSYPTASK	**13** (47)	**6** (20)	0.04	3
Tb427.10.5880	Proteophosphoglycan	VTPDGGKGsNITSSR	**8** (47)	**1** (20)	0.01	2
Tb427.10.5910	hypothetical protein, conserved	ANVESGSSTRPPsR	**5** (15)	**0** (6)	0.13	2
Tb427.10.5990	hypothetical protein, conserved	HLVNIsGHsAER	**5** (4)	**1** (0)	0.05	3
Tb427.10.6000	hypothetical protein, conserved	VAtVLtEstEHDVSDFYR	**10** (10)	**2** (5)	0.00	3
Tb427.10.7790	ubiquitin fusion degradation protein	VEFERPLDmPPsPTESER	**11** (15)	**4** (4)	0.44	2
Tb427.10.8000	hypothetical protein, conserved	AVtPLsPYEVTSVHEVPmIHR	**15** (17)	**3** (4)	0.01	3
Tb427.10.840	WD domain, G-beta repeat, (FAZ6)	AGsETETSLLTEVQVLR	**11** (46)	**0** (18)	0.24	3
Tb427.10.840	WD domain, G-beta repeat, (FAZ6)	GAPHssSDAIAELLPDR	**4** (46)	**1** (18)	0.25	2
Tb427.10.840	WD domain, G-beta repeat, (FAZ6)	GTSPSAtPPGK	**8** (46)	**3** (18)	0.08	3
Tb427.10.8780	AAA domain containing protein	EAMSSVSYSEMsSGGIPEVR	**12** (13)	**3** (7)	0.39	2
Tb427.10.8820	Bilobe protein, conserved	TIGTTSGHSTTNLssHTPEK	**6** (17)	**0** (5)	0.03	3
Tb427.10.8930	paraflagellar rod component	VASSGKEDTEEAPsASSETGVSTPGDEK	**11** (27)	**5** (12)	0.18	3
Tb427.10.970	Tetratricopeptide repeat	IALsSVFESKDAR	**10** (16)	**5** (13)	0.33	3
Tb427tmp.01.0230	hypothetical protein, conserved	ALKFsLsPVtTR	**7** (18)	**1** (10)	0.06	3
Tb427tmp.01.1170	hypothetical protein, conserved	KAsGDQPADDTALTGSFVNVLSSHcDAR	**7** (105)	**3** (65)	0.37	2
Tb427tmp.01.1170	hypothetical protein, conserved	LHEGSTSQHsR	**4** (105)	**1** (65)	0.25	2
Tb427tmp.01.1960	hypothetical protein, conserved	KRPSsIGRPSSR	**9** (31)	**2** (5)	0.12	3
Tb427tmp.01.1960	hypothetical protein, conserved	KTsSAPsLLPQIK	**20** (31)	**2** (5)	0.03	3
Tb427tmp.01.3000	paraflagellar rod component (PFC17)	LPPIVPLVYDFDEDDLSNYcSSTADsR	**28** (31)	**6** (9)	0.32	2
Tb427tmp.01.3720	hypothetical protein	SRPRtPAsPAAPR	**8** (13)	**2** (7)	0.14	3
Tb427tmp.01.3960	Bilbo1	HAsFHGsTSNALVPR	**20** (41)	**7** (26)	0.10	3
Tb427tmp.01.3960	Bilbo1	LMSEASsFLGNLR	**5** (41)	**0** (26)	0.04	3
Tb427tmp.01.4850	hypothetical protein, conserved	FEAILsNLRASGTR	**12** (60)	**2** (38)	0.03	3
Tb427tmp.01.6790	hypothetical protein, conserved	MAScDSsVDRNQYHTEYEGR	**10** (46)	**3** (52)	0.28	3
Tb427tmp.01.6900	hypothetical protein, conserved	VESsVGPVDsAHMSR	**4** (9)	**1** (1)	0.25	2
Tb427tmp.01.7450	hypothetical protein, conserved	NQsESsALRPSISPSTR	**12** (40)	**0** (1)	0.15	3
Tb427tmp.01.7450	hypothetical protein, conserved	SEKHPGDtPDsVISTSK	**17** (40)	**1** (1)	0.00	3
Tb427tmp.01.7450	hypothetical protein, conserved	SQAVAADAVDGAcHsISNESSSR	**4** (40)	**0** (1)	0.12	2
Tb427tmp.01.7450	hypothetical protein, conserved	tVSTNLSSVLPAR	**4** (40)	**0** (1)	0.12	2
Tb427tmp.01.8190	hypothetical protein, conserved	TVGGGRPssGRPsGR	**10** (29)	**1** (20)	0.00	3
Tb427tmp.01.8330	zinc-finger of a C2HC-type	RSEVPASSEVAGNTSVsVDsR	**19** (33)	**1** (22)	0.00	3
Tb427tmp.01.8640	leucine-rich repeat protein (LRRP)	DLTSLHTESVVTsIR	**9** (11)	**1** (2)	0.02	3
Tb427tmp.01.8770	leucine-rich repeat protein (LRRP)	LDASSTDETSTSAPAPmPGAAQALAAALNS	**46** (115)	**12** (78)	0.35	2
Tb427tmp.02.1410	hypothetical protein, conserved	SHAVESHAYSYSTtPR	**13** (20)	**1** (4)	0.16	3
Tb427tmp.02.3050	hypothetical protein, conserved	GGETGSGTRtPEGLSPSR	**21** (23)	**8** (11)	0.24	3
Tb427tmp.02.3880	Flagellar-associated PapD-like	LSAPQtSHSSTAEmIPLFDDIPK	**8** (15)	**1** (3)	0.26	2
Tb427tmp.02.4290	hypothetical protein, conserved	SSPTsNGGFTVTAVFGAPDSTSR	**9** (8)	**0** (0)	0.04	3
Tb427tmp.03.0020	hypothetical protein, conserved	VRLEDLPTIESAGGScGsLSSFEGD	**8** (8)	**1** (1)	0.26	2
Tb427tmp.03.0300	hypothetical protein, conserved	SLTVDVmsPIIsEEGEAK	**12** (15)	**0** (7)	0.25	3
Tb427tmp.03.0760	repressor activator protein 1	sVsPGGVHPQTAAVSALSR	**9** (11)	**3** (5)	0.07	3
Tb427tmp.160.0400	hypothetical protein, conserved	IGLNTAFVAtPtSSEAETTYR	**8** (9)	**3** (4)	0.08	3
Tb427tmp.160.0650	Fibronectin type III domain containing protein	HAASSSGsSPAPGGVK	**13** (37)	**5** (22)	0.04	3
Tb427tmp.160.1120	hypothetical protein, conserved	FNLPINSPLGTAPVmSPQsGsGR	**18** (18)	**0** (0)	0.04	3
Tb427tmp.160.1790	hypothetical protein, conserved	SAVNLFVAEGDssDDDEVTEDALR	**7** (15)	**3** (6)	0.12	3
Tb427tmp.160.3060	hypothetical protein	ASSAHRSPGMLLVPFGPTR **	**5** (5)	**0** (0)	0.13	2
Tb427tmp.211.3300	Peroxin 19	EGEGSGTSLsDGDDDKPSEEELATIR	**9** (10)	**4** (5)	0.25	3
Tb427tmp.211.4270	ubiquitin carboxyl-terminal hydrolase	TDTTDsQLFSLADLQLAR	**6** (6)	**1** (3)	0.24	2
Tb427tmp.47.0011	Right handed beta helix region	KVsHSNTSVLLPNVR	**7** (14)	**2** (2)	0.02	3
Tb427tmp.47.0027	hypothetical protein, conserved	sRtESVETPsLDLPIPLVR	**45** (46)	**9** (11)	0.00	3
Tb427tmp.50.0001	hypothetical protein, conserved	sVsADENGEDPAVASGADIPAHVmR	**13** (28)	**6** (20)	0.21	3
Tb427tmp.50.0002	SCAMP family	GSHDTPTNMEEMNVFSEsDESLHR	**16** (38)	**8** (44)	0.43	3

Supplemental Table 2.3. *Phospho-peptides with increased abundance after treatment with AEE788 for (4 h)*. Phospho-peptides from trypanosomes treated with DMSO (0.1%) or AEE788 (5 μM) were enriched over an IMAC column. LC-MS/MS was used to monitor the abundance of observed phospho-peptides over three independent experiments. The phospho-peptides listed here demonstrated an increase (2-fold, or greater) in abundance in at least two out of three biological replicates. The phosphosite is highlighted in red (phosphoRS [104] score above 80%). Spectral counts indicate the combined number of times a phospho-peptide was observed over the three independent experiments. The number in parenthesis is the summation of all unique peptides detected (IMAC elution and flow through) for each protein reported. A Student's t-test was used to determine if the change in abundance was statistically significant ($p \leq 0.05\%$). For phospho-peptides observed in two out of three experiments, only the two experiments were used for statistical analysis. Phospho-peptides listed in Table 2.1 or Table 2.2 are highlighted in yellow. ** no phosphosite with a phosphoRS probability of at least 80% was identified.

Gene ID	Predicted Protein Product	Peptide Sequence	Spectral Counts		p-Value	# of Repeats
			DMSO	AEE788		
Tb427.01.2100	calpain-like cysteine peptidase	AEEASPAPSPAGEsDEKAsKSEHESEAK	**20** (88)	**44** (99)	0.02	3
Tb427.01.3220	GTPase activating protein	SEAPAGTTNTSSSSLSETHGDSAVVSK **	**2** (2)	**10** (10)	0.15	3
Tb427.02.5010	pleckstrin homology	TNsLYSSSVNGER	**2** (7)	**4** (4)	0.42	2
Tb427.04.4510	protein phosphatase 2C	GsAADHSETSDTcHGLSASPTVSR	**3** (8)	**6** (12)	0.16	3
Tb427.04.5020/Tb42	RNA polymerase IIA subunit (RPB1)	DHDAtPFVNNAsLFLR	**2** (19)	**6** (17)	0.02	3
Tb427.05.1680	hypothetical protein, conserved	NHsLPsNFSTYDFVK	**4** (18)	**9** (16)	0.19	3
Tb427.05.1950	hypothetical protein, conserved	LSASEEsHTPGSLEDELVHSSVR	**0** (1)	**6** (16)	0.12	2
Tb427.05.1950	hypothetical protein, conserved	SATDIKHsGGPLsDGLLR	**1** (1)	**7** (16)	0.01	3
Tb427.05.2500	hypothetical protein, conserved	ERtPPtPVR	**2** (3)	**7** (8)	0.02	3
Tb427.07.1240	sphingosine kinase A, B	ADsFYSSTALPHsR	**6** (12)	**14** (22)	0.24	3
Tb427.07.7000	Bilobe protein, conserved	YATPKDDVssNEEDDQEVLK	**2** (22)	**4** (25)	0.42	2
Tb427.08.5580	hypothetical protein, conserved	AKNSESDsDDALASTAPVVAQR	**3** (14)	**6** (14)	0.16	3
Tb427.08.8000	hypothetical protein, conserved	GVDTRDsLFADGGELDsFYAK	**3** (4)	**6** (7)	0.16	3
Tb427.10.13250	hypothetical protein, conserved	YGDTPGSPLSEITTHSSDSEVPEYFYAGSQTIR	**4** (9)	**8** (9)	0.42	2
Tb427.10.8830	hypothetical protein, conserved	GAmVsGssAPQTAPAHQR	**5** (7)	**12** (12)	0.32	3
Tb427.10.9330	hypothetical protein, conserved	ASGEVNAESNVHsPASVTAK	**6** (9)	**13** (15)	0.44	3
Tb427tmp.01.0300	hypothetical protein, conserved	SAmAATDGGAPSSTRtsVVGNASR	**2** (3)	**8** (8)	0.14	3
Tb427tmp.01.0680	leucine rich repeat (TbLRRP1)	TSGVPsREETVDLR	**6** (61)	**13** (48)	0.23	3
Tb427tmp.01.1170	hypothetical protein, conserved	KAsGDQPADDTALTGSFVNVLSSHcDAR	**4** (86)	**8** (77)	0.30	3
Tb427tmp.01.8330	zinc-finger of a C2HC-type	RLsVSSLTHPTTAEGAHDVGSTEGAPR	**3** (42)	**11** (47)	0.02	3
Tb427tmp.02.4210	AAA ATPase	EAEIDVLGssGsRDDNHDREEK	**2** (5)	**6** (6)	0.06	3
Tb427tmp.160.4020	cysteine peptidase	SATDsVHAEEEHLEK	**0** (2)	**4** (4)	0.12	2

Supplemental Table 2.4. *Phospho-peptides with increased abundance after treatment with AEE788 for (9 h)*. Phospho-peptides from trypanosomes treated with DMSO (0.1%) or AEE788 (5 μM) were enriched over an IMAC column. LC-MS/MS was used to monitor the abundance of observed phospho-peptides over three independent experiments. The phospho-peptides listed here demonstrated an increase (2-fold, or greater) in abundance in at least two out of three biological replicates. The phospho-site is highlighted in red (phosphoRS [104] score above 80%). Spectral counts indicate the combined number of times a phospho-peptide was observed over the three independent experiments. The number in parenthesis is the summation of all unique peptides detected (IMAC elution and flow through) for each protein reported. A Student's t-test was used to determine if the change in abundance was statistically significant ($p \leq 0.05\%$). For phospho-peptides observed in two out of three experiments, only the two experiments were used for statistical analysis. Phospho-peptides listed in Table 2.1 or Table 2.2 are highlighted in yellow. ** no phospho-site with a phosphoRS probability of at least 80% was identified.

Gene ID	Predicted Protein Product	Peptide Sequence	Spectral Counts		p-Value	# of Repeats
			DMSO	AEE788		
Tb427.01.1020	leucine-rich repeat-containing protein	sCELsTVERPIR	**1** (4)	**5** (9)	0.05	3
Tb427.01.1020	leucine-rich repeat-containing protein	LAsPGSLsR	**2** (4)	**7** (9)	0.09	3
Tb427.01.2100	calpain-like cysteine peptidase	DGLDAHAEEASPAPSPAGEsDEKAsKSEHESEAK	**21** (93)	**46** (128)	0.21	3
Tb427.01.2100	calpain-like cysteine peptidase	SERESGTADGSSGRPEEVSHAFSPNR **	**6** (93)	**12** (128)	0.44	3
Tb427.02.4050	hypothetical protein, conserved	ETETSAttPTPLHSDAGVR	**2** (3)	**6** (5)	0.06	3
Tb427.03.3940	RNA-binding protein	TPLNNESGPGTSSSGSHSSSSNVPVASLR **	**1** (4)	**8** (8)	0.23	2
Tb427.03.4970	hypothetical protein, conserved	SVPTLQLPAsVGGsAK	**2** (2)	**6** (7)	0.18	2
Tb427.04.310	SPRY domain/HECT-domain	TTLSKsAHVsHER	**3** (3)	**8** (9)	0.04	3
Tb427.04.3970	hypothetical protein, conserved	RSSSGHRVSVLTDDTNASSGAASR **	**1** (3)	**12** (24)	0.01	3
Tb427.04.3970	hypothetical protein, conserved	LPDscVsVSAPIR	**0** (3)	**5** (24)	0.04	2
Tb427.04.3970	hypothetical protein, conserved	AFVsFLPsPR	**2** (3)	**8** (24)	0.10	3
Tb427.05.1950	hypothetical protein, conserved	SATDIKHsGGPLsDGLLR	**0** (0)	**18** (29)	0.11	3
Tb427.05.1950	hypothetical protein, conserved	HsGGPLsDGLLR	**0** (0)	**5** (29)	0.04	3
Tb427.05.1950	hypothetical protein, conserved	LSAsEEsHTPGSLEDELVHSSVR	**0** (0)	**4** (29)	0.07	2
Tb427.05.2620	hypothetical protein, conserved	MTTGDGSSTVsGGsGSSIR	**0** (27)	**7** (28)	0.02	3
Tb427.05.2820	protein kinase	NPSVTRSPSVLsNSPAPDNLR	**8** (9)	**16** (20)	0.29	3
Tb427.06.4710	calmodulin	LLssKEDSASLPTK	**1** (10)	**6** (6)	0.08	3
Tb427.07.1020	hypothetical protein, conserved	KLHYLTHsDsD	**3** (5)	**6** (6)	0.23	3
Tb427.07.2140	ZC3H18	EIAFVGEDASSTGsGLHHSR	**0** (4)	**10** (20)	0.04	2
Tb427.07.2660	ZC3H2	SVTLGDAsVTTQPAVVR	**0** (0)	**11** (12)	0.07	2
Tb427.07.3550	hypothetical protein, conserved	ELsNEKEEEGSSPR	**3** (198)	**7** (141)	0.15	2
Tb427.07.3610	hypothetical protein, conserved	sHEsLKLPVIR	**3** (7)	**6** (9)	0.29	2
Tb427.07.5250	hypothetical protein, conserved	FVSGTPGTFDTNGGAPPsGR	**1** (9)	**7** (12)	0.05	2
Tb427.07.6640	hypothetical protein, conserved	SPSSSIGsVTGAAANDGAAAGSERPISVEAK	**2** (29)	**6** (23)	0.18	2
Tb427.07.7000	Bilobe protein, conserved	TSSHIsEHGLDR	**0** (38)	**10** (67)	0.02	3
Tb427.07.7000	Bilobe protein, conserved	SGSDMISTVHsDAEVTVR	**6** (38)	**17** (67)	0.28	3
Tb427.08.5710	recombination initiation protein NBS1	DTFRSPsPMVR	**2** (8)	**5** (10)	0.10	3
Tb427.08.5730	STE20 Protein Kinaes	LADFGVSTELSHSLsR	**2** (1)	**6** (6)	0.05	2
Tb427.08.840	hypothetical protein, conserved	MSLPEDTSNLGDsIDR	**0** (0)	**5** (4)	0.04	3
Tb427.10.14770	Associated kinase of Tb14-3-3 (AKB1)	LANSsLPVsHTSTR	**7** (13)	**15** (18)	0.02	3
Tb427.10.14950	RNA binding protein (ZC3H40)	GGGGINSGNNtANNStANADIAtPTATGR	**3** (7)	**9** (13)	0.20	2
Tb427.10.15700	hypothetical protein, conserved	STSGVSTALTIGTK **	**1** (6)	**7** (17)	0.20	2
Tb427.10.2930	hypothetical protein, conserved	KSDsNDNALASIIR	**4** (16)	**12** (21)	0.02	3
Tb427.10.3700	AMP-activated PK, gamma reg subunit	GVSADTAMSSSITsR	**4** (8)	**11** (17)	0.13	3
Tb427.10.570	Sec8 domain containing protein	LsVDSALNTPHHVASTR	**2** (3)	**4** (5)	0.11	2
Tb427.10.5870	hypothetical protein, conserved	VEDTHVAAVSLTSsR	**2** (11)	**7** (16)	0.02	3
Tb427.10.6240	ras-like small GTPase (TbRHP)	RTPSLVGVAVAsR	**6** (6)	**13** (13)	0.30	3
Tb427.10.8780	AAA domain containing protein	AEDsAVLEPSAAEGVEENsGEVPK	**1** (13)	**6** (7)	0.04	3
Tb427.10.9700	hypothetical protein, conserved	AKSYAssADAFSSSAQR	**3** (12)	**9** (11)	0.22	3
Tb427tmp.01.0300	hypothetical protein, conserved	SAmAATDGGAPSSTRTsVVGNASR	**1** (4)	**9** (14)	0.02	3
Tb427tmp.01.0390	dynein heavy chain	LDSQSLTAtDTVsERPK	**1** (6)	**4** (4)	0.10	2
Tb427tmp.02.2890	hypothetical protein, conserved	EVEDAPPDmSGITSVmPsEHVY	**0** (3)	**20** (20)	0.29	2
Tb427tmp.02.4210	AAA ATPase	DEsVDSSITDESLRR	**0** (4)	**10** (13)	0.21	3
Tb427tmp.02.4750	hypothetical protein, conserved	TTsLHVsPVR	**0** (0)	**4** (5)	0.18	2
Tb427tmp.02.5190	pantothenate kinase subunit	LyASSSEDLSGAVSSSPDSNPTLHDAVAPTLASHGK	**0** (1)	**7** (9)	0.14	2
Tb427tmp.160.4020	cysteine peptidase	sATDsVHAEEEHLEK	**0** (1)	**4** (5)	0.18	2
Tb427tmp.160.4770	AAK1	AVTALssDTASTDPEVLAYR	**0** (9)	**12** (33)	0.18	2
Tb427tmp.160.4770	AAK1	DEAAASsVKscTAAQESGDNDQmVLK	**1** (9)	**11** (33)	0.09	2
Tb427tmp.18.0003	dynein intermediate chain IC140	VEAFRPEEDTmsLSELDGDGADTR	**0** (2)	**10** (10)	0.04	2
Tb427tmp.46.0003	protein kinase	KNsNDGsPTPDHAGDEPIDVR	**0** (1)	**4** (4)	0.18	2
Tb427tmp.52.0002	hypothetical protein, conserved	KLGESDEGLAsRPVSPSPESGK	**6** (38)	**16** (44)	0.07	3

2.6 References

1. Lejon, V. and P. Buscher, *Review Article: cerebrospinal fluid in human African trypanosomiasis: a key to diagnosis, therapeutic decision and post-treatment follow-up.* Trop Med Int Health, 2005. **10**(5): p. 395-403.

2. Kennedy, P.G.E., *Clinical features, diagnosis, and treatment of human African trypanosomiasis (sleeping sickness).* The Lancet Neurology, 2013. **12**(2): p. 186-194.

3. Babokhov, P., et al., *A current analysis of chemotherapy strategies for the treatment of human African trypanosomiasis.* Pathog Glob Health, 2013. **107**(5): p. 242-52.

4. Patel, G., et al., *Kinase scaffold repurposing for neglected disease drug discovery: discovery of an efficacious, lapatinib-derived lead compound for trypanosomiasis.* J Med Chem, 2013. **56**(10): p. 3820-32.

5. DiMasi, J.A., R.W. Hansen, and H.G. Grabowski, *The price of innovation: new estimates of drug development costs.* Journal of Health Economics, 2003. **22**(2): p. 151-185.

6. Traxler, P., et al., *AEE788: a dual family epidermal growth factor receptor/ErbB2 and vascular endothelial growth factor receptor tyrosine kinase inhibitor with antitumor and antiangiogenic activity.* Cancer Res, 2004. **64**(14): p. 4931-41.

7. Daniela Meco, T.S., Gian Franco Zannoni, Enrica Marinelli, Maria Grazia Prisco, Chiara de Waure and Riccardo Riccardi, *Dual inhibitor AEE788 reduces tumor growth in preclinical models of medulloblastoma.* Translational oncology, 2010. **3**: p. 326-335.

8. Behera, R., S.M. Thomas, and K. Mensa-Wilmot, *New Chemical Scaffolds for Human African Trypanosomiasis Lead Discovery from a Screen of Tyrosine Kinase Inhibitor Drugs.* Antimicrob Agents Chemother, 2014.

9. Katiyar, S., et al., *Lapatinib-binding protein kinases in the african trypanosome: identification of cellular targets for kinase-directed chemical scaffolds.* PLoS One, 2013. **8**(2): p. e56150.

10. Dar, A.C. and K.M. Shokat, *The evolution of protein kinase inhibitors from antagonists to agonists of cellular signaling.* Annu Rev Biochem, 2011. **80**: p. 769-95.

11. Sherwin, T. and K. Gull, *The cell division cycle of Trypanosoma brucei brucei: timing of event markers and cytoskeletal modulations.* Philos Trans R Soc Lond B Biol Sci, 1989. **323**(1218): p. 573-88.

12. Woodward, R. and K. Gull, *Timing of nuclear and kinetoplast DNA replication and early morphological events in the cell cycle of Trypanosoma brucei.* J Cell Sci, 1990. **95 (Pt 1)**: p. 49-57.

13. Jensen, R.E. and P.T. Englund, *Network news: the replication of kinetoplast DNA.* Annu Rev Microbiol, 2012. **66**: p. 473-91.

14. Gluenz, E., et al., *The kinetoplast duplication cycle in Trypanosoma brucei is orchestrated by cytoskeleton-mediated cell morphogenesis.* Mol Cell Biol, 2011. **31**(5): p. 1012-21.

15. Siegel, T.N., D.R. Hekstra, and G.A. Cross, *Analysis of the Trypanosoma brucei cell cycle by quantitative DAPI imaging.* Mol Biochem Parasitol, 2008. **160**(2): p. 171-4.

16. Zhou, Q., H. Hu, and Z. Li, *New insights into the molecular mechanisms of mitosis and cytokinesis in trypanosomes.* Int Rev Cell Mol Biol, 2014. **308**: p. 127-66.

17. Hammarton, T.C., *Cell cycle regulation in Trypanosoma brucei.* Mol Biochem Parasitol, 2007. **153**(1): p. 1-8.

18. Li, Z., *Regulation of the cell division cycle in Trypanosoma brucei.* Eukaryot Cell, 2012. **11**(10): p. 1180-90.

19. Ogbadoyi, E.O., D.R. Robinson, and K. Gull, *A high-order trans-membrane structural linkage is responsible for mitochondrial genome positioning and segregation by flagellar basal bodies in trypanosomes.* Mol Biol Cell, 2003. **14**(5): p. 1769-79.

20. Robinson, D.R. and K. Gull, *Basal body movements as a mechanism for mitochondrial genome segregation in the trypanosome cell cycle.* Nature, 1991. **352**(6337): p. 731-3.

21. Lacomble, S., et al., *Basal body movements orchestrate membrane organelle division and cell morphogenesis in Trypanosoma brucei.* J Cell Sci, 2010. **123**(Pt 17): p. 2884-91.

22. Lacomble, S., et al., *Three-dimensional cellular architecture of the flagellar pocket and associated cytoskeleton in trypanosomes revealed by electron microscope tomography.* J Cell Sci, 2009. **122**(Pt 8): p. 1081-90.

23. Kohl, L., T. Sherwin, and K. Gull, *Assembly of the paraflagellar rod and the flagellum attachment zone complex during the Trypanosoma brucei cell cycle.* J Eukaryot Microbiol, 1999. **46**(2): p. 105-9.

24. Kohl, L., D. Robinson, and P. Bastin, *Novel roles for the flagellum in cell morphogenesis and cytokinesis of trypanosomes.* EMBO J, 2003. **22**(20): p. 5336-46.

25. Robinson, D.R., et al., *Microtubule polarity and dynamics in the control of organelle positioning, segregation, and cytokinesis in the trypanosome cell cycle.* J Cell Biol, 1995. **128**(6): p. 1163-72.

26. Esson, H.J., et al., *Morphology of the trypanosome bilobe, a novel cytoskeletal structure.* Eukaryot Cell, 2012. **11**(6): p. 761-72.

27. Zhou, Q., et al., *A comparative proteomic analysis reveals a new bi-lobe protein required for bi-lobe duplication and cell division in Trypanosoma brucei.* PLoS One, 2010. **5**(3): p. e9660.

28. Bangs, J.D., *Replication of the ERES:Golgi junction in bloodstream-form African trypanosomes.* Mol Microbiol, 2011. **82**(6): p. 1433-43.

29. Field, M.C., et al., *Chapter 1 Macromolecular Trafficking and Immune Evasion in African Trypanosomes.* 2009. **278**: p. 1-67.

30. Schell, D., N.K. Borowy, and P. Overath, *Transferrin is a growth factor for the bloodstream form ofTrypanosoma brucei.* Parasitology Research, 1991. **77**(7): p. 558-560.

31. Guyett, P.J., et al., *Glycogen Synthase Kinase 3β Promotes the Endocytosis of Transferrin in the African Trypanosome.* ACS Infectious Diseases, 2016. **2**(7): p. 518-528.

32. Hesse, F., et al., *A novel cultivation technique for long-term maintenance of bloodstream form trypanosomes in vitro.* Mol Biochem Parasitol, 1995. **70**(1-2): p. 157-66.

33. Ajoko, C. and D. Steverding, *A cultivation method for growing bloodstream forms of Trypanosoma brucei to higher cell density and for longer time.* Parasitol Res, 2015. **114**(4): p. 1611-2.

34. Kaufmann, D., et al., *Regulation and spatial organization of PCNA in Trypanosoma brucei.* Biochem Biophys Res Commun, 2012. **419**(4): p. 698-702.

35. Cavanagh, B.L., et al., *Thymidine analogues for tracking DNA synthesis.* Molecules, 2011. **16**(9): p. 7980-93.

36. Liu, B., et al., *Fellowship of the rings: the replication of kinetoplast DNA.* Trends Parasitol, 2005. **21**(8): p. 363-9.

37. Povelones, M.L., *Beyond replication: Division and segregation of mitochondrial DNA in kinetoplastids.* Mol Biochem Parasitol, 2014.

38. Tiengwe, C., C.A. Marques, and R. McCulloch, *Nuclear DNA replication initiation in kinetoplastid parasites: new insights into an ancient process.* Trends Parasitol, 2014. **30**(1): p. 27-36.

39. Borst, P., et al., *On the DNA content and ploidy of trypanosomes.* Mol Biochem Parasitol, 1982. **6**(1): p. 13-23.

40. Andre, J., et al., *An alternative model for the role of RP2 protein in flagellum assembly in the African trypanosome.* J Biol Chem, 2014. **289**(1): p. 464-75.

41. Ikeda, K.N. and C.L. de Graffenried, *Polo-like kinase is necessary for flagellum inheritance in Trypanosoma brucei.* J Cell Sci, 2012. **125**(Pt 13): p. 3173-84.

42. He, C.Y., M. Pypaert, and G. Warren, *Golgi duplication in Trypanosoma brucei requires Centrin2.* Science, 2005. **310**(5751): p. 1196-8.

43. Forsythe, G.R., R. McCulloch, and T.C. Hammarton, *Hydroxyurea-induced synchronisation of bloodstream stage Trypanosoma brucei.* Mol Biochem Parasitol, 2009. **164**(2): p. 131-6.

44. Archer, S.K., et al., *The cell cycle regulated transcriptome of Trypanosoma brucei.* PLoS One, 2011. **6**(3): p. e18425.

45. Kabani, S., M. Waterfall, and K.R. Matthews, *Cell-cycle synchronisation of bloodstream forms of Trypanosoma brucei using Vybrant DyeCycle Violet-based sorting.* Mol Biochem Parasitol, 2010. **169**(1): p. 59-62.

46. Mutomba, M.C. and C.C. Wang, *Effects of aphidicolin and hydroxyurea on the cell cycle and differentiation of Trypanosoma brucei bloodstream forms.* Mol Biochem Parasitol, 1996. **80**(1): p. 89-102.

47. Hu, H., et al., *The Centriole Cartwheel Protein SAS-6 in Trypanosoma brucei Is Required for Probasal Body Biogenesis and Flagellum Assembly.* Eukaryot Cell, 2015. **14**(9): p. 898-907.

48. Garner Dl Fau - Pinkel, D., et al., *Assessment of spermatozoal function using dual fluorescent staining and flow cytometric analyses.* 1986(0006-3363 (Print)).

49. Steverding, D., et al., *ESAG 6 and 7 products of Trypanosoma brucei form a transferrin binding protein complex.* (0171-9335 (Print)).

50. Pal, A., et al., *Differential endocytic functions of Trypanosoma brucei Rab5 isoforms reveal a glycosylphosphatidylinositol-specific endosomal pathway.* J Biol Chem, 2002. **277**(11): p. 9529-39.

51. Morriswood, B. and K. Schmidt, *A MORN Repeat Protein Facilitates Protein Entry into the Flagellar Pocket of Trypanosoma brucei.* Eukaryot Cell, 2015. **14**(11): p. 1081-93.

52. Field, M.C., et al., *New approaches to the microscopic imaging of Trypanosoma brucei.* Microsc Microanal, 2004. **10**(5): p. 621-36.

53. Nolan, D.P., M. Geuskens, and E. Pays, *N-linked glycans containing linear poly-N-acetyllactosamine as sorting signals in endocytosis in Trypanosoma brucei.* Curr Biol, 1999. **9**(20): p. 1169-72.

54. de Graffenried, C.L., et al., *Polo-like kinase phosphorylation of bilobe-resident TbCentrin2 facilitates flagellar inheritance in Trypanosoma brucei.* Mol Biol Cell, 2013. **24**(12): p. 1947-63.

55. Portman, N. and K. Gull, *The paraflagellar rod of kinetoplastid parasites: from structure to components and function.* Int J Parasitol, 2010. **40**(2): p. 135-48.

56. Giannakouros, T., et al., *Serine-arginine protein kinases: a small protein kinase family with a large cellular presence.* FEBS J, 2011. **278**(4): p. 570-86.

57. Hu, H., Q. Zhou, and Z. Li, *SAS-4 Protein in Trypanosoma brucei Controls Life Cycle Transitions by Modulating the Length of the Flagellum Attachment Zone Filament.* J Biol Chem, 2015. **290**(51): p. 30453-63.

58. Morriswood, B., et al., *Novel bilobe components in Trypanosoma brucei identified using proximity-dependent biotinylation.* Eukaryot Cell, 2013. **12**(2): p. 356-67.

59. Fry, A.M., et al., *Cell cycle regulation by the NEK family of protein kinases.* J Cell Sci, 2012. **125**(Pt 19): p. 4423-33.

60. Bonhivers, M., et al., *Biogenesis of the trypanosome endo-exocytotic organelle is cytoskeleton mediated.* PLoS Biol, 2008. **6**(5): p. e105.

61. Inoue, M., et al., *Identification and characterization of a cell division-regulating kinase AKB1 (associated kinase of Trypanosoma brucei 14-3-3) through proteomics study of the Tb14-3-3 binding proteins.* J Biochem, 2015. **158**(1): p. 49-60.

62. Wang, S.A., et al., *Phosphorylation of p300 increases its protein degradation to enhance the lung cancer progression.* Biochim Biophys Acta, 2014. **1843**(6): p. 1135-49.

63. Ishida, N., et al., *Phosphorylation at serine 10, a major phosphorylation site of p27(Kip1), increases its protein stability.* J Biol Chem, 2000. **275**(33): p. 25146-54.

64. Ulery, P.G., G. Rudenko, and E.J. Nestler, *Regulation of DeltaFosB stability by phosphorylation.* J Neurosci, 2006. **26**(19): p. 5131-42.

65. Vazquez, F., et al., *Phosphorylation of the PTEN tail regulates protein stability and function.* Mol Cell Biol, 2000. **20**(14): p. 5010-8.

66. Yamamoto, H., et al., *Phosphorylation of axin, a Wnt signal negative regulator, by glycogen synthase kinase-3beta regulates its stability.* J Biol Chem, 1999. **274**(16): p. 10681-4.

67. Machida, Y.J. and A. Dutta, *Cellular checkpoint mechanisms monitoring proper initiation of DNA replication.* J Biol Chem, 2005. **280**(8): p. 6253-6.

68. Nishitani, H. and Z. Lygerou, *Control of DNA replication licensing in a cell cycle.* Genes Cells, 2002. **7**(6): p. 523-34.

69. Berriman, M., et al., *The genome of the African trypanosome Trypanosoma brucei.* Science, 2005. **309**(5733): p. 416-22.

70. Parsons, M., et al., *Comparative analysis of the kinomes of three pathogenic trypanosomatids: Leishmania major, Trypanosoma brucei and Trypanosoma cruzi.* BMC Genomics, 2005. **6**: p. 127.

71. Sheu, Y.J. and B. Stillman, *The Dbf4-Cdc7 kinase promotes S-phase by alleviating an inhibitory activity in Mcm4.* Nature, 2010. **463**(7277): p. 113-7.

72. Sheu, Y.J. and B. Stillman, *Cdc7-Dbf4 phosphorylates MCM proteins via a docking site-mediated mechanism to promote S-phase progression.* Mol Cell, 2006. **24**(1): p. 101-13.

73. Zou, L. and B. Stillman, *Assembly of a complex containing Cdc45p, replication protein A, and Mcm2p at replication origins controlled by S-phase cyclin-dependent kinases and Cdc7p-Dbf4p kinase.* Mol Cell Biol, 2000. **20**(9): p. 3086-96.

74. Tanaka, S., et al., *CDK-dependent phosphorylation of Sld2 and Sld3 initiates DNA replication in budding yeast.* Nature, 2007. **445**(7125): p. 328-32.

75. Tu, X., et al., *Distinct cytoskeletal modulation and regulation of G1-S transition in the two life stages of Trypanosoma brucei.* J Cell Sci, 2005. **118**(Pt 19): p. 4353-64.

76. Tu, X. and C.C. Wang, *Pairwise knockdowns of cdc2-related kinases (CRKs) in Trypanosoma brucei identified the CRKs for G1/S and G2/M transitions and demonstrated distinctive cytokinetic regulations between two developmental stages of the organism.* Eukaryot Cell, 2005. **4**(4): p. 755-64.

77. Tu, X. and C.C. Wang, *The involvement of two cdc2-related kinases (CRKs) in Trypanosoma brucei cell cycle regulation and the distinctive stage-specific phenotypes caused by CRK3 depletion.* J Biol Chem, 2004. **279**(19): p. 20519-28.

78. Gheiratmand, L., et al., *Biochemical characterization of the bi-lobe reveals a continuous structural network linking the bi-lobe to other single-copied organelles in Trypanosoma brucei.* J Biol Chem, 2013. **288**(5): p. 3489-99.

79. Okuzumi, T., et al., *Inhibitor hijacking of Akt activation.* Nat Chem Biol, 2009. **5**(7): p. 484-93.

80. Holderfield, M., et al., *RAF inhibitors activate the MAPK pathway by relieving inhibitory autophosphorylation.* Cancer Cell, 2013. **23**(5): p. 594-602.

81. Gould, C.M., et al., *Active site inhibitors protect protein kinase C from dephosphorylation and stabilize its mature form.* J Biol Chem, 2011. **286**(33): p. 28922-30.

82. Zhang, F., et al., *Inhibitory phosphorylation of glycogen synthase kinase-3 (GSK-3) in response to lithium. Evidence for autoregulation of GSK-3.* J Biol Chem, 2003. **278**(35): p. 33067-77.

83. Wan, X., et al., *Rapamycin induces feedback activation of Akt signaling through an IGF-1R-dependent mechanism.* Oncogene, 2007. **26**(13): p. 1932-40.

84. Hodges, M.E., et al., *Reconstructing the evolutionary history of the centriole from protein components.* J Cell Sci, 2010. **123**(Pt 9): p. 1407-13.

85. Schmidt, T.I., et al., *Control of centriole length by CPAP and CP110.* Curr Biol, 2009. **19**(12): p. 1005-11.

86. Pelletier, L., et al., *Centriole assembly in Caenorhabditis elegans.* Nature, 2006. **444**(7119): p. 619-23.

87. Gogendeau, D., et al., *Sas-4 proteins are required during basal body duplication in Paramecium.* Mol Biol Cell, 2011. **22**(7): p. 1035-44.

88. Leidel, S. and P. Gönczy, *SAS-4 Is Essential for Centrosome Duplication in C. elegans and Is Recruited to Daughter Centrioles Once per Cell Cycle.* Developmental Cell, 2003. **4**(3): p. 431-439.

89. Novak, Z.A., et al., *Cdk1 Phosphorylates Drosophila Sas-4 to Recruit Polo to Daughter Centrioles and Convert Them to Centrosomes.* Dev Cell, 2016. **37**(6): p. 545-57.

90. Benz, C., et al., *Depletion of 14-3-3 proteins in bloodstream-form Trypanosoma brucei inhibits variant surface glycoprotein recycling.* Int J Parasitol, 2010. **40**(5): p. 629-34.

91. Lundgren, D.H., et al., *Role of spectral counting in quantitative proteomics.* Expert Rev Proteomics, 2010. **7**(1): p. 39-53.

92. Old, W.M., et al., *Comparison of label-free methods for quantifying human proteins by shotgun proteomics.* Mol Cell Proteomics, 2005. **4**(10): p. 1487-502.

93. Kislinger, T., et al., *Global survey of organ and organelle protein expression in mouse: combined proteomic and transcriptomic profiling.* Cell, 2006. **125**(1): p. 173-86.

94. Takadate, T., et al., *Novel prognostic protein markers of resectable pancreatic cancer identified by coupled shotgun and targeted proteomics using formalin-fixed paraffin-embedded tissues.* International Journal of Cancer, 2013. **132**(6): p. 1368-1382.

95. Xie, X., et al., *A comparative phosphoproteomic analysis of a human tumor metastasis model using a label-free quantitative approach.* Electrophoresis, 2010. **31**(11): p. 1842-52.

96. Dammer, E.B., et al., *Quantitative Phosphoproteomics of Alzheimer's Disease Reveals Crosstalk between Kinases and Small Heat Shock Proteins.* Proteomics, 2015. **15**(0): p. 508-519.

97. Singec, I., et al., *Quantitative Analysis of Human Pluripotency and Neural Specification by In-Depth (Phospho)Proteomic Profiling.* Stem Cell Reports, 2016. **7**(3): p. 527-42.

98. Zhang, B., et al., *Detecting differential and correlated protein expression in label-free shotgun proteomics.* J Proteome Res, 2006. **5**(11): p. 2909-18.

99. Leal, S., et al., *Virulence of Trypanosoma brucei strain 427 is not affected by the absence of glycosylphosphatidylinositol phospholipase C.* Mol Biochem Parasitol, 2001. **114**(2): p. 245-7.

100. Hirumi, H.H.a.K., *Axenic Culture of Arican Trypanosome Bloodstream Forms.* Parasitology Today, 1994. **10**(2): p. 80-84.

101. Licklider, L.J., et al., *Automation of nanoscale microcapillary liquid chromatography-tandem mass spectrometry with a vented column.* Anal Chem, 2002. **74**(13): p. 3076-83.

102. Eng, J.K., A.L. McCormack, and J.R. Yates, *An approach to correlate tandem mass spectral data of peptides with amino acid sequences in a protein database.* J Am Soc Mass Spectrom, 1994. **5**(11): p. 976-89.

103. Kall, L., et al., *Semi-supervised learning for peptide identification from shotgun proteomics datasets.* Nat Methods, 2007. **4**(11): p. 923-5.

104. Taus, T., et al., *Universal and confident phosphorylation site localization using phosphoRS.* J Proteome Res, 2011. **10**(12): p. 5354-62.

CHAPTER 3

REGULATION OF MITOCHONDRIAL GENOME DIVISION AND BASAL BODY DUPLICATION BY A CASEIN KINASE IN THE AFRICAN TRYPANOSOME[2]

[2] Catherine Sullenberger, Justin Wiedeman, Yuko Ogata, David Swinney, and Kojo Mensa-Wilmot.
To be submitted to Journal of Biological Chemistry, August 2017

3.1 Abstract

Trypanosoma brucei causes the potentially fatal disease, Human African Trypanosomiasis (HAT). The mitochondrial genome of *Trypanosoma brucei* is an interlocked network of thousands of circular DNAs sequestered in a kinetoplast (mitochondrial nucleoid). The kinetoplast is tethered to a basal body through a tripartite attachment complex (TAC) and it is widely-held that a mechanical force accompanying basal body separation causes scission of the replicated kDNA network. However, molecular pathways required for division of the catenated mitochondrial nucleoid remain elusive. Trypanosome casein kinase 1 (TbCK1.2) has been implicated in this process. Using both small-molecule and genetic approaches, we found that reduced TbCK1.2 activity inhibited kinetoplast division without preventing kDNA synthesis, basal body duplication/separation, or flagellum biogenesis. Accordingly, we conclude that basal body separation is not sufficient to cause kinetoplast division. In light of this data we postulate that a set of proteins ("kinetoplast division factors" or KDFs) are recruited to regions proximal to the kinetoplast to facilitate biochemical resolution of the kDNA network after basal bodies have moved to the kinetoplast poles. We theorize that TbCK1.2 regulates activity/localization of KDFs. Additionally, we demonstrate that knockdown of TbCK1.2 promoted multiple rounds of basal body duplication. Conversely, overexpression of TbCK1.2 inhibited basal body biogenesis. Taken together these data suggest that TbCK1.2 controls basal body copy number. In attempts to discover proteins in the TbCK1.2 signaling pathway, we identified proteins with altered phosphorylation after knockdown of TbCK1.2. We identified

four basal body proteins (TbBBP59, TbBBP268, TbBBP110, and TbBBP590) as putative TbCK1.2 effectors, consistent with detection of the enzyme at the basal body. Collectively we show that TbCK1.2 regulates division of the kDNA network, independent of basal body separation and additionally restricts basal body duplication during trypanosome division.

3.2 Introduction

The protozoan parasite *Trypanosoma brucei* causes human African trypanosomiasis (HAT) in some rural regions of sub-Saharan Africa (reviewed in [1]). The trypanosome basal body, a microtubule-organizing center, plays a pivotal role in parasite viability (reviewed in [2]). The basal body is important for flagellum biogenesis (reviewed in [3]), organization and duplication of cytoskeleton-associated organelles [2, 4], and inheritance of the mitochondrial genome [5-7]. Several trypanosome basal body proteins have been characterized [8-16], but the pathways which regulate biogenesis of the organelle are not understood.

In *T. brucei* the basal body consists of two centriole-like structures: a mature basal body (mBB) and an adjacent immature probasal body (pBB) [17]. The mature basal body nucleates the flagellar axoneme [17] which is essential for motility and cytokinesis [18, 19]. Shortly after nucleation, the flagellum exits the cell body and traverses the length of the trypanosome, attached to the plasma membrane via the flagellar attachment zone (FAZ) (reviewed in [20]). Proper assembly of the FAZ and flagellum influence the site of cleavage furrow ingression during cytokinesis [19, 21, 22].

The mitochondrial genome is sequestered within a kinetoplast (mitochondrial nucleoid) (reviewed in [23, 24]). Kinetoplast DNA (kDNA) is composed of two classes of circular, double-stranded DNAs (minicircles and maxicircles) that form a compact, catenated network (reviewed in [23-25]). The kinetoplast is physically tethered to the basal body through the “tripartite attachment complex” (TAC) [26] which is associated with accurate segregation of the kDNA network into daughter cells [6, 7].

Duplication of both the kinetoplast and basal body are coordinated with trypanosome division [2, 17, 27]. In G1 trypanosomes possess a single kinetoplast (K), nucleus (N), and basal body (1K1N 1mBB/1pBB). In S-phase DNA synthesis occurs in the kinetoplast and nucleus, with kDNA replication terminating prior to nuclear DNA synthesis [27, 28]. Probasal body maturation, marked by recruitment of a transition zone protein, TbRP2 [16], occurs before division of the kinetoplast [4, 17, 29]. The newly matured basal body nucleates a daughter flagellum and two new probasal bodies are assembled adjacent to each mature basal body generating 1K1N 2mBB/2pBB trypanosomes with two flagella [4, 17, 28, 29]. Separation of basal body pairs (mBB/pBB) is thought to cause division of the kinetoplast [5]. However, given the nature of the interlocked kDNA network, it is likely that an enzyme capable of initiating double-strand DNA breaks is required to biochemically resolve the replicated kDNA network [23, 24, 30]. Division of the kinetoplast occurs prior to mitosis yielding 2K1N 2mBB/2pBB trypanosomes [17, 27]. Division of the nuclear genome during mitosis produces 2K2N 2mBB/2pBB

trypanosomes. Cytokinesis segregates the kinetoplast-basal body pairs into daughter cells (two 1K1N 1mBB/1pBB trypanosomes).

Defects in basal body duplication or separation are associated with inhibition of kinetoplast division [10-12, 31]. Failed kinetoplast scission does not prevent duplication of the nucleus which can lead to the emergence of trypanosomes with a single kinetoplast and two nuclei (1K2N) [10-12, 31, 32]. Genetic knockdown of the trypanosome casein kinase 1 homolog (TbCK1.2) results in the production of 1K2N trypanosomes [32]. Consequently, we sought to determine whether TbCK1.2 regulated kinetoplast division by modulating basal body biogenesis.

Employing both chemical and genetic approaches, we found that reduction of TbCK1.2 activity inhibited kinetoplast division without preventing basal body duplication/separation, or flagellum biogenesis. This surprising result led us to hypothesize that basal body separation is not sufficient to cause division of the kinetoplast, as is widely-accepted. In light of this data we postulate that a set of proteins (“kinetoplast division factors” or KDFs) are recruited to regions proximal to the kinetoplast to facilitate division of the kDNA network, in a TbCK1.2-dependent fashion. Additionally, we found that loss of TbCK1.2 activity permitted multiple rounds of basal body duplication to occur within a single trypanosome division cycle. Conversely, overexpression of TbCK1.2 inhibited basal body biogenesis. Knockdown of TbCK1.2 altered phosphorylation of some trypanosome basal body proteins; consistent with our detection of the enzyme at the basal body. Taken together our work indicates that TbCK1 restricts basal body reduplication

during trypanosome cell division, highlighting a novel function of a casein kinase in an early-branching eukaryote.

3.3 Results

Kinetoplast DNA replicates but fails to divide following knockdown of TbCK1.2

A trypanosome casein kinase 1 homolog, TbCK1.2, is essential for trypanosome proliferation and division of the mitochondrial genome (Supplemental Figures 3.1A-3.1B) [32, 33]. To further characterize the role of TbCK1.2 in separation of the kinetoplast (mitochondrial nucleoid), we generated a tetracycline-inducible TbCK1.2 RNAi line [33] in which one TbCK1.2 allele was endogenously tagged with a V5 epitope at the N-terminus (V5-TbCK1 RNAi line). Western blotting showed that a 24-hour knockdown of TbCK1.2 reduced protein levels of V5-TbCK1.2 by 60% (Figure 3.1A) and caused an arrest of trypanosome replication (Supplemental Figure 3.1A).

We monitored duplication of the kinetoplast and nucleus by staining the DNA-containing organelles with DAPI (Supplemental Figure 3.1B). During trypanosome division, the kinetoplast duplicates prior to mitosis such that two kinetoplasts are visualized prior to segregation of the nuclear genome (2K1N) [17, 27]. After genetic knockdown of TbCK1.2, 20% of the trypanosome population had a single kinetoplast and two nuclei (1K2N) (Supplemental Figure 1B) [32] indicating that these cells had failed kinetoplast division, but duplication of the nucleus proceeded normally. Appearance of 1K2N trypanosomes correlates with a decrease in the percentage of 1K1N (G1) cells which may be symptomatic of failed cytokinesis, consistent with the emergence of trypanosomes (8.5%) with more than

two kinetoplasts and/or nuclei (“other”) (Supplemental Figure 3.1B) [32, 33]. Additionally, knockdown of TbCK1.2 caused an increase in the percentage of trypanosomes which two nuclei and a 4C equivalent of nuclear DNA (Supplemental Figure 3.1C).

To determine if reduced levels of TbCK1.2 affected kinetoplast DNA (kDNA) content, we examined fluorescence intensity of DAPI-stained kDNA networks (Supplemental Figure 3.1D). Synthesis of kDNA occurs in 1K1N trypanosomes [27]. Accordingly, there is a mixture of unreplicated and replicating kDNA networks in this population. The median kDNA fluorescence intensity in control (-Tet) 1K1N trypanosomes was almost twice that observed in each kinetoplast of control 2K1N and 2K2N cells (Supplemental Figure 3.1D), as expected. In 1K2N trypanosomes (+Tet), the median fluorescence intensity of DAPI-stained kinetoplasts was increased, as compared to unreplicated kDNA networks in the control (2K1N and 2K2N) (Supplemental Figure 3.1D). The median kDNA fluorescence intensity in 1K2N cells was twice that of uninduced 1K1N trypanosomes (Supplemental Figure 3.1D), and in some cases kDNA fluorescence intensity in 1K2N cells exceeded measurements from control population (Supplemental Figure 3.1D). Thus, kDNA is replicated in 1K2N trypanosomes.

Separation of duplicated trypanosome basal bodies is believed to drive division of the kinetoplast [5]. Knockdown or overexpression of proteins important for basal body duplication or separation have been associated with defects in kinetoplast division leading to the emergence of 1K2N trypanosomes [5, 10-12, 15,

31]. Consequently, we sought to determine if TbCK1.2's role in kinetoplast division was rooted in control of basal body biogenesis.

Knockdown of TbCK1.2 causes amplification of basal bodies

The trypanosome basal body consists of a mature basal body (mBB) and adjacent immature probasal body (pBB) (1mBB/1pBB) [17]. Duplication of the organelle yields trypanosomes with two mature basal bodies and two new probasal bodies (2mBB/2pBB) [17]. Accordingly, the number of mBBs and pBBs per trypanosome can be used to monitor probasal body maturation and assembly [11, 12, 15]. To track basal body biogenesis, we used anti-TbSAS6 to visualize mature and immature basal bodies [15], and YL1/2 (anti-Tyr-α-tubulin antibody) which labels mature basal bodies in *T. brucei* [16] (Figure 3.1B). We detected foci positive for Tb-SAS6 away from the basal body (Supplemental figure 3.2) which may represent non-specific binding of the polyclonal antibody; alteration of image display setting (brightness/contrast) was employed to reduce background (Figure 3.1B).

Dual staining with anti-TbSAS and YL1/2 (Figure 3.1B) in control cells (-Tet) showed a near equal distribution of unduplicated (1mBB/1pBB) or duplicated (2mBB/2pBB) basal bodies (Figure 3.1C). Knockdown of TbCK1.2 (24 h) skewed this distribution, as determined using a χ^2 test, by reducing the number of trypanosomes with unduplicated basal bodies from 42% to 12% ($p = 1.9 \times 10^{-33}$) (Figure 3.1C). Correspondingly, in 39% of induced trypanosomes basal body copy number exceeded that of control cells (> 2mBB/2pBB) (Figures 3.1B-3.1C), while the percentage of cells with two basal bodies (2mBB/2pBB) was unchanged (Figure 3.1C). Surprisingly, we observed basal bodies, labeled with both YL1/2 and

anti-TbSAS6, that were distant from the kinetoplast ("distal basal bodies") in approximately 10% of trypanosomes after knockdown of TbCK1.2 (Figure 3.1D). Together these data show that reduced TbCK1.2 protein abundance causes amplification of basal bodies.

Because separation of duplicated basal bodies is postulated to drive kinetoplast division [5, 26], we examined the number of basal bodies in 1K2N trypanosomes to determine if basal body biogenesis was inhibited (Figure 3.2A). We found that approximately 80% of 1K2N trypanosomes completed basal body duplication, with the majority (47%) demonstrating increased copy number of the organelle (Figure 3.2B). Thus, failed kinetoplast division was not caused by a block in basal body biogenesis, leading us to speculate that duplicated basal bodies of 1K2N cells were not capable of separation.

Separation of duplicated basal bodies occurs prior to division of the mitochondrial nucleoid [34]. Thus, it was not surprising to detect basal bodies at the kinetoplast poles in control 1K1N trypanosomes with two basal bodies (Figure 3.2A). Following knockdown of TbCK1.2, we observed 1K2N trypanosomes with two basal bodies (2mBB/2pBB) which remained next to each other, as well as 1K2N cells with well separated basal bodies (Figure 3.2A). To quantitate the extent of basal body separation, we measured the distance between YL1/2-postivie mature basal bodies (inter-basal body distance) in TbCK1.2 RNAi cells incubated in the absence or presence of tetracycline (Figure 3.2C). In control (-Tet) 1K1N cells with two basal bodies, the inter-basal body distances ranged from 0.35 μm to 2.7 μm with an average distance of 1.2 μm (Figure 3.2C). The inter-basal body

distance doubled after division of the kinetoplast in both 2K1N and 2K2N control cells with an average inter-basal body distance of 2.2 μm and 2.3 μm, respectively.

For 1K2N trypanosomes with two mature basal bodies, the inter-basal body distances measured were similar to control cells with a single kinetoplast, ranging from 0.34 μm to 2.6 μm with a median distance of 1.1 μm (Figure 3.2C). Additionally, the average inter-basal body distances measured in induced 1K1N (1.1 μm), 2K1N (2 μm), and 2K2N (2.1 μm) trypanosomes were not reduced, as compared to control cells (Figure 3.2C). We conclude that knockdown of TbCK1.2 does not impair basal body migration. Unexpectedly in approximately 40% of trypanosomes with a single kinetoplast (-Tet or +Tet), the inter-basal body distance exceeded the minimum distance measured in control 2K1N cells (1.17 μm) which have completed kinetoplast division (Figure 3.2C). This data points to a possibility that basal body separation alone may not be sufficient to drive division of the kinetoplast.

The capacity of duplicated basal bodies to nucleate a flagellar axoneme was examined by double labeling trypanosomes with the antibody YL1/2 [16] (mature basal bodies) and anti-PFR2, a component of the flagellum-associated paraflagellar rod (PFR) (reviewed in [35]) (Figure 3.3A). In the uninduced control population, trypanosomes possessed a single flagellum (48.5%) or two flagella (51.5%) (Figure 3.3B). Knockdown of TbCK1.2 altered this distribution, as determined with a χ^2 test, reducing the percentage of cells with a single flagellum from 48.5% to 19% ($p = 8 \times 10^{-20}$) (Figure 3.3B). Concomitantly, the percentage of cells with two flagella increased from 51.5% to 66% and 15% of the population had

more than two flagella (Figure 3.3B). Detection of trypanosomes with multiple flagella demonstrates that supernumerary basal bodies are able to form flagella. Further, 82% of 1K2N trypanosomes had two flagella (Figure 3.3C). Accordingly, we conclude that knockdown of TbCK1.2 does not impair flagellum assembly in 1K2N trypanosomes. Lastly, we observed distal basal bodies with flagella indicating that they are functional basal bodies (Figure 3.3A).

Our data reveals that knockdown of TbCK1.2 inhibits kinetoplast division without blocking kDNA replication (Supplemental Figure 3.1D), basal body duplication (Figure 3.1), basal body separation (Figure 3.2), or flagellum biogenesis (Figure 3.3). Accordingly, TbCK1.2 regulates division of the kinetoplast without impeding normal basal body function.

SB-431542 inhibits kinase activity of TbCK1.2 and causes basal body overduplication

To validate the role of TbCK1.2 in controlling basal body copy number (Figures 3.1-3.2), we sought to identify a small molecule inhibitor of TbCK1.2 and test if the inhibitor would cause basal body overduplication in *T. brucei*. A Selleck^{TM} library of 70 protein kinase inhibitors was tested against recombinant TbCK1.2 (see Materials and Methods). From this screen, we identified SB-431542 [36, 37] as an inhibitor of purified TbCK1.2 with an IC_{50} of 49.2 nM (Figure 3.4). We then tested the possibility that SB-431542 could inhibit TbCK1.2 in vivo. As an ATP-competitive inhibitor [38], the potency of SB-431542 is influenced by the intracellular concentration of ATP. In vitro studies with SB-431542 and purified TbCK1.2 were performed in the presence of 20 μM ATP (Figure 3.4), 100-fold

lower than the intracellular ATP concentration in *T. brucei* [39]. Consequently, we increased the SB-43152 concentration for in vivo studies and found that SB-451542 (10 μM) inhibited trypanosome proliferation in a 10 h assay (Supplemental Figure 3.3A).

To determine if SB-431542 affected basal body biogenesis, trypanosomes were treated with SB-431542 (10 μM) or DMSO (drug vehicle), and basal bodies detected by co-staining trypanosomes with the antibodies YL1/2 (mature basal bodies [16]) and anti-TbSAS6 (all basal bodies [15]) (Figure 3.5A). In the control DMSO-treated population, 49% of trypanosomes had one basal body (1mBB/1pBB) and 37% had two basal bodies (2mBB/2pBB) (Figure 3.5B). SB-43152 treatment decreased the percentage of cells with 1mBB/1pBB to 28%, increased the number of trypanosomes with 2mBB/2pBB to 50%, and permitted basal body reduplication in 13% of the population (> 2mBB/2pBB) (Figure 3.5B). The difference in the distribution of basal bodies per cell, as assessed using a χ^2 test, was statistically significant after SB-431542 treatment ($p = 3.9 \times 10^{-17}$).

To determine if SB-431542 also disrupted kinetoplast division, we used DAPI to enumerate the number of kinetoplasts and nuclei per trypanosome following drug treatment. We found that SB-431542 (10 μM, 10 h) reduced the number of 1K1N trypanosomes from 49% to 27.5%, impaired kinetoplast division in 12% of the population (1K2N), and produced cells (16%) with more than two kinetoplasts and/or nuclei (“other”) (Supplemental Figure 3.3B), similar to knockdown of TbCK1.2 (Supplemental Figure 3.3B). SB-43152 treatment also reduced the number of 2K1N cells from 15% to 5% of the population

(Supplemental Figure 3.3B). SB-431542 treatment did not alter TbCK1.2 protein levels (Supplemental Figure 3.3C), indicating that loss of kinase activity, and not the protein itself, disrupts basal body copy number and kinetoplast division.

Inhibition of basal body duplication by overexpression of TbCK1.2

The role of TbCK1.2 in basal body duplication was probed further by monitoring biogenesis of the organelle after overexpressing the enzyme (Figure 3.6). For this goal, a tetracycline-inducible version of TbCK1.2, with a C-terminal hemagglutinin (HA) tag, was integrated into the VSG-G4 locus of minichromosomes in single marker (SM) trypanosomes [40]. The pGad9-V4 expression plasmid [41], uses a single T7 promoter to drive expression of TbCK1.2 and the selectable marker which results in expression of TbCK1.2-HA in the absence of exogenous tetracycline (Figure 3.6A). Addition of tetracycline (1μg/ml) to the medium significantly increased TbCK1.2-HA expression (Figure 3.6A) and impaired trypanosome proliferation (Supplemental Figure 3.4). Compared to a cell line expressing TbCK1.2-HA from its endogenous promoter, the ectopic T7 promoter increased expression 3-fold (Supplemental Figure 3.5).

We used markers for mature basal bodies (YL1/2 [16]) and immature probasal bodies (anti-TbSAST [15]) to track probasal body maturation and assembly after overexpression of TbCK1.2 (Figure 3.6B). In the uninduced control population, 42% of trypanosomes contained a single mature basal body (1mBB), while in trypanosomes overexpressing TbCK1.2 the percentage of trypanosomes with 1mBB increased to 64% (Figure 3.6C). Conversely, the proportion of trypanosomes with two mature basal bodies (2mBB) dropped from 57% in the

uninduced population to 24% after tetracycline induction (Figure 3.6C). Unexpectedly, a mature basal body, positive for YL1/2 and TbSAS6, was not paired with a TbSAS6-positive probasal body (1mBB/0pBB) in 14% of TbCK1.2-overexpressing trypanosomes (Figures 3.6B-3.6C). The change in basal body distribution per trypanosome was statistically significant as a result of TbCK1.2 overexpression (12 h), as determined by a χ^2 test (p = 9.4 x 10^{-9}). We conclude that elevated expression of TbCK1.2 suppresses basal body biogenesis.

We theorized that if inhibition of basal body duplication was the result of increased TbCK1.2 activity, basal body biogenesis would be rescued by SB-431542 treatment since the small molecule inhibits TbCK1.2 activity (Figure 3.4). To test this hypothesis, we incubated a TbCK1.2 overexpression line with tetracycline for six hours, then added SB-431542 (7 μM) or equal volume DMSO (drug solvent), and incubated the cultures an additional six hours (Figure 3.6C). Uninduced control cells treated with SB-431542 (7 μM, 6 h) maintained the same distribution of basal bodies per cell as uninduced trypanosomes treated with DMSO, as determined using a χ^2 test (p = 0.5) (Figure 3.6C). Importantly, SB-43152 rescued probasal body maturation and assembly in trypanosomes overexpressing TbCK1.2 (+Tet +SB-431542); the proportion of trypanosomes with two mature basal bodies increased from 24% (+Tet +DMSO) to 43% and the percentage of 1mBB/0pBB trypanosomes dropped from 15% (+Tet +DMSO) to 5% (Figure 3.6C). The difference in the distribution of basal bodies per cell in the uninduced control population treated with DMSO (-Tet +DMSO) was not statistically significant from TbCK1.2-overexpressing trypanosomes treated with

SB-431542 (+Tet +SB-431542), as determined using a χ^2 test ($p = 7 \times 10^{-2}$). These data are consistent with SB-431542 rescuing basal body biogenesis by reducing activity of the overexpressed enzyme.

TbCK1.2 is detected in the cytoplasm, flagellum and at basal bodies

We entertained a possibility that TbCK1.2's effect on basal body duplication (Figure 3.1) or kinetoplast division (Figure 3.2 and Supplemental Figure 3.1B) might be explained, at least in part, by its intracellular location. Using the uninduced V5-TbCK1.2 RNAi line (Figure 3.1A), we employed an antibody directed against the V5 epitope to localize TbCK1.2 in bloodstream trypanosomes (Figure 3.7). Fixation of trypanosomes with paraformaldehyde (PFA) followed by detergent permeabilization retains a majority of the cytoplasmic content, as compared to protocols which simultaneously fix and permeabilize cells such as methanol (fixatives are reviewed in [42]). Under these conditions V5-TbCK1.2 was detected in puncta in the cytoplasm (Figures 3.7A). We also detected TbCK1.2 along the flagellum and at YL1/2-positive mature basal bodies (Figure 3.7A).

Fixation/permeabilization with methanol eliminated most of the cytoplasmic V5 signal (Figure 3.7B). However, co-localization with the anti-centrin antibody 20H5 [11] demonstrated that V5-TbCK1.2 was retained at the flagellum, basal bodies, and parts of the bilobe [11, 43] (Figure 3.7B). V5-TbCK1.2 was detected at the basal body in approximately 50% of the population, independent of cell cycle stage (based on the number of kinetoplasts and nuclei per cell).

Knockdown of V5-TbCK1.2, by the addition of tetracycline (1 µg/ml) to the V5-TbCK1.2 RNAi line, dramatically reduced the detectable V5 signal in most

trypanosomes (Supplemental Figure 3.6) indicating that the V5 antibody is specific to V5-TbCK1.2.

Knockdown of TbCK1.2 alters phosphorylation of select basal body, bilobe, and mitochondrial proteins

To identify protein components of TbCK1.2 signaling pathways we used a comparative phosphoproteomics approach to identify proteins whose phosphorylation changed after knockdown of TbCK1.2. We expected that TbCK1.2 substrates, as well downstream effectors, would show decreased phosphorylation if TbCK1.2 activity was reduced. We first employed a semi-quantitative, label-free shotgun proteomics strategy [44, 45] in which spectral counts were used to compare the abundance of specific phospho-peptides in the uninduced and induced (24h) TbCK1.2 RNAi line. We identified over 100 putative TbCK1.2 pathway proteins with either decreased or increased phosphorylation. Proteins with increased phosphorylation are not likely to be substrates of TbCK1.2, but could be effectors of TbCK1.2 signaling. Altered phosphorylation of protein kinases and phosphatases after knockdown of TbCK1.2 (Table 3.1) could explain the increased phosphorylation of some trypanosome proteins.

We used a SILAC (stable isotope labeling of amino acids in culture) (reviewed in [46]) phosphoproteomics approach [47] to validate candidates identified by our label-free strategy. As a control for biological variation we compared the phosphoproteome profile between the uninduced TbCK1.2 RNAi line grown in heavy medium or light medium (Supplemental Figure 3.7). The phospho-peptide abundance ratios (heavy:light) clustered around 1.0 indicating

that the majority of phospho-peptides were found at the same abundance in control cells grown in either heavy or light medium (Supplemental Figure 3.7).

Comparison of trypanosomes with reduced TbCK1.2 activity (light medium) to control cells (heavy medium) demonstrates that phosphorylation of select peptides has increased or decreased (Figure 3.8). Only peptides that were matched to spectra with 95% accuracy, or greater (PEP value < 0.05) are reported in Figure 3.8. Phospho-peptides with an abundance ratio of two or greater in the control experiment (Supplemental Figure 7) were removed from the dataset presented in Figure 3.8. In some instances, a phospho-peptide was only detected in the uninduced control or the induced sample which prevented calculation of an abundance ratio. Such proteins are not shown in Figure 3.8, but are listed in Table 3.1 and Supplemental Tables 3.1-3.2.

Following knockdown of TbCK1.2, the abundance of 113 phospho-peptides was decreased 2-fold or greater, and the abundance of 257 phospho-peptides was increased 2-fold or greater, as compared to the uninduced control (Figure 8). We generated a list of putative TbCK1.2 effectors that were observed using both label-free and SILAC methods; this list includes 65 proteins with decreased phosphorylation (Supplemental Table 3.1) and 143 proteins with increased phosphorylation (Supplemental Table 3.2).

Of the 208 putative effectors identified, here we choose to focus on proteins that could explain TbCK1.2's role in basal body duplication (Figure 3.1) or kinetoplast division (Figure 3.2 and Supplemental Figure 3.1B). Following knockdown of TbCK1.2, phosphorylation of some basal body proteins was

decreased (TbBBP268 [12] and TbBBP59 [12]) and others increased (TbBBP110 [12] and TbBBP590 [12]) (Table 3.1). Additionally, a homolog to the centrosomal protein, tubulin binding cofactor C (TBCC) [48], was dephosphorylated (Table 3.1). Protein components of the bilobe (TbLRRP1 [49]) and flagellar attachment zone (TbFAZ2 [50]) also demonstrated altered phosphorylation (Table 3.1). Lastly, proteins in the outer mitochondrial membrane (POMP25 and POMP12 [51]) were identified as putative TbCK1.2 pathway proteins (Table 3.1).

3.4 Discussion

TbCK1.2 prevents amplification of basal bodies during trypanosome division

We discovered that TbCK1.2, a trypanosome casein kinase 1 homolog, regulates basal body copy number. Genetic knockdown of TbCK1.2 caused amplification of basal bodies (Figures 3.1-3.2). Conversely, overexpression of TbCK1.2 inhibited basal body biogenesis (Figure 3.6). A small molecule inhibitor of TbCK1.2 increased basal body copy number in wildtype trypanosomes (Figure 3.5) and rescued basal body duplication in TbCK1.2-overexpressing cells (Figure 3.6C), confirming that TbCK1.2 kinase activity is important in regulation of basal body copy number. The fact that a 2 to 3-fold change in TbCK1.2 expression disrupts the basal body duplication cycle (Figures 3.1 and 3.6) suggests that endogenous TbCK1.2 activity is tightly regulated.

Restricting the copy number of microtubule-organizing centers (MTOCs) has also been documented in other organisms [52-54]. Amplification of centrosomes, which are structurally similar to basal bodies (reviewed in [2, 55, 56]), is associated with cancer [57] and other diseases (reviewed in [58-61]). While

proteins such as polo-like kinase 4 (PLK4) and polo-like kinase 1 (PLK1) are important regulators of centrosome copy number [62-65], the single trypanosome PLK homolog (TbPLK1) is not essential for probasal body biogenesis or maturation [31]. Thus, the molecular pathways that control centriole/basal body copy number in humans are different in *T. brucei*.

Our hypothesis that TbCK1.2 functions in basal body duplication is supported by detection of the enzyme at the basal body (Figure 3.7). Further, phosphorylation of several basal body proteins was either decreased or increased following knockdown of TbCK1.2 (Table 3.1). These data point to a TbCK1.2 phospho-signaling pathway that controls basal body copy number. Amplification of trypanosome basal bodies has also been reported in *T. brucei* following overexpression of TbNRKC [9] or knockdown of TbCEP57 [12], TbBBP46 [12], and TbLRTP [14]. Since these proteins were not detected as putative TbCK1.2 effectors in our phosphoproteomics experiments, we speculate that multiple pathways exist for cell cycle control of basal body duplication in *T. brucei*. Alternatively, though not mutually exclusive, these basal body regulators may be of low abundance and not detected in our proteomics analysis.

Surprisingly, knockdown of TbCK1.2 produced a small population of trypanosomes with basal bodies which were distant from a kinetoplast (Figure 3.1D). The data may suggest that TbCK1.2 normally suppresses a de novo basal body biogenesis pathway in which the organelle is assembled in the absence of a preexisting basal body (reviewed in [66]). Interestingly, the presence of both templated and de novo centriole/basal body assembly pathways have been

reported in a variety of organisms [62, 67-70]. It is possible that TbCK1.2 regulates stability of TbSAS6 at the cartwheel which is essential for basal body assembly [15]. This idea is consistent with the finding that TbCK1.2 overexpression resulted in a small population of trypanosomes that lacked a TbSAS6-positive probasal body (1mBB/0pBB) (Figures 3.6C-3.6D), similar to knockdown of TbSAS6 [15], TbBLD10 [12], or TbPOC11 [12].

A novel role for TbCK1.2 in kinetoplast division

Genetic knockdown of TbCK1.2 inhibited kinetoplast division (Supplemental Figure 3.1B), but not kDNA replication (Supplemental Figure 3.1D) or basal body duplication producing 1K2N trypanosomes with two, or more, basal bodies (Figure 3.2) competent of seeding flagella (Figure 3.3). It is unlikely that defects in kinetoplast division are directly linked to basal body overduplication after TbCK1.2 knockdown (Figures 3.1-3.2) because the literature provides many examples in which kinetoplast division is blocked but basal body copy number is unaffected [8, 10, 12, 15]. Hence, the pathways are separable genetically. Accordingly, we postulate that TbCK1.2 regulates basal body duplication and kinetoplast division through distinct pathways without excluding a possibility that molecular components are shared.

Current dogma in the field points to basal body separation as the driving force behind kinetoplast division [5]. Based on this model we assumed that basal body separation would be impaired in 1K2N trypanosomes. However, the distance between duplicated basal bodies (inter-basal body distance) in 1K2N trypanosomes was not reduced as compared to control 1K1N cells (Figure 3.2C).

This data suggests that initial basal body migration along the kinetoplast was successful following knockdown of TbCK1.2. Additionally, in trypanosomes with two kinetoplasts (2K1N or 2K2N), the inter-basal body distances measured after TbCK1.2 knockdown were similar to those detected in control trypanosomes with two kinetoplasts (Figure 3.2C). Thus, failure of the kinetoplast to divide following knockdown of TbCK1.2 is not the result of impaired basal body movements. From this data, we infer that separation of basal bodies is not sufficient to drive kinetoplast scission.

Further, when comparing the inter-basal body distance in trypanosomes with two basal bodies and either a single kinetoplast (2BB/1K) or two kinetoplasts (2BB/2K), the distance measured in 40% of 2BB/1K cells exceeded the minimum distance measured in 2BB/2K trypanosomes (Figure 3.2C). This data is at odds with the current dogma which would posit that the inter-basal body distance of 2BB/2K *T. brucei* is always greater than that of 2BB/1K cells. Accordingly, we believe that it is important to revisit the role of basal body separation in kinetoplast scission.

In a seminal paper, small molecule inhibitors were used to study the relationship between basal body migration and kinetoplast division [5]. A microtubule-destabilizing agent (ansamitocin) was used to block basal body separation and two topoisomerase inhibitors (teniposide and ethidium bromide) to prevent kinetoplast division [5]. Ansamitocin prevented kinetoplast division, while compounds used to disrupt kinetoplast scission had no effect on basal body separation suggesting that basal body separation was necessary for kinetoplast

division [5]. However, because inhibitors could block kinetoplast division without inhibiting basal body separation, the data hints at the possibility that basal body migration is not sufficient to drive this process. Our genetic data supports this interpretation of the data. When considering that basal body separation is not sufficient to cause scission of the kinetoplast, it is important to acknowledge the complexity of the kDNA network; it consists of thousands of interlocked circular, double-stranded DNAs (reviewed in [23-25]) that must undergo decatenation before the kinetoplast can separate. Consequently, it is unlikely that mechanical force alone would be able resolve the interlocked circular DNA molecules.

From a biochemical perspective, it is likely that a mitochondrial topoisomerase would be required to promote division of the replicated kDNA network [24, 30]. This principle is consistent with topoisomerase inhibitors preventing kinetoplast division, independent of basal body separation [5]. However, genetic knockdown TbTopoII$_{mt}$, the only mitochondrial type II topoisomerase (Topo II) does not inhibit kinetoplast division [71-73]. Thus, the molecular mechanisms leading to scission of the kinetoplast remain elusive.

In light of published literature and data presented in this manuscript, we postulate that a set of factors that promote kinetoplast division ("kinetoplast division factors" or KDFs) act in a TbCK1.2-dependent manner to execute kinetoplast scission (Figure 3.9). It is reported that kinetoplast division occurs almost an hour after the termination of kinetoplast DNA (kDNA) synthesis [28]. During this lag between kDNA network synthesis and division, the basal bodies duplicate (Figure 3.9, step 1) [28] and migrate to the kinetoplast poles (Figure 3.9, step 2). We

propose that KDFs are recruited around this time period (Figure 3.9, step 3) and may be components of the basal body, TAC, or mitochondrial membrane. We envision that KDFs may influence Topo II activity or localization to ensure that its decatenation activity is directed along a symmetric cleavage plane of the replicated kDNA network. This hypothesis parallels regulatory aspects of Topo II in other eukaryotes which are required for mitosis: i) the tumor suppressor BRCA1 regulates decatenation activity of topo II during S-phase to promote proper segregation of the nuclear genome [74], ii) the condesin complex modifies chromatin structure in order to recruit topo II to the centromere [75] where its action is required for resolution sister chromatids [76, 77]. We hypothesize that TbCK1.2 may regulate the activity or localization of KDFs, or potentially TbTopoII$_{mt}$ itself (Figure 3.9, step 3), to promote kinetoplast division, after basal body separation (Figure 3.9, step 4). Finally, separation of kinetoplast-basal body pairs, in association with the TAC, influence kinetoplast segregation (Figure 3.9 step, 5) [6, 7, 78].

Our hypothesis makes clear predictions about the effect of genetic knockdown of KDFs. We expect that kinetoplast division would be inhibited (1K2N), but kDNA replication, basal body duplication/segregation, or flagellum biogenesis, would be successful, similar to knockdown of TbCK1.2 (Figures 3.1-3.3). In support of these concepts, genetic knockdown of either TbBBP46 or TbCEP57 appear to satisfy these criteria; knockdown of either protein produced 1K2N trypanosomes with duplicated basal bodies (and flagella) that migrated to the kinetoplast poles [12]. It will be important to analyze other properties inherent

to KDFs including inter-basal body distance and kDNA synthesis before TbBBP46 or TbCEP57 can be considered true KDFs.

SB-431542 can be used to study TbCK1.2 signaling pathways in the trypanosome

SB-431542 inhibits the enzyme activity of recombinant TbCK1.2 (Figure 3.4). Additionally, SB-431542 treatment of *T. brucei* phenocopies genetic knockdown of TbCK1.2; treatment inhibited kinetoplast division (Supplemental Figure 3.3B) and increased basal body copy number (Figure 3.5). Thus, we used two independent approaches to confidently show that TbCK1.2 activity regulates kinetoplast scission and basal body duplication. The ability of SB-431542 to inhibit TbCK1.2 kinase activity in vivo suggests that it may a useful chemical tool to study the signaling pathway in *T. brucei*.

There are advantages to using chemical approaches to study protein function. First, it takes less time to chemically inhibit enzyme activity as compared to RNAi-mediated protein depletion which is influenced by protein stability. Second, use of a small molecule reduces kinase activity but may preserve kinase-independent functions (reviewed in [79]), assuming protein levels remain constant following drug treatment as was the case with SB-431542 (Supplemental Figure 3.3C). Drawbacks to using small molecules include so-called “off-target” effects resulting from small molecule interaction with multiple proteins [37, 80, 81]. “Off-target” effects of SB-431542 may explain the observed decrease in 2K1N trypanosomes following drug treatment (Supplemental Figure 3.3B) since that effect was not observed after genetic knockdown of TbCK1.2 (Supplemental Figure 3.1B). Alternatively, the discrepancy could be explained by differences in

the degree to which TbCK1.2 activity was reduced following knockdown of TbCK1.2 or SB-431542 treatment.

TbCK1.2 effectors and signaling proteins

A phosphoproteomics analysis identified putative TbCK1.2 pathway proteins (Figure 3.8, Table 3.1, and Supplemental Tables 3.1-3.2). We were particularly interested in proteins that may regulate kinetoplast division or basal body biogenesis (Table 3.1). Several trypanosome-specific basal body proteins were identified as putative TbCK1.2 effectors, including TbBBP59 [12], TbBBP268 [12], TbBBP110 [12], and TbBBP590 [12]. These candidate TbCK1.2 effectors were found in proximity to either TbCEP57 or TbBBP46 [12]. Knockdown of either TbCEP57 or TbBBP46 resulted in basal body overduplication [12] similar to knockdown of TbCK1.2 (Figures 3.1-3.2). Intriguingly distal basal bodies were detected after knockdown of TbCK1.2 (Figures 3.1D) and TbCEP57 [12]. Knockdown of TbCEP57 or TbBB46 also blocked kinetoplast division, but not migration of duplicated basal bodies to the kinetoplast poles [12]. Similarly, two other putative effectors (TbFAZ2 and TbLRRP1) have been associated with kinetoplast division; knockdown of the flagellar attachment zone (FAZ) protein TbFAZ2 or the bilobe protein TbLRRP1 produces 1K2N trypanosomes [49, 50]. Thus, identified TbCK1.2 effectors (Table 3.1) are linked to the control of kinetoplast scission and basal body copy number in the literature.

We hypothesize that some KDFs localize to the mitochondrion or mitochondrial membrane to which the kinetoplast is anchored via the TAC [26]. Consequently, the identification of two proteins present in the outer mitochondrial

membrane (POMP25 and POMP12) [51] as TbCK1.2 effectors (Table 3.1) was particularly interesting. It is possible that these mitochondrial proteins serve as docking sites for KDFs. In future work, we will employ genetic approaches to study the function and localization of putative TbCK1.2 effectors (Table 3.1 and Supplemental Tables 3.1-3.2) as KDFs or regulators of basal body copy number.

3.5 Materials and Methods

Parasite cultures

Bloodstream *T. brucei* CA427, single marker (SM) [40], or TbCK1.2 transfectant cell lines (see below) were cultured in HMI-9 medium supplemented with 10% Fetal Bovine Serum (Atlanta Biologicals; Flowery Branch, GA), 10% Serum Plus™ (SAFC Biosciences; Lenexa, KS), and 1% antibiotic-antimycotic solution (Corning; Corning, NY) at 37 °C, 5% CO_2 [82]. Transfectant lines were continuously cultured in the presence of selection antibiotics (see below). For all experiments trypanosomes were harvested in logarithmic phase (i.e. less than 1 x 10^6 cells/ml).

Generation of TbCK1.2 transfectant cell lines

TbCK1.2 RNAi line: A p2T7 RNAi construct targeting TbCK1.2 [33] was provided by Dr. Mick Urbaniak (Lancaster University). The TbCK1.2 RNAi construct (10 µg) was linearized with Not1-HF (New England Biolabs, Ipswich, MA) and transfected into SM trypanosomes via electroporation following a previously published protocol [83]. Following transfection, trypanosomes were added to HMI-9 medium (20 ml) and incubated for 24 hours. To obtain clonal lines, the culture was diluted serially (1:10, 1:100, 1:1000) and plated (1 ml/well) in 24-well plates. Stable transfectant

clones were selected in the presence of G418 (6.5 μg/ml) and Hygromycin B (5 μg/ml).

TbCK1.2 overexpression: Chromosomal DNA was isolated from CA427 trypanosomes [84] and used as a template for PCR amplification of full-length TbCK1.2 using high-fidelity Phusion® polymerase (New England Biolabs). The forward primer was engineered with a 5' HindIII cleavage site and the reverse primer with a KpnI site to facilitate cloning into a pGad9-V4 expression plasmid [41]. The forward and reverse primer sequences, respectively, were: aagcttATGAGCGTAGAGCTTCGTGTGG and ggtaccTTAGACGGGATGTTCATCTTCC (lower case characters indicate restriction sites). After amplification, the Phusion® polymerase was removed (PCR clean-up kit, Qiagen; Venlo, Netherlands), and 3'-adenosine overhangs were added using Taq DNA polymerase (New England Biolabs) and dATP (0.25 mM, final) following a protocol from New England Biolabs. TbCK1.2 was first cloned into the pCR™ 2.1-TOPO® vector (Thermo Fisher Scientific; Waltham, MA) before subcloning into pGAD9-V4 [41].

The TbCK1.2 expression construct (10 μg) was linearized with BamHI (New England Biolabs) and transfected into SM trypanosomes [40] via electroporation as previously described [83]. Stable transfectant clones were isolated by addition of G418 (6.5 μg/ml) and Hygromycin B (5 μg/ml), and serial dilution as described above.

TbCK1.2-HA overexpression: TbCK1.2 was amplified from a pET21-TbCK1.2 construct (Mensa-Wilmot lab, unpublished) with a high-fidelity Phusion® polymerase (New England Biolabs). The forward primer was engineered with a 5' HindIII restriction site and the reverse primer with an XhoI site to facilitate cloning into a pLew100-HA expression plasmid [40] (pLew100-TbTLK-HA [85] was kindly provided by Dr. Ching Wang at the University of California San Francisco). The forward and reverse primer sequences, respectively were: aagcttATGAGCGTAGAGCTTCGTGTGGGAAAC and ctcgagGACGGGATGTTCATCTTCCTTTTC (lowercase letters indicate restriction sites). After amplification, Phusion® polymerase was removed using a PCR clean-up kit (Qiagen). Subsequently, 3'-adenosine overhangs were added to the amplified TbCK1.2 gene using Taq DNA polymerase (New England Biolabs; Ipswich, MA) and dATP (0.25 mM, final) to allow cloning into a pCR™ 2.1-TOPO® vector. After performing a restriction digest with HindIII and XhoI (New England Biolabs), TbCK1.2 was isolated from pCR™ 2.1-TOPO® (Fisher) and subcloned into a pLew100-HA backbone. TbCK1.2-HA was PCR amplified from pLew100-TbCK1.2-HA with 5' HindIII and 3' Kpn1 restriction sites to facilitate cloning into pGAD9-V4 [41] with the same forward primer used to amplify TbCK1.2 from the pET21 plasmid. The sequence for the reverse primers was ggtaccCTCAAGCGTAATCTGGTACGTCGTATGGG (lowercase letters indicate restriction cut sites).

pGAD9-V4-TbCK1.2-HA construct was transfected into SM trypanosomes [40] by nucleofection [86]. Briefly, SM trypanosomes (4×10^7) were washed in

PBSG (3000 x g, 5 min) and resuspended in 100 µl of Amaxa human T-cell nucleofection solution (Lonza Group; Basel, Switzerland) containing BamHI-linearized pGAD9-V4-TbCK1.2-HA (10 µg). Trypanosomes were nucleofected with one pulse using protocol X-001 on a Nucleofector 2b device (Lonza Group) [86]. Following nucleofection, trypanosomes were incubated in 30 ml of HMI-9 medium for 18 h. Stable clones were then selected under the pressure of G418 (6.5 µg/ml) and Hygromycin B (5 µg/ml), after serial dilution (as described above).

V5-TbCK1.2 RNAi line: A bla/V5 plasmid [87] (provided by Dr. Chris Tschudi at Yale University) was used as a template (1 ng/µl) to amplify a bla/V5 tagging cassette flanked by sequences specific to TbCK1.2 in order to integrate a V5 epitope tag at the N-terminus of a TbCK1.2 allele. The forward primer included 90 bases of 3' UTR of TbCK1.2, and the reverse primer contained 91 bases from the 5' ORF of TbCK1.2. The PCR product was precipitated with ethanol, and resuspended in 100 µl of Amaxa human T-cell nucleofection solution. The tagging cassette was transfected into TbCK1.2 RNAi trypanosomes (4 x 10^7) by nucleofection [86] (described above). The forward primer sequence was: CAGCGGTGACAGCGGCAATAATCCAACCAAAATCAAACAAAAAAAAAAGAGA AGAAAGAGAATCAAAAACAGAAACTGTCGGTTATAAACAcccgggATGGCCAA GCCTTTGTCTCAAGAAG (lower case letters indicate a linker sequence separating BlaR- and TbCK1.2-specific sequences). The reverse primer sequence was: GAATATTTGTCCCCCGGAATATTTCACCAAAC GAACCGGAACCAATTTTTTGCCCGATGCGGAATCGGTTTCCCACACGAAGC TCTACGCTcccgggCGTAGAATCGAGACCGAGGAGAGGGTTAG (lower case

letters indicate a linker sequence separating V5- and TbCK1.2-specific sequences). Stable clones were then selected under the pressure of G418 (6.5 µg/ml), blasticidin (10 µg/ml), and Hygromycin B (5 µg/ml), after serial dilution (as described above).

TbCK1.2-HA line: pMoTag4H [88] was used as a template (1 ng/ul) to amplify an HA-HygroR cassette tagging cassette with flanking sequences to target the PCR product to the C-terminus of an endogenous TbCK1.2 allele. PCR amplification and recovery of the PCR product for transfection were performed as described previously [88]. The forward primer sequence was: GTTGCAAGAGGGCCGTGCGGATCAGCAGCAGCAGCAACAACAACAGCAGC AACGGCGTGGATCTGAAAAGGAAGATGAACATCCCGTCGGTACCGGGCCC CCCCTCGAG. The reverse primer sequence was ATGGGCAGTTCACCCTCTTTCTCTCTCTTATTCTCTTCTTCTCTTATTTCCTTC TTTTCTTTTTTTTTTTCCTTCTCCTTTTCTTCTATCTTCGTCTCTTGGCGGCCG CTCTAGAACTAGTGGAT. The PCR product was transfected into CA427 cells (4 x 10^7) using nucleofection as described above. Stable clones were then selected under the pressure of Hygromycin B (5 µg/ml), after serial dilution (as described above).

Analysis of V5-TbCK1.2 protein levels after genetic knockdown of TbCK1.2

The V5-TbCK1.2 RNAi line (5 x 10^4 cells/ml) was incubated in HMI-9 medium, with or without tetracycline (1 µg/ml), for 24 hours (37 ºC, 5%). Induced and uninduced trypanosomes were pelleted (3000 x g, 5 min) and processed for western blotting

(see “western blotting”) with an anti-V5 antibody (see “antibodies”). Three biological replicates were performed.

Quantitation of the number of nuclei, kinetoplasts, basal bodies, and flagella per trypanosome after knockdown of TbCK1.2

The TbCK1.2 RNAi line (5 x 10^4 cells/ml) was incubated in HMI-9 medium, with or without tetracycline (1 µg/ml), for 24 hours (37 ºC, 5%) and processed accordingly. Quantitation of the number of kinetoplasts and nuclei, per trypanosome, was performed after staining trypanosomes with 4’,6-diamidino-2-phenylindole (DAPI) (see “enumeration of kinetoplasts and nuclei by DAPI staining”). DAPI staining was executed for four biological replicates (n = 125/experiment). Visualization and quantitation of basal bodies was achieved by co-staining trypanosomes with the antibodies YL1/2 [16] and anti-TbSAS6 [15]. Staining was performed for three biological replicates (n = 125/experiment). Quantitation of flagella was performed after co-staining trypanosomes with YL1/2 [16] and anti-PFR2 (GenScript®) antibodies. Enumeration of flagella was executed for three biological replicates (n = 125/experiment). Refer to “immunofluorescence assays” for staining conditions and “antibodies” for concentrations used.

Enumeration of kinetoplasts and nuclei after DAPI staining

Trypanosomes (~1.5 x 10^6) were resuspended in 500 µl of 4% paraformaldehyde (PFA) in phosphate buffered saline (PBS) (Affymetrix; Santa Clara, CA). Cells were fixed for one minute (25 °C) and pelleted at 3000 x g for three minutes. The cell pellet was resuspended in 10 µl of supernatant (PFA/PBS) and adhered to

poly-L-lysine (Sigma Adlrich; St. Louis, MO) coated coverslips for 15 minutes. Coverslips were briefly rinsed with PBS prior to mounting onto microscope slides using VectaSheild® Mounting Medium (Vector Labs; Burlingame, CA) supplemented with 1.5 µM DAPI.

Western blotting

Trypanosomes (8 x 10^5 per sample) were washed in 1 ml of PBSG and centrifuged (3000 x, 5 min). The cell pellet was lysed in 12 µl of SDS gel loading buffer: 50 mM Tric-HCl (pH 6.8), 2% sodium dodecyl sulfate (SDS), 10% glycerol, 0.1% bromophenol blue, 50 mM β-mercaptoethanol. The lysate was heated at 95 ºC for five minutes. Proteins were separated on a TGX Stain-Free™ FastCast™ 12% acrylamide gel (Bio-Rad; Hercules, CA). Prior to transfer, the stain-free gel was activated by exposure to UV light for five minutes using a ChemiDoc MP system (Bio-Rad). Subsequently, proteins were transferred from the polyacrylamide gel to a PVDF membrane using the Trans-Blot® Turbo™ RTA Transfer Kit (Bio-Rad) and Trans-Blot® Turbo™ Transfer System (Bio-Rad). The PVDF membrane was blocked with 5% milk in tris-buffered saline containing 0.1% Tween-20 (TBST) and washed thrice in TBST, five minutes each. Primary antibody was incubated with the membrane in 10 ml of bovine serum albumin (BSA) (5%) in TBST for one hour. The membrane was washed in TBST, as described above, before exposure to the secondary antibody (conjugated to alkaline phosphatase) in TBST with 5% BSA for one hour. The membrane was washed as described previously and incubated with Immun-Star™ chemiluminescent alkaline phosphatase (AP) substrate (Bio-

Rad) for three minutes. Chemiluminescence was detected using a ChemiDoc MP system. All steps were carried out at 25 °C.

Western blot normalization was performed with Image Lab™ Software. Briefly, the stain-free blot (detected under UV light) was used to estimate total protein in each lane. Image Lab™ then normalized band intensity (either for V5-TbCK1.2 or TbCK1.2-HA at ~39 kDa) to the total protein detected in the corresponding lane of the stain-free blot. All western blots were performed in triplicate, and the normalized band intensities obtained for either the uninduced or induced samples were averaged.

Immunofluorescence assays

Trypanosomes (8×10^5) in 1 ml of PBSG were pelleted (3000 x g, 5 min). The cell pellet was resuspended in 10 µl of PBSG and adhered to poly-L-lysine coated coverslips for five minutes. Once the cells adhered, the coverslip was quickly air-dried (~3 minutes) and placed in methanol at -20 ºC for twenty minutes. Coverslips were rinsed briefly with PBS before exposure to blocking solution (1% BSA in PBS) for one hour. Next, the coverslips were incubated with primary antibody in blocking solution for one hour (25 °C) followed by three washes in PBS, five minutes each. The coverslip was then exposed to a fluorescent secondary antibody in blocking solution for one hour (25 °C). The coverslip was then washed as described previously and mounted onto a microscope slide with VectaSheild® Mounting Medium supplemented with 1.5 µM DAPI. Trypanosomes were visualized by fluorescence microscopy on an Applied Precision DeltaVision II microscope

System (GE Healthcare; Issaquah, WA). Images were captured with a cooled CCD camera.

Antibodies

Western blotting: The anti-V5 rabbit monoclonal antibody (Cell Signaling; Danvers, MA) and anti-HA rabbit polyclonal antibody (Abcam; Cambridge, UK) were used at a dilution of 1:2000. Anti-rabbit secondary antibody conjugated to alkaline phosphatase (Bio-Rad) was used at a dilution of 1:3000.

Immunofluorescence assays: The YL1/2 [16] monoclonal rat anti-tubulin antibody (EMD Millipore; Billerica, MA) was used at a dilution of 1:1000. The polyclonal rabbit anti-TbSAS6 antibody [15], provided by Dr. Ziyin Li (University of Texas Health Science Center), was used at a dilution of 1:500. The mouse monoclonal anti-centrin antibody 20H5 [11] (EMD Millipore) was used at a dilution of 1:500. The rabbit polyclonal anti-PFR2 antibody, used at a dilution of 1:500, was produced by GenScript® (Piscataway Township, NJ) using a synthetic peptide from the trypanosome protein. The rabbit monoclonal anti-V5 antibody (Cell Signaling) was used at a dilution of 1:250. All secondary antibodies were conjugated to either AlexaFluorophore-488 (AF-488) or AF-594 and used at a dilution of 1:3000.

When specified, trypanosomes were fixed with paraformaldehyde (PFA) and permeabilized with detergent. Briefly, cells (2×10^6 per sample) were pelleted (3000 x g, 5 min) and was rinsed with 1 ml of PBSG. The cell pellet was resuspended in 500 µl of 4% PFA in PBS. Trypanosomes were incubated with PFA for one minute, pelleted, and adhered to a poly-L-lysine coated coverslip in 10 µl of the supernatant (4% PFA in PBS). Trypanosomes were allowed to adhere to the

coverslip for 15 minutes. Subsequently the coverslip was rinsed with PBS and aldehydes quenched with 0.15 M glycine in PBS (500 µl). The coverslip was then incubated with 0.15% triton X-100 in PBS (500 µl) for 25 minutes at room temperature. After rinsing off the detergent, trypanosomes were stained using the immunofluorescence assay described above.

Measurement of inter-basal body distances

The distance between basal bodies (inter-basal body distance) in trypanosomes with two mature basal bodies was determined using ImageJ software. A line was drawn between the center of YL1/2-positive mature basal bodies (see "immunofluorescence assays"), and the distance of the line was converted from pixels to µm based on the size of the scale bar (µm) in ImageJ. Trypanosomes from five independent immunofluorescence assays were analyzed (n = 97 (1K1N –Tet), n = 94 (1K1N +Tet), n = 95 (1K2N +Tet), n = 81 (2K1N –Tet), n = 61 (2K1N +Tet), n = 84 (2K2N –Tet), n = 51 (2K2N +Tet)).

Enzyme assays with purified, recombinant TbCK1.2

Full-length recombinant TbCK1.2 was expressed as a fusion with maltose-binding protein at the N-terminus, and a hexahistidine tag at the C-terminus in *E. coli* BL21 (DE3) [89]. The enzyme was purified by double affinity chromatography on (i) maltose, and then (ii) metal affinity chromatography [90]. In a final step, size exclusion chromatography was employed, resulting in 90% pure recombinant TbCK1.2 (as assessed by coomassie blue staining) and was used for our enzyme assays.

Reaction mixtures for protein kinase assays were prepared on ice with purified TbCK1.2 (50 nM) and a peptide substrate pS7 (20 μM) (Anaspec; Fremont, CA) in reaction buffer: 50 mM 4-(2-hydroxyethyl)-1-piperazineethanesulfonic acid (HEPES), pH 7.6, 5 mM $MgCl_2$, 2 mM dithiothreitol (DTT), and 150 mM NaCl. SB-431542 (1 μl) was added to the reaction (19 μl) from a 20X stock of each desired concentration (on ice). Equal volume (1 μl) of the drug vehicle, dimethyl sulfoxide (DMSO), was used as a control. ATP/ATP-[$\boldsymbol{\gamma}$-^{33}P] was added at a final concentration of 20 μM (1 μCi). Reaction components were thoroughly mixed via pipetting and incubated for 20 minutes at 30 °C. The reaction was halted by the addition of two volumes of ice cold 10% trichloroacetic acid (TCA). The terminated reaction was dotted onto Whatman P-81 paper, which was then loaded onto a vacuum manifold, washed three times with 75 mM phosphoric acid (H_3PO_4), and dried with acetone. Peptide[$\boldsymbol{\gamma}$-^{33}P] on Whatman P-81 filter paper was measured with a scintillation counter (TriCarb 4810 TR). The experiment was performed in triplicate, using technical replicates in each experiment. Counts per minute (CPM) were converted to percent activity by assigning activity of the DMSO control as 100%. For each experiment, the average CPM of technical replicates was used to determine percent activity as compared to the DMSO control. The percent activity from each experiment was averaged and the data analyzed with GraphPad Prism 6. A four-parameter non-linear regression analysis was used to fit a line to the points and to determine the IC_{50} (inhibitory concentration that reduces activity by 50%).

SB-431542 treatment of single marker trypanosomes

The effect of SB-431542 treatment on proliferation, kinetoplast division, and basal body duplication was determined in SM cells (parental background of TbCK1.2 RNAi line). All experiments used a starting trypanosome density of 5 x 10^5 cells/ml. SB-431542 was added to cell cultures (from a 1000X stock) at a final concentration of 10 μM. Equal volume (1 μl/ml) DMSO (drug vehicle) was a used as a control. Cells were incubated with DMSO or SB-431542 for 10 hours (37 ºC, 5%).

Trypanosome proliferation was assessed by determining the cell density at 0 hours (start) and 10 hours after treatment with DMSO or SB-431542. Samples were diluted 50-fold in filtered Beckman Coulter isoton II buffer (Z-series Pak) (Beckman Coulter; Crea, CA) and cell density measured on a Z-series Coulter Counter (Beckman Coulter). Trypanosome density was measured in three biological replicates and the average cell density determined.

Kinetoplast division was visualized via DAPI staining (see “enumeration of kinetoplasts and nuclei by DAPI staining”). Quantitation of the number of kinetoplast and nuclei were performed for three biological replicates (n = 100/experiment). Basal bodies were detected with the antibodies YL1/2 [16] and anti-TbSAS6 [15] (see “immunofluorescence assays” and “antibodies”). Quantitation of basal body numbers was executed for three biological replicates (n = 125/experiment).

Detection of TbCK1.2-HA protein levels after overexpression of TbCK1.2

A TbCK1.2-HA overexpression line (5 x 10^4 cells/ml) was incubated in HMI-9 medium, with or without tetracycline (1 μg/ml), for 12 hours (37 ºC, 5%). Induced

and uninduced trypanosomes were processed for western blotting (see “western blotting”) using an anti-HA antibody (see “antibodies”). The average band intensity of triplicate experiments, determined by Image Lab™ (described in “western blotting”), is reported.

Assessment of basal body duplication in TbCK1.2-overexpressing trypanosomes in the presence of DMSO or SB-431542

A TbCK1.2 overexpression line (5 x 10^4 cells/ml) was incubated in HMI-9 medium with or without tetracycline (1 µg/ml), for six hours (37 ºC, 5%). The uninduced and induced cultures were each divided into two flasks. One uninduced and one induced sample was treated with a 1000X stock of SB-431542 (7 µM, final). The remaining samples were treated with equal volume (1 µl/ml) DMSO (drug vehicle). The cultures were incubated an additional six hours at 37 ºC, 5% (i.e. induced samples were in the presence of tetracycline for 12 hours). Trypanosomes were then collected and basal bodies detected using YL1/2 [16] and anti-TbSAS6 [15] antibodies (see “immunofluorescence assay” and “antibodies”). Staining and quantitation was performed for three biological replicates.

Quantitation of fluorescence intensity from DAPI-stained kinetoplasts

Images of trypanosomes stained with YL1/2 [16] and DAPI (see above) were captured on a DeltaVision II microscope System under the same brightness and exposure conditions. Additionally, the brightness and contrast settings of display images were kept identical. Using ImageJ software, a box was drawn over each kinetoplast or nucleus and the sum of the pixels in the selection measured (raw

integrated density). To control for background fluorescence, a box with the same dimensions used for each kinetoplast or nucleus was drawn at two areas near the organelle of interest, and the raw integrated density determined. The average of the two background fluorescence measurements was then subtracted from the integrated density of the respective kinetoplast or nucleus. Images were analyzed from three independent immunofluorescence assays (n = 100 (1K1N –Tet), n = 71 (1K2N +Tet), n = 88 (2K1N –Tet), n = 84 (2K2N –Tet)).

Analysis of nuclear DNA content following knockdown of TbCK1.2

The TbCK1.2 RNAi line (5 x 10^4 cells/ml) was incubated in HMI-9 medium with or without tetracycline (1 µg/ml) for 24 hours (37 ºC, 5%). Trypanosomes (1 x 10^5) were fixed in 1 mL of methanol (40%) in PBS for 30 minutes (25 °C) and pelleted by centrifugation at 3000 x g for 3 minutes. The cell pellet was resuspended in 1 ml of PBS with RNase A (40 µg/ml) and propidium iodide (50 µg/ml). The samples were incubated away from light at 37 ºC for 30 minutes. Samples were then moved to ice and propidium iodide fluorescence measured on a Beckman Coulter Cyan flow cytometer. FlowJo software (FlowJo, LLC; Ashland, OR) was used to quantitate propidium iodide fluorescence in trypanosome populations as identified by forward and side scatter properties of the cells.

Effect of SB-431542 treatment on V5-TbCK1.2 expression

The V5-TbCK1.2 RNAi line (5 x 10^4 cells/ml) was incubated in HMI-9 medium (without tetracycline) in the presence of SB-431542 (10 µM) or equal volume (1 µl/ml) DMSO (drug vehicle) for 10 hours (37 ºC, 5%). Trypanosomes treated with

DMSO or SB-431542 were processed for western blotting (see “western blotting”) using an anti-V5 antibody (see “antibodies”). The normalized band intensity (see “western blotting”) of V5-TbCK1.2 was averaged over triplicate biological replicates.

SILAC and label-free preparation of trypanosome peptides for LC-MS/MS

Preparation of labeled trypanosome peptides for LC-MS/MS: A tetracycline-inducible TbCK1.2 RNAi line was cultured for five days (17 doublings) in HMI-9 medium modified for SILAC [46, 91]; IMDM medium depleted of Lys and Arg (Gibco Laboratories; Gaithersburg, MD) was supplemented with either L-Arg (120μM) and L-Lys (240 μM) (“light” medium), or $^{13}C_6$ -L-Arg (120 μM) and $^{2}H_4$-L-Lys (240 μM) (“heavy” medium). Knockdown of TbCK1.2 was induced for 24 hours in cells grown in light medium. Subsequently, induced (light medium) and uninduced (heavy medium) trypanosomes (3 x 10^7 cells per sample) were combined and pelleted (3000 x g, 5 min, 4 ºC). Cells were washed with 10 ml of PBSG containing phosphatase inhibitors (2 mM imidazole, 1 mM sodium fluoride, 4 mM sodium tartate, 1.15 mM sodium molybdate, 1 mM β-glycerophosphate, and 5 μM phenylarsine oxide, final concentrations) and pelleted as before. Trypanosomes were lysed by sonication in 500 μl of lysis buffer (8 M urea, 4 mM DTT, 50 mM HEPES, pH 7.6, and phosphatase inhibitors described above), and alkylated with iodoacetamide (9 mM) for twenty minutes (protected from light). The cell lysate was then diluted with 50 mM HEPES, pH 7.6, containing phosphatase inhibitors and digested by trypsin immobilized-agarose beads (Thermo Scientific) at 37 °C for 30 hours. Tryptic peptides were bound to a Sep-Pak C18 column and

eluted by a step gradient of acetonitrile (1%, 25%, and 50%) in trifluoroacetic acid (TFA). As a control for biological variation, uninduced trypanosomes (3 x 10^7 cells per sample) grown in heavy and light medium were combined and processed as described above. Phospho-peptides were enriched using immobilized metal affinity chromatography described below.

Preparation of label-free trypanosome peptides for LC-MS/MS: Trypanosomes with a tetracycline-inducible RNAi construct (5 x 10^4 cells/ml) were incubated in the presence or absence of tetracycline in HMI-9 medium for 24 hours. Trypanosomes (6 x 10^7 per sample) were collected and processed as described above for cells grown in SILAC medium, except that the uninduced and induced samples were prepared individually and never combined. Two label-free experiments were performed.

Phospho-peptide enrichment and LC-MS/MS analysis

Phospho-peptides were enriched by $FeCl_3$ charged metal affinity chromatography (IMAC) using a previously published protocol [92]. Phospho-peptide elutions were desalted twice in this case, yielding two fractions from the same sample, in order to enhance the amount phospho-peptides recovered for MS analysis. The desalted phospho-peptides were dried in a speed vac.

LC-MS/MS analysis was performed with an Easy-nLC 1000 (Thermo Scientific) coupled to an Orbitrap Fusion mass spectrometer (Thermo Scientific) as described previously [92] with following modifications: i) phospho-peptides were dissolved in 10 µL of 2% acetonitrile and 0.1% formic acid in water, and 7 µL was

loaded, ii) the chromatographic separation was achieved over a 139-min gradient from 2% to 50% B (2-5% B for 2min, 5–30% B for 120 min, 30–50% B for 15 min, and 50% B for 2 min) at a flow rate of 300 nL/min, and iii) an inclusion list was used during analysis of the second label-free experiment.

The inclusion list consisted of 17 unique peptides which demonstrated the greatest decrease in phospho-peptide abundance in the first label-free experiment. Multiple phospho-isoforms, as well as dephosphorylated versions, of the peptide were included generating a list of 105 peptides total. During the survey scan, precursor ions that matched the mass to charge ratios in the inclusion list were isolated first for MS/MS analysis before analyzing the most abundant ions. The mass to charge ratios used to search for peptides were based on measurements made from the first label-free LC-MS/MS analysis, or predicted based on amino acid sequence for peptide isoforms not previously detected.

Proteome Discoverer™ version 2.1 (Thermo Scientific) was used for data analysis. As previously reported [92], the data were searched using SEAQUEST [93] against *T. brucei* protein database v. 4.2 (tritrypdb.org), and PhoshoRS [94] was used to evaluate the site of phosphorylation. Phosphorylation sites were reported if the PhosphoRS probability was greater than 79%. Phospho-peptides that demonstrated at least a 2-fold decrease (or increase) in our SILAC experiment and a spectral count experiment are reported as putative TbCK1.2 effectors.

Figure 3.1. *Knockdown of casein kinase 1 causes amplification of trypanosome basal bodies*. One allele of TbCK1.2 was tagged with a V5 epitope (N-terminal) in a cell line harboring a tetracycline-inducible TbCK1.2 RNAi construct. Trypanosomes were incubated in the absence (-Tet) or presence (+Tet) of tetracycline (1 µg/ml) for 24 h. (***A***) Western blot using an anti-V5 antibody to probe lysate from uninduced (-Tet) and induced trypanosomes (+Tet). The average normalized band intensity (see materials and methods) of V5-CK1 (39 kDa), with standard deviation, is shown graphically from three biological replicates. (***B***) Trypanosomes co-stained with anti-TbSAS6 to label mature basal bodies (mBB) and probasal bodies (pBB), and the antibody YL1/2 to mark mature basal bodies. Trypanosomes were counterstained with DAPI to visualize DNA. K = kinetoplast; N = nucleus; Arrowheads = basal bodies. The scale bar is 6 µm. Gray box: control cell with two basal bodies (2mBB/2pBB). Green box: induced trypanosome with increased basal body copy number (> 2mBB/2pBB). (***C***) Average percentage of trypanosomes with the indicated number of mature basal bodies (mBB) ($YL1/2^{+}$) and probasal bodies (pBB) ($YL1/2^{-}$ and $TbSAS6^{+}$). Error bars represent standard deviation from triplicate biological replicates. The distribution of trypanosomes with different numbers of mBBs and pBBs, between control (-Tet) and experimental (+Tet) samples was compared using a χ^2 test ($p = 1.9 \times 10^{-33}$). (***D***) Detection of trypanosomes with distal basal bodies (DBBs) (white arrowheads) labeled with anti-TbSAS6 and YL1/2 antibodies, as described above. The average percentage of trypanosomes with DBBs from three biological replicates is presented with

standard deviation. A student's t-test was used to compare the proportion of cells with DBBs between uninduced and induced TbCK1.2 RNAi line (p = 0.002).

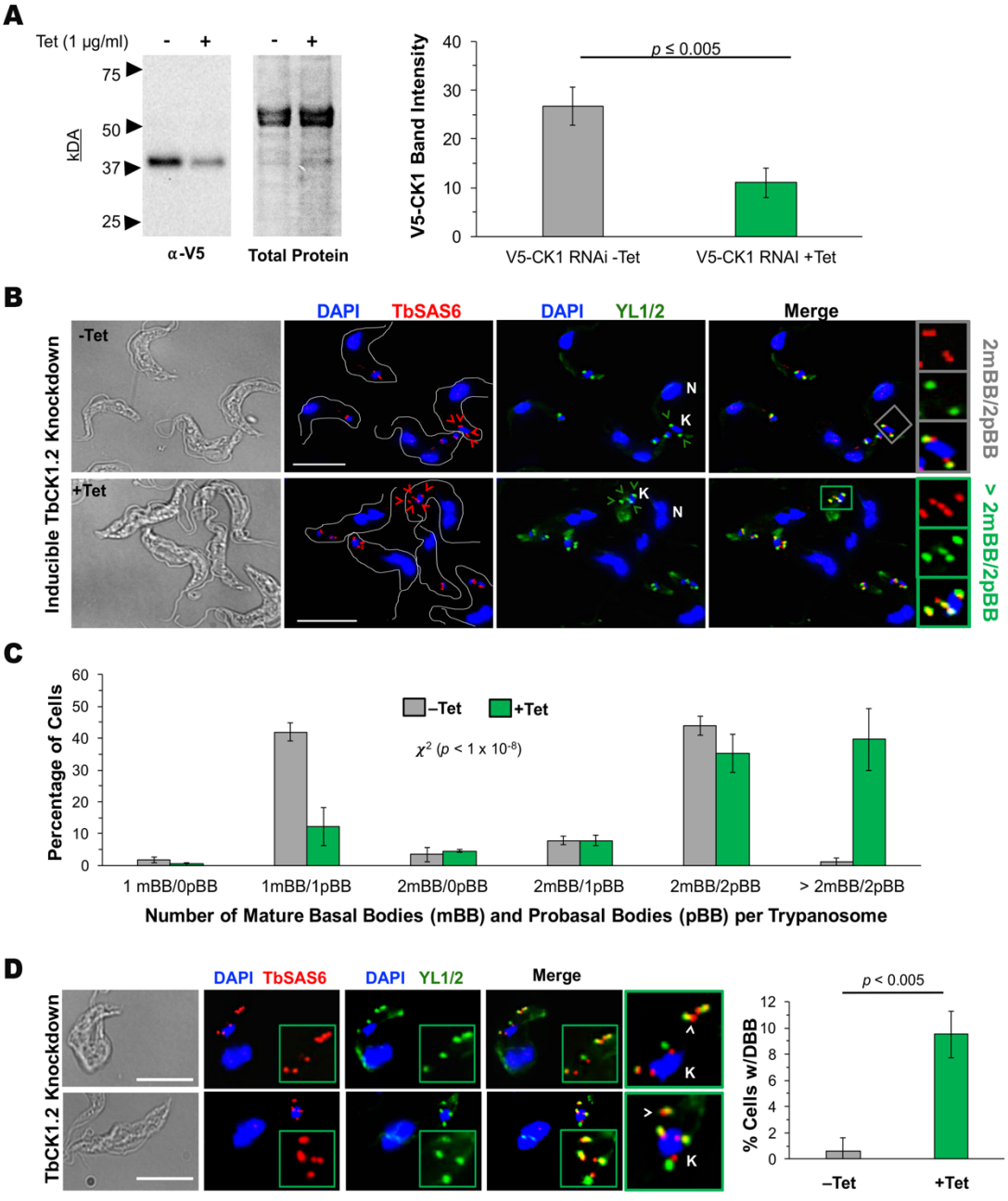

Figure 3.2. *Knockdown of TbCK1.2 inhibits kinetoplast division but not basal body duplication or segregation*. (***A***) Labeling of basal bodies in 1K2N trypanosomes following induction of TbCK1.2 RNAi (+Tet, 24 h) with anti-TbSAS6 (all basal bodies) and YL1/2 (mature basal bodies). Trypanosomes were counterstained with DAPI to visualize DNA in the kinetoplast (K) and nucleus (N). Gray and white boxes: representative pattern of basal bodies in control (-Tet) 1K1N cells with two basal body pairs (2mBB/2pBB). Green boxes: basal body staining in 1K2N cells (+Tet) that have two basal bodies (2mBB/2pBB) or overduplicated basal bodies (> 2mBB/2pBB). The scale bar is 6 μm. (***B***) The average percentage of 1K2N trypanosomes with indicated the number of mature basal bodies (mBBs) and probasal bodies (pBB). The average and standard deviation of three biological replicates are presented. (***C***) The distance (μM) between mature, YL1/2-positive basal bodies (inter-basal body distance) was measured in trypanosomes with two mature basal bodies using ImageJ. The average inter-basal body distance, with standard deviation, for each cell population is indicated. YL12-stained trypanosomes from four biological replicates were combined.

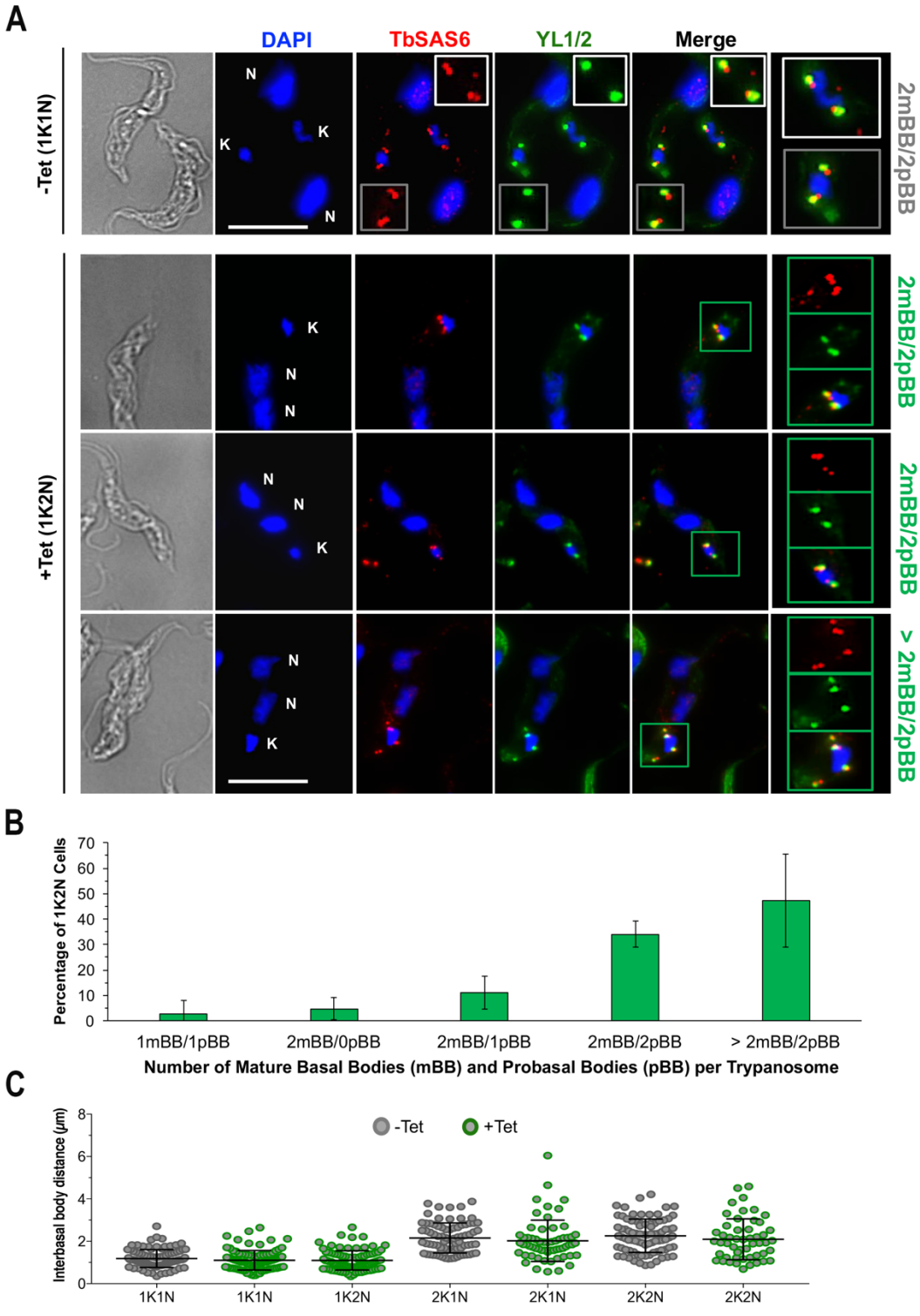
A
DAPI
TbSAS6
YL1/2
Merge
-Tet (1K1N)
+Tet (1K2N)
2mBB/2pBB
2mBB/2pBB
2mBB/2pBB
> 2mBB/2pBB
B
Percentage of 1K2N Cells
1mBB/1pBB
2mBB/0pBB
2mBB/1pBB
2mBB/2pBB
> 2mBB/2pBB
Number of Mature Basal Bodies (mBB) and Probasal Bodies (pBB) per Trypanosome
C
Interbasal body distance (μm)
-Tet
+Tet
1K1N
1K1N
1K2N
2K1N
2K1N
2K2N
2K2N

Figure 3.3. *Flagella are detected in 1K2N cells and on supernumerary basal bodies and distal bodies following knockdown of TbCK1.2.* (***A***) TbCK1.2 RNAi cells incubated with (+Tet) or without (-Tet) tetracycline (1 µg/ml) for 24-hours were co-stained with the antibodies YL1/2 (detects mature basal bodies) and anti-PFR2 (detects the paraflagellar rod or PFR) to monitor flagellum biogenesis. A control (-Tet) cell with two flagella is shown in the first row followed by an induced (+Tet) 1K2N trypanosome with two flagella (2^{nd} row), an induced cell with more than two flagella (3^{rd} row), and a flagellated distal basal body (DBB) (yellow arrowhead) in the last row. DAPI was used to visualize DNA in the kinetoplast (K) and nucleus (N). Arrowheads = basal bodies; arrows = PFR. The scale bar is 6 µm. (***B***) The number of flagella per cell were quantitated and the average percentage, with standard deviation, from three biological replicates is shown. A χ^2 test was used to determine if the distribution of cells with one, two, or more than two flagella differed, statistically, after knockdown of TbCK1.2 ($p = 8 \times 10^{-20}$). (***C***) Average percentage of 1K2N cells with the indicated number of flagella. Error bars represent standard deviation from triplicate experiments.

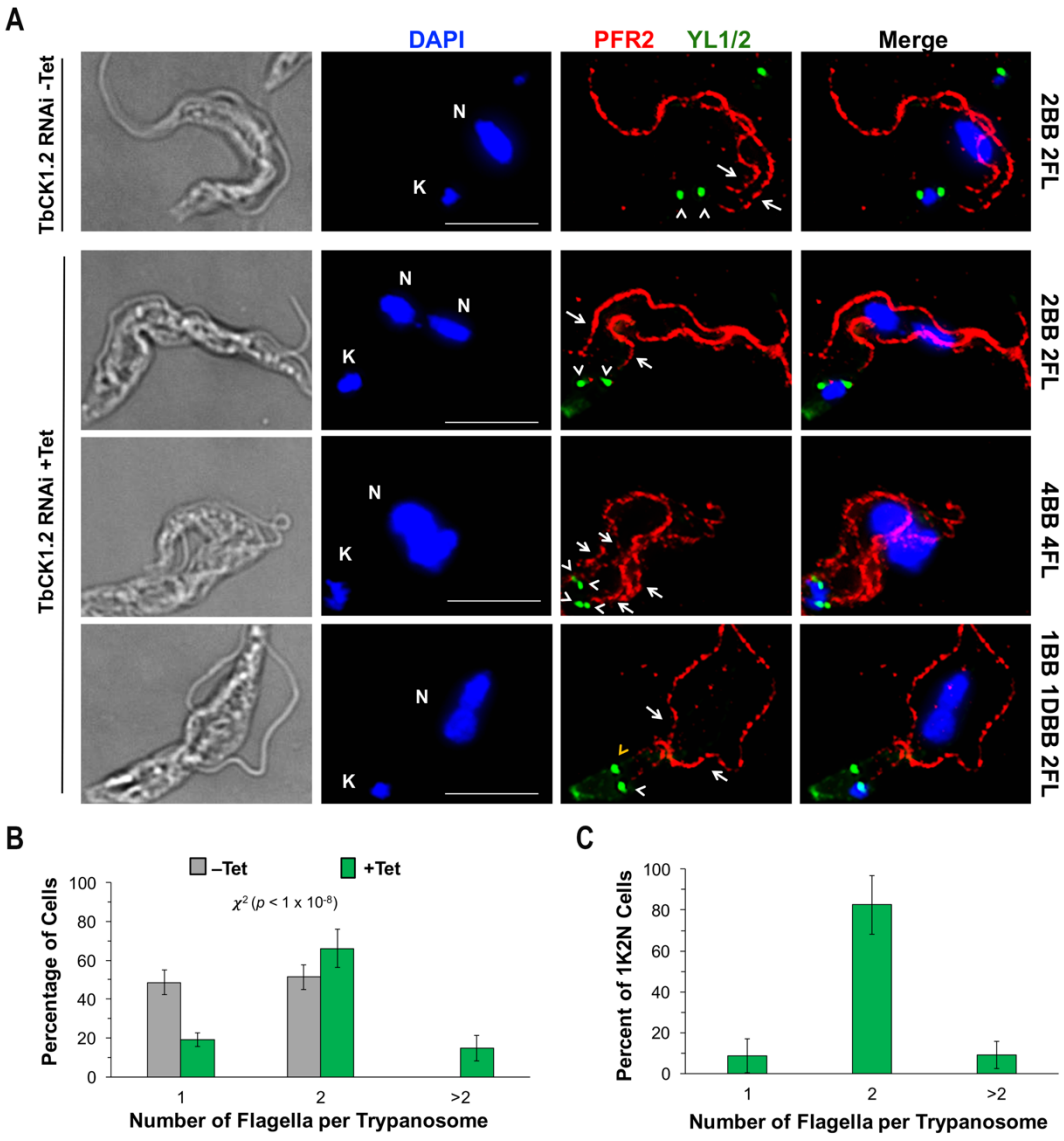
A
DAPI
PFR2
YL1/2
Merge
TbCK1.2 RNAi -Tet
TbCK1.2 RNAi +Tet
2BB 2FL
2BB 2FL
4BB 4FL
1BB 1DBB 2FL
N
K
B
–Tet
+Tet
χ^2 (p < 1 x 10^{-8})
Percentage of Cells
Number of Flagella per Trypanosome
C
Percent of 1K2N Cells
Number of Flagella per Trypanosome

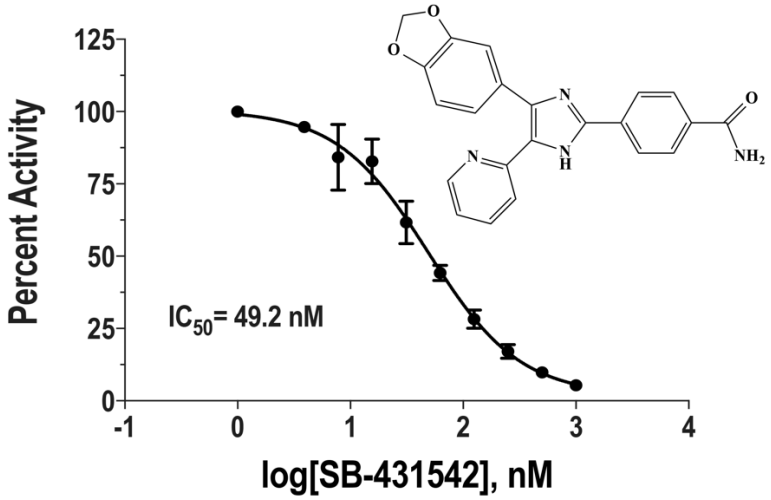

Figure 3.4. *SB-431542 is a small molecule inhibitor of purified TbCK1.2*. A dose-response curve demonstrating the effect of increased SB-431542 (structure shown) concentrations on enzyme activity of purified, recombinant TbCK1.2.

Figure 3.5. (***A***) Trypanosome basal bodies were visualized using an anti-TbSAS6 antibody (all basal bodies) and the antibody YL1/2 (mature basal bodies) after treatment with SB-431542 (10 μM, 10 h) or equal volume (1 μl) DMSO (drug vehicle). DNA was visualized with DAPI. K = kinetoplast; N = nucleus. Gray box: DMSO-treated cell with duplicated basal bodies (2mBB/2pBB). Blue box: SB-431542-treated trypanosome with overduplicated basal bodies (> 2mBB/2pBB). The scale bar is 6 μm. (***B***) The average percentage of cells with indicated numbers of mature basal bodies (mBB) and probasal bodies (pBB) after treatment with DMSO or SB-43142 (10 μM, 10 h). Error bars represent the standard deviation in three independent experiments. A χ^2 test was used to determine whether the distribution of basal bodies (mBBs/pBBs) differed, statistically, between cell populations treated with DMSO or SB-431542 ($p = 9.8 \times 10^{-14}$).

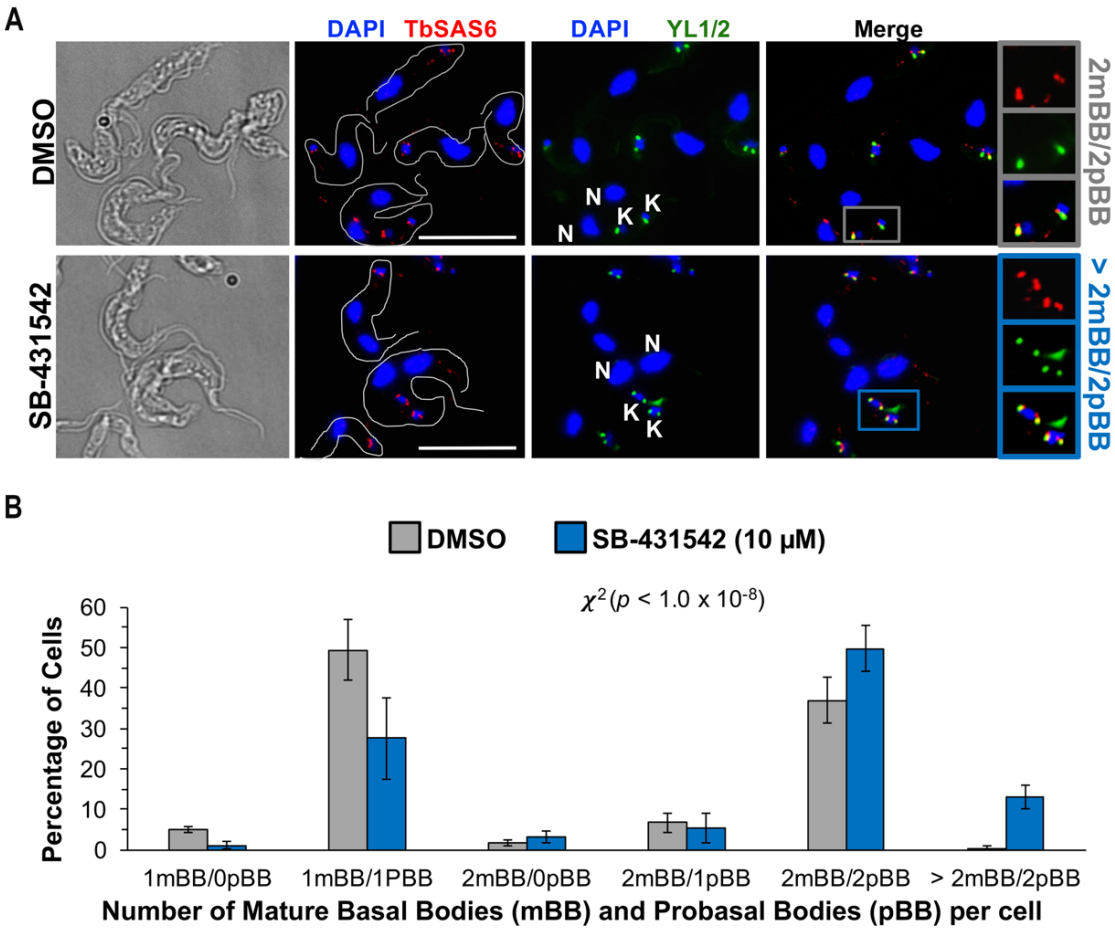
A
DAPI TbSAS6
DAPI YL1/2
Merge
DMSO
SB-431542
N
K
2mBB/2pBB
> 2mBB/2pBB
B
DMSO
SB-431542 (10 µM)
$\chi^2(p < 1.0 \times 10^{-8})$
Percentage of Cells
60
50
40
30
20
10
0
1mBB/0pBB
1mBB/1PBB
2mBB/0pBB
2mBB/1pBB
2mBB/2pBB
> 2mBB/2pBB
Number of Mature Basal Bodies (mBB) and Probasal Bodies (pBB) per cell

Figure 3.6. *Overexpression of TbCK1.2 inhibits basal body duplication*. A tetracycline (Tet) inducible TbCK1.2-HA expression construct was integrated into minichromosomes of single marker (SM) trypanosomes for regulated TbCK1.2 expression. (***A***) Anti-HA western blot of trypanosome lysate collected from the TbCK1.2-HA overexpression line incubated with (+Tet) or without (-Tet) exogenous tetracycline (12 h). The average normalized band intensity (see materials and methods) of TbCK1.2-HA (40 kDA), with standard deviation, from three biological replicates is presented as a bar graph. (***B***) Images depicting mature basal bodies (mBBs) and probasal bodies (pBBs) after TbCK1.2 overexpression (12 h). DNA in the kinetoplast (K) and nucleus (N) was visualized using DAPI. The scale bar is 6 μm. Gray box: control trypanosome with two mature basal bodies and two probasal bodies (2mBB/2pBB). Green box: TbCK1.2-overexpressing cell with a single mature basal body (1mBB/0pBB). (***C***) Experimental strategy for assessing the effect of TbCK1.2 overexpression on basal body duplication in the presence or absence of SB-431542 (7 μM). The TbCK1.2 overexpression line was incubated in medium with (+Tet) or without (-Tet) tetracycline for 6 h. Subsequently, SB-431542 (7 μM) or equal volume DMSO (drug vehicle) was added to uninduced (-Tet) or induced (+Tet) trypanosomes for an additional 6 h. Cells were then collected for staining with anti-TbSAS6 (mature basal bodies and probasal bodies) and YL1/2 (mature basal bodies). The average percentage of trypanosomes with indicated numbers of mature basal bodies (mBBs) and probasal bodies (pBBs) is shown for each treatment. Error bars represent the standard deviation in three biological replicates. The distribution of

trypanosomes with different numbers of mBBs and pBBs was compared using a χ^2 test: uninduced cells treated with DMSO (-Tet; +DMSO) to induced cells treated with DMSO (+Tet; +DMSO) (p = 9.4 x 10^{-9}) or uninduced cells treated with DMSO (-Tet +DMSO) to induced cells treated with SB-431542 (+Tet +SB-431542) (p = 7 x 10^{-2}).

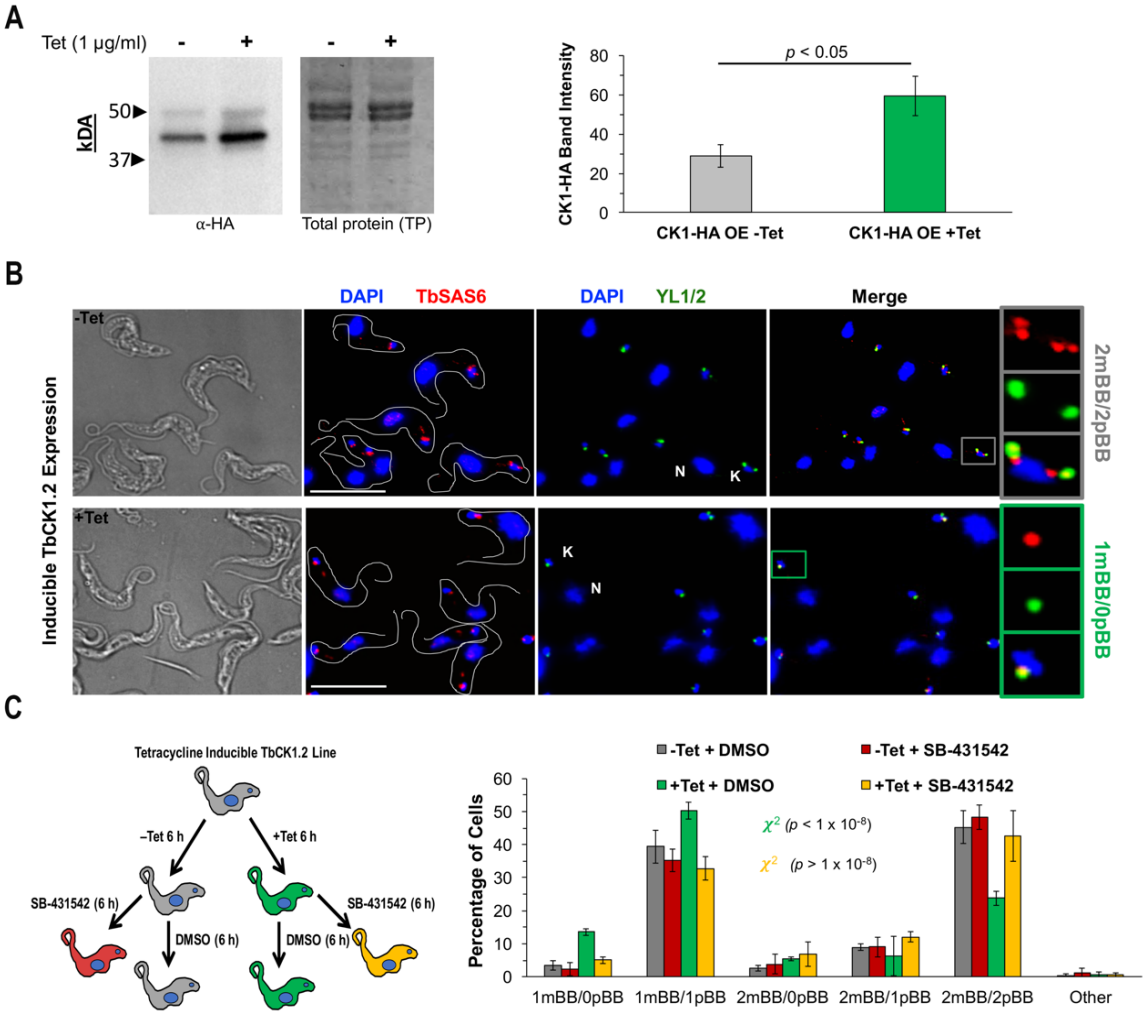

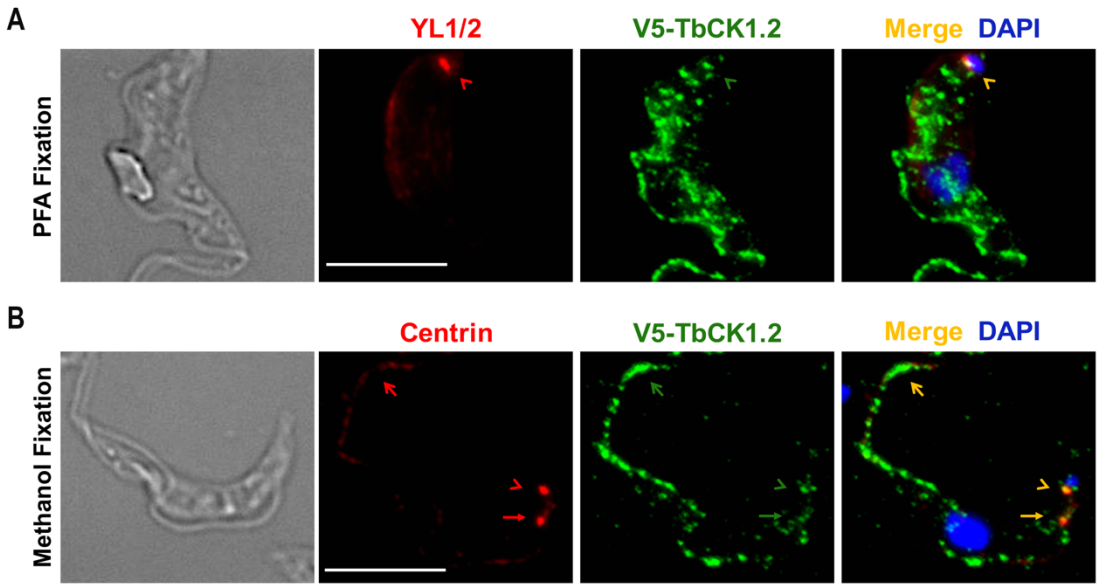

Figure 3.7. *TbCK1.2 is detected in the cytoplasm, flagellum, and at basal bodies*. Localization of TbCK1.2 in bloodstream trypanosomes was determined by immunofluorescence detection of V5-TbCK1.2 with an anti-V5 antibody in the V5-TbCK1.2 RNAi line (in the absence of tetracycline). (***A***) Trypanosome fixed with paraformaldehyde (PFA) and co-stained with YL1/2 (mature basal bodies) and anti-V5 antibodies. DAPI was used to stain DNA in the kinetoplast. Arrowhead = basal body. The scale bar is 6 μm. (***B***) Trypanosome fixed with methanol and co-stained with the anti-centrin antibody 20H5 and anti-V5. DAPI was used to stain DNA in the kinetoplast and nucleus. Arrowhead = basal body; open arrow = flagellum; closed arrow = bilobe. The scale bar is 6 μm.

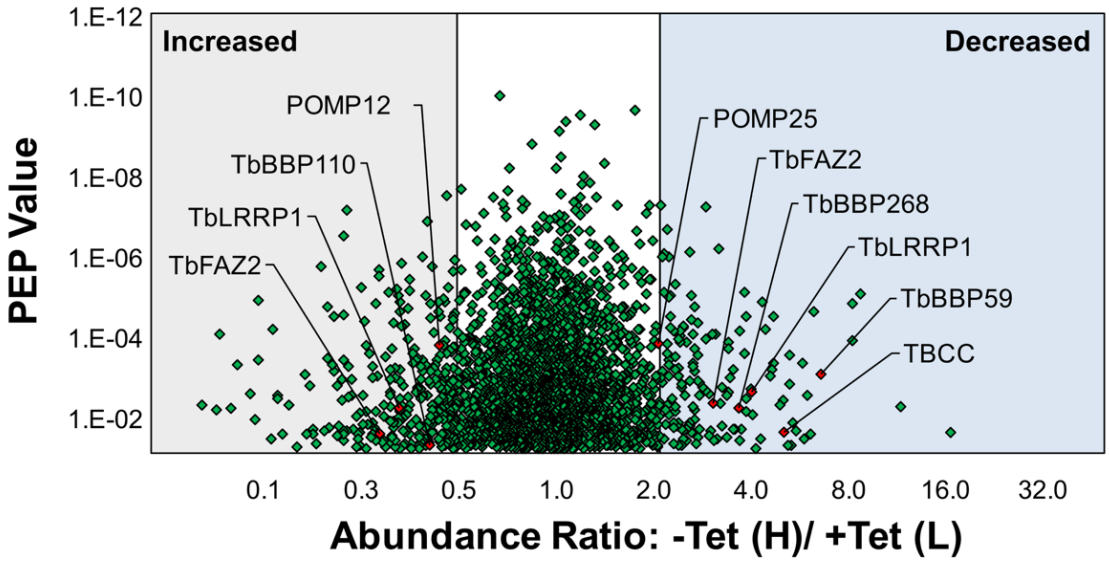

Figure 3.8. *Knockdown of TbCK1.2 perturbs homeostasis of select trypanosome phospho-peptides*. A tetracycline-inducible TbCK1.2 RNAi cell line was cultured in either light (L) or heavy (H) HMI-9 medium (SILAC) (see materials and methods). Knockdown of TbCK1.2 was induced with tetracycline (1 µg/ml) for 24 h in trypanosomes grown in light medium. Uninduced control cells (3×10^7) grown in heavy medium were combined with induced trypanosomes (3×10^7) followed by cell lysis. The parasite lysate was digested with trypsin and phospho-peptides enriched over an IMAC column before analysis by LC-MS/MS. Abundance ratios (H/L) of identified phospho-peptides are plotted as a function of their PEP value (probability that spectra-peptide match is incorrect). Only peptides with a score of 5×10^{-2} (5% chance of error), or lower, are shown. The area shaded in gray represents phospho-peptides with a 2-fold, or greater, increase in abundance, while the blue zone indicates peptides with a 2-fold, or greater, decrease in abundance.

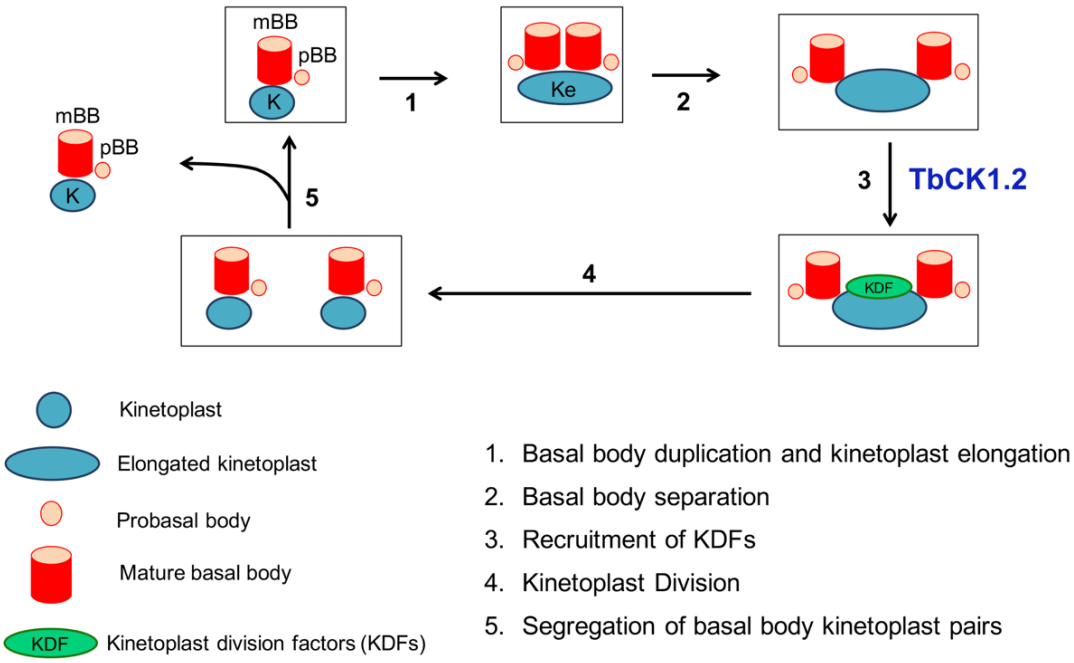

Figure 3.9. *Putative role for TbCK1.2 in regulation of kinetoplast division factors*. The basal body (mBB/pBB) is closely associated with a single kinetoplast (K) at the start of the cell division cycle. Basal body duplication is associated with kinetoplast elongation (Ke) (step 1). Prior to division of the kinetoplast the basal bodies begin to migrate, away from one another, to the kinetoplast poles (step 2). Our data demonstrates that basal body separation is not sufficient to divide the catenated kDNA network. Thus, we propose that TbCK1.2 regulates the activity and/or localization of factors ("kinetoplast division factors" or KDFs) (step 3) which promote biochemical separation of the kDNA network (step 4). Following kinetoplast division, the paired basal bodies and kinetoplasts continue to separate in preparation segregation during cytokinesis (step 5).

Table 3.1 *Putative TbCK1.2 effectors associated with the basal body, kinetoplast, or phospho-signaling*. Following a 24-h knockdown of TbCK1.2, phospho-peptides were harvested from uninduced and induced cells and phospho-peptides enriched over an IMAC column. Phospho-peptide abundance was calculated in each sample using a labeled proteomics (SILAC) and label-free approach (spectral counting (SC)) (see materials and methods). Select phospho-peptides identified with decreased or increased abundance (at least 2-fold) in each phosphoproteomics strategy are listed below. Peptides shaded in gray show increased phosphorylation. Phosphorylation sites are indicated in red (PhosphoRS [94] value >79%). * indicates the number of phospho-sites which could not be accurately identified. The fold change in phospho-peptide abundance, as compared to the uninduced control, is shown. ~ indicates that the phospho-peptide was only present in the control or induced population, preventing calculation of an abundance ratio. The probability that spectra was incorrectly matched with the specified peptide is presented (PEP Value).

Gene ID	Predicted Protein Product	Sequence	Fold Change		PEP Value	
			SILAC	SC	SILAC	SC
Basal Body, Bilobe and Flagellar Proteins						
Tb427.10.350	TbBBP59 (Dual Specificity Protein Kinase)	VSSAGSTPSVTAAR**	6.6	3	7.7E-04	1.0E-03
Tb427.10.10280	TbBBP268	RHSFTASSEADAAVVK**	3.7	5.5	5.2E-03	2.2E-04
Tb427tmp.01.0680	TbLRRP1	LGRPPSTTNDDASHPAK**	4.0	6	2.2E-03	1.0E-03
Tb427.01.4310	TbFAZ2	FDYLSDQRPR	3.1	2	4.2E-03	3.7E-03
Tb427.10.15290	Tubulin Binding Cofactor C	SSMEGAGSVSSDEEADSAHIGR**	5.0	2.5	2.2E-02	2.3E-05
Tb427.10.12950	TbBBP110	EESHCPGASAAPSSR	2.5	~99	4.7E-02	7.2E-04
Tb427tmp.01.2430	TbBBP590	VSGASTVSGMQTAASSSSSSAR	~99	~99	2.8E-05	1.4E-04
Tb427tmp.01.0680	TbLRRP1	SASAVELYSLR	3.1	3	5.5E-03	2.1E-04
Tb427.01.4310	TbFAZ2	SSGTALPAGAGVSEMMHTCR	3.5	~99	2.5E-02	1.4E-04
Mitochondrial Proteins						
Tb427.03.3520	TbPOMP25	EGSGFECSSGVLTQEER	2.1	~99	1.4E-04	1.6E-04
Tb427tmp.02.0350	TbPOMP12	DGSHTTNDSTDCSTVTSAR**	2.3	2.0	1.4E-04	5.8E-03
Phospho-signaling Proteins						
Tb427.06.2840	Rio2 Kinase	SIDSAINVAAQQR	~99	4.3	1.7E-04	6.35E-05
Tb427.10.15300	S/T Protein Kinase	DQPFYSNGSGHGER	2.7	~99	5.7E-03	2.5E-03
Tb427tmp.211.2360/2410	Protein Kinase A catalytic subunit isoform 1/2	SPGDTSNFESYPESGDK	2.1	2.0	8.9E-04	1.4E-04
Tb427.02.1820	Protein Kinase (SNF1/CBL-interacting)	SPHSATTAAEASITSFAK*	2.1	4.0	3.5E-02	2.6E-04
Tb427.04.1700	Protein Kinase (Tau-tubulin Kinase)	GHSASPEPPPPFQR	2.2	~99	4.9E-03	1.1E-03
Tb427.10.13780	glycogen synthase kinase 3	STGSLVAIK	~99	~99	2.8E-02	2.4E-02
Tb427.10.14300	MEKK-related kinase 1 (MRK1)	DASESDPNDDDDDNSSTSTAGPPGSTR**	~99	~99	1.9E-03	1.7E-05
Tb427tmp.01.4320	kinetoplastid-specific protein phosphatase	EGSLASDGLVSHR	2.4	2.0	3.3E-05	8.3E-06

Supplemental Figure 3.1. *Knockdown of TbCK1.2 impairs trypanosome proliferation and kinetoplast duplication without disrupting DNA synthesis*. A TbCK1.2 RNAi cell line was incubated in the absence (-Tet) or presence (+Tet) of tetracycline (1 μg/ml) for 24 h. (***A***) Trypanosome density was determined 12 h, 16 h, or 24 h after the addition of tetracycline, starting from a density of 5 x 10^4 cells/ml. The average cell density and standard deviation of triplicate biological experiments are shown. (***B***) The number of kinetoplasts (K) and nuclei (N) per trypanosome was assessed by staining with DAPI following knockdown of TbCK1.2. The average percentage of trypanosomes with indicated numbers of kinetoplasts and nuclei is presented. Error bars represent standard deviation in three biological experiments. Examples of trypanosomes (+Tet) with defective kinetoplast division (1K2N) are shown. A χ^2 test was employed to determine whether the distribution, based on enumeration of kinetoplasts and nuclei, was statistically different after knockdown of TbCK1.2 (p = 3.3 x 10^{-22}). (***C)*** DNA content per trypanosome was analyzed by flow cytometry (see materials and methods). The distribution of cells with unreplicated (2C), replicating (2C-4C), or replicated (4C) DNA are shown. The inset shows the average percentage of cells with one, two, or more than two nuclei in uninduced (-Tet) or induced (+Tet) trypanosomes, as determined by DAPI staining of nuclei (see panel B). (***D***) The fluorescence intensity of DAPI-stained kinetoplasts was determined by ImageJ following knockdown of TbCK1.2. The average fluorescence intensity, with standard deviation, is provided for each cell population. DAPI-stained trypanosomes from four biological replicates were combined.

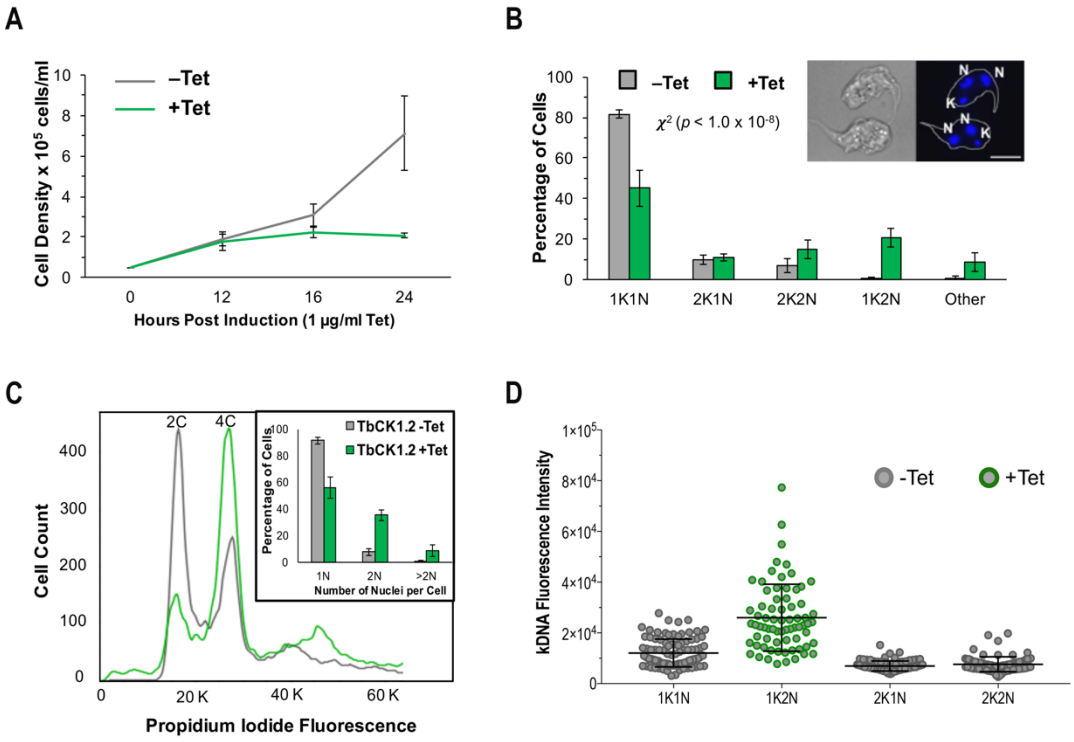
A
Cell Density x 10^5 cells/ml
–Tet
+Tet
Hours Post Induction (1 µg/ml Tet)
B
Percentage of Cells
–Tet
+Tet
χ² (p < 1.0 x 10⁻⁸)
1K1N
2K1N
2K2N
1K2N
Other
C
Cell Count
2C
4C
TbCK1.2 -Tet
TbCK1.2 +Tet
Percentage of Cells
Number of Nuclei per Cell
Propidium Iodide Fluorescence
D
kDNA Fluorescence Intensity
-Tet
+Tet

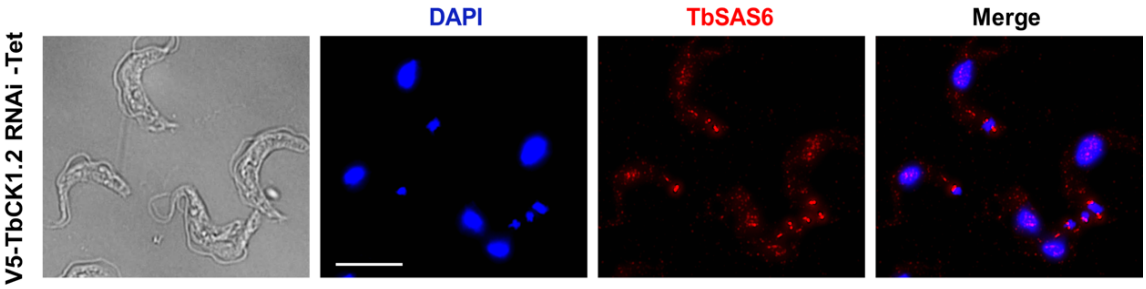

Supplemental Figure 3.2. *Background staining from the anti-TbSAS6 antibody*. Uninduced TbCK1.2 RNAi cells from the panel in Figure 3.1B without adjustments to brightness/contrast to remove signal from the anti-TbSAS6 antibody which is not detected at the basal body.

Supplemental Figure 3.3. *Effect of SB-431542 on trypanosome proliferation, kinetoplast division, and TbCK1.2 expression*. Trypanosome density was determined after treating cells (10 h) with DMSO (drug vehicle) or SB-431542 (10 μM). "Start" indicates the cell density (5 x10^5 cell/ml) at which DMSO or drug was added. The average density is presented and error bars represent standard deviation in three biological replicates. (***B***) DNA in the kinetoplast and nucleus was stained with DAPI after treatment (10 h) with DMSO (drug vehicle) or SB-431542 (10 μM) and the number of kinetoplasts and nuclei per cell quantitated. The average percentage of cells with the indicated number of kinetoplasts and nuclei are shown. Error bars indicate standard deviation in three biological experiments. A χ^2 test was used to compare the distribution between cells treated with SB-431542 or DMSO (p = 1.6 x 10^{-27}). (***C***) A cell line in which one allele of TbCK1.2 was tagged with a V5 epitope was treated with DMSO (drug vehicle) or SB-431542 (10 μM) for 10 h. Following treatment, cell lysate was probed with an anti-V5 antibody by western blotting. The average normalized band intensity (see materials and methods) for V5-TbCK1.2 and standard deviation from three biological replicates are shown.

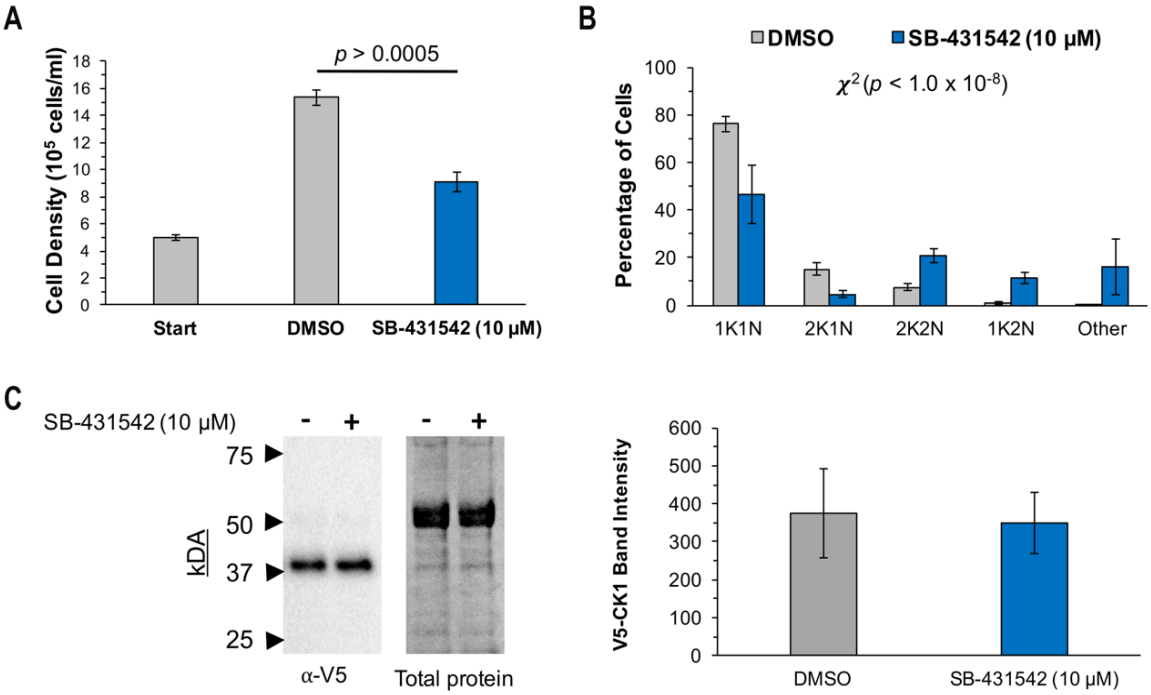
A
Cell Density (10^5 cells/ml)
p > 0.0005
Start
DMSO
SB-431542 (10 µM)
B
DMSO
SB-431542 (10 µM)
χ² (p < 1.0 x 10^-8)
Percentage of Cells
1K1N
2K1N
2K2N
1K2N
Other
C
SB-431542 (10 µM)
kDA
75
50
37
25
α-V5
Total protein
V5-CK1 Band Intensity
DMSO
SB-431542 (10 µM)

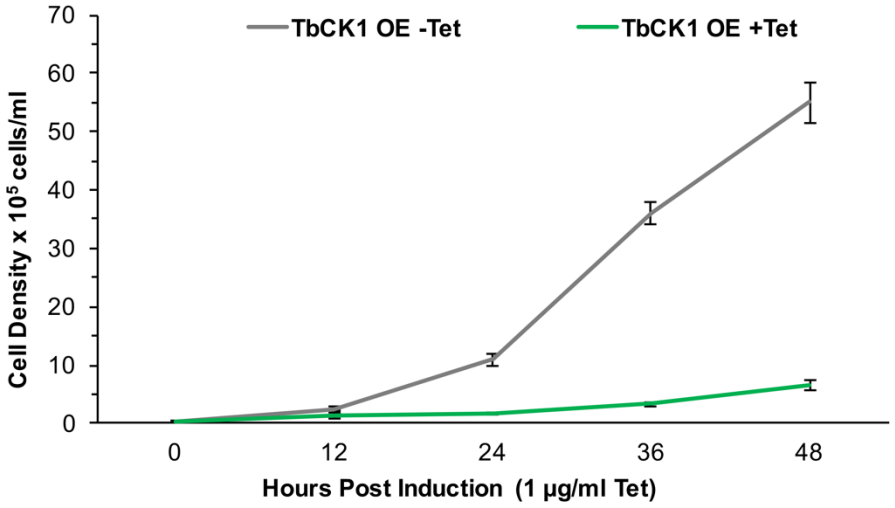

Supplemental Figure 3.4. *Overexpression of TbCK1.2 arrests trypanosome proliferation*. A cell line harboring an ectopic, tetracycline-inducible copy of TbCK1.2 was incubated in the presence (+Tet) or absence (-Tet) of tetracycline for 48 h. Cell density was determined every 12 h. The average cell density with standard deviation in three biological replicates are shown.

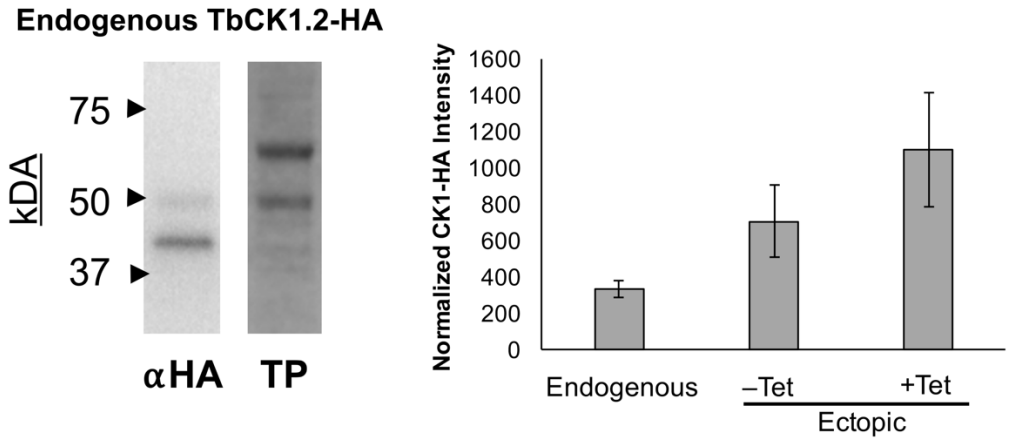

Supplemental Figure 3.5. *Expression of TbCK1.2-HA from its endogenous promoter*. One allele of TbCK1.2 was tagged with an HA epitope at the C-terminus in CA427 trypanosomes. Cell lysate collected from the TbCK1.2-HA was probed with anti-HA antibody by western blotting. TbCK1.2-HA corresponds to the band at ~40 kDA (as expected). Total protein (TP) is shown as a load control. The average normalized (see materials and methods) CK1-HA band intensity from cells expressing TbCK1.2-HA from an endogenous or ectopic promoter (see Figure 3.6A) are shown. Error bars represent standard deviation in three biological replicates.

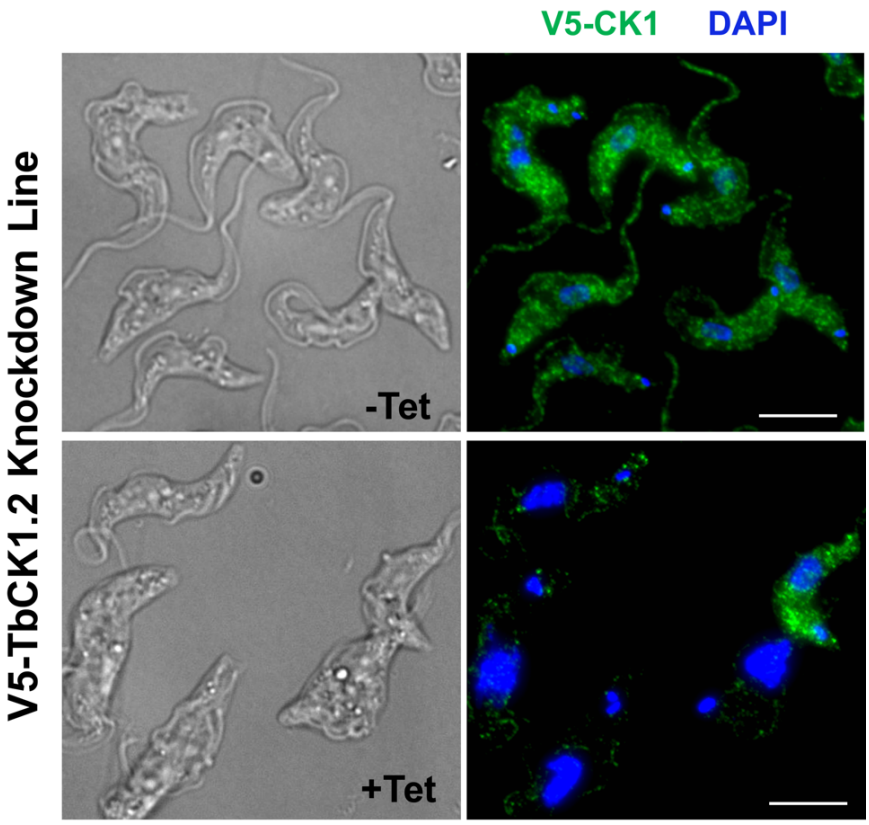

Supplemental Figure 3.6. *Immunofluorescence evaluation of TbCK1.2 knockdown.* A V5-TbCK1.2 RNAi line was incubated in the absence (-Tet) or presence (+Tet) of tetracycline for 24 hours. Uninduced and induced cells were fixed with paraformaldehyde (PFA), permeabilized with detergent, and probed with an anti-V5 antibody. The scale bar is 6 μm.

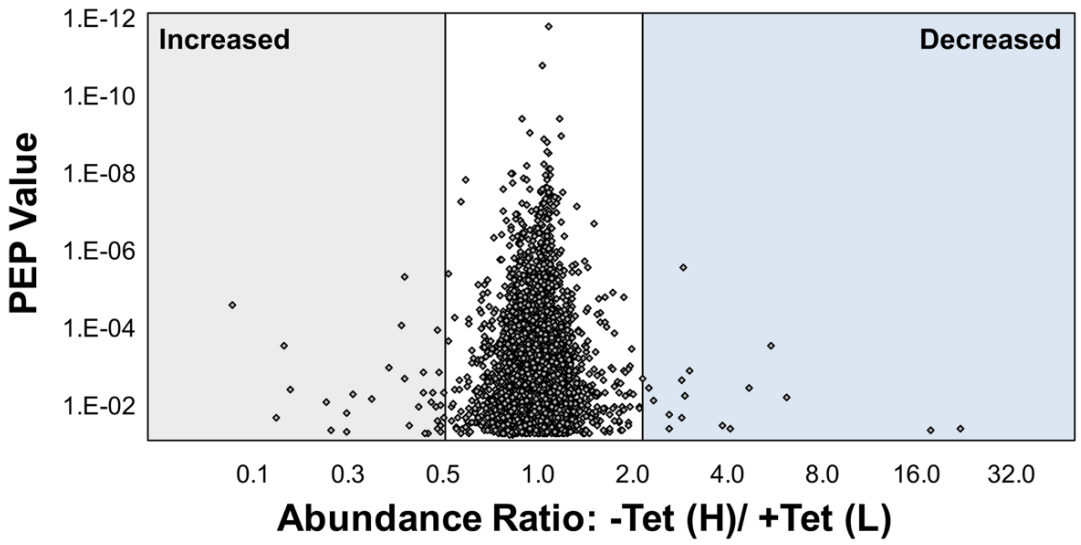

Supplemental Figure 3.7. *Biological variation of phospho-peptide abundance in a TbCK1.2 RNAi line (-Tet) grown in heavy or light SILAC medium.* The TbCK1.2 RNAi cell line (-Tet) was cultured in either light (L) or heavy (H) HMI-9 medium (SILAC). Trypanosomes grown in light medium (3×10^7) were combined with cells grown in heavy medium (3×10^7), lysed, tryspinzed, and phospho-peptides enriched over an IMAC column before analysis by LC-MS/MS. The abundance ratio (H/L) of identified phospho-peptides are plotted as a function of their PEP value (probability that spectra-peptide match was incorrect). Only peptides with a score of 5×10^{-2} (5% chance of error), or lower, are shown. Gray and blue areas indicated phospho-peptides with increased and decreased abundance (two-fold or greater), respectively.

Supplemental Table 3.1. *Putative TbCK1.2 effectors with decreased phospho-peptide abundance after knockdown of TbCK1.2*. Following a 24-h knockdown of TbCK1.2, phospho-peptides were harvested from uninduced and induced cells and phospho-peptides enriched over an IMAC column (see materials and methods). Phospho-peptide abundance was calculated in each sample using a labeled proteomics (SILAC) and label-free approach (spectral counting (SC)) (see materials and methods). Phospho-peptides identified with decreased abundance (at least 2-fold) in each phosphoproteomics strategy are listed below. Phosphorylation sites are indicated in red (PhosphoRS [94] value >79%). * indicates the number of phospho-sites which could not be accurately identified. The fold change in phospho-peptide abundance, as compared to the uninduced control, is shown. ~ indicates that the phospho-peptide was only present in the control or induced population, preventing calculation of an abundance ratio. All peptides had a PEP value (probability that spectra-peptide match was incorrect) of 5% or less. N/A = specific phospho-isoform of a peptide was identified by one approach, but not the other.

Gene ID	Predicted Protein Product	Sequence	Fold Decrease	
			SILAC	SC
Tb427.01.1880	WD40 repeat-conatining protein	SSQSAVTTSEVGGCSPQR*	2.5	2
Tb427.01.4280	Hypothetical	VSASSTPQFSR	3.1	4
Tb427.01.4310	FAZ Protein 2	FDYLSDQRPR	3.1	2
Tb427.02.5810	Hypothetical	GDVGDPAVSDGDGTDIGR	3	3
Tb427.03.1010	Hypothetical	AVASLVTDEASEQAAAAPQNR	8.7	3.5
Tb427.03.3240	Hypothetical	GNNSNSLNGSVNGPR	N/A	2
Tb427.03.3240	Hypothetical	GNNSNSLNGSVNGPR	2.6	N/A
Tb427.03.3520	Outer Mitochondrial Membrane Protein (POMP25)	EGSGFECSSGVLTQEER	2.1	~99
Tb427.03.3940	RNA binding protein (DRBD11)	TPLNNESGPGTSSSGSHSSSSNVPVASLR**	N/A	5
Tb427.03.3940	RNA binding protein (DRBD11)	TPLNNESGPGTSSSGSHSSSSNVPVASLR*	2.5	N/A
Tb427.03.5040	Hypothetical	GLQDGVESDGCSTVFSHSGQR	2.2	N/A
Tb427.03.5040	Hypothetical	GLQDGVESDGCSTVFSHSGQR*	N/A	4
Tb427.04.2750	Hypothetical	LPTRGSQQPLDEDEDR	2.2	N/A
Tb427.04.2750	Hypothetical	LPTRGSQQPLDEDEDR*	N/A	~99
Tb427.04.2920	Hypothetical	NSVTFSDATETR	2	N/A
Tb427.04.2920	Hypothetical	NSVTFSDATETR	N/A	2.5
Tb427.05.360	ISG75 (ivariant surface glycoprotein)	DDISIGEANAK	2	2
Tb427.05.3610	adaptor complex protein (AP) 3 delta subunit 1	VVGATGSISNR	2	N/A
Tb427.05.3610	adaptor complex protein (AP) 3 delta subunit 1	VVGATGSISNR	N/A	~99
Tb427.06.2840	Rio2 Kinase	SIDSAINVAAQQR	~99	4.3
Tb427.06.3490	ZFP-1 (Zinc finger binding protein 1)	SENSLSFSGSR	5.3	2
Tb427.06.4390	Kinesin	DGTPSPNNTQNENLQR	2	N/A
Tb427.06.4390	Kinesin	DGTPSPNNTQNENLQR	N/A	2
Tb427.06.4440	RNA binding protein 42	TGAVEKEPSCAEGK	4.3	~99
Tb427.07.2300	TbNup132 (nucleoporin)	SEMETMSAPADPLSEK	16.6	N/A
Tb427.07.2300	TbNup132 (nucleoporin)	SEMETMSAPADPLSEK**	N/A	~99
Tb427.07.3550	Cytoskeleton Associated Protein	AAEGKPSTSEAESSDVGAAANTR	3.2	N/A
Tb427.07.3550	Cytoskeleton Associated Protein	AAEGKPSTSEAESSDVGAAANTR**	N/A	3.5
Tb427.07.5030	Hypothetical	GGSESEVYDTLNGSNSNNK	2.4	2
Tb427.08.3870	SRP40, C-terminal domain containing protein	KPVAPDSSSDDDEPVR	2.4	N/A
Tb427.08.3870	SRP40, C-terminal domain containing protein	KPVAPDSSSDDDEPVRKPLVK	N/A	2.5
Tb427.08.4400	Hypothetical	NSVVAGTSDYNQR	2.6	2
Tb427.08.6660	PFC1 (PFR componenet)	MMTMPDADGAADSNKGSLDTGSVPK*	2.1	18
Tb427.08.7080	Hypothetical	SLDESTQHTISAPSK	3.2	2.5
Tb427.08.7760	Hypothetical	TSATFLASPLQPVR*	5.2	N/A
Tb427.08.7760	Hypothetical	TSATFLASPLQPVR	N/A	~99
Tb427.10.10280	TbBBP268	RHSFTASSEADAAVVK*	3.7	N/A
Tb427.10.10280	TbBBP268	RHSFTASSEADAAVVK	N/A	5.5
Tb427.10.11990	RNA binding protein (Nip7 homolog)	TTGNNGSNDDDDGDDGEEQNSQQTYVFR*	4	3
Tb427.10.13800	Hypothetical	VSSTTQPAAEAAVEKPADSGAPAVPDAEAETR**	N/A	~99
Tb427.10.13800	Hypothetical	VSSTTQPAAEAAVEKPADSGAPAVPDAEAETR*	2.264	N/A
Tb427.10.14480	Hypothetical	EALQGLGASEGSQTGR*	2	N/A

(Supplemental Table 3.1 continued)

Tb427.10.14480	Hypothetical	EALQGLGASEGSQTGR	N/A	~99
Tb427.10.14500	Hypothetical	SATPPQGTIVMPGTVR	8.2	N/A
Tb427.10.14500	Hypothetical	SATPPQGTIVMPGTVR	N/A	2.9
Tb427.10.15290	tubulin binding cofactor c	SSMEGAGSVSSDEEADSAHIGR	5.N/A33	N/A
Tb427.10.15290	tubulin binding cofactor c	SSMEGAGSVSSDEEADSAHIGR	N/A	2.5
Tb427.10.15300	S/T Protein Kinase	DQPFYSNGSGHGER	2.676	~99
Tb427.10.350	TbBBP59 (Protein Kinase)	VSSAGSTPSVTAAR*	N/A	3
Tb427.10.350	TbBBP59 (Protein Kinase)	VSSAGSTPSVTAAR*	6.556	N/A
Tb427.10.5200	Hypothetical	SGGDDVDDIDGSGLAK	3.85	2
Tb427.10.5450	NLP (ISWI complex)	EENSVNGDETNTTLPR	2.387	2
Tb427.10.970	Hypothetical	SGPSSQDPFVCSTTAK*	2.213	N/A
Tb427.10.970	Hypothetical	SGPSSQDPFVCSTTAK**	N/A	3
Tb427tmp.01.0680	TbLRRP1	LGRPPSTTNDDASHPAK	.N/AN/A	N/A
Tb427tmp.01.0680	TbLRRP1	LGRPPSTTNDDASHPAK*	N/A	6
Tb427tmp.01.3730; T	Hypothetical	SPSSDQLDVVK	3.726	N/A
Tb427tmp.01.3730; T	Hypothetical	SPSSDQLDVVK*	N/A	~99
Tb427tmp.01.4780	Hypothetical	ANGDGCSDAEDLLR	2.N/A61	2
Tb427tmp.01.6790	Bilobe Protein	LDEEVPNIGQLSDGGGSPK	4.651	2.3
Tb427tmp.02.0990	Dpy-30 motif/AAA domain containing protein	SRQSLPTVIDLGTQAEK	4.5	2.2
Tb427tmp.211.1070	ZC3H28	QQGPAGSQVDEHEEDGDLEDSR	2.986	2
Tb427tmp.211.2360;	protein kinase A catalytic subunit isoform 1/2	SPGDTSNFESYPESGDK	2.14	N/A
Tb427tmp.211.2360	protein kinase A catalytic subunit isoform 1	SPGDTSNFESYPESGDKR	N/A	2
Tb427tmp.244.2660	CHAT domain containing protein	STAQEADVDEKPQCLANR	3.718	4

Supplemental Table 3.2. *Putative TbCK1.2 effectors with increased phospho-peptide abundance after knockdown of TbCK1.2*. Following a 24-h knockdown of TbCK1.2, phospho-peptides were harvested from uninduced and induced cells and phospho-peptides enriched over an IMAC column (see materials and methods). Phospho-peptide abundance was calculated in each sample using a labeled proteomics (SILAC) and label-free approach (spectral counting (SC)) (see materials and methods). Phospho-peptides identified with decreased abundance (at least 2-fold) in each phosphoproteomics strategy are listed below. Phosphorylation sites are indicated in red (PhosphoRS [94] value >79%). * indicates the number of phospho-sites which could not be accurately identified. The fold change in phospho-peptide abundance, as compared to the uninduced control, is shown. ~ indicates that the phospho-peptide was only present in the control or induced population, preventing calculation of an abundance ratio. All peptides had a PEP value (probability that spectra-peptide match was incorrect) of 5% or less. N/A = specific phospho-isoform of a peptide was identified by one approach, but not the other.

Gene ID	Predicted Protein Product	Sequence	Fold Decrease	
			SILAC	SC
Tb427.01.2100	Calpain-like cysteine peptidase	ANKSEGESVTKDGSDGHAEETSPVQSPEGEVGER	~99	3
Tb427.01.4310	FAZ Protein 2	SSGTALPAGAGVSEMMHTCR	3.5	~99
Tb427.02.1820	Protein Kinase (SNF1/CBL-interacting)	SPHSATTAAEASITSFAK*	2.1	4
Tb427.02.5760	Flagellar Member 8	KSASPSELNSPVMK*	N/A	5
Tb427.02.5760	Flagellar Member 8	KSASPSELNSPVMK	2	N/A
Tb427.02.5760	Flagellar Member 8	SDLPSSPSSPLCIK	N/A	3
Tb427.02.5760	Flagellar Member 8	SDLPSSPSSPLCIK	2.1	N/A
Tb427.03.1010	Hypothetical	GAADVNENPTSSATPR*	N/A	4
Tb427.03.1010	Hypothetical	GAADVNENPTSSATPR	~99	N/A
Tb427.03.1010	Hypothetical	GGSVESAATRPSGGGAALTQDAVDAGGSAADSNA	N/A	2.7
Tb427.03.1010	Hypothetical	GGSVESAATRPSGGGAALTQDAVDAGGSAADSNA	~99	N/A
Tb427.03.3800	Hypothetical	EHPPSFQSPTPTVEGPLVSPR	4	3
Tb427.03.3880	Hypothetical	EPMSPLPTQPTSVPSVASLK	~99	~99
Tb427.03.3940	RNA-binding protein (DRBD11)	SLGISGHGSAR	2.9	2
Tb427.03.4180	Hypothetical	VSSPLPPIDASEHGSPR*	11.1	~99
Tb427.03.4270	Hypothetical	FPALSGSVVR	N/A	0
Tb427.03.4270	Hypothetical	FPALSGSVVR	2.1	N/A
Tb427.03.4270	Hypothetical	LTESLQNVNDR	3.2	2
Tb427.03.4710	Hypothetical	LSETSSSSVAASR**	~99	~99
Tb427.03.4710	Hypothetical	SHSSNVESGCTSR	N/A	~99
Tb427.03.4710	Hypothetical	SHSSNVESGCTSR*	2.7	N/A
Tb427.03.4970	Hypothetical	GQTGAGGSGPGPSGAVESDLLQK*	~99	4
Tb427.03.5020	Flagellar Member 6	RPNADPDEKSDSGTHSEGEHTMEK**	N/A	~99
Tb427.03.5020	Flagellar Member 6	RPNADPDEKSDSGTHSEGEHTMEK*	~99	N/A
Tb427.04.1700	Protein Kinase (Tau-tubulin Kinase)	GHSASPEPPPPFQR	2.2	~99
Tb427.04.2370	Hypothetical	HTTNSSFSSNIGSR*	5.7	~99
Tb427.04.2820	Hypothetical	STSTTASHALQQGGAETSDQSR**	2.4	N/A
Tb427.04.2820	Hypothetical	STSTTASHALQQGGAETSDQSR*	N/A	~99
Tb427.04.3140	SBDS protein C-terminal domain containing protein	SVGGGGGSHQTGSSSNPTQCLNNNNK*	2.1	~99
Tb427.04.3330	EF-hand domain pair	TVGDSSKNASTSSVTNAVK	5.9	N/A
Tb427.04.3330	EF-hand domain pair	TVGDSSKNASTSSVTNAVK**	N/A	~99
Tb427.04.4280	Hypothetical	VLCSEPPTPPCEQK	~99	2.5
Tb427.05.2620	Hypothetical	RPVSSPIACGHGSR	3	~99
Tb427.05.3030	IFT122B	LDGTTTSLQLTNPSK**	N/A	0
Tb427.05.3030	IFT122B	LDGTTTSLQLTNPSK*	4.5	N/A
Tb427.05.3030	IFT122B	VGHGVGPAGGGAGGVGGTTR	2.7	4
Tb427.06.1180	Hypothetical	RVESDPSQLADSPEPQKPPR	2.1	2
Tb427.06.1920	Hypothetical	NSQTLQDGMGSSSR*	~99	3.3
Tb427.06.2860	Hypothetical	GSTISCSSPQRPQAVVNELHR*	N/A	8
Tb427.06.2860	Hypothetical	GSTISCSSPQRPQAVVNELHR*	2.4	N/A
Tb427.06.4390	KIF3/5 Heavy Chain	GPSPFDAAR	~99	3
Tb427.06.5010	Hypothetical	DASEHLPALPSAR	3.1	N/A

(Supplemental Table 3.2 continued)

Tb427.06.5010	Hypothetical	DASEHLPALPSAR*	N/A	3
Tb427.06.620	Hypothetical	TPLSPVSSR	3.6	~99
Tb427.06.870	myotubularin	SLPFLDER	3.2	~99
Tb427.07.1420	Hypothetical	RASFAFGDSCAASPR	2.6	~99
Tb427.07.2320	Hypothetical	VLQPLSSGSPSPR*	2.1	3
Tb427.07.2660	ZC3H20	SVTLGDASVTTQPAVVR	4.5	~99
Tb427.07.3130	Hypothetical	EVSQRPVGVSPGDAATDTSPLK	3.6	N/A
Tb427.07.3130	Hypothetical	EVSQRPVGVSPGDAATDTSPLK**	N/A	~99
Tb427.07.3130	Hypothetical	TATETATEGYSQPPSVTVYPHVNR	3.2	N/A
Tb427.07.3130	Hypothetical	TATETATEGYSQPPSVTVYPHVNR	N/A	~99
Tb427.07.3700	Hypothetical	AASFESPSDDTLR	3.9	2
Tb427.07.3790	ras-like small GTPase (ras-like small GTPase)	SNVSSPLLSK	7.2	2
Tb427.07.4410	Hypothetical	SSFNAVETHR	~99	2
Tb427.07.4410	Hypothetical	SSVSPVSSTTTATETHHPETTSSSTR**	N/A	~99
Tb427.07.4410	Hypothetical	SSVSPVSSTTTATETHHPETTSSSTR*	2.4	N/A
Tb427.07.4500	PX domain containing protein	EQPQPVAVVDSTPPPAPK*	5.1	2
Tb427.07.4870	Hypothetical	MASAASTDIR	2	N/A
Tb427.07.4870	Hypothetical	MASAASTDIR*	N/A	~99
Tb427.07.5140	Hypothetical	DAEAVLSPTSDPDAK*	~99	~99
Tb427.07.5180; Tb42	60S ribosomal protein L23a	LSASYDALDTANK	7.2	~99
Tb427.07.6790	Hypothetical	NGASIQPSCDETTPDKVQNALTESSVVSR*	4.5	~99
Tb427.07.6950	Hypothetical	VGHVPGVQLSPK	~99	~99
Tb427.07.7000	Hypothetical	SQLEVQAPAR	2.6	~99
Tb427.07.7250	Ankyrin repeats (3 copies)	HSISSQQR	2	~99
Tb427.08.2640	ubiquitin-activating enzyme e1 (UBA1)	ATTECAQGDNSPTGASSSLR	~99	2
Tb427.08.3180	DUF3250	SSSFTLVPR	2	~99
Tb427.08.3590	Hypothetical	TGSIFSGEK	2.2	2
Tb427.08.4400	Hypothetical	GSCFTDSVTNGIVPIGGGK*	4.9	2.5
Tb427.08.4780	Flagellar Member 3	DQTPSLQDLLR	3.4	N/A
Tb427.08.6050	Hypothetical	AVISPQEKPLTSSSSGEALGGSGNEVK*	~99	~99
Tb427.08.6370	cytoskeleton associated protein	EEGSLSPYLR	6.3	~99
Tb427.08.6660	PFR component 1	ITLDKSQISK	4.5	5
Tb427.08.6950; Tb42	dynein light chain 2B	MEFNASTTNER	3.6	~99
Tb427.08.7820	DNA-binding domain containing protein	IASPPPPSR	~99	~99
Tb427.08.7850	Hypothetical	AGPISHVEGSPSR	~99	~99
Tb427.08.790	Hypothetical	KGSCACSTTNISDTNAAQNSR*	N/A	~99
Tb427.08.790	Hypothetical	KGSCACSTTNISDTNAAQNSR*	~99	N/A
Tb427.10.11880	Hypothetical	ANASTESAGVSGEDALER	N/A	4
Tb427.10.11880	Hypothetical	ANASTESAGVSGEDALER	2.6	N/A
Tb427.10.12950	BBP110	EESHCPGASAAPSSR	2.5	~99
Tb427.10.13780	glycogen synthase kinase 3	STGSLVAIK	~99	~99
Tb427.10.14300	MEKK-related kinase 1 (MRK1)	FNDASESDPNDDDDDNSSTSTAGPPGSTR**	~99	~99
Tb427.10.14490	Hypothetical	TNGSGSTGSGEAAAGEPNAQK	~99	~99

(Supplemental Table 3.2 continued)

Tb427.10.1810	RING-H2 zinc finger	MEEAAAEGMPLSQEQGEQK	2.1	3
Tb427.10.3500	RNA-binding protein	TSQNDGAIVPLLAEDVEK*	2.6	3
Tb427.10.4440	predicted SAP domain protein	ASTGSVSESGHVSGLK	N/A	~99
Tb427.10.4440	predicted SAP domain protein	ASTGSVSESGHVSGLK*	4	N/A
Tb427.10.4860	Hypothetical	SCTPPPGDSDVSR	~99	~99
Tb427.10.5350	dynein heavy chain	SELQASQVGASSETAVVR*	2.1	~99
Tb427.10.5880	Proteophosphoglycan	SASLDSSVTAK	~99	~99
Tb427.10.5880	Proteophosphoglycan	SNISSTCLTPGR*	2.6	2
Tb427.10.6410	mismatch repair protein (MSH6)	TSEGPTQEFTQASGTQCGSK*	~99	~99
Tb427.10.6580	hypothetical protein	HASLPSNSTPVK**	N/A	2
Tb427.10.6580	hypothetical protein	HASLPSNSTPVK*	3.7	N/A
Tb427.10.7230	Flagellar Member 1	DGTASTPTQERHSTLGEETEGPMTVSSR**	2.1	~99
Tb427.10.9330	hypothetical protein	ASGEVNAESNVHSPASVTAK	3.7	~99
Tb427.10.9330	hypothetical protein	VEGDGSPELLATR	2	~99
Tb427.10.9700	predicted C2 domain protein	SYASSADAFSSSAQR*	2.6	~99
Tb427.10.9700	predicted C2 domain protein	TTASTACTSSGYNTAR	2.9	~99
Tb427tmp.01.0680	TbLRRP1	SASAVELYSLR	3.1	3
Tb427tmp.01.0920	ADP-ribosylation factor GTPase activating protein	GPSQGNFQAPAVDAK	2.4	2
Tb427tmp.01.1050	FAZ Protein 20	MLNNIPSQR	2.2	~99
Tb427tmp.01.2330	eukaryotic translation initation factor 4 gamma	CSQSTNDLTR	2.2	3
Tb427tmp.01.2430	BBP590	VSGASTVSGMQTAASSSSSSAR	~99	~99
Tb427tmp.01.3960	BILBO1	VTPNGSLSMQGALAPYNGSR	2.3	2
Tb427tmp.01.4320	kinetoplastid-specific phospho-protein phosphatase	EGSLASDGLVSHR	2.4	2
Tb427tmp.01.4400	hypothetical protein	KDSSPPRPPFR	3.4	~99
Tb427tmp.01.4400	hypothetical protein	SPSTMSQPQQLEYETR	N/A	~99
Tb427tmp.01.4400	hypothetical protein	SPSTMSQPQQLEYETR*	3.1	N/A
Tb427tmp.01.4480	PH domain containing protein	LSKPQQPSNSSGGDSK	~99	2.5
Tb427tmp.01.4920	hypothetical protein	GGTSGDDSATPSTLDDDESRGSGEEK	N/A	~99
Tb427tmp.01.4920	hypothetical protein	GGTSGDDSATPSTLDDDESRGSGEEK	~99	N/A
Tb427tmp.01.6770	hypothetical protein	KNADDYSETSGTALPGEAGEK*	4	~99
Tb427tmp.01.6770	hypothetical protein	SSSEIVASTGGGTDTHRDSGSSGNNGAAPNDNEK*	~99	10
Tb427tmp.01.6790	hypothetical protein	STSALLSSLGGK	2	2.3
Tb427tmp.01.6900	hypothetical protein	LEGTPTSDSNAPR	3.9	~99
Tb427tmp.01.8190	hypothetical protein	TEAVPLSR	3.7	2
Tb427tmp.01.8770	leucine-rich repeat protein (LRRP)	SAITGPVAAGPPECESIK	5	~99
Tb427tmp.02.0350	Outer Mitochondrial Membrane Protein (POMP12)	DGSHTTNDSTDCSTVTSAR**	N/A	2
Tb427tmp.02.0350	Outer Mitochondrial Membrane Protein (POMP12)	DGSHTTNDSTDCSTVTSAR*	2.3	N/A
Tb427tmp.02.1420	hypothetical protein	YSPLHFCSSK	3.1	4
Tb427tmp.02.1600	ubiquitin-like protein	FEGTQTPQQTR	3.1	~99
Tb427tmp.02.4290	hypothetical protein	GSVATSASNQEATCAANPSGIDSSR*	N/A	2.3
Tb427tmp.02.4290	hypothetical protein	GSVATSASNQEATCAANPSGIDSSR	3.7	N/A
Tb427tmp.02.4290	hypothetical protein	GVSTHSAGCQSESGASSVVSSTEHVQNNK**	N/A	~99
Tb427tmp.02.4290	hypothetical protein	GVSTHSAGCQSESGASSVVSSTEHVQNNK	2.4	N/A

(Supplemental Table 3.2 continued)

Tb427tmp.02.4640	tubulin-tyrsoine ligase-like protein	EESMGGAAGTGHISEDGGSK	8.3	2
Tb427tmp.02.4950	cytoplasmic translation associated protein	HLSSADLFK*	N/A	~99
Tb427tmp.02.4950	cytoplasmic translation associated protein	HLSSADLFK	~99	N/A
Tb427tmp.160.1440	EB1-like C-terminal motif containing protein	SGSRGESSSEGDSAVAAAALLK*	2.8	2
Tb427tmp.160.1440	EB1-like C-terminal motif containing protein	TNNAGSSSGVLSGSGDISER	3	2
Tb427tmp.160.2980	GTPase activating protein	SASVTMEGESVR	~99	~99
Tb427tmp.160.3020	hypothetical protein	SAGNDDKSHPPTQGGFR	2.2	2
Tb427tmp.160.3990	cation transporter	EASPGSATLLDSPAATGMSTR	8.5	~99
Tb427tmp.160.4700	peroxisomal membrane protein (Pex16)	DRSSETVGEDADFSEAGK	~99	2
Tb427tmp.211.3890	hypothetical protein	DHASPAEGSGSNVTVVSGVCSAER	N/A	3
Tb427tmp.211.3890	hypothetical protein	DHASPAEGSGSNVTVVSGVCSAER*	3.3	N/A
Tb427tmp.211.4840	mismatch repair protein (PMS1)	TSSPDATASPTSTTNR	N/A	~99
Tb427tmp.211.4840	mismatch repair protein (PMS1)	TSSPDATASPTSTTNR*	3.2	N/A
Tb427tmp.39.0006	translation initiation factor eIF2B delta subunit	SPGNWSPLSHGSR	2.5	4
Tb427tmp.55.0019	hypothetical protein	SKSPPAPLVPR	5.6	3

3.6 References

1. Brun, R., et al., *Human African trypanosomiasis.* Lancet, 2010. **375**(9709): p. 148-59.

2. Vaughan, S. and K. Gull, *Basal body structure and cell cycle-dependent biogenesis in Trypanosoma brucei.* Cilia, 2015. **5**: p. 5.

3. Ralston, K.S., et al., *The Trypanosoma brucei flagellum: moving parasites in new directions.* Annu Rev Microbiol, 2009. **63**: p. 335-62.

4. Lacomble, S., et al., *Basal body movements orchestrate membrane organelle division and cell morphogenesis in Trypanosoma brucei.* J Cell Sci, 2010. **123**(Pt 17): p. 2884-91.

5. Robinson, D.R. and K. Gull, *Basal body movements as a mechanism for mitochondrial genome segregation in the trypanosome cell cycle.* Nature, 1991. **352**(6337): p. 731-3.

6. Zhao, Z., et al., *p166, a link between the trypanosome mitochondrial DNA and flagellum, mediates genome segregation.* EMBO J, 2008. **27**(1): p. 143-54.

7. Trikin, R., et al., *Correction: TAC102 Is a Novel Component of the Mitochondrial Genome Segregation Machinery in Trypanosomes.* PLoS Pathog, 2016. **12**(7): p. e1005750.

8. Hu, H., Q. Zhou, and Z. Li, *A Novel Basal Body Protein That Is a Polo-like Kinase Substrate Is Required for Basal Body Segregation and Flagellum Adhesion in Trypanosoma brucei.* J Biol Chem, 2015. **290**(41): p. 25012-22.

9. Pradel, L.C., et al., *NIMA-related kinase TbNRKC is involved in basal body separation in Trypanosoma brucei.* J Cell Sci, 2006. **119**(Pt 9): p. 1852-63.

10. Li, Z. and C.C. Wang, *KMP-11, a basal body and flagellar protein, is required for cell division in Trypanosoma brucei.* Eukaryot Cell, 2008. **7**(11): p. 1941-50.

11. He, C.Y., M. Pypaert, and G. Warren, *Golgi duplication in Trypanosoma brucei requires Centrin2.* Science, 2005. **310**(5751): p. 1196-8.

12. Dang, H.Q., et al., *Proximity Interactions among Basal Body Components in Trypanosoma brucei Identify Novel Regulators of Basal Body Biogenesis and Inheritance.* MBio, 2017. **8**(1).

13. McKean, P.G., et al., *Gamma-tubulin functions in the nucleation of a discrete subset of microtubules in the eukaryotic flagellum.* Curr Biol, 2003. **13**(7): p. 598-602.

14. Morgan, G.W., et al., *An evolutionarily conserved coiled-coil protein implicated in polycystic kidney disease is involved in basal body duplication and flagellar biogenesis in Trypanosoma brucei.* Mol Cell Biol, 2005. **25**(9): p. 3774-83.

15. Hu, H., et al., *The Centriole Cartwheel Protein SAS-6 in Trypanosoma brucei Is Required for Probasal Body Biogenesis and Flagellum Assembly.* Eukaryot Cell, 2015. **14**(9): p. 898-907.

16. Andre, J., et al., *An Alternative Model for the Role of RP2 Protein in Flagellum Assembly in the African Trypanosome.* J Biol Chem, 2014. **289**(1): p. 464-75.

17. Sherwin, T. and K. Gull, *The cell division cycle of Trypanosoma brucei brucei: timing of event markers and cytoskeletal modulations.* Philos Trans R Soc Lond B Biol Sci, 1989. **323**(1218): p. 573-88.

18. Ralston, K.S., et al., *Flagellar motility contributes to cytokinesis in Trypanosoma brucei and is modulated by an evolutionarily conserved dynein regulatory system.* Eukaryot Cell, 2006. **5**(4): p. 696-711.

19. Kohl, L., D. Robinson, and P. Bastin, *Novel roles for the flagellum in cell morphogenesis and cytokinesis of trypanosomes.* EMBO J, 2003. **22**(20): p. 5336-46.

20. Sunter, J.D. and K. Gull, *The Flagellum Attachment Zone: 'The Cellular Ruler' of Trypanosome Morphology.* Trends Parasitol, 2016. **32**(4): p. 309-24.

21. Rotureau, B., et al., *Flagellar adhesion in Trypanosoma brucei relies on interactions between different skeletal structures in the flagellum and cell body.* J Cell Sci, 2014. **127**(Pt 1): p. 204-15.

22. Vaughan, S., et al., *A repetitive protein essential for the flagellum attachment zone filament structure and function in Trypanosoma brucei.* Protist, 2008. **159**(1): p. 127-36.

23. Liu, B., et al., *Fellowship of the rings: the replication of kinetoplast DNA.* Trends Parasitol, 2005. **21**(8): p. 363-9.

24. Jensen, R.E. and P.T. Englund, *Network news: the replication of kinetoplast DNA.* Annu Rev Microbiol, 2012. **66**: p. 473-91.

25. Shapiro, T.A. and P.T. Englund, *The structure and replication of kinetoplast DNA.* Annu Rev Microbiol, 1995. **49**: p. 117-43.

26. Ogbadoyi, E.O., D.R. Robinson, and K. Gull, *A high-order trans-membrane structural linkage is responsible for mitochondrial genome positioning and segregation by flagellar basal bodies in trypanosomes.* Mol Biol Cell, 2003. **14**(5): p. 1769-79.

27. Woodward, R. and K. Gull, *Timing of nuclear and kinetoplast DNA replication and early morphological events in the cell cycle of Trypanosoma brucei.* J Cell Sci, 1990. **95 (Pt 1)**: p. 49-57.

28. Sullenberger, C., et al., *AEE788 Inhibits Basal Body Assembly and Blocks DNA Replication in the African Trypanosome.* Mol Pharmacol, 2017. **91**(5): p. 17.

29. Gluenz, E., et al., *The kinetoplast duplication cycle in Trypanosoma brucei is orchestrated by cytoskeleton-mediated cell morphogenesis.* Mol Cell Biol, 2011. **31**(5): p. 1012-21.

30. Povelones, M.L., *Beyond replication: division and segregation of mitochondrial DNA in kinetoplastids.* Mol Biochem Parasitol, 2014. **196**(1): p. 53-60.

31. Ikeda, K.N. and C.L. de Graffenried, *Polo-like kinase is necessary for flagellum inheritance in Trypanosoma brucei.* J Cell Sci, 2012. **125**(Pt 13): p. 3173-84.

32. Jones, N.G., et al., *Regulators of Trypanosoma brucei Cell Cycle Progression and Differentiation Identified Using a Kinome-Wide RNAi Screen.* PLoS Pathog, 2014. **10**(1): p. e1003886.

33. Urbaniak, M.D., *Casein kinase 1 isoform 2 is essential for bloodstream form Trypanosoma brucei.* Mol Biochem Parasitol, 2009. **166**(2): p. 183-5.

34. Robinson, D.R., et al., *Microtubule polarity and dynamics in the control of organelle positioning, segregation, and cytokinesis in the trypanosome cell cycle.* J Cell Biol, 1995. **128**(6): p. 1163-72.

35. Portman, N. and K. Gull, *The paraflagellar rod of kinetoplastid parasites: from structure to components and function.* Int J Parasitol, 2010. **40**(2): p. 135-48.

36. Inman, G.J., et al., *SB-431542 is a potent and specific inhibitor of transforming growth factor-beta superfamily type I activin receptor-like kinase (ALK) receptors ALK4, ALK5, and ALK7.* Mol Pharmacol, 2002. **62**(1): p. 65-74.

37. Vogt, J., R. Traynor, and G.P. Sapkota, *The specificities of small molecule inhibitors of the TGFss and BMP pathways.* Cell Signal, 2011. **23**(11): p. 1831-42.

38. Ogunjimi, A.A., et al., *Structural basis for specificity of TGFbeta family receptor small molecule inhibitors.* Cell Signal, 2012. **24**(2): p. 476-83.

39. Bienen, E.J., et al., *Non-cytochrome mediated mitochondrial ATP production in bloodstream form Trypanosoma brucei brucei.* Eur J Biochem, 1993. **216**(1): p. 75-80.

40. Wirtz, E., et al., *A tightly regulated inducible expression system for conditional gene knock-outs and dominant-negative genetics in Trypanosoma brucei.* Mol Biochem Parasitol, 1999. **99**(1): p. 89-101.

41. Wickstead, B., K. Ersfeld, and K. Gull, *The frequency of gene targeting in Trypanosoma brucei is independent of target site copy number.* Nucleic Acids Res, 2003. **31**(14): p. 3993-4000.

42. Schnell, U., et al., *Immunolabeling artifacts and the need for live-cell imaging.* Nat Methods, 2012. **9**(2): p. 152-8.

43. Esson, H.J., et al., *Morphology of the trypanosome bilobe, a novel cytoskeletal structure.* Eukaryot Cell, 2012. **11**(6): p. 761-72.

44. Lundgren, D.H., et al., *Role of spectral counting in quantitative proteomics.* Expert Rev Proteomics, 2010. **7**(1): p. 39-53.

45. Zhang, B., et al., *Detecting differential and correlated protein expression in label-free shotgun proteomics.* J Proteome Res, 2006. **5**(11): p. 2909-18.

46. Mann, M., *Functional and quantitative proteomics using SILAC.* Nat Rev Mol Cell Biol, 2006. **7**(12): p. 952-8.

47. Urbaniak, M.D., D.M. Martin, and M.A. Ferguson, *Global quantitative SILAC phosphoproteomics reveals differential phosphorylation is widespread between the procyclic and bloodstream form lifecycle stages of Trypanosoma brucei.* J Proteome Res, 2013. **12**(5): p. 2233-44.

48. Garcia-Mayoral, M.F., et al., *The solution structure of the N-terminal domain of human tubulin binding cofactor C reveals a platform for tubulin interaction.* PLoS One, 2011. **6**(10): p. e25912.

49. Zhou, Q., et al., *A comparative proteomic analysis reveals a new bi-lobe protein required for bi-lobe duplication and cell division in Trypanosoma brucei.* PLoS One, 2010. **5**(3): p. e9660.

50. Zhou, Q., et al., *Assembly and maintenance of the flagellum attachment zone filament in Trypanosoma brucei.* J Cell Sci, 2015. **128**(13): p. 2361-72.

51. Niemann, M., et al., *Mitochondrial outer membrane proteome of Trypanosoma brucei reveals novel factors required to maintain mitochondrial morphology.* Mol Cell Proteomics, 2013. **12**(2): p. 515-28.

52. O'Toole, E.T. and S.K. Dutcher, *Site-specific basal body duplication in Chlamydomonas.* Cytoskeleton (Hoboken), 2014. **71**(2): p. 108-18.

53. Ruthnick, D. and E. Schiebel, *Duplication of the Yeast Spindle Pole Body Once per Cell Cycle.* Mol Cell Biol, 2016. **36**(9): p. 1324-31.

54. Nigg, E.A., *Centrosome duplication: of rules and licenses.* Trends Cell Biol, 2007. **17**(5): p. 215-21.

55. Bettencourt-Dias, M. and D.M. Glover, *Centrosome biogenesis and function: centrosomics brings new understanding.* Nat Rev Mol Cell Biol, 2007. **8**(6): p. 451-63.

56. Dawe, H.R., H. Farr, and K. Gull, *Centriole/basal body morphogenesis and migration during ciliogenesis in animal cells.* J Cell Sci, 2007. **120**(Pt 1): p. 7-15.

57. Levine, M.S., et al., *Centrosome Amplification Is Sufficient to Promote Spontaneous Tumorigenesis in Mammals.* Dev Cell, 2017. **40**(3): p. 313-322 e5.

58. Chan, J.Y., *A clinical overview of centrosome amplification in human cancers.* Int J Biol Sci, 2011. **7**(8): p. 1122-44.

59. Nigg, E.A. and J.W. Raff, *Centrioles, centrosomes, and cilia in health and disease.* Cell, 2009. **139**(4): p. 663-78.

60. Godinho, S.A. and D. Pellman, *Causes and consequences of centrosome abnormalities in cancer.* Philos Trans R Soc Lond B Biol Sci, 2014. **369**(1650).

61. Chavali, P.L., M. Putz, and F. Gergely, *Small organelle, big responsibility: the role of centrosomes in development and disease.* Philos Trans R Soc Lond B Biol Sci, 2014. **369**(1650).

62. Peel, N., et al., *Overexpressing centriole-replication proteins in vivo induces centriole overduplication and de novo formation.* Curr Biol, 2007. **17**(10): p. 834-43.

63. Kleylein-Sohn, J., et al., *Plk4-induced centriole biogenesis in human cells.* Dev Cell, 2007. **13**(2): p. 190-202.

64. Shukla, A., et al., *Plk1 relieves centriole block to reduplication by promoting daughter centriole maturation.* Nat Commun, 2015. **6**: p. 8077.

65. Loncarek, J., P. Hergert, and A. Khodjakov, *Centriole reduplication during prolonged interphase requires procentriole maturation governed by Plk1.* Curr Biol, 2010. **20**(14): p. 1277-82.

66. Beisson, J. and M. Wright, *Basal body/centriole assembly and continuity.* Curr Opin Cell Biol, 2003. **15**(1): p. 96-104.

67. Marshall, W.F., Y. Vucica, and J.L. Rosenbaum, *Kinetics and regulation of de novo centriole assembly. Implications for the mechanism of centriole duplication.* Curr Biol, 2001. **11**(5): p. 308-17.

68. Khodjakov, A., et al., *De novo formation of centrosomes in vertebrate cells arrested during S-phase.* J Cell Biol, 2002. **158**(7): p. 1171-81.

69. Mizukami, I. and J. Gall, *Centriole replication. II. Sperm formation in the fern, Marsilea, and the cycad, Zamia.* J Cell Biol, 1966. **29**(1): p. 97-111.

70. Heath, I.B., S.G. Kaminskyj, and T. Bauchop, *Basal body loss during fungal zoospore encystment: evidence against centriole autonomy.* J Cell Sci, 1986. **83**: p. 135-40.

71. Wang, Z., et al., *Inhibition of Trypanosoma brucei gene expression by RNA interference using an integratable vector with opposing T7 promoters.* J Biol Chem, 2000. **275**(51): p. 40174-9.

72. Wang, Z. and P.T. Englund, *RNA interference of a trypanosome topoisomerase II causes progressive loss of mitochondrial DNA.* EMBO J, 2001. **20**(17): p. 4674-83.

73. Lindsay, M.E., et al., *A new function of Trypanosoma brucei mitochondrial topoisomerase II is to maintain kinetoplast DNA network topology.* Mol Microbiol, 2008. **70**(6): p. 1465-76.

74. Lou, Z., K. Minter-Dykhouse, and J. Chen, *BRCA1 participates in DNA decatenation.* Nat Struct Mol Biol, 2005. **12**(7): p. 589-93.

75. Coelho, P.A., J. Queiroz-Machado, and C.E. Sunkel, *Condensin-dependent localisation of topoisomerase II to an axial chromosomal structure is required for sister chromatid resolution during mitosis.* J Cell Sci, 2003. **116**(Pt 23): p. 4763-76.

76. Coelho, P.A., et al., *Dual role of topoisomerase II in centromere resolution and aurora B activity.* PLoS Biol, 2008. **6**(8): p. e207.

77. Rattner, J.B., et al., *Topoisomerase II alpha is associated with the mammalian centromere in a cell cycle- and species-specific manner and is required for proper centromere/kinetochore structure.* J Cell Biol, 1996. **134**(5): p. 1097-107.

78. Gheiratmand, L., et al., *Biochemical characterization of the bi-lobe reveals a continuous structural network linking the bi-lobe to other single-copied organelles in Trypanosoma brucei.* J Biol Chem, 2013. **288**(5): p. 3489-99.

79. Kung, J.E. and N. Jura, *Structural Basis for the Non-catalytic Functions of Protein Kinases.* Structure, 2016. **24**(1): p. 7-24.

80. Dolloff, N.G., et al., *Off-target lapatinib activity sensitizes colon cancer cells through TRAIL death receptor up-regulation.* Sci Transl Med, 2011. **3**(86): p. 86ra50.

81. Bain, J., et al., *The selectivity of protein kinase inhibitors: a further update.* Biochem J, 2007. **408**(3): p. 297-315.

82. Hirumi, H.H.a.K., *Axenic Culture of Arican Trypanosome Bloodstream Forms.* Parasitology Today, 1994. **10**(2): p. 80-84.

83. Subramanya, S. and K. Mensa-Wilmot, *Regulated cleavage of intracellular glycosylphosphatidylinositol in a trypanosome. Peroxisome-to-endoplasmic reticulum translocation of a phospholipase C.* FEBS J, 2006. **273**(10): p. 2110-26.

84. Medina-Acosta, E. and G.A. Cross, *Rapid isolation of DNA from trypanosomatid protozoa using a simple 'mini-prep' procedure.* Mol Biochem Parasitol, 1993. **59**(2): p. 327-9.

85. Li, Z., S. Gourguechon, and C.C. Wang, *Tousled-like kinase in a microbial eukaryote regulates spindle assembly and S-phase progression by interacting with Aurora kinase and chromatin assembly factors.* J Cell Sci, 2007. **120**(Pt 21): p. 3883-94.

86. Burkard, G., C.M. Fragoso, and I. Roditi, *Highly efficient stable transformation of bloodstream forms of Trypanosoma brucei.* Mol Biochem Parasitol, 2007. **153**(2): p. 220-3.

87. Shen, S., et al., *In vivo epitope tagging of Trypanosoma brucei genes using a one step PCR-based strategy.* Mol Biochem Parasitol, 2001. **113**(1): p. 171-3.

88. Oberholzer, M., et al., *A vector series for rapid PCR-mediated C-terminal in situ tagging of Trypanosoma brucei genes.* Mol Biochem Parasitol, 2006. **145**(1): p. 117-20.

89. Studier, F.W., et al., *Use of T7 RNA polymerase to direct the expression of cloned genes.* Methods in Enzymology, 1990. **185**: p. 60-89.

90. Cass, B., et al., *Purification of recombinant proteins from mammalian cell culture using a generic double-affinity chromatography scheme.* Protein Expr Purif, 2005. **40**(1): p. 77-85.

91. Butter, F., et al., *Comparative proteomics of two life cycle stages of stable isotope-labeled Trypanosoma brucei reveals novel components of the parasite's host adaptation machinery.* Mol Cell Proteomics, 2013. **12**(1): p. 172-9.

92. Guyett, P.J., et al., *Novel Effects of Lapatinib Revealed in the African Trypanosome by Using Hypothesis-Generating Proteomics and Chemical Biology Strategies.* Antimicrob Agents Chemother, 2017. **61**(2).

93. Eng, J.K., A.L. McCormack, and J.R. Yates, *An approach to correlate tandem mass spectral data of peptides with amino acid sequences in a protein database.* J Am Soc Mass Spectrom, 1994. **5**(11): p. 976-89.

94. Taus, T., et al., *Universal and confident phosphorylation site localization using phosphoRS.* J Proteome Res, 2011. **10**(12): p. 5354-62.

CHAPTER 4

CONCLUSIONS AND DISCUSSION

4.1 Utility of AEE788 as a chemical tool for studying trypanosome biology

In Chapter 2 we demonstrated that the small molecule AEE788 inhibits DNA synthesis in both the kinetoplast and nucleus, and prevents duplication of the basal body and bilobe, after a short-term treatment (4 h). Taken together, these data suggest that AEE788 blocks S-phase entry in bloodstream trypanosomes, as each of these independent events occur during this time [1-5]. Remarkably, removal of AEE788 from trypanosome culture allowed these processes to resume. Thus, for the first time, pre-S-phase bloodstream trypanosomes were reversibly enriched from an asynchronous culture. Accordingly, we postulate that phospho-proteins affected by AEE788 treatment are likely to include novel regulators of the G1/S transition; an exciting possibility given the lack of knowledge regarding signaling pathways that promote G1 progression and initiation of chromosomal DNA synthesis in *T. brucei*. Using a comparative phospho-proteomics analysis we identified proteins whose phosphorylation was altered as a result of AEE788 treatment ("AEE788 effectors") (Chapter 2). Future genetic studies will focus on assessing the role of AEE788 effectors in promoting S-phase entry. Additionally, we are interested in identifying protein kinases targeted by AEE788. Knowledge of

AEE788 targets and effectors will be beneficial for mapping novel phospho-signaling pathways that regulate S-phase entry in bloodstream trypanosomes.

In Chapter 2 we also showed that AEE788 selectively disrupts transferrin endocytosis and trypanosome morphology. Importantly, ongoing work in our lab suggests that a previously uncharacterized protein kinase (Tb427tmp.160.4770) is hyper-phosphorylated after AEE788 treatment and regulates transferrin endocytosis. These findings serve as a proof-of-principle for our "discovery chemical biology" strategy outlined in Figure 1.1. In this approach, we first used phenotypic studies to document the physiological pathways disrupted by AEE788 (global "mode of action" studies). Then, using a comparative phospho-proteomics analysis, we identified a list of putative AEE788 effectors whose phosphorylation was influenced by the drug. Given that a putative AEE788 effector (Tb427tmp.160.4770) regulates an AEE788-disrupted pathway (transferrin endocytosis), our strategy for studying trypanosome biology with small molecules is genetically validated. This data makes us confident that future functional studies with other putative AEE788 effectors will identify novel regulators of: i) S-phase entry, ii) DNA synthesis, iii) basal body duplication, and iv) trypanosome morphology.

4.2 Biological functions of TbCK1.2

New perspectives on division of the kinetoplast

Chapter 3 characterized a function of TbCK1.2 in division of the kDNA network. We observed that knockdown of TbCK1.2 blocked kinetoplast scission without perturbation of kDNA synthesis, basal body duplication/separation, or flagellum

biogenesis. These data are at odds with the current dogma which presents basal body separation as the mechanical force that drives kinetoplast division [6]. Our data demonstrates that basal body separation is not sufficient to cause division of the kinetoplast. Accordingly, we outlined a new hypothesis in which TbCK1.2 promotes activity or recruitment of “kinetoplast division factors” (KDFs) to biochemically resolve interlocked DNAs of the replicated kDNA network (Figure 3.9).

We hypothesize that KDFs regulate the activity of mitochondrial topoisomerases which, through decatenation of interlocked minicircles and maxicircles, biochemically separate the doubled-sized mitochondrial nucleoid into two equivalent daughter kDNA networks after completion of kDNA synthesis. Accordingly, topoisomerase activity would need to be directed to specific positions within the kDNA network, as random decatenation could lead to asymmetric division or kinetoplast fragmentation. We propose that KDFs may impose “directed decatenation” activity on topoisomerases to ensure symmetric division of the kDNA network. It is also possible that TbCK1.2 directly regulates topoisomerase activity through phosphorylation as has been documented for casein kinase II in other eukaryotes [7-9].

Additionally, it is imperative that activity of the topoisomerases be coordinated with kDNA replication such that division proceeds after the kDNA network is fully replicated. From our kinetic studies in Chapter 2, we know that kinetoplast division occurs in G2. It is therefore possible that KDFs are upregulated during this time in order to coordinate topoisomerase activity with kDNA replication

and kDNA network division. In the kinetoplastid *Crithidia fasciculate*, mRNA stability of mitochondrial topoisomerase II is regulated such that protein expression peaks during kinetoplast duplication [12, 13]. It is possible that TbCK1.2 regulates mRNA stability of KDFs or topoisomerases as several RNA-binding proteins had altered phosphorylation following knockdown of TbCK1.2 (Supplemental Tables 3.1-3.2). Alternatively, morphological changes in kDNA network organization, observed after the kDNA network has doubled in size [1, 10, 11], might allow topoisomerases to distinguish between the replicated and unreplicated kDNA network. Thus, TbCK1.2 and KDFs may regulate topoisomerase activity or localization through modification of kDNA network organization, protein-protein interactions, and post-translational modifications; similar regulatory mechanisms have been described for topoisomerase II in other eukaryotes [7, 8, 14-17] (reviewed in [18]).

Although mitochondrial topoisomerases have received a lot of attention as the enzymes required to resolve daughter kDNA networks [19, 20], it is possible that other proteins with nuclease activity are important in this process. A structure-specific endonuclease (TbSSE1) localizes at the kinetoplast antipodal sites [21, 22] (protein assemblies that form at kinetoplast poles during S-phase), similar to mitochondrial topoisomerase II ($TbTOPII_{mt}$) [23]. Knockdown of either protein results in asymmetric division. Accordingly, KDFs may influence nuclease activity of proteins other than a topoisomerase to direct biochemical resolution of the kDNA network.

Our KDF hypothesis recognizes an important role of basal body separation in segregation of duplicated kDNA networks into daughter trypanosomes (Figure 3.9) [6]. We propose that KDFs act after initial migration of basal bodies along the kinetoplast, prior to division of the KDNA network in G2 (Figure 3.9). In future work, it will be important to know if basal body separation influences KDF recruitment or activity to gain a better understanding of the relationship between kinetoplast division and basal body separation.

The "AEE788 block-and-release" protocol (Chapter 2) allowed us to distinguish the times at which kDNA synthesis, kDNA network elongation, and kinetoplast division occurred following AEE788 washout. Accordingly, AEE788 will be a useful tool for the future study of KDFs. For example, using the AEE788 "block-and-release" protocol we can track localization of putative KDFs during different stages of kinetoplast duplication. It will be useful to know if a trypanosome topoisomerase or TbSSE1 localizes to the plane of division on the kDNA network prior to separation of the mitochondrial nucleoid, which we know occurs 3-3.5 h after AEE788 washout. Similarly, it will be interesting to disrupt protein function of $TopoII_{mt}$ or TbSSE1 at specific points during kinetoplast duplication to determine if the proteins have multiple functions in kDNA replication and/or network division.

Regulation of basal body copy number

Data presented in Chapter 3 identified TbCK1.2 as a regulator of basal body copy number. Reduced TbCK1.2 activity promotes amplification of basal bodies, while increased activity inhibits basal body biogenesis. Consistent with these observations, we detected TbCK1.2 at the basal body and identified basal body

proteins with altered phosphorylation following knockdown of TbCK1.2. The function of these putative TbCK1.2 effectors remains unknown and will be the focus of future studies. Given that phosphorylation of two basal body proteins was consistently reduced (Tb427.10.10280 and Tb427.10.350) (Table 3.1) after knockdown of TbCK1.2, we are interested in determining if they could be direct biochemical substrates of enzyme. Towards this goal, our lab has established an in vitro protein kinase assay that uses synthetic peptides corresponding to putative TbCK1.2 effectors as substrates for purified recombinant TbCK1.2. Our initial studies have shown that several identified TbCK1.2 effectors are phosphorylated by TbCK1.2. Therefore, our phospho-proteomics analysis is capable of identifying proteins in the TbCK1.2 phospho-signaling pathway. Once TbCK1.2 substrates are known, mutation of the enzyme's phospho-site in vivo will allow us to gain a better understanding of how the substrate is influenced by TbCK1.2 phospho-signaling.

Basal body duplication is coordinated with the trypanosome division cycle [2, 3], occurring during nuclear S-phase [28]. Consequently, one explanation for the phenotypes described after TbCK1.2 knockdown (Chapter 3) could be that TbCK1.2 regulates S-phase events in the trypanosome. Preliminary data in our lab indicates that knockdown of TbCK1.2 promotes aberrant DNA synthesis. In mammalian cells, proteins that control both DNA synthesis and centriole duplication (occurs in S-phase) have been reported [29-31]. Future characterization of TbCK1.2 effectors will allow us to determine which proteins function in basal body duplication and/or DNA synthesis.

4.3 References

1. Gluenz, E., et al., *The kinetoplast duplication cycle in Trypanosoma brucei is orchestrated by cytoskeleton-mediated cell morphogenesis.* Mol Cell Biol, 2011. **31**(5): p. 1012-21.

2. Woodward, R. and K. Gull, *Timing of nuclear and kinetoplast DNA replication and early morphological events in the cell cycle of Trypanosoma brucei.* J Cell Sci, 1990. **95 (Pt 1)**: p. 49-57.

3. Sherwin, T. and K. Gull, *The cell division cycle of Trypanosoma brucei brucei: timing of event markers and cytoskeletal modulations.* Philos Trans R Soc Lond B Biol Sci, 1989. **323**(1218): p. 573-88.

4. He, C.Y., M. Pypaert, and G. Warren, *Golgi duplication in Trypanosoma brucei requires Centrin2.* Science, 2005. **310**(5751): p. 1196-8.

5. Zhou, Q., H. Hu, and Z. Li, *New insights into the molecular mechanisms of mitosis and cytokinesis in trypanosomes.* Int Rev Cell Mol Biol, 2014. **308**: p. 127-66.

6. Robinson, D.R. and K. Gull, *Basal body movements as a mechanism for mitochondrial genome segregation in the trypanosome cell cycle.* Nature, 1991. **352**(6337): p. 731-3.

7. Ackerman, P., C.V. Glover, and N. Osheroff, *Phosphorylation of DNA topoisomerase II by casein kinase II: modulation of eukaryotic topoisomerase II activity in vitro.* Proc Natl Acad Sci U S A, 1985. **82**(10): p. 3164-8.

8. DeVore, R.F., A.H. Corbett, and N. Osheroff, *Phosphorylation of topoisomerase II by casein kinase II and protein kinase C: effects on enzyme-mediated DNA cleavage/religation and sensitivity to the antineoplastic drugs etoposide and 4'-(9-acridinylamino)methane-sulfon-m-anisidide.* Cancer Res, 1992. **52**(8): p. 2156-61.

9. Ahn, B.H., T.H. Kim, and Y.S. Bae, *Mapping of the interaction domain of the protein kinase CKII beta subunit with target proteins.* Mol Cells, 2001. **12**(2): p. 158-63.

10. Gluenz, E., M.K. Shaw, and K. Gull, *Structural asymmetry and discrete nucleic acid subdomains in the Trypanosoma brucei kinetoplast.* Mol Microbiol, 2007. **64**(6): p. 1529-39.

11. Povelones, M.L., *Beyond replication: division and segregation of mitochondrial DNA in kinetoplastids.* Mol Biochem Parasitol, 2014. **196**(1): p. 53-60.

12. Pasion, S.G., et al., *Sequences within the 5' untranslated region regulate the levels of a kinetoplast DNA topoisomerase mRNA during the cell cycle.* Mol Cell Biol, 1996. **16**(12): p. 6724-35.

13. Pasion, S.G., et al., *Periodic expression of nuclear and mitochondrial DNA replication genes during the trypanosomatid cell cycle.* J Cell Sci, 1994. **107 (Pt 12)**: p. 3515-20.

14. Lou, Z., K. Minter-Dykhouse, and J. Chen, *BRCA1 participates in DNA decatenation.* Nat Struct Mol Biol, 2005. **12**(7): p. 589-93.

15. Coelho, P.A., et al., *Dual role of topoisomerase II in centromere resolution and aurora B activity.* PLoS Biol, 2008. **6**(8): p. e207.

16. Coelho, P.A., J. Queiroz-Machado, and C.E. Sunkel, *Condensin-dependent localisation of topoisomerase II to an axial chromosomal structure is required for sister chromatid resolution during mitosis.* J Cell Sci, 2003. **116**(Pt 23): p. 4763-76.

17. Goswami, P.C., J.L. Roti Roti, and C.R. Hunt, *The cell cycle-coupled expression of topoisomerase IIalpha during S-phase is regulated by mRNA stability and is disrupted by heat shock or ionizing radiation.* Mol Cell Biol, 1996. **16**(4): p. 1500-8.

18. Nitiss, J.L., *DNA topoisomerase II and its growing repertoire of biological functions.* Nat Rev Cancer, 2009. **9**(5): p. 327-37.

19. Jensen, R.E. and P.T. Englund, *Network news: the replication of kinetoplast DNA.* Annu Rev Microbiol, 2012. **66**: p. 473-91.

20. Liu, B., et al., *Fellowship of the rings: the replication of kinetoplast DNA.* Trends Parasitol, 2005. **21**(8): p. 363-9.

21. Liu, Y., S.A. Motyka, and P.T. Englund, *Effects of RNA interference of Trypanosoma brucei structure-specific endonuclease-I on kinetoplast DNA replication.* J Biol Chem, 2005. **280**(42): p. 35513-20.

22. Engel, M.L. and D.S. Ray, *The kinetoplast structure-specific endonuclease I is related to the 5' exo/endonuclease domain of bacterial DNA polymerase I and colocalizes with the kinetoplast topoisomerase II and DNA polymerase beta during replication.* Proc Natl Acad Sci U S A, 1999. **96**(15): p. 8455-60.

23. Melendy, T., C. Sheline, and D.S. Ray, *Localization of a type II DNA topoisomerase to two sites at the periphery of the kinetoplast DNA of Crithidia fasciculata.* Cell, 1988. **55**(6): p. 1083-8.

24. Wang, Z., et al., *Inhibition of Trypanosoma brucei gene expression by RNA interference using an integratable vector with opposing T7 promoters.* J Biol Chem, 2000. **275**(51): p. 40174-9.

25. Wang, Z. and P.T. Englund, *RNA interference of a trypanosome topoisomerase II causes progressive loss of mitochondrial DNA.* EMBO J, 2001. **20**(17): p. 4674-83.

26. Jessop, L. and M. Lichten, *Mus81/Mms4 endonuclease and Sgs1 helicase collaborate to ensure proper recombination intermediate metabolism during meiosis.* Mol Cell, 2008. **31**(3): p. 313-23.

27. Klein, F., et al., *A central role for cohesins in sister chromatid cohesion, formation of axial elements, and recombination during yeast meiosis.* Cell, 1999. **98**(1): p. 91-103.

28. Sullenberger, C., et al., *AEE788 Inhibits Basal Body Assembly and Blocks DNA Replication in the African Trypanosome.* Mol Pharmacol, 2017. **91**(5): p. 17.

29. Xu, X., et al., *DNA replication licensing factor Cdc6 and Plk4 kinase antagonistically regulate centrosome duplication via Sas-6.* Nat Commun, 2017. **8**: p. 15164.

30. Adon, A.M., et al., *Cdk2 and Cdk4 regulate the centrosome cycle and are critical mediators of centrosome amplification in p53-null cells.* Mol Cell Biol, 2010. **30**(3): p. 694-710.

31. Hemerly, A.S., et al., *Orc1 controls centriole and centrosome copy number in human cells.* Science, 2009. **323**(5915): p. 789-93.